

Report No. FAA-RD-74-119,1

11

ILS GLIDE SLOPE STANDARDS

Part I: A Review of Flight Inspection Standards Affecting Landing Performance and Comparison With Limits Evolved From System Analysis

Lee Gregor Hofmann, Warren F. Clement,
Dunstan Graham, Gary L. Teper

Systems Technology, Inc.
Hawthorne, California

Bryon L. Wiscons, David L. Hemmel

Collins Radio Co.
Cedar Rapids, Iowa

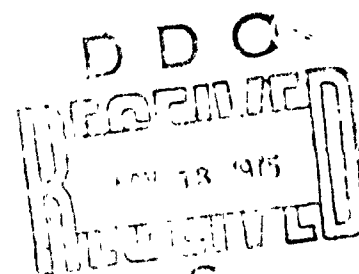
Richard H. McFarland, Avionics Consultant

Athens, Ohio



June 1975

Final Report



Document is available to the public through the
National Technical Information Service,
Springfield, Virginia 22161.

Prepared for

U.S. DEPARTMENT OF TRANSPORTATION
FEDERAL AVIATION ADMINISTRATION
Systems Research & Development Service

ADA017087

NOTICE

This document is disseminated under the sponsorship of the Department of Transportation in the interest of information exchange. The United States Government assumes no liability for its contents or use thereof.

ACCESSION FOR	NTIS	DOC	UNCLASSIFIED	RESTRICTED
BY	DISTRIBUTION/AVAILABILITY STATEMENT			
Dist.	EXPL. and or Special			
A				

1. Report No. 18 FAA-RD-74-119 1	2. Government Accession No. 12 304 P.	3. Recipient's Catalog No.	
6 ILS Glide Slope Standards: Part I, A Review of Flight Inspection Standards Affecting Landing Performance and Comparison with Limits Evolved From System Analysis.		5. Report Date June 1975	6. Performing Organization Code 14 STI-1043-1
7. Author(s) 15 L. G. Hofmann, W. F. Clement, D. Graham, 'cont'd at 15)	8. Performing Organization Report No. TR-1043-1		
9. Performing Organization Name and Address SYSTEMS TECHNOLOGY, INC. 13766 South Hawthorne Boulevard Hawthorne, California 90250	10. Work Unit No. (TRAIS) 071-313-013		
12. Sponsoring Agency Name and Address Federal Aviation Administration Systems Research and Development Service 800 Independence Avenue, S. W. Washington, D. C. 20591	11. Contract or Grant No. 15 DOT-FA74WA-3340		
13. Type of Report and Period Covered FINAL, PHASE I 8/20/73 to 8/20/74	14. Sponsoring Agency Code FAA/ARD-322		
15. Supplementary Notes G. L. Teper, Systems Technology, Inc.; B. L. Wiscons, D. L. Hemmel, Collins Radio Co.; and R. H. McFarland, Avionics Consultant 9 Final report 20 Aug 73 - 20 Aug 74. Phase I.			
<p>Abstract</p> <p>System analysis techniques are used to determine maximum levels for ILS Glide Slope beam structure characteristics which will result in acceptable approach and landing outcomes. Results are based upon a power spectral density signature for ILS Glide Slopes obtained from a nonstationary statistical analysis of flight inspection data for 17 Category II and II-training facilities. Maximum levels and standard deviation time histories for typical aircraft-control system response; indicated glide path deviation, actual glide path deviation and actual glide path deviation rate; are used as the basis for recommending revisions to the ILS Glide Slope flight inspection data processing procedures, and for recommending relaxed flight inspection standards.</p> <p>The maximum extent to which current Glide Slope flight inspection standards might be relaxed is indicated to be very considerable along the entire approach path for Category I service. Relaxation of the standards in ILS Approach Zone 3 is also possible for Category II service. An additional finding is that the maximum extent to which flight inspection standards might be relaxed is exactly the same for Category II and III services.</p> <p>Further findings are that any distinctions between the approach performance obtained using manual flight director controlled approach coupling, automatic approach coupling, or inertially augmented automatic approach coupling do not warrant ILS Glide Slope flight inspection standards which are specific to the airborne user's method of coupling. Glide Slope approach couplers incorporating inertial augmentation produce significantly lower touchdown dispersion, but comparable missed approach rates. The dominant influence on missed approaches for a light straight-wing twin was not ILS Glide Slope structure, but was rather wind gusts and shears.</p> <p>Recommended revisions to flight inspection data processing would include filtering the "differential trace" to obtain additional traces representing typical airborne system responses. Data analysis would be revised in that 2σ boundaries appropriate to each filter output and category of ILS service would be applied to each trace by means of transparent overlays. The 2σ boundaries must then not be exceeded more than 5 percent of the time interval after passage of the outer marker in order that a trace indicate acceptability.</p> <p><i>The original information was filed in the Flight Inspection Standards File.</i></p> <p><i>Excluded from the file.</i></p>			
17. Key Words Instrument Landing System (ILS) Automatic Landing System Flight Control System Flight Inspection Standards		18. Distribution Statement Document is available to the public through the National Technical Information Service, Springfield, Virginia 22161.	
19. Security Classif. (of this report) Unclassified	20. Security Classif. (of this page) Unclassified	21. No. of Pages 305	22. Price

DN

FOREWORD

The research reported here was accomplished for the United States Department of Transportation by Systems Technology, Inc., Hawthorne, California, under Phase I of Contract DOT-FA74WA-3340. The program was sponsored by the Federal Aviation Administration, (FAA) Systems Research and Development Service, Washington, D. C.

This research, conducted from August 1973 to August 1974, was accomplished under the general direction of Mr. Dunstan Graham at Systems Technology, Inc., and, at the Collins Co., under the direction of Mr. John C. Hall. Mr. John F. Hendrickson served as Technical Officer for the FAA. Valuable guidance throughout the course of this research was provided by Messrs. Henry H. Butts, Richard D. Munnikhuysen and John F. Hendrickson of the FAA.

The authors are especially indebted to Mr. Gerry J. Bierman of the Jet Propulsion Laboratories for sharing his considerable experience in numerical covariance propagation algorithms with them.

The manuscript was released by the authors in June 1975.

TABLE OF CONTENTS

	<u>Page</u>
I. INTRODUCTION AND RATIONALE FOR THE TECHNICAL APPROACH	1
Rationale for the Technical Approach	3
Organization of Report	8
II. OVERALL ILS GLIDE SLOPE SYSTEM PERFORMANCE ANALYSIS	9
Limits of Acceptable Overall System Performance	9
Overall System Performance Model	11
Mathematical Basis for the Overall System Performance Model . .	12
Overall System Performance Analysis	19
Summary of the Procedure for Using the Atmospheric, Aircraft, Flight Control System and Glide Slope Models to Determine Overall System Performance Characteristics . . .	20
Summary of Key Results and Conclusions	24
III. DEVELOPMENT OF REVISED FLIGHT INSPECTION STANDARDS AND PROCEDURES	28
Data Collection	28
Data Processing	31
Data Analysis	34
Numerical Tolerance Values	47
Comparison of Tolerances with Current Standards	59
IV. A REVIEW OF CURRENT FAA AND ICAO STANDARDS	69
Approach and Landing Performance	69
ILS Flight Inspection Standards Review	73
Glide Path Receiver Standards	81
V. CONCLUSIONS	84

APPENDIX A:	ANALYSIS OF THE COLLINS RADIO CO. GLIDE SLOPE DATA..	88
APPENDIX B:	MODELS USED FOR ILS GLIDE SLOPE; WIND, WIND SHEAR AND TURBULENCE; AIRCRAFT; APPROACH COUPLERS AND FLIGHT CONTROL SYSTEM	185
APPENDIX C:	STATISTICAL CHARACTERIZATION OF THE TOUCHDOWN EVENT	224
APPENDIX D:	TRAJECTORIES FOR MEAN AND STANDARD DEVIATION OF SYSTEM RESPONSE VARIABLES	228
APPENDIX E:	AN ALTERNATIVE FILTER SYSTEM FOR GENERATING TYPICAL AIRCRAFT RESPONSES TO GLIDE SLOPE STRUCTURE.	275
REFERENCES:	283

LIST OF FIGURES

1. Block Diagram of the Deterministic Section of the Complete Model	13
2. Block Diagram of the Stochastic Section of the Complete Model	14
3. Airborne Flight Inspection Equipment Configuration	32
4. Block Diagram for Filter System Which Generates Typical Aircraft Indicated Deviation and Actual Path Deviation and Actual Path Deviation Rate Responses	33
5. Tolerances for the η_p Trace for Category II and III ILS Glide Slope Service	45
6. Illustrative Application of Tolerances for the η_p Trace for Category II and III ILS Glide Slope Service	46
7. Comparison of Variation of Estimated Tracking Error with ILS Glide Slope Variation Function	48
8. 2σ Tolerance Level Curves for the Differential Trace	51
9. 2σ Tolerance Level Curves for Typical Aircraft Actual Path Deviation Response.	52
10. 2σ Tolerance Level Curves for Typical Aircraft Actual Path Deviation Rate Response	53
11. 2σ Tolerance Level Curves for Typical Aircraft Indicated Glide Path Deviation Response	54
12. Comparison of Current Structure Standard for Category I with the 2σ Tolerance Level for the Differential Trace	61
13. Comparison of Current Structure Standard for Category II with the 2σ Tolerance Level for the Differential Trace	62
14. Comparison of Current FAA Slope Change/Reversal Standard with the 2σ Tolerance Level for the Typical Aircraft Path Deviation Rate Response for Category I, II, and III	63
15. Comparison of Current FAA Average Path Alignment Standard for Category II with the 3σ Tolerance Level for the Typical Aircraft Path Deviation Response (Filter System No. 1)	64
16. Relation Between Decision Height Window and Maximum Allowable Deviations Above and Below the Glide Slope Beam	70

	<u>Page</u>
A-1. Frequency Points at Which $\hat{\Phi}$ (W, NS, NC, ND) is Evaluated . . .	100
A-2. Normalized Confidence Interval for Estimates of the Mean as a Function of Total Effective Number of Degrees of Freedom.	103
A-3. Normalized Confidence Interval for Variance as a Function of Total Effective Number of Degrees of Freedom.	104
A-4. Lag Windows D_0 and D_1 ; Spectral Windows Q_0 and Q_1 (From Ref. 24)	109
A-5. Estimates of Differential Trace Mean Values.	112
A-6. Estimates of Differential Trace Total Standard Deviation . . .	114
A-7. Estimate for Differential Trace Stationary Power Spectral Density.	116
A-8. Obtaining a Model for $\hat{\sigma}_\eta$	117
A-9. Estimate of Differential Trace Power Spectral Density.	118
B-1. Basic Geometry Determining Ideal O DDM Path and the Far- Field Asymptote.	187
B-2. Wind Profile Associated with 10 Knot Wind at 10 ft Altitude (From Ref. 10).	194
B-3. Scenario for Approach and Landing for System Performance Analysis	198
B-4. Perturbed Coordinates Locating the Aircraft.	199
B-5. Lear-Siegler Automatic Landing System for Convair 880 (Ref. 17).	213
B-6. Inertially Smoothed Glide Slope Deviation.	216
B-7. Flight Director System of Convair 880.	218
B-8. Automatic Coupler and Manual Landing System Model for Piper PA-30.	220
B-9. Autothrottle for Piper PA-30	221
D-1. Mean Responses: CV-880, LSI, Cat I, M	230
D-2. Standard Deviation Responses: CV-880, LSI, Cat I, M	232

	<u>Page</u>
D-3. Mean Responses: CV-880, FD, Cat II, M.	235
D-4. Mean Responses: CV-880, FD, Cat II, M.	237
D-5. Standard Deviation Responses: CV-880, FD, Cat II, M.	239
D-6. Standard Deviation Responses: CV-880, FD, Cat II, M.	242
D-7. Mean Responses: CV-880, LSI, Cat II, III	245
D-8. Mean Responses: CV-880, LSI, Cat II, III	247
D-9. Standard Deviation Responses: CV-880, LSI, Cat II, III	249
D-10. Standard Deviation Responses: CV-880, LSI, Cat II, III	252
D-11. Mean Responses: CV-880, IS, Cat II, III.	253
D-12. Mean Responses: CV-880, IS, Cat II, III.	257
D-13. Standard Deviation Responses: CV-880, IS, Cat II, III.	259
D-14. Standard Deviation Responses: CV-880, IS, Cat II, III.	262
D-15. Mean Responses: PA-30, Invented, Cat II, M	265
D-16. Mean Responses: PA-30, Invented, Cat II, M	267
D-17. Standard Deviation Responses: PA-30, Invented, Cat II, M . . .	269
D-18. Standard Deviation Responses: PA-30, Invented, Cat II, M . . .	272
E-1. Block Diagram for Alternative Filter System which Generates Typical Aircraft Indicated Deviation, Actual Path Deviation and Actual Path Deviation Rate Responses (Filter System No. 2).	276
E-2. 2 σ Tolerance Level Curves for Typical Aircraft Actual Path Deviation Response (Filter System No. 2).	277
E-3. 2 σ Tolerance Level Curves for Typical Aircraft Actual Path Deviation Rate Response (Filter System No. 2)	278
E-4. 2 σ Tolerance Level Curves for Typical Aircraft Indicated Glide Path Deviation Response (Filter System No. 2)	279
E-5. Comparison of Current FAA Slope Change Reversal Standard with the 2 σ Tolerance Level for the Typical Aircraft Path Deviation Rate Response for Cat I, II and III (Filter System No. 2) . . .	281
E-6. Comparison of Current FAA Average Path Alignment Standard for Cat II with the 3 σ Tolerance Level for the Typical Aircraft Path Deviation Response (Filter System No. 2)	282

LIST OF TABLES

	<u>Page</u>
1. Representative Limits on Acceptable Glide Slope System Performance	10
2. Critical Levels for Overall System Performance Metrics	19
3. Simulation Results Summary	25
4. Flight Inspection Check List Items for which Data Processing is Recommended	35
5. Guide to Corresponding Check List Items for the Current and Revised Glide Path Flight Inspection Data Analysis	39
6. Estimated Bounds on Dynamic Tracking Error in Elevation	49
7. Overall ILS Glide Slope System Performance Requirements	71
8. ICAO and FAA Definitions Used in Connection with Glide Slope Standards	74
9. Salient Glide Path Standards for the Signal in Space, (Ref. 4 and 5)	78
10. Summary of Recent Changes on Category II ILS Glide Path Tolerances Resulting from Change Order 8240.29 (Ref. 21)	82
11. Salient Airborne Glide Path Receiver Standards	83

ABBREVIATIONS, SYMBOLS AND
SPECIAL NOTATION

ABBREVIATIONS

DDM	Difference in depth of modulation
FAA	Federal Aviation Administration
ICAO	International Civil Aviation Organization
ILS	Instrument Landing System
ILS Point "A"	An imaginary point on the glide path/localizer course measured along the runway centerline extended, in the approach direction, 4 nautical miles from the runway threshold
ILS Point "B"	An imaginary point on the glide path/localizer course measured along the runway centerline extended, in the approach direction, 3500 feet from the runway threshold
ILS Point "C"	A point through which the downward extended straight portion of the glide path (at the commissioned angle) passes at a height of 100 feet above the horizontal plane containing the runway threshold
ILS Approach Zone 1	The distance from the coverage limit of the localizer/glide path to Point "A" (four miles from the runway threshold)
ILS Approach Zone 2	The distance from Point "A" to Point "B"
ILS Approach Zone 3	The distance from Point "B" to Point "C" for evaluations of Category I and Category II training systems. The distance from Point "B" to the runway threshold for evaluations of Category II operational systems
PHT	Typical aircraft path absolute altitude at runway threshold
RTCA	Radio Technical Commission for Aeronautics
RTT	Radio telemetering theodolite
TCH	Threshold crossing height

TRS Theodolite recording system

SYMBOLS

a_z or AZ	Normal acceleration measured along the z body axis of the aircraft at the center of gravity	ft/sec ²
A_o	Nominal effective altitude difference between the glide path receiver antenna and the lowest point on the landing gear with the aircraft in landing attitude	ft
b	Wing span	ft
c	Elevation of the ideal 0 DDM surface above the antenna mast base	ft
\bar{c}	Mean aerodynamic chord	ft
CRF, CSF, CTF	Factors used to scale magnitude of wind and wind shear, ILS Glide Slope alignment error and structure, and turbulence	
d or D	Actual glide path deviation in linear units	ft
\bar{d}_c	Distance between the ideal 0 DDM locus for the commissioned angle from the straight-line asymptote as measured in the vertical plane containing the runway centerline, measured normal to the straight-line asymptote	ft
d_e or DE	Indicated glide path deviation in linear units	ft
D	Total aircraft drag	lbs
e	Base of natural logarithm, 2.718 . . .	
f	Cyclic frequency, $\omega/(2\pi)$	Hz
F	Gaussian probability distribution function	
g	Gravitational acceleration, 32.16	ft/sec ²
\hat{G}	Smoothed, and frequency averaged power spectral density estimate for prewhitened ILS Glide Slope record ensemble	$\mu A^2/Hz$
h^*	Total altitude of aircraft center of gravity above GPIF on runway	ft
\dot{h}_e	Low-pass filtered rate of climb error	ft/sec

h_{ocg}	Aircraft center of gravity altitude with respect to GPIF at touchdown	ft
H	Total altitude of aircraft above GPIF on runway	ft
\dot{H} or HD	Actual rate of climb	ft/sec
H_1	Trim component of H	ft
H_2 or $H2$	Perturbation component of H	ft
i, i', i''	Record sample index	
I_y	Pitch moment of inertia	slug-ft ²
k	Discrete frequency index	
K	Aerodynamic ground effect proximity function	
K_0	Constant, 12278., converting Glide Slope displacement in radian units to microampere units	$\mu A/rad$
K_1	Course softening gain function	
K_2	Flare multiplier gain	
K_{sz}	Normal acceleration gain	rad/(ft/sec ²)
K_{ASC}	Airspeed command to autothrottle	ft/sec
K_{GSI}	Glide Slope coupler integrator gain	1/sec
K_h	Instantaneous vertical speed gain	rad/(ft/sec)
K_{IAS} or K_u	Airspeed gain in autothrottle	volts/(ft/sec)
K_{Iu}	Integral of airspeed error feedback gain in autothrottle	lbs/ft
K_s	Effective servo and elevator gain	
K_T	Gain for thrust response to jet engine power command	lbs/volt
K_{T_θ} or K_{θ}	Pitch attitude gain in autothrottle	volts/rad
K_w	Mean wind altitude profile function	

K_x	Range variation signature function for ILS Glide Slope structure	
K_θ or K_q	Pitch damper gain	sec
K_U	Glide Slope coupler gain	(ft/sec)/ μ A
L	Total aircraft lift	lbs
L_1	Characteristic length in ILS Glide Slope structure standard deviation range variation	ft
L_u	Characteristic length for longitudinal gusts	ft
L_w	Characteristic length for normal gusts	ft
L_η	Characteristic length of ILS Glide Slope structure	ft
m	Aircraft mass, or mean for prewhitened ILS Glide Slope record segment	slugs or μ A
M	Pitching moment applied to aircraft	ft-lbs
M_q	$(1/I_y)(\partial M/\partial q)$	1/sec
M_u	$(1/I_y)(\partial M/\partial u)$	1/sec
M_w	$(1/I_y)(\partial M/\partial w)$	1/sec
$M_{\dot{w}}$	$(1/I_y)(\partial M/\partial \dot{w})$	1/ft
M_δ	$(1/I_y)(\partial M/\partial \delta)$	1/sec ²
NC	ILS Glide Slope record segment center time	sec
NND or N	Number of ensemble members	
NS	ILS Glide Slope record segment length	sec
NTS	Number of points in the average over frequency	
p	Effective pedestal height of the runway	ft
P	Probability of event designated by argument or subscripts	
q or Q	Pitching component of aircraft angular velocity	rad/sec
Q_1	Effective spectral window in the frequency domain corresponding to a rectangular data window	

r	Ratio $\sigma_{\eta_{RTT_{dyn}}} / \sigma_{\eta_{r_{dyn}}}$	
R	Range from base of ILS Glide Slope antenna mast to center of gravity for the approaching aircraft	ft
\hat{R}	Double-sided raw power spectral density estimate for prewhitened ILS Glide Slope record ensemble	$\mu A^2/Hz$
s	Laplace transform variable	rad/sec
S	Wing area	ft^2
S_u	Switch function on airspeed feedback	
S_η	Switch function on ILS Glide Slope structure inputs	
S_θ	Switch function on pitch attitude feedback	
t	Time	sec
$t_{K;\alpha}$	Value of t in the student t -distribution corresponding to the 100 α percentile for K degrees of freedom	
T	Specific time interval length in local context	sec
T_o	Trimmed engine thrust	lbs
u	Longitudinal (x) component of perturbed translational velocity of aircraft	ft/sec
u'	Low-pass filtered u_{AS}	ft/sec
u''	Time integral of scaled u'	ft
u_A	Longitudinal component of the deterministic atmospheric disturbance environment	ft/sec
u_{AS} or UAS	Airspeed perturbation from trim	ft/sec
\hat{u}_{AS}	Airspeed perturbation from trim, exclusive of turbulence	ft/sec
u_g	Longitudinal gust velocity component	ft/sec
u_w	Horizontal longitudinal wind component	ft/sec
U_o^*	x Body axis component of trimmed inertial velocity in presence of steady wind	ft/sec
V'	Equalized jet engine power command	volts

V_{A_0}	Trimmed airspeed	ft/sec
V_{HW_0}	Initial value of the mean wind, \bar{u}_w	ft/sec
$V_{T_0}^*$	Trim speed in presence of steady wind	ft/sec
w	Normal (z) component of perturbed translational aircraft velocity	ft/sec
w_g	Normal gust velocity component	ft/sec
w_A	Normal component of the deterministic atmospheric disturbance environment	ft/sec
W_e or W_E	Effective statistical bandwidth of a random process	rad/sec
W_{min}	Minimum main gear wheel threshold clearance in normal operation	ft
W_0^*	z Body axis component of trimmed inertial velocity in presence of steady wind	ft/sec
x_1, y_1, z_1	Coordinates of base of ILS Glide Slope antenna mast with respect to the GPIF on the runway	ft
x_t, y_t, z_t	Coordinates of the runway centerline at the threshold with respect to the GPIF on the runway	ft
X	Total horizontal displacement of aircraft center of gravity from GPIF on the runway in the direction of the centerline, or longitudinal force applied to aircraft	ft or lbs
X_1	Trim component of X	ft
X_2 or X_2	Perturbation component of X	ft
X_u	$(1/m)(\partial X/\partial u)$	1/sec
X_w	$(1/m)(\partial X/\partial w)$	1/sec
X_δ	$(1/m)(\partial X/\partial \delta)$	ft/sec ²
z_j	Thrust line offset with respect to aircraft center of gravity	ft
Z	Normal force applied to aircraft	lbs
Z_u	$(1/m)(\partial Z/\partial u)$	1/sec

Z_w	$(1/m)(\partial Z/\partial w)$	1/sec
Z_δ	$(1/m)(\partial Z/\partial \delta)$	ft/sec ²
α_{A_0}	Trimmed aerodynamic angle of attack in presence of steady wind	rad
β	Complement of the confidence level $1 - \beta$	
γ_{A_0}	Trimmed flight path angle with respect to air mass in steady horizontal translation	rad
γ_0	Trimmed flight path angle	rad
δ	Control variable, used with subscript e or T	
δ_e or DEL E	Elevator deflection angle	rad
δ_T or DEL T	Engine thrust perturbation	lbs
ΔA	Difference between the nominal and actual altitude difference between the glide path receiver antenna and the lowest point on the landing gear for a <u>particular aircraft in landing attitude</u>	ft
Δw_{ge}	Apparent change in aerodynamic plunge velocity arising from ground effect	ft/sec
$\Delta \Theta$	$\Theta_1 - \Theta$	deg
η	Indicated glide path deviation in angular units before low-pass filtering in glide path receiver	μA
η' , η_c or ETAE	Indicated glide path deviation in angular units	μA
η''	Time integral of scaled η'	ft/sec
η_c or ETAC	Intermediate variable in ILS Glide Slope structure model	μA
η_c^*	ILS Glide Slope structure component	μA
η_p or ETAP	Actual glide path deviation in angular units at fixed range	μA
$\dot{\eta}_p$ or ETAPD	Actual glide path deviation rate in angular units	$\mu A/\text{sec}$
η_r or ETAR	Differential trace referenced to the commissioned or desired angle, in angular units	μA

θ or θ_{THETA}	Pitch attitude perturbation	rad
θ'	High-pass or low-pass filtered θ	rad
θ_o^*	Trimmed pitch attitude in presence of steady wind	rad
Θ or Θ_T	Commissioned or desired ILS Glide Slope angle	deg
Θ_1	Actual Glide Slope angle	deg
K	Total effective number of degrees of freedom in an ensemble of N records	
K'	Effective number of degrees of freedom in a single record	
$\hat{\mu}$	Estimate of ensemble mean for corresponding ILS Glide Slope record segments	μA
$\hat{\mu}_r$	Estimated of mean value for a given ILS Glide Slope record segment	μA
$v_{\pm 75}$	Difference between 0 μA reference line and 0 μA reference mark used in applying the tolerance on sensitivity and linearity of the typical aircraft off-path response	μA
ϵ_j	Thrust line inclination with respect to aircraft x body axis	deg
ρ	Probability density function, or correlation coefficient if subscripted	
σ	Denotes one standard deviation in general. May be particularized by subscript	
$\hat{\sigma}_r$	Estimate of standard deviation for a given ILS Glide Slope record segment	μA
$\sigma_{\text{RTT acc}}$	Standard deviation of calibration and resolution error for the RTT	
$\sigma_{\text{RTT dyn}}$	Standard deviation of dynamic tracking error arising from operation of the RTT	
$\sigma_{\text{RX insp}}$	Standard deviation of glide path receiver centering error for inspecting aircraft	μA
$\sigma_{\text{RX op}}$	Standard deviation of glide path receiver centering error for operating aircraft	μA
$\hat{\sigma}_t$	Estimate of ensemble standard deviation for corresponding ILS Glide Slope record segments	μA

$\hat{\sigma}_{\Delta\theta}$	Estimate of standard deviation of ILS Glide Slope alignment error with respect to the commissioned or desired angle	μA
$\hat{\sigma}_{\eta}$	Estimate of standard deviation for ILS Glide Slope structure	μA
$\hat{\sigma}_{\mu_r}$	Estimate of the ensemble standard deviation of the ILS Glide Slope record segment means for corresponding segments	μA
τ_e	Effective servo and elevator time constant	sec
τ_E	Effective engine thrust response time constant	sec
τ_{IV}	Autothrottle lead equalization time constant	sec
τ_R	Glide path receiver time constant	sec
τ_u	Airspeed low-pass filter time constant	sec
τ_{θ}	Pitch attitude high-pass or low-pass filter time constant	sec
Φ	Assumed actual power spectral density for ILS Glide Slope	$\mu A^2/Hz$
$\hat{\Phi}$	Power spectral density estimate for ILS Glide Slope record ensemble	$\mu A^2/Hz$
$\chi^2_{K;\alpha}$	Value of χ^2 in the χ^2 -distribution corresponding to to the 100 α percentile for K degrees of freedom	
ω or W	Angular frequency	rad/sec
ω_{RC}	Rate of climb response bandwidth for typical aircraft	rad/sec

MATRIX AND VECTOR SYMBOLS

A	System matrix
B	Input distribution matrix
C	Covariance matrix for x
D	Covariance matrix for y
\dot{G}	Input-to-output distribution matrix

H	State-to-output distribution matrix
n	Dimension of the state vector x
Q	Power spectral density matrix for w
u	Input vector
w	Process noise vector
x	State vector
y	Output vector
y_0	Constant term in output vector
y_1	Linearly time dependent term in output vector

SPECIAL NOTATION

$E[.]$	Expected value of $[.]$
$(\cdot)_{TD}$	Touchdown-related value of (\cdot)
$(\hat{\cdot})$	Denotes estimate of (\cdot)
$(\bar{\cdot})$	Denotes mean or expected value of (\cdot)
$(\dot{\cdot})$	Derivative with respect to time of (\cdot)
$(\cdot)'$	Transpose of matrix (\cdot)
$ (\cdot) $	Absolute value of scalar quantity (\cdot) , or determinant of square matrix (\cdot)
$(\cdot)_{max}$	Maximum allowable value for (\cdot)
$(\cdot)_{min}$	Minimum allowable value for (\cdot)

METRIC CONVERSION FACTORS

Approximate Conversions to Metric Measures

Symbol	When You Know	Multiply by	To Find	Symbol
LENGTH				
in	inches	2.5	centimeters	cm
ft	feet	30	centimeters	cm
yd	yards	0.9	meters	m
mi	miles	1.6	kilometers	km
AREA				
m ²	square inches	6.5	square centimeters	cm ²
ft ²	square feet	0.09	square meters	m ²
yd ²	square yards	0.8	square meters	m ²
mi ²	square miles	2.6	square kilometers	km ²
	acres	0.4	hectares	ha
MASS (weight)				
oz	ounces	28	grams	g
lb	pounds	0.45	kilograms	kg
	short tons (2000 lb)	0.9	tonnes	t
VOLUME				
tap	teaspoons	5	milliliters	ml
Tabsp	tablespoons	15	milliliters	ml
fl oz	fluid ounces	30	milliliters	ml
c	cups	0.24	liters	l
p	pints	0.47	liters	l
qt	quarts	0.96	liters	l
gal	gallons	3.8	liters	l
ft ³	cubic feet	0.03	cubic meters	m ³
yd ³	cubic yards	0.76	cubic meters	m ³
TEMPERATURE (exact)				
°F	Fahrenheit temperature	5/9 (after subtracting 32)	Celsius temperature	°C

Symbol	When You Know	Multiply by	To Find	Symbol
LENGTH				
mm	millimeters	0.04	inches	in
cm	centimeters	0.4	inches	in
m	meters	3.3	feet	ft
km	kilometers	1.1	miles	mi
		0.6	miles	mi
AREA				
cm ²	square centimeters	0.15	square inches	in ²
m ²	square meters	1.2	square yards	yd ²
km ²	square kilometers	0.4	square miles	mi ²
ha	hectares (10,000 m ²)	2.5	acres	ac
MASS (weight)				
g	grams	0.035	ounces	oz
kg	kilograms	2.2	pounds	lb
t	tonnes (1000 kg)	1.1	short tons	st
VOLUME				
ml	milliliters	0.03	fluid ounces	fl oz
l	liters	2.1	pints	pt
		1.06	quarts	qt
		0.28	gallons	gal
m ³	cubic meters	36	cubic feet	ft ³
		1.3	cubic yards	yd ³
TEMPERATURE (exact)				
°C	Celsius temperature	9/5 (then add 32)	Fahrenheit temperature	°F



* 1 in = 2.54 (exactly). For other exact conversions and more detailed tables, see NBS Mon. Publ. 286, Units of Length and Masses, Price \$2.25, SD Catalog No. C13.10.286.

SECTION I
INTRODUCTION AND RATIONALE FOR
THE TECHNICAL APPROACH

The standard aid to low-visibility approach and landing in commercial aviation is the Instrument Landing System (ILS). Two radio beams (the "Glide Slope" and the "Localizer") are formed to guide an aircraft on the proper approach glide path and along the extended runway centerline in the landing direction. Unfortunately, because of the way in which the beams are formed, the "on-course" signals can be distorted by radio energy reflected by objects such as hangars or by features of the terrain. Some sites for the ILS facilities are problem situations in which the beam "bends" or structure may make the ILS difficult to fly.

In the United States, the Federal Aviation Administration (FAA) has formulated "standards" for the quality of the ILS signals and makes periodic flight inspections of all commissioned ILS facilities to insure that the standards are complied with. Actually, there is not a single set of standards but three, corresponding to three "categories" of aircraft low visibility landing operations. Category I implies instrument flight possibly down to a decision height of 200 ft. The pilot then completes the landing by visual reference to the runway. Category II is similar except that the decision height is 100 ft. In Category III, there is no decision height limitation. The operation is to and along the surface of the runway with external visual reference during the final phase of the landing. Naturally, the standards on the geometry, alignment and structure characteristics of the ILS beams are more stringent and difficult to comply with as one progresses from Category I through Category II to Category III operations.

Because problem situations obtain at many locations, and because of the stringent standards, the rate of commissioning of Category II and especially of Category III facilities has been somewhat disappointing. The difficulties, in many cases, reside in obtaining the proper characteristics for the ILS Glide Slope.

It is also a fact that the standards covering major elements of the

airborne system have not been evolved in a way which assures consistency of those standards with the standards for the ground system, or for that matter, with the standards for the complete approach and landing system. All this suggests that there may be tradeoffs to be made between the ground based and airborne portions of the system, and that, very likely, the requirements embodied in the existing standards might be relaxed at least in certain zones or regions of the approach and landing operation. (This, of course, may only be done with no decrement in safety or pilot acceptance.) If the standards could be relaxed and the efficiency of the inspection procedure improved, many more facilities might be commissioned, and the schedule reliability and safety of airline and business aircraft operations would be improved.

For these reasons, a system analysis to devise new, improved models and standards for quality of Category I, II and III ILS Glide Slope airborne and ground system performance is in order. The conduct of such a system analysis is the object of the research reported herein.

The purpose of the research is for UHF ILS Glide Slopes to:

- Review the existing standards for the ground and airborne portions of approach and landing system performance
- Analyze data on beam geometry, alignment and structure
- Model the system and design and conduct simulation experiments to determine, for large air carrier and business aircraft equipped with a representative number of different airborne systems, standards for Category I, II and III overall approach and landing system performance
- Budget the error allowable within the bounds of acceptable system landing performance among the system elements in order to recommend revised standards for the ground system performance, the airborne system performance, and the overall system performance
- Develop a practical method for the collection of flight inspection data compatible with the analysis technique. ("Practical" may here be interpreted to mean that no large or drastic changes in inspection procedures nor in instrumentation should be required

- Develop a method for the analysis of flight inspection data to determine the suitability of a given ILS Glide Slope facility for Category I, II or III operations

RATIONALE FOR THE TECHNICAL APPROACH

Fortunately, a landing accident is a very rare event. Landing accidents attributable to the poor performance of ILS ground facilities and/or the airborne equipment complement of aircraft using these facilities are even rarer. It is, therefore, extremely difficult to obtain a sufficient number of cases so as to have confidence in the statistics representing the distribution of landing outcomes to be expected with any particular combination of ground facilities, aircraft, airborne system, and operating personnel. Time-consuming and costly flight operations are used in the inspection, test, and certification programs required by the Federal Aviation Administration. These establish, more or less satisfactorily, that a particular combination of facility, aircraft, airborne equipment complement, and operating personnel is safe when looked at as a total system. Flight testing, however, cannot reasonably be used to answer questions such as, "What are the required ILS characteristics?" or, "Can we trade looser tolerances on the ground facility performance for tighter tolerances on the airborne system?" This is because a totally, impractically enormous number of approaches and landings would be required to establish confidence in the association of approach or landing outcomes with changes in the characteristics of the overall system.

On the other hand, dynamic system analysis and simulation presents a feasible alternative. This is because a sophisticated system analysis is fully capable of relating the real-world sensitivity of approach and landing outcomes to the governing characteristics and design parameters of the elements of the system. The results of such an analysis can be used to partition the causes of various undesirable approach and landing outcomes (e.g., missed approaches; and long, short, hard landings) among the contributing imperfections of the ground facility, aircraft dynamic response, airborne system, operating personnel and the meteorological environment. Indeed, such system analyses and simulations have been used in the past to assist in

setting standards for ILS signal quality (Ref. 1, 2 and 3) as well as almost universally in the design of compatible automatic flight control systems, approach couplers, landing systems, flight directors, and auto-throttles.

In part, however, in the past, the setting of standards for ILS signal quality (Ref. 4 and 5) as well as, for example, the recommendation of models representing atmospheric disturbances (Ref. 6) has been functionally and organizationally separated from the determination of the actual criteria to which the airborne equipment complement is designed. The lack of established standards for airborne equipment has allowed the designers of this equipment great latitude in meeting requirements, but the lack of a standard for overall system performance has precluded realistic and practical tradeoffs between ground and airborne system performance. Not only is this the case, but also it is a fact that the last system study used in setting standards for the ground system performance is now ten years old. It concentrated on Category III approaches down to a height of 50 ft. In the meantime, there have been great advances in the technology of computing machinery, computational algorithms, and analytical methods. (These now easily allow us to perform digital simulation, make use of time-varying models and spectral characteristics, and to avoid grossly inefficient Monte Carlo simulation, for example.)

The basic assumption underlying the rationale of our proposed approach, upon whose validity we would suppose that there is widespread agreement, is that dynamic system analysis and simulation may indeed be made to serve the purposes of the research outlined above. Analysis and simulation can be used to establish the critical nature or lack thereof of the many factors involved with approach and landing. In turn, the results can be used to help the FAA in the formulation and recommendation of realistic standards (or subsystem and equipment tolerances) with much higher probabilities of exceedence than are appropriate to accidents. Such standards or tolerances are more easily applied because of the greater observability the higher probability of exceedence provides.

Compatible standards developed following a logical and consistent plan of analysis and simulation would require no more than the number of ILS

inspection and commissioning flights as are used in present practice. On the other hand, the flight inspections would be sufficient to verify with a high confidence that the ground facility is performing within its allotted tolerance, because that tolerance has been deliberately established at a higher level of observational probability, and the relative influence of that tolerance on overall landing system performance would be known. A similar conclusion holds for flight tests, certification flights or other tests required in the application of compatible standards to aircraft, flight control systems or other system elements. It is by appealing to probabilistic observational concepts, analysis and simulation that we may obviate the limitations mentioned at the beginning of this subsection with respect to the enormous number of in-flight approaches and landings which would otherwise be required to evolve a set of compatible system standards.

It is also possible, even in the presence of a number of random disturbances, to obviate the necessity for time-domain simulation of an equivalently enormous number of approaches and landings. This is precisely what we have done by means of simulating the statistics of the system variables in the time domain in distinction to the system variables themselves. The result is a large savings in time and computer costs.

The approach, and its rationale, depend on having, at hand, a unique combination of constituent linearized models and analytical methods. It should be further understood that these models and methods must be complete in the sense that they must include representative aircraft and airborne system characteristics, ILS Glide Slope geometry, alignment and structure* characteristics, a well developed model for atmospheric disturbances at low altitudes,†

*Models for the ILS Glide Slope in terms useful for dynamic system analysis were not altogether adequate for this study at the start of the program. In particular, there were no statistical models for the ILS Glide Slope which accounted for the range dependence of the characteristic parameters. This range dependence is known to be important (e.g., Ref. 8) since typical ILS Glide Slope data fails statistical tests for stationarity. Therefore, a range-varying statistical model was developed in this program so as to overcome the serious limitations of existing models. The range-varying statistical model is based on a nonstationary statistical analysis of flight inspection data from 17 Category II and II-training ILS Glide Slopes (Ref. 9). The nonstationary statistical analysis procedure, results and model are described in Appendix A.

†Models for atmospheric disturbances appropriate to approach and landing are discussed in detail in Ref. 10 and 11, which present a justification for the choice of particular levels and shaping.

and measures of performance, safety and pilot acceptability. These models and methods establish an analytical framework for measuring the interactions among the subsystem elements, disturbance inputs, and the relative influence of changes in the several system elements (especially, the ground facility and airborne system) on the precision of control, pilot acceptance, precision of measurement in the inspection procedures, and available margins of safety.

Confidence in the results from any application of the approach and landing system models, however, will always be in proportion to confidence in the analytical description of the environment in which the airplane and its various subsystems operate. One cannot evolve comprehensive standards and tolerances for the ILS Glide Slope with respect to overall approach and landing system performance standards without characterizing all of the important inputs and disturbances which affect approach and landing success. There are six types of inputs and disturbances encountered during an approach to touchdown which must be considered. These are:

- Steady winds of random magnitude
- Wind shears based upon the steady wind magnitude
- Stochastic atmospheric turbulence
- ILS Glide Slope ideal path shape
- ILS Glide Slope alignment
- ILS Glide Slope structure

All must be considered because measures determining acceptable landing performance (e.g., pilot acceptance of aircraft attitude variability, dimensions of the touchdown footprint, etc.) are the result of a combination of inputs and disturbances. The development of revised standards for the ILS Glide Slope must account for the fact that portions of each of these measures (within levels for the measures which are critical for approach and landing success) must be reserved for the contributions of wind, wind shear and turbulence disturbances. The margin remaining may be used to accommodate the ILS Glide Slope inputs.

The levels of the measures which are critical for approach and landing success have been drawn from sources such as Ref. 1 and 6. While these "critical levels" might be somewhat conservative with respect to, say, a "one-in-ten million" landing accident goal, they do have the virtues of a successful history and of being the result of a consensus on requirements for safe operation. This background for the critical levels tends to assure that if they are in error, it is, indeed, by being conservative.

These critical levels for the measures, taken together, provide the bounds upon overall system performance. The extent to which performance requirements upon the ground system (ILS) and the airborne system may be relaxed while remaining at or within the critical levels for each of the measures is the result sought in this study. This result will provide a basis which may later assist the FAA in revising ILS flight inspection standards and in formulating standards of performance for airborne systems.

An additional aspect of this research is concerned with the conduct of ILS flight inspections and the application of revised flight inspection standards similar to those recommended on the basis of the above study. The revised flight inspection is envisioned to include tolerances upon typical aircraft actual glide path deviation, actual glide path deviation rate and indicated glide path deviation response arising from ILS inputs. These responses are generated by passing the "differential trace" signal from the existing flight inspection equipment through a filter which, in fact, would be a simplified aircraft/control system simulation. Appropriate tolerances may be applied to the filter responses using transparent overlays. (This is in distinction to constructing the tolerance levels on oscillograph records by hand as is currently the practice.) The tolerances are set at 2 σ levels so that the tolerance level may be exceeded for as much as 5 per cent of the record length and still be acceptable. Manual processing of the flight inspection data involving considerable human judgement and some arbitrariness in execution in the current flight inspection data analysis procedure (e.g., construction of the "graphical average path"), is replaced either by the filtering function or by manual determination of whether or not the 5 per cent exceedence criterion is met.

The total effect of this technical approach is to produce tolerances for typical aircraft actual glide path deviation, actual glide path deviation rate,

and indicated glide path deviation responses to ILS Glide Slope inputs which are based upon landing performance for the overall system. Furthermore, these three variables have direct relevance to landing operations (whereas the "differential trace" itself does not). Actual glide path deviation and deviation rate have a strong influence upon conditions at touchdown and hence safety. Indicated glide path deviation is one variable upon which missed approach decisions are based. Hence, that variable governs the practical utility of the ILS Glide Slope guidance. In addition, procedures for applying the tolerances to flight inspection data are suggested here which are simple to execute, and which require less artistry in application.

ORGANIZATION OF THE REPORT

The next Section describes in detail the formulation and results of the overall ILS Glide Slope system performance analysis. That Section is supported by Appendices B and C which give specific equations and numerical parameter values for the ILS Glide Slope, wind and wind shear, turbulence, aircraft, flight control system, and landing event models which were used. Section II is further supported by Appendix D which contains time histories for the mean and standard deviation of several key system variables for the four aircraft/control system combinations investigated.

Section III contains recommendations for revised flight inspection standards and procedures, and presents a comparison of the recommended standards with the current FAA and ICAO flight inspection standards.

Section IV presents a review of standards governing overall system landing performance. This includes the FAA and ICAO flight inspection standards, FAA automatic landing system standards and FAA and RTCA ILS Glide Slope receiver standards.

Section V presents a summary of the conclusions resulting from this investigation.

The nonstationary statistical analysis of 17 Category II and II-training ILS Glide Slope "differential trace" records which led to the analytical ILS Glide Slope structure model used in this study is presented, as has been mentioned, in Appendix A.

SECTION II

OVERALL ILS GLIDE SLOPE SYSTEM PERFORMANCE ANALYSIS

The purpose of this Section is to explain the method for determining the most generous (permissive) tolerances upon ILS Glide Slope beam alignment and structure consistent with acceptable overall system performance. The first concern must necessarily be defining "acceptable overall system performance". This is followed by a description of the actual method for determining the tolerances.

LIMITS OF ACCEPTABLE OVERALL SYSTEM PERFORMANCE

The key to arriving at rational revised standards for ILS Glide Slope beam alignment and structure lies in recognizing what the real or ultimate system performance objectives are. Basically, there are two such objectives:

- Land the aircraft on the runway with a precision adequate for safety
- Regulate the aircraft attitude, airspeed and normal acceleration deviations to levels which are small enough so as to be acceptable to pilots on the basis of confidence and safety

A third performance objective which is "artificial" in that it is the result of operating regulations rather than the survival instinct is:

- Regulate aircraft indicated glide path deviation and airspeed deviation (exclusive of gusts) to meet the Category II approach window requirements when applicable

From more specific statements of these three objectives, all other specifications on overall ILS Glide Slope system performance may be derived. The level of error allowable under these specifications upon the overall system, may then be budgeted among the various ground and airborne subsystems.

Fortunately, more specific statements of these three objectives are available from existing FAA performance requirements (see Table 1), ICAO statements of specification intent, and RTCA standard performance criteria. Furthermore, the first two sources state some of the requirements in terms

TABLE 1
REPRESENTATIVE LIMITS ON ACCEPTABLE
GLIDE SLOPE SYSTEM PERFORMANCE

<u>Item</u>	<u>Objective/Basis</u>	<u>Source</u>
Touchdown Dispersion for All Causes	1500 ft about nominal touchdown point/ 2σ contained interval 200 ft to 2500 ft from threshold	Ref. 6
Aircraft Deviation at 50 ft Arising from Path Bends	± 4 ft/ 2σ	Ref. 4
Aircraft Pitch Attitude Deviation at 50 ft Arising from Path Bends	± 2 deg/ 2σ	Ref. 4
Aircraft Pitch Attitude Deviation Post-Capture to 50 ft from all Causes	± 6 deg/ $3\sigma^*$	Ref. 1
Aircraft Normal Acceleration Post-Capture to 50 ft from all Causes	± 0.5 g/ $3\sigma^*$	Ref. 1
Category II and III Approaches		
Indicated Glide Slope Deviation from all Causes (Larger of)	± 35 μ A or ± 12 ft/ $2\sigma^\dagger$	Ref. 12, 13
Airspeed Deviation from all Causes except Turbulence	± 5 kts/ $2\sigma^\dagger$	Ref. 13

*These are "not to be exceeded" values which, in turn, have been re-interpreted to be 3σ values (i.e., a value which would be exceeded less than 0.26 per cent of the time).

† These values must not be exceeded if the approach is to be continued. An upper limit on the missed approach probability (rate), from each cause, of 5 per cent has been used to re-interpret these values as 2σ values.

of a "95 per cent probability basis" or a "2 σ basis". These are equivalent descriptors and they are especially well-suited for use with our analysis method.

OVERALL SYSTEM PERFORMANCE MODEL

The overall system performance model, as its name implies, models system performance in a comprehensive way. The model includes parts representing

- Steady wind and wind shear
- Atmospheric turbulence
- ILS Glide Slope geometry, alignment and structure

inputs, a dynamic model of aircraft response to the above atmospheric inputs and to control inputs obtained from dynamic models of

- Approach coupler response to ILS inputs and aircraft motions
- Flight control system response to aircraft motions and inputs from the approach coupler

Of course, different aircraft models, different approach coupler models and different flight control system dynamic models have been used to investigate, for example, the relative differences in overall system performance for large transport aircraft and business aircraft for approach couplers with and without inertial smoothing, and flight control systems with and without advanced wind and wind shear proofing features.

The complete model is such that it makes the mean value and the variance of every input and response variable available as a function of time (equivalent to a function of range at constant velocity). The complete model has two sections, namely:

- A deterministic section which produces the mean value of every input and response variable
- A stochastic section which produces the covariance matrix* for the input and response variables

*The diagonal elements of the covariance matrix are the variances or σ^2 values of the input and response variables.

Consider next these two sections of the complete model.

Deterministic Section of the Complete Model

The deterministic section is described by the block diagram in Fig. 1. The mean values of variables are denoted by the bars over the variables in this figure. The block diagram indicates that the mean values of the aircraft, flight control system and coupler response are obtained as the result of forcing the model with the mean wind, \bar{u}_w , and the mean glide path, $\bar{\alpha}_c$. The mean glide path, $\bar{\alpha}_c$, is obtained from the geometrical shape of the ideal Glide Slope with respect to its straight-line asymptote. The level of the mean wind, \bar{u}_w , is the average headwind magnitude with respect to active runway landing direction.

The models in the blocks of Fig. 1 will be the dynamic equations describing the particular subsystem. For example, the longitudinal aircraft equations of motion (e.g., Ref. 14 or 15) are the aircraft dynamic model, and so on, for the approach coupler and flight control system dynamic models. The complete details of the models actually used for the ILS Glide Slope; wind, wind shear and turbulence environment; the aircraft; approach couplers and flight control systems, are given in Appendix B.

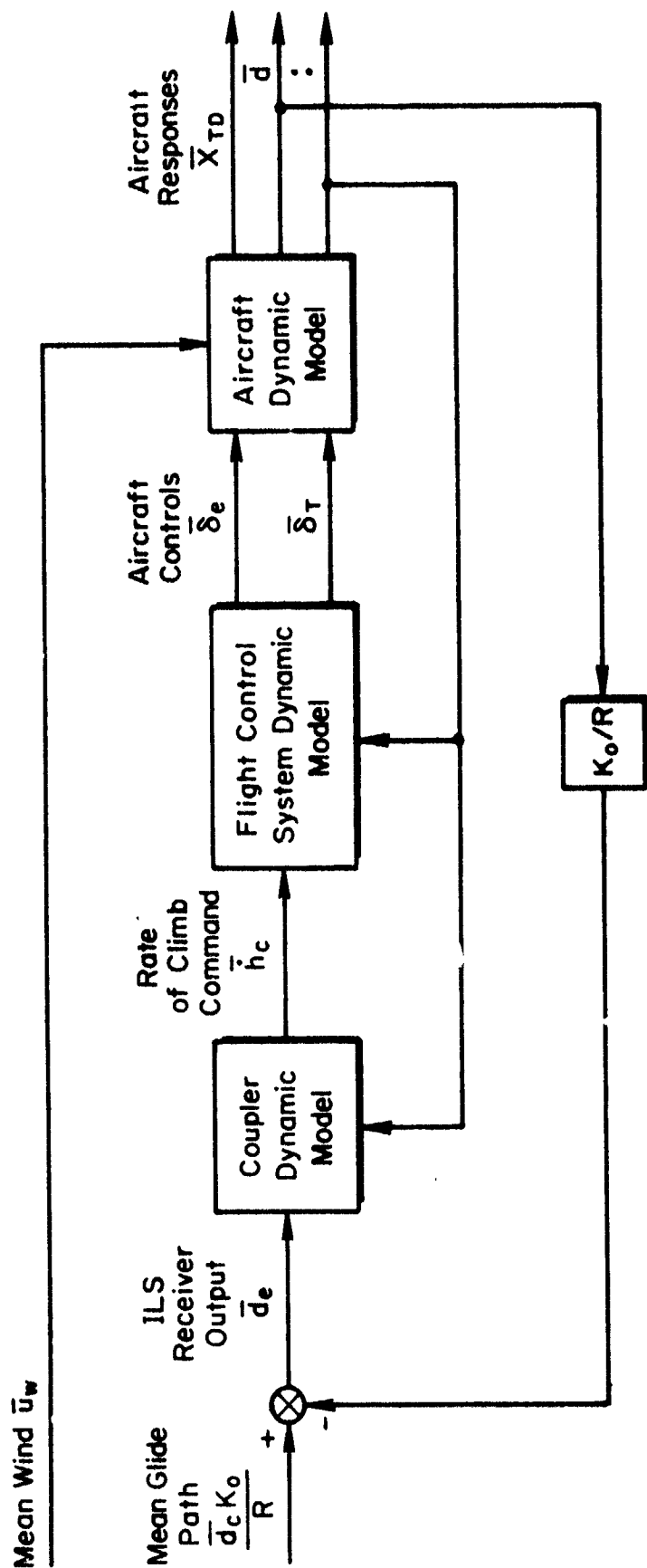
The model shown in Fig. 1 will not be linear in general. However, between Glide Slope capture completion and touchdown an approximate linearized model of the complete system can be shown to be accurate.

Stochastic Section of the Complete Model

The stochastic section of the model is described by the block diagram in Fig. 2. Here the variances of the variables are denoted by σ_i^2 with the particular variable designated by the subscript. The dynamic models of the aircraft, flight control system and approach coupler in Fig. 2 blocks are different from, but are closely related to the corresponding blocks of Fig. 1.

MATHEMATICAL BASIS FOR THE OVERALL SYSTEM PERFORMANCE MODEL

Between Glide Slope capture completion and touchdown, the dynamic models in the blocks of Fig. 1 can be described by linear differential equations. It can be shown that the time histories for the atmospheric and ILS inputs can also be described by linear differential equations (operating upon white noise).



Note: $(\bar{\cdot})$ indicates the mean or average value of (\cdot)

Figure 1. Block Diagram of the Deterministic Section of the Complete Model

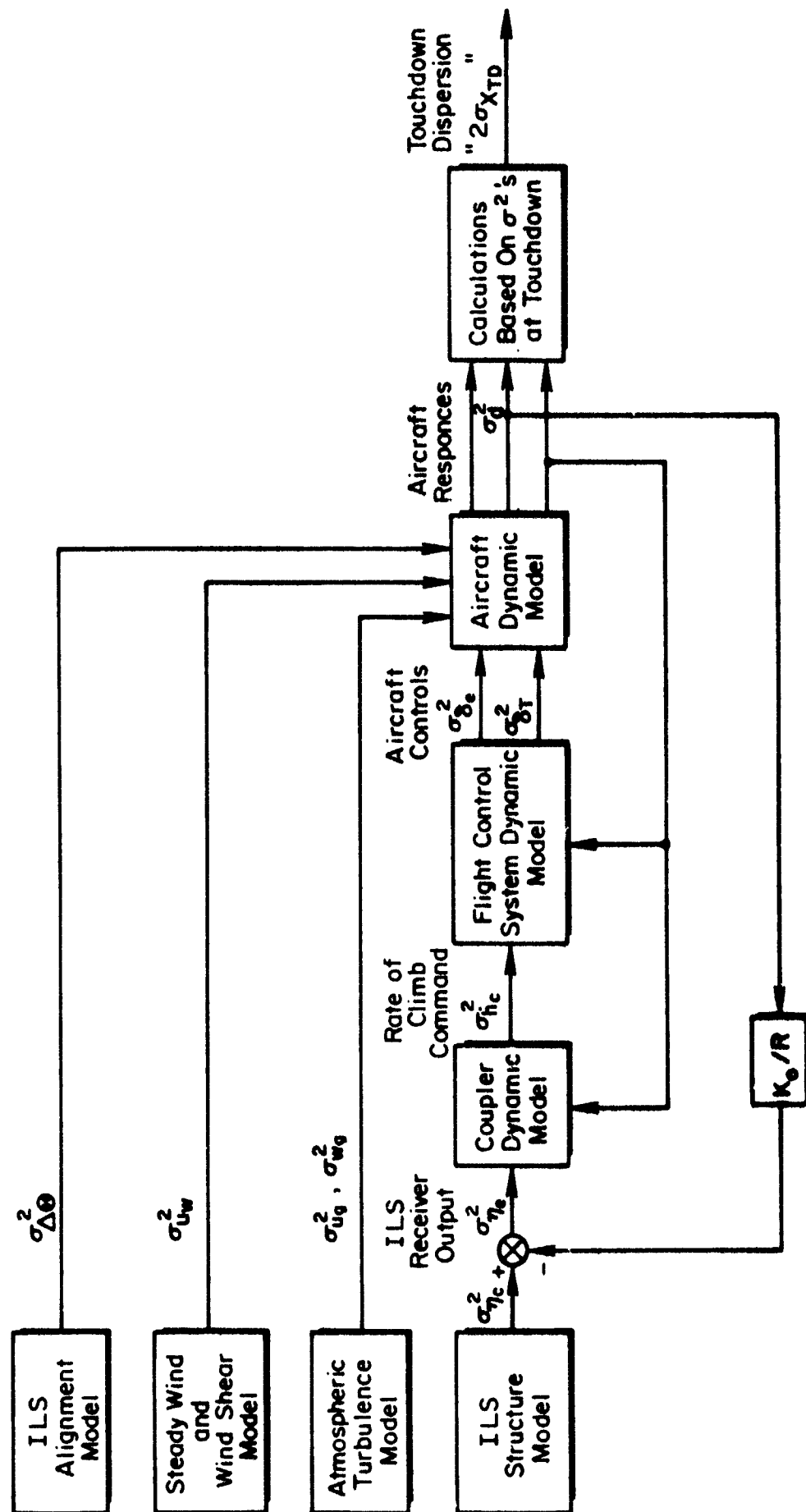


Figure 2. Block Diagram of the Stochastic Section of the Complete Model

When this is the case, the entire system model can be written in the form of a first order vector differential equation and a vector algebraic equation. These are of the form

$$\dot{x} = A(t)x + B(t)u(t) + w(t), \quad x(0) = x_0 \quad (1)$$

$$y = H(t)x + G(t)u(t) + y_0 + y_1 t \quad (2)$$

where $w(t)$ is a vector of independent white noise processes with zero means. If we let $E[\cdot]$ denote the expected value of $[\cdot]$, then define the mean or expected value for x as \bar{x} , the differential and algebraic equations for the mean values are

$$\dot{\bar{x}} = A(t)\bar{x} + B(t)u(t), \quad \bar{x}(0) = \bar{x}_0 \quad (3)$$

$$\bar{y} = H(t)\bar{x} + G(t)u(t) + y_0 + y_1 t \quad (4)$$

given that $E[w] = 0$ and assuming that $E[wu'] = 0$ u is a deterministic input vector. The covariance matrix for x , $E[x(t)x'(t)]$, is C . The differential equations for the covariance matrix are (e.g., Ref. 16):

$$\dot{C} = A(t)C + CA'(t) + Q(t), \quad C(0) = C_0 \quad (5)$$

where $E[w(t)w'(t + \tau)] = Q(t)\delta(\tau)$. The covariance for the output, $E[y(t)y'(t)]$ is D .

$$D = H(t)CH'(t) \quad (6)$$

Now the importance of Eq 3 through 6 derives from the fact that $\bar{x}(t)$ and $C(t)$ completely determine the joint probability density function for $x(t)$ as a function of time.

Namely,

$$\rho(x_1, \dots, x_n, t) = \frac{e^{-(1/2)(x - \bar{x})^T C^{-1} (x - \bar{x})}}{(2\pi)^{n/2} \sqrt{|C|}} \quad (7)$$

where $\rho(x_1, \dots, x_n, t)$ denotes the n-dimensional joint Gaussian probability density function for $x(t)$. $\bar{y}(t)$ and $D(t)$ similarly define the joint probability density function for $y(t)$. And, of course, $x_1, x_2 \dots$ and $y_1, y_2 \dots$ can be used to represent all of the overall system variables in the problem of interest to us here. The above equation for C (Eq 5) and the last equation for D (Eq 6) constitute the whole stochastic section for the complete model shown in Fig. 2 except for the final calculations based upon the values of selected variances at touchdown. This model is "closely related" to the one in Fig. 1 in that the same parameter matrices (which represent aircraft stability derivatives, flight control system and approach coupler gains, etc.) $A(t)$, $B(t)$, $G(t)$ and $H(t)$, characterize the equations for \dot{x} and y as well as the equations for \dot{C} and D .

The final calculation, in which the longitudinal dimension of the touchdown footprint is determined, is based upon the joint probability density function for sink rate ($-\dot{H}$), altitude (H), and longitudinal displacement (X). That is, upon $\rho(-\dot{H}, H, X, t)$. The longitudinal dimensions of the 2σ touchdown footprint is approximately the minimum interval, $(X_{TD2} - X_{TD1})$ satisfying

$$0.9544 = \int_{X_{TD1}}^{X_{TD2}} dX \int_0^{(-\dot{H}_{TD})_{\max}} d(-\dot{H}) \int_{-\infty}^{\infty} dt \left[\frac{\rho(-\dot{H}, H, X, t)}{\rho(H, t)} \right]_{H=0} \rho_{TD}(t)$$

$$\doteq \int_{X_{TD1}}^{X_{TD2}} dX \left[\frac{e^{-1/2 \left(\frac{X - \bar{X}}{\sigma_X \sqrt{1 - \rho_{XH}^2}} \right)^2}}{\sqrt{2\pi} \sigma_X \sqrt{1 - \rho_{XH}^2}} \right]_{\bar{H}=0} \quad (8)$$

where $(-\dot{H}_{TD})_{\max}$ is the maximum allowable sink rate at touchdown which will still result in an acceptable landing. The approximate expression in Eq 8 is developed and justified in Appendix C along with the development for the exact expression. Since the probability density function in the approximate expression is Gaussian:

$$X_{TD_2} - X_{TD_1} = 4 \left[\sigma_X \sqrt{1 - \rho_{XH}^2} \right] \bar{H} = 0 \quad (9)$$

ρ_{XH} is the correlation coefficient for X and H, and σ_X is the standard deviation for X.

An additional important feature of the model is the manner in which decisions to continue an approach or to execute a missed approach are represented. This decision is made at, or prior to, reaching the Category II Decision Height (100 ft) on Category II approaches. We shall assume that missed approaches executed because of inadequate visibility are not of interest. (Missed approaches executed for reasons of inadequate visibility are not the result of inadequate overall system performance capability.) However, missed approaches resulting from inadequate airspeed regulation (exclusive of turbulence effects), inadequate indicated glide path deviation regulation, or both are of interest because they are the result of overall system performance capability.

The missed approach probability (P_{MA}) is determined on the basis of the expected fraction of all approaches which, at the nominal time of reaching the Category II Decision Height (100 ft) are out of tolerance (± 5 kts or ± 8.45 ft/sec) in airspeed regulation (exclusive of turbulence effects), out of tolerance (± 12 ft or $\pm 77.2 \mu A$) in indicated glide path deviation, or both (Ref. 12 and 13). The computation is made using the joint probability density function for airspeed deviation exclusive of turbulence (\tilde{u}_{AS}) and indicated glide path deviation (d_e).

$$P_{MA} = 1 - \int_{-12.}^{12.} d(d_e) \int_{-8.45}^{8.45} d\tilde{u}_{AS} \left[\rho(d\tilde{u}_{AS}, d_e) \right] \bar{H} = 100 \text{ ft} \quad (10)$$

The probability of a missed approach for Category III approaches is also computed on the basis of Eq 10 even though there is no prescribed lower limit for the actual decision altitude (Ref. 13). The possibility of a lower decision altitude for Category III approaches renders the missed approach probability computed by Eq 10 conservative.

In the case of Category I approaches, there are no regulatory tolerances corresponding to those for Category II and III approaches. Consequently, no mechanism exists in our model for producing missed approaches in Category I operations. That is, it is assumed that all Category I approaches are continued to touchdown. This results in the model being somewhat conservative in that computed touchdown dispersions would be expected to be somewhat enlarged with respect to actual touchdown dispersions because, in fact, some Category I approaches may be terminated with missed approach execution for reasons other than inadequate visibility.

Since out-of-tolerance Category II and III approaches are converted to missed approaches at the decision height in our model, there must also be a correction of the joint probability density function for all problem variables at the decision height so that only those approaches which are continued to touchdown are represented. Just prior to the decision height the joint probability density function is

$$\left[\rho(\tilde{u}_{AS}, d_e, x_3, \dots, x_n, t) \right]_{\bar{H} = 100 \text{ ft}}$$

Just after the decision height it is

$$(1 - P_{MA})^{-1} \left[\rho(\tilde{u}_{AS}, d_e, x_3, \dots, x_n, t) \right]_{\bar{H} = 100 \text{ ft}}$$

for $-8.45 \leq \tilde{u}_{AS} \leq 8.45$ and $-12 \leq d_e \leq 12$, and is zero elsewhere.

The joint probability density function just after the decision height is obviously non-Gaussian. In our model this non-Gaussian joint probability density function is approximated by a Gaussian one having the same first and second moments. These first and second moments, i.e., the means and covariance, provide the initial conditions (refer to Eq 7) for continuing the

solution of Eq 3 through 6 from the decision height to touchdown for Category II and III landing operations.

OVERALL SYSTEM PERFORMANCE ANALYSIS

The overall system performance analysis constitutes the exercise of the overall system performance model (for various aircraft/control system combinations and categories of landing operations). The model is exercised repetitively for increasing levels of ILS Glide Slope alignment error and structure until one or more performance metrics reach a critical level. Critical levels used for performance metrics involving pilot acceptance, missed approach probability and touchdown dispersion aspects of overall system performance are given in Table 2.

TABLE 2

CRITICAL LEVELS FOR OVERALL SYSTEM PERFORMANCE METRICS

Pilot Acceptance (during Glide Slope track phase only)

Pitch Attitude: $\sigma_{\theta} \leq 2.0 \text{ deg (0.035 rad)}$

Normal Acceleration: $\sigma_{a_z} \leq 0.167 \text{ g (5.36 ft/sec}^2\text{)}$

Missed Approach Probability: $P_{MA} \leq 0.05$

2 σ Touchdown Footprint Dimension (for touchdowns having sink rates from 0 to 8 ft/sec only)

$$(X_{TD_2} - X_{TD_1}) \leq 1500 \text{ ft}$$

The levels of ILS Glide Slope alignment error and structure which cause one or more of the performance metrics to reach a critical level are the maximum permissible levels for the ILS Glide Slope which, in turn, may be used to recommend revised flight inspection standards.

SUMMARY OF THE PROCEDURE FOR USING THE ATMOSPHERIC, AIRCRAFT, FLIGHT CONTROL SYSTEM AND GLIDE SLOPE MODELS TO DETERMINE OVERALL SYSTEM PERFORMANCE CHARACTERISTICS

This Summary is a concise description of the procedure for determining overall system performance characteristics. This procedure governs the implementation of the material presented in the three previous subsections.

The procedure is described below in terms of steps. Many of these steps are purely computational [designated (C)]. Some steps in computation require user interaction (I) at decision points. Other steps in computation require hard-copy output (O) or the generation of data files for subsequent processing (F). A very few steps are manual (M).

The first stage of the procedure results in selection of an aircraft/control system combination and a category of approach for analysis. Initialization computations are performed, followed by propagation of the mean state vector and covariance matrix to the Category II decision height (or to the runway in the case of Category I approaches). The covariance is propagated in three separate components in this stage. This is done in order that the contributions to the covariance of various groups of inputs which we may wish to scale differently are maintained as separate quantities to permit rescaling without recomputation.

The No. 1 component of the covariance represents the effects of variability of the mean wind from one approach to another. This component is scaled from a nominal value by the parameter, CRF, (see Eq B-17). The No. 2 component of the covariance represents the effects of ILS Glide Slope anomalies. This component is scaled from a nominal value by the parameter, CSF, (see Eq B-6, 7 and 10). The No. 3 component of the covariance represents the effects of stochastic gusts. This component is scaled from a nominal value by the parameter, CTF, (see Eq B-23 and 24). Only CSF is varied in the course of this study. CRF and CTF are taken to be unity throughout.

The second stage of the procedure combines the three component covariances into a single covariance, No. 4, for specific values of CRF, CSF and CTF. Covariance No. 4 plus the mean state defines the probability density function for the state vector at the Category II decision height (or at the runway for Category I). The truncation effects of the Category II approach window are applied to the probability density function if appropriate. The mean state

and covariance after truncation are then propagated to the runway. The 2σ touchdown dispersion is computed from the state probability density function at the runway.

Stage 2 may then be recycled for a new value of CSF until the FAA 2σ dispersion of 1500 ft is matched, or until the missed approach probability or the pilot acceptance metrics, which are also evaluated at the beginning of Stage 2, assume their respective critical values.

The third stage is simply a rerun of the first stage. However, the mean wind variability and stochastic gust effects are ignored; the final value of CSF in Stage 2 is used; and a simplified, typical aircraft/control system model which also represents the filter to be used in the revised flight inspection procedure replaces the detailed aircraft/control system model used in Stages 1 and 2. This rerun is terminated at 50 ft altitude. This rerun also provides the 1σ time history specifications for the ILS Glide Slope beam and typical aircraft response variables against which flight inspection records would be compared under the revised flight inspection procedure. The Stage 3 computations, in effect, serve to calibrate the filter outputs.

Steps in the Procedure

Stage 1. Select the data file for a particular aircraft/control system combination (choose 1 of 4 available).

Select category of ILS Glide Slope service to be investigated (choose Category I, Category II with manual landing, or Category III or Category II with automatic landing.) (I)

Compute the trimmed flight condition. This provides the initial value for the mean of the state vector. (C)

For nominal levels of variability in the mean wind and wind shear, ILS Glide Slope anomalies (using unity for the scale factor parameter, CSF), and stochastic gust disturbances, compute the steady-state covariance matrices for the three corresponding covariance components at the initial value for the mean of the state vector. These provide the initial conditions for the Stage 1 covariance propagation.

Propagate the mean state and covariance components No. 1, No. 2 and No. 3. (C)

Output the mean state and variances. (O)

Output and create a data file for the pilot acceptance variance components No. 1, No. 2, and No. 3 (involving pitch attitude and normal acceleration) for the maximum value of the pitch attitude variance component No. 3 and for the maximum value of the normal acceleration variance component No. 3. (O, F)

Compute, output, and create data file for the mean state, variances, and covariance matrices No. 1, No. 2, and No. 3 at the Category II decision height or at the runway as is appropriate. (C, O, F)

Stop mean state and covariance propagation at Category II decision height for Category II and Category III investigations, or at the runway for Category I investigation. (C)

Stage 2. Select values for CRF, CSF, and CTF. (I)

Compute covariance No. 4 according to

$$C^{(4)} = (CRF)^2 C^{(1)} + (CSF)^2 C^{(2)} + (CTF)^2 C^{(3)}$$

and similarly compute the pilot acceptance variances No. 4 using pilot acceptance variance components No. 1, No. 2, and No. 3. (C)

Output the root-mean-square pitch attitude and normal acceleration pilot acceptance metrics. (O)

* Compute and output the correlation matrix for covariance No. 4 (C, O)

* Compute approximations to the first 4 central moments for the state vector probability density function as truncated by missed approach execution at the Category II decision height. (C)

* Output the first 4 central moments. (O)

* Compute and output the missed approach probability. (C, O)

Steps preceded by () do not apply for Category I approaches.

* Reinitialize the mean state vector and covariance matrix No. 4 using the correlation matrix and the first 2 central moments for the truncated state vector probability density function. (C)

* Propagate the mean state and covariance. (C)

* Output the mean state and variances. (O)

* Stop mean state and covariance propagation at the runway. (C)

* Output and create data file for the mean state, variances, and covariance matrix at the runway. (O, F)

Compute and output the longitudinal dimension of the 2σ touchdown footprint, the mean touchdown point and the mean and standard deviation of sink rate at touchdown. (C, O)

Return to the beginning of Stage 2 and use an increased value for CSF if neither the pilot acceptance measures, the probability of a missed approach, nor the longitudinal touchdown footprint dimension exceeds the critical (2σ) levels. If any one critical level is equalled, stop. If any one tolerance level is exceeded, use a reduced value for CSF. (I)

Stage 3. For the final CSF value of Stage 2, the simplified, typical aircraft/control system model, and with the mean wind and wind shear variability (CRF) and stochastic gusts (CTF) set to zero, repeat the first 6 steps of Stage 1 for the mean state and covariance component No. 2. (I, C, O)

Stop mean state and covariance propagation at 50 ft altitude. (C)

Plot $\pm 2\sqrt{\text{variance}}$ for the ILS Glide Slope beam structure; for indicated aircraft Glide Slope deviation (in μA units); for aircraft deviations from the ideal path (in μA units); and for the rate of aircraft deviations from the ideal path (in $\mu A/\text{sec}$ units). These plots provide the " 2σ " tolerance envelopes which will form part of the suggested revised inspection standards. (M)

The manner in which the plots resulting from the last step above would be used as a standard in flight inspection is described in Section III. Different tolerances (plots) would, of course, be appropriate for each category of ILS service.

Steps preceded by () do not apply for Category I approaches.

SUMMARY OF KEY RESULTS AND CONCLUSIONS

Key results of exercising the overall system performance model are summarized in Table 3. For each aircraft/control system combination, (except the one involving the Piper PA-30) the scale factor amplifying the level of ILS Glide Slope alignment error and structure (CSF in Eq B-6, 7 and 10) was increased until one of the performance metric critical levels was equalled. This produced the critical value of the scale factor. The results in Table 3 are for the critical value of this scale factor.

The Piper PA-30 required special consideration because, for the flight control system and the given disturbance environment, both the probability of missed approach and the longitudinal dimension of the 2σ touchdown footprint exceeded the critical levels given in Table 2 even in the complete absence of ILS Glide Slope alignment error and structure. Furthermore, the ILS contributions to the probability of missed approach and to the longitudinal dimension of the 2σ touchdown footprint are quite small in comparison to the contributions from wind, wind shear and gusts. Since this was found to be the case, we merely evaluated the Piper PA-30 landing performance for the smallest critical value of the scale factor found for the other cases, 1.50. The extent to which the critical level of the 2σ touchdown footprint longitudinal dimension is exceeded is minor, and, in fact, the 1500 ft critical level really only applies for automatic landings while the Piper PA-30 system model is for manual landings. The very high missed approach probability cannot be rationalized away, however. It might be the case that the existing Category II approach window for automatic approaches (± 12 ft, Ref 19) is inappropriate for slow, low wing-loading aircraft such as the Piper PA-30. Nevertheless, the approach window dimension would have to be increased to ± 32 ft in order to lower the probability of missed approach to 0.05. This change in the approach window dimension, if introduced, could then cause a substantial increase in the longitudinal dimension of the 2σ touchdown footprint.

The critical values of the scale factor in the ILS Glide Slope alignment error and structure models (Eq B-6, 7 and 10) are 3.00 for Category I approaches and 1.50 for Category II and III approaches. (The 1.50 will serve also for the 1.53 and 1.58 critical values in Table 3 because the 5 per cent increase over 1.50 does not warrant separate flight inspection

TABLE 3
SIMULATION RESULTS SUMMARY

AIRCRAFT, SYSTEM, CATEGORY	CRITICAL VALUE OF SCALE FACTOR	PROBABILITY OF MISSED APPROACH	STANDARD DEVIATION			MEAN TOUCHDOWN		220 TOUCHDOWN FOOTPRINT DIMENSION (ft)
			PITCH (deg)	NORMAL ACCELERATION (g's)	TOUCHDOWN SINK RATE (ft/sec)	SINK RATE (ft/sec)	LOCATION (ft)	
CV-880 LSI I, M	3.00	NA	2.06 ^c	0.061	0.54	2.76	300.	777.
CV-880 FD II, M	1.50	0.05 ^c	1.31	0.058	0.48	2.50	405.	557.
CV-880 LSI II, III	1.53	0.05 ^c	1.19	0.039	0.40	2.72	518.	629.
CV-880 IS II, III	1.58	0.05 ^c	0.71	0.028	0.39	2.74	487.	454.
PA-30 Invented II, M	1.50	0.47 ^a	1.76	0.037	0.73	3.04	338.	1636 ^a
		(ILS Effects Alone Give Prob. of Missed Approach = .00093)						
CRITICAL VALUE(S)		0.05	2.00	0.17	$p(0 \leq -\frac{H}{TD} \leq 8) \geq 0.95$		30./338.	1500.

- ()^c Denotes Critical Limitation Upon Critical Scale Factor
 ()^a Denotes Critical Limitation in Absence of ILS Glide Slope Alignment Error and Structure
 LSI Lear Seigler Automatic Landing System (Ref. 17)
 FD Flight Director System Using LSI Control Laws
 IS Inertially Smoothed Version of LSI System
 Invented Hypothetical Approach Coupler and Autothrottle System for a Light Twin Aircraft (Ref. 18)
 M Flight Continued Manually by Visual Reference to Ground Below Decision Height

data analysis.)

Identification of these critical levels fulfills a key objective of the study.

Trajectories for the mean and standard deviation of several system response variables of interest have been plotted for all five aircraft/control system combinations listed in Table 3. The plotted results are voluminous and only moderately interesting. These plots form Appendix D to the report.

Conclusions reached as the result of exercising the overall system performance model are as follows:

- Pitch attitude excursions during final approach limit relaxation of ILS Glide Slope standards for jet transport Category I operations
- Landing performance for jet transport Category II operations is similar for automatic or manual flight director approach and landing, and for direct or inertially smoothed coupling to the Glide Slope
- Inertial smoothing gives a reduction in touchdown dispersion
- Manual landing gives a small reduction in touchdown dispersion
- Category II and III requirements upon ILS Glide Slope alignment and structure are identical
- Category II and III approaches which would result in excessive touchdown dispersion are converted to missed approaches at the Category II decision height
- Missed approach probability in excess of 5 per cent limits relaxation of the ILS Glide Slope specification for jet transport Category II and III operations
- Touchdown dispersion limits Category II landing performance for low wing-loading, straight-wing aircraft
- Missed approaches and touchdown dispersion for low wing-loading, straight-wing aircraft are almost entirely from wind, wind shear and gusts

- The existing Category II Glide Slope tracking accuracy requirement is probably inappropriate for low wing-loading, straight-wing aircraft
- ILS Glide Slope beam alignment is critical (for clearance in "low" direction and for sink rate arrest in flare in the "high" direction) for values only beyond those actually investigated

The next Section presents suggestions for revised flight inspection standards and procedures based upon the results of the overall system performance analysis.

SECTION III

DEVELOPMENT OF REVISED FLIGHT INSPECTION STANDARDS AND PROCEDURES

This Section presents recommendations for revisions to flight inspection data collection, processing and analysis. Two separate subsections recommend numerical tolerance values for flight inspection data analysis and compare the recommended numerical tolerance values with the current flight inspection standards.

DATA COLLECTION

Three aspects of the data collection process are affected by recommended changes in flight inspection procedures. These are theodolite placement, generation of an archive data tape and oscillograph records, and the airborne equipment configuration.

Theodolite Placement Recommendation

Specifications for radio telemetering theodolite (RTT) placement in Para. 217.32(2)(a) Ref. 5 are strictly appropriate only for highly idealized runway and ground plane configurations for which the far-field asymptote in the vertical plane containing the runway centerline intersects the runway at a point [the glide path initial point (GPIP)] opposite the Glide Slope antenna mast. An idealized case of practical importance, the so-called "pedestal case," Ref. 20, is not entirely appropriately accommodated by current RTT placement specifications, and neither are idealized cases which may be thought of as a hybrid combination of the two. In the latter two cases, the true GPIP is not opposite the Glide Slope antenna mast, but rather it is offset in the direction of the runway threshold.

The present specification for locating the RTT does not, in general, correctly account for:

- The true GPIP location in consideration of the difference in elevation between the runway and the ground plane at the Glide Slope antenna mast and the ground plane grade angle

- The true location of the idealized 0 difference in depth of modulation (DDM) line in the vertical plane containing the runway centerline

Only the latter item, however, affects the flight inspection procedure.

A recommended revision to the RTT placement specification involves determining the effective elevation above the ground plane at the antenna mast for the origin of an equivalent erect conical reference system*. This effective elevation should be determined as part of the Glide Slope commissioning process. This effective elevation replaces the "difference in elevation between the ground plane at the base of the antenna mast and the center of the runway opposite the mast" in Para. 217.32(2)(a)1 of Ref. 5. In Para. 217.32(2)(a)4, the marker pole setting would be 124 in. (two times the standard theodolite eyepiece height of 62 in.) minus the effective elevation. The steps in positioning the theodolite in Para. 217.32(2)(a) would be otherwise unchanged†.

When the RTT is positioned in this manner, the intersection of its reference surface with the vertical plane containing the runway centerline is nearly identical to the intersection of the idealized 0 DDM surface with that vertical plane, and the asymptotes to these two curves are identical. This procedure is advantageous with respect to the current placement procedure whenever a "pedestal" exists. The effective pedestal elevation results in a constant vertical distance offset between the RTT reference and idealized 0 DDM path when the current placement specification is used. This constant offset can be significant when measured in μA at points close to the runway threshold. A 2 ft effective pedestal elevation results in a 22.8 microamperes (μA) deviation at the runway threshold for example. Elimination of this source of systematic deviation through revision of the RTT placement procedure may make a larger portion of the tolerances available to accommodate other sources of deviation.

*The RTT establishes an erect conical reference system, while on the other hand, the 0 DDM cone is tilted from vertical by the grade angle. The equivalent erect conical reference is equivalent to the ideal 0 DDM cone in the sense that the curves formed at their intersections with a vertical plane through the runway centerline have coincident asymptotes.

†These steps merely serve to shift the origin of the theodolite reference system slightly in order to provide a comfortable eyepiece height (62 in.) for the theodolite operator.

It must be appreciated that the suggested revision in RIT placement procedure will not affect the true location of the GPIP since only the RIT reference is changed. The change will result in displacement of the GPIP implied by the RIT reference system from its current location (the point on the runway centerline opposite the antenna mast). The revised location would be displaced a distance along the runway centerline from the current location. The displacement is in the direction of the runway threshold when the runway is effectively on a pedestal with respect to the ground plane.

A further recommendation is that "permanent" theodolite benchmarks be installed after commissioning (or recommissioning) in order to expedite RIT set-up for ensuing flight inspections. This would reduce the flight inspection workload in a small way, and would eliminate a possible source for human error.

Data Tape and Oscillograph Record Recommendations

It is recommended that all signals which are oscillograph recorded in the current flight inspection process plus barometric altitude be recorded on magnetic tape as part of the theodolite recording system (TRS). The magnetic tapes could be recorded in FM or digital formats. Digital format is recommended for ease in labelling individual data records on the tape, and for the opportunity afforded for further data processing beyond the requirements for specific flight inspections. If a digital format is used, continuous signals should be sampled at a rate of at least 10/sec. The magnetic tape recordings should be the primary data record.

Oscillograph records are required for the application of tolerances to the signals in the revised flight inspection procedure. These oscillograph records may be produced on-line during inspection flights, or off-line using data previously tape recorded. Duplicate oscillograph records may be obtained off-line in this manner.

The advantages of these recommendations are:

- No new oscillograph recording capability will be required. The channel capacity of the existing oscillographs will be sufficient together with the off-line capability provided by the magnetic tape records

- The magnetic tape will provide a compact permanent record of the basic inspection data which is in a form that may be readily subjected to more extensive analysis should additional investigative or research needs arise

Recommended Airborne Equipment Configuration

The recommended configuration for the airborne equipment is shown in Fig. 3. Additional equipment required beyond that presently installed for flight inspection includes analog-to-digital and digital-to-analog converters, digital tape write and read capability, the filter system, and a precision barometric altimeter. The details of the filter system are presented in the following subsection.

The recommended configuration is only one of several possible alternatives. (For example, digital-to-analog conversion could be omitted if all channels could be oscillograph recorded simultaneously on-line during the inspection flight. The ability to produce duplicate oscillograph records in the field would be sacrificed however.)

It is strongly recommended that the entire process of producing magnetic tape and oscillograph records be under the direction and control of the flight inspection engineer in the field. Specifically, it is recommended that no equipment configuration be adopted which requires that responsibility be delegated to personnel at remote facilities for data processing.

DATA PROCESSING

Data Processing requirements in the recommended procedure are modest. In addition to forming the difference between the receiver and theodolite signals as in the present theodolite recording system, a filter system is required to generate typical aircraft glide path indicated deviation and actual path deviation and actual path deviation rate responses. The inputs to the filter system are barometric altitude with respect to the runway elevation at GPIP, the difference between the receiver and theodolite signals and the commissioned angle. A block diagram for the filter system is shown in Fig. 4. A similar alternative filter system is given in Appendix E.

It is anticipated that the commissioned angle, Θ , in Fig. 4 would be hand-set on a ganged potentiometer. Barometric altitude, H , might be obtained as an electrical signal from the inspecting aircraft's air data system, but a

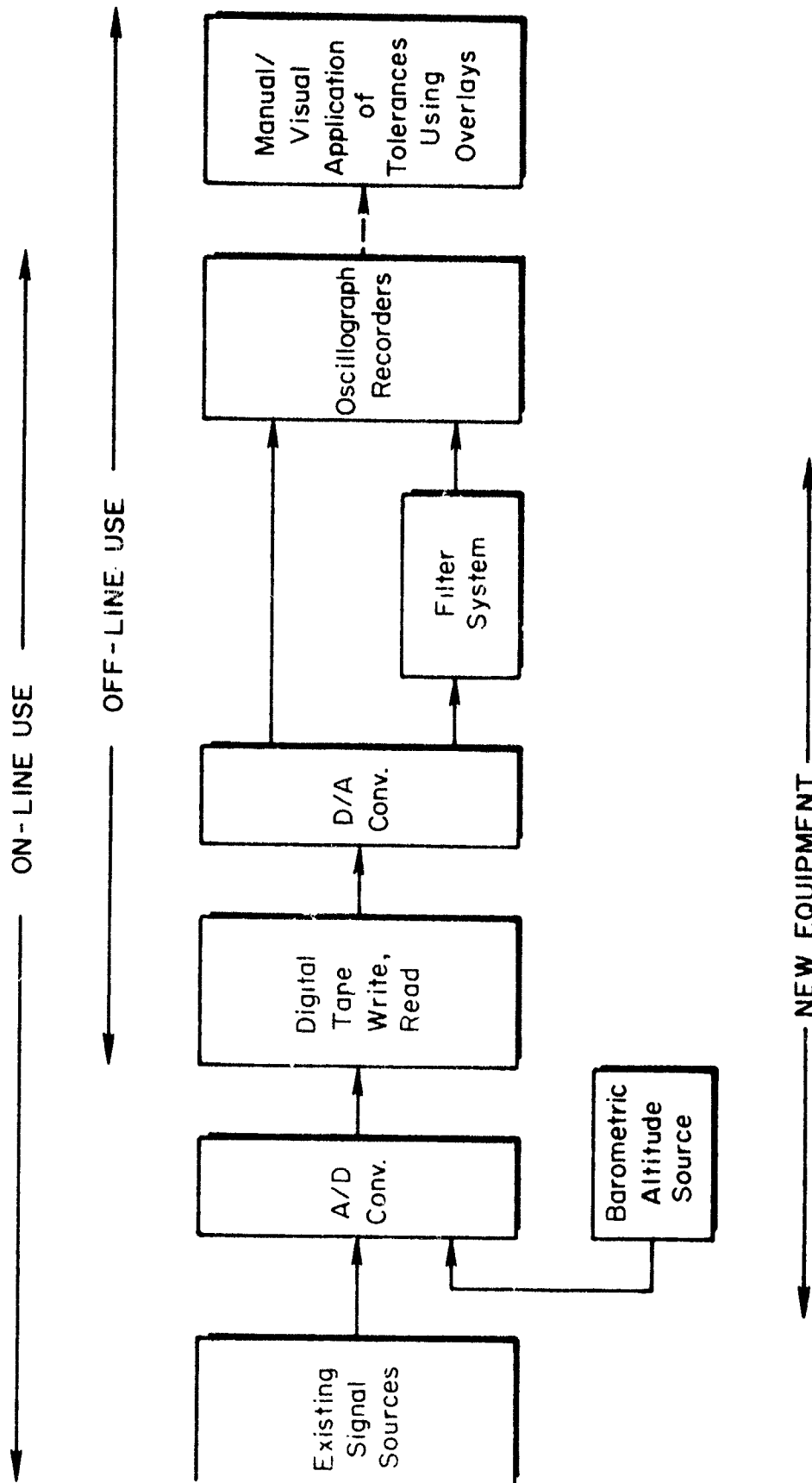


Figure 3. Airborne Flight Inspection Equipment Configuration

ω_{RC} Typical aircraft rate of climb
 response bandwidth, 0.2 (rad/sec)

K_0 Conversion constant 12,278. ($\mu A/rad$)

K_1 Course softening gain function, $K_1 = 1.0$,
 $H \approx 600$ ft; decreasing linearly to zero at
 $H = 0$; $K_1 = 0$, $H \approx 0$ ft

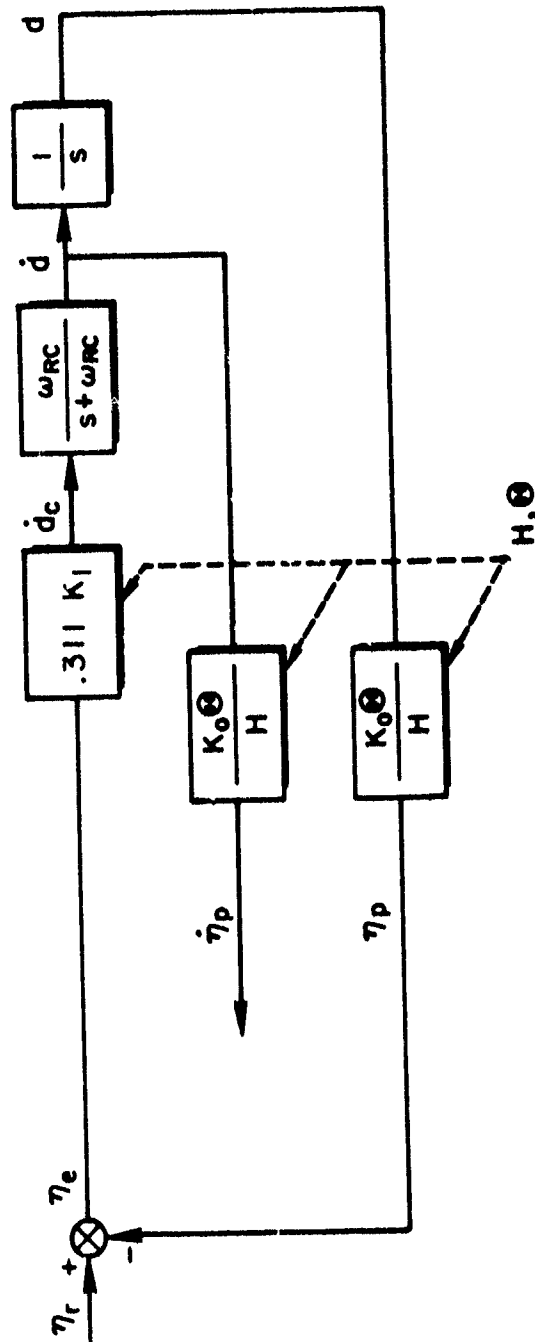


Figure 4. Block Diagram for Filter System Which Generates Typical Aircraft Indicated Deviation and Actual Path Deviation and Actual Path Deviation Rate Responses (Filter System No. 1)

separate precision barometric altimetry system dedicated to the flight inspection function is more desirable.

The filter system itself might be implemented on a small, general purpose analog computer or a special purpose analog computer depending upon the relative costs and the number of installations required. Notice that three integrators, two divisions and one multiplication and some logic (for K_1) are required as a minimum for implementation using general purpose analog elements.

The role of the filter system is three-fold in that it:

- Substitutes data processing for that part of the current inspection workload devoted to determining average path angle, width, structure and changes/reversals in slope
- Provides conditioned signals which are similar to the indicated deviation and actual path deviation and actual path deviation rate responses of aircraft that will use the ILS facility
- Improves the confidence level in the results of flight inspection in that the variables to which the tolerances are applied are directly relevant to landing success

DATA ANALYSIS

The proposed revisions to the data analysis procedure presented below have been formulated to emphasize application of rational tolerances to filtered flight inspection measurements which have direct operational relevance to the successful completion of landings. The revised procedure includes application of tolerances to all features of the ILS beam which are checked under the current procedure. Table 4 has been constructed to identify features receiving analysis under the current procedure which will be aided by data processing (filtering) under the recommended revised procedure.

The filtered flight inspection measurements have operational relevance because the filter used is, in fact, a simplified simulation of an aircraft and Glide Slope coupler. Variables within the filter are simulations of indicated glide path deviation, actual glide path deviation and actual glide path deviation rate. Each of these responses to the ILS Glide Slope guidance affects the landing approach outcome in a key way. Indicated glide path deviation is the primary source of aircraft Glide Slope tracking accuracy for

TABLE 4

FLIGHT INSPECTION CHECK LIST ITEMS
FOR WHICH DATA PROCESSING IS RECOMMENDED

<u>Glide Path Check List Item</u>	<u>Approach Zone 2</u>	<u>Approach Zones 1 and 3</u>
Angle	"Actual Glide Path Angle" is an arithmetic mean angle of all deviations of the differential output of the TRS.* A stationary mean is assumed, but no test for stationarity is presently applied. Data processing which will allow inferential determination of mean deviations is recommended.	"Graphical Average Path Angle" is described by a curved line drawn visually through the mean of short term deviations in the differential output of the TRS and which line follows long term trends (1500 ft or more). Non-stationarity is assumed. Data processing which will allow inferential determination of mean deviations is recommended.
Threshold Crossing Height	The height of a straight line extension of the trend of the graphical average path at ILS Point C to the runway threshold. Data processing is recommended to determine the path response for a typical aircraft at the threshold.	
Change/ Reversal in Slope of the Path	Visual inspection of the differential output of the TRS for changes and/or reversals in the trend of the slope of the path record which extend for at least 1500 ft on one side of the change or reversal. Data processing to expose slope changes/reversals is recommended.	Same procedure and same recommendation as for Zone 2

*Thecdolite recording system

TABLE 4 (CONCLUDED)

<u>Glide Path Check List Item</u>	<u>Approach Zone 2</u>	<u>Approach Zones 1 and 3</u>
Structure	2 σ variability tolerances are applied visually about the "Actual Glide Path Angle." Non-stationary variability is assumed. Data processing is recommended to separate the structure into parts producing aircraft path response and indicated path deviation response with separate tolerances for each part.	2 σ variability tolerances in Zones 1 and 3 are applied visually about the "Graphical Average Path Angle." Otherwise present procedure is the same as for Zone 2 and recommendations are the same as listed for Zone 2.
Sensitivity (Path Width)	"Mean Width" is the difference between the "Actual $\pm 75\mu A$ Path Angles," which are arithmetic means of all deviations of the differential output of the TRS. (Same recommendations apply as are cited for Angle above.)	Only level flight checks are prescribed. Computation of two vertical angles does not warrant data processing.
Symmetry of Path Width	"Mean Width" must be distributed within fixed percentages above and below the "on-path" position. Data processing is recommended for computation of averaged deviations from "Actual $\pm 75\mu A$ Path Angles."	

the pilot. This indication has a major influence upon the missed approach decision. Actual glide path deviation and deviation rate have been shown to make the principal ILS Glide Slope related contributions to longitudinal touchdown dispersion in Section III of Ref. 7. Longitudinal touchdown dispersion together with sink rate at touchdown are the principal determinants of landing success insofar as the longitudinal degrees of freedom of the problem are concerned.

The practice of applying separate tolerances* to operationally significant variables will tend to reduce the number of ILS Glide Slope facilities which do not meet the existing standards but which are nevertheless judged "flyable" by experienced pilots. This will be the result of having made the tolerances more pointed with respect to operationally relevant variables rather than by any unwarranted relaxation of standards presently applied to less relevant variables. The effect on the flight inspection process will be to eliminate restrictions on those features of the ILS Glide Slope guidance signal which do not affect approach and landing success.

The "rational" characteristic of the newly developed tolerances arises not only from the fact that these tolerances will be applied to operationally relevant variables, but also from the fact that these tolerances are based upon exceedences of 2σ levels. The 2σ levels have a much higher observational probability of exceedence than do the levels (say, $n\sigma$) which result in landing accidents. However, by applying the 2σ tolerance level (which is easily applied and gives a high confidence verification of facility acceptability) the required safety margin is implicitly preserved since both the tolerance level and the safety requirement are proportional to σ .

The current procedure makes use of a zone concept in applying standards. This is largely to facilitate construction of the limits directly upon the oscillograph records. The revised procedure does not make use of the zone concept (although the designated ILS Points remain useful). Under the revised procedure the tolerances are to be applied to the oscillograph records using transparent overlays.

*"Tolerances" will be used to denote limits developed as the result of this research. The term "standards" will be used to denote the existing flight inspection standards. Hopefully, the newly developed tolerances will form the basis for revised flight inspection standards.

The following subsections present the revised procedures for applying the newly developed tolerances to the flight inspection records. Since the revised analysis procedure applies tolerances to inspection record features which do not have a one-to-one correspondence with the features examined in the current analysis procedure, Table 5 has been provided as a guide to the correspondence of items in the two inspection check lists.

Tolerance on Actual Path Angle and Typical Aircraft Path Response

Two tolerances are actually applied in this part of the analysis. One is upon the alignment of the actual path with the commissioned angle or desired path. The second tolerance is upon the typical aircraft path deviation response induced by long wave length bends. The inspection record to which these tolerances are applied is the η_p trace.

The overlay providing the $\pm 2\sigma$ limits for the η_p trace and the actual path alignment limits appropriate to the category of ILS service (I, II, III) is selected and placed over the η_p trace with the runway threshold markings in alignment. The overlay is then shifted in the $\pm \mu A$ direction in such a manner as to center the η_p trace within the $\pm 2\sigma$ limits (or in such a manner as to equalize the total time that the $+2\sigma$ limit and -2σ limit are each exceeded). The $0 \mu A$ line of the η_p oscillograph record must lie between the actual path alignment limits indicated on the overlay. The total $+2\sigma$ level exceedence time for the η_p oscillograph trace must not exceed 2.5 percent of the total record time for the interval from the outer marker to ILS Point C for Category I service, or to the runway threshold for Category II and Category III services. Similarly, the total -2σ level exceedence time must not exceed 2.5 percent of the same total record time.

If the $0 \mu A$ line of the η_p oscillograph record does not lie between the actual path alignment limits, then the Glide Slope alignment to the commissioned or desired angle is deficient. If either or both of the 2σ level exceedence times exceeds 2.5 percent of the total record time, then the long wave length bends are excessive as indicated by the typical aircraft path response trace, η_p .

TABLE 5

GUIDE TO CORRESPONDING CHECK LIST ITEMS
FOR THE CURRENT AND REVISED GLIDE PATH
FLIGHT INSPECTION DATA ANALYSIS

<u>Current Glide Path Check List Item</u>	<u>Revised Glide Path Check List Item</u>
Angle	Angle (and typical aircraft path deviation response)
Threshold crossing height	Typical aircraft path absolute altitude at runway threshold (PHT)
Change/reversal in slope of the path	Typical aircraft path deviation rate response
Structure	(Angle and) typical aircraft path deviation response Typical aircraft indicated glide path deviation
Sensitivity (path width) Symmetry of path width distribution	Sensitivity and linearity of typical aircraft off-path response

Tolerance on Typical Aircraft Path Altitude at Threshold Crossing for
Category II and Category III ILS Facilities

The inspection record to which this tolerance is applied is the η_p trace. The tolerance is calculated using the parameters specific to each ILS Glide Slope installation. It is based upon a requirement that the typical aircraft path cross the runway threshold between the absolute altitudes above the threshold of $(PHT)_{\min}$ and $(PHT)_{\max}$ ft.*

The tolerances are calculated in terms of μA units by the following equations.

(Tolerance on deviation above the 0 μA reference path
[Below the 0 μA line on the oscillograph record]) =

$$\frac{12\ 278.37}{\sqrt{(x_t - x_1)^2 + y_1^2}} \left[(PHT)_{\max} - \tan \Theta_T \sqrt{(x_t - x_1)^2 + y_1^2} + p - z_t \right] \mu A \quad (11)$$

(Tolerance on deviation below the 0 μA reference path
[Above the 0 μA line on the oscillograph record]) =

$$\frac{12\ 278.37}{\sqrt{(x_t - x_1)^2 + y_1^2}} \left[\tan \Theta_T \sqrt{(x_t - x_1)^2 + y_1^2} - p + z_t - (PHT)_{\min} \right] \mu A \quad (12)$$

The reference path is that established by the RMT when set at the commissioned or desired angle Θ_T . $(x_t - x_1)$ is the distance in feet between the point on the runway centerline opposite the Glide Slope antenna mast and the runway threshold. z_t is the elevation in feet of the GPIP with respect to the runway threshold. z_t is positive when the GPIP elevation exceeds the threshold elevation. p is the effective pedestal height of the runway in feet.

The tolerances on deviation above and below the 0 μA reference path are marked on the η_p oscillograph record at the runway threshold crossing mark. The η_p oscillograph trace must pass between these two tolerance marks at the point of runway threshold crossing. If one of the above tolerances is violated, it can only be corrected by changes in the ILS

* $(PHT)_{\min}$ and $(PHT)_{\max}$ loosely correspond to $(TCH)_{\min}$ and $(TCH)_{\max}$ in the current standards. The intent of these specifications is similar. The latter quantities are 47 ft and 60 ft respectively in the current Flight Inspection Standards (Ref. 5).

Glide Slope siting arrangement. This is because the tolerances are absolute with respect to the runway threshold, and are independent of the RTT measurement system.

Tolerance on Typical Aircraft Path Deviation Rate Response

This tolerance is applied to assure that excessive rate of descent changes or excessive pitch attitude changes will not be required to follow the ILS Glide Slope guidance. The inspection record to which this tolerance is applied is the $\dot{\eta}_p$ trace.

The overlay providing the $\pm 2\sigma$ limits for the $\dot{\eta}_p$ trace appropriate to the category of ILS service (I, II, III) is selected and placed over the $\dot{\eta}_p$ trace with the runway threshold markings and 0 μA lines in alignment. The total $+2\sigma$ level exceedence time for the $\dot{\eta}_p$ oscillograph trace must not exceed 2.5 percent of the total record time for the interval from the outer marker to ILS Point C for Category I service, or to the runway threshold for Category II and Category III service. Similarly, the total -2σ level exceedence time must not exceed 2.5 percent of the same total record time.

Tolerance on Typical Aircraft Indicated Glide Path Deviation

This tolerance is applied to assure that excessive indicated glide path deviations will not be encountered in following the ILS Glide Slope guidance. Excessive indicated glide path deviations will result in frequent missed approach execution. The inspection record to which this tolerance is applied is the η_e trace.

The overlay providing the $\pm 2\sigma$ limits for the η_e trace appropriate to the category of ILS service (I, II, III) is selected and placed over the η_e trace with the runway threshold markings and 0 μA lines in alignment. The total $+2\sigma$ level exceedence time for the η_e oscillograph trace must not exceed 2.5 percent of the total record time for the interval from the outer marker to ILS Point C for Category I service, or to the runway threshold for Category II and Category III service. Similarly, the total -2σ exceedence time must not exceed 2.5 percent of the same total record time.

Tolerance on Sensitivity and Linearity of the Typical Aircraft Off-Path Response

Two tolerances are actually applied in this part of the analysis. One is upon the sensitivity of the off-path indication as measured by the path width obtained from the typical aircraft path deviation responses for flight inspection approaches flown at $+75 \mu\text{A}$ and $-75 \mu\text{A}$ indicated deviation*. The second tolerance is applied to the same data. It is upon the linearity of the off-path indication as measured by the symmetry in distribution of the path width about the actual path angle. The inspection records to which these tolerances are applied are the η_{p+75} and η_{p-75} traces.

These tolerances are applied to assure adequate dynamic path deviation response characteristics for aircraft in following the ILS Glide Slope guidance.

The location of the $0 \mu\text{A}$ reference mark of the overlay with respect to the $0 \mu\text{A}$ line on the η_p trace (resulting from application of the tolerance on actual path angle and typical aircraft path response) is located with respect to the $0 \mu\text{A}$ line on the η_{p+75} and η_{p-75} oscillograph records. A reference line is then drawn at this constant μA value on the two records.

The overlay providing the $\pm 2\sigma$ limits for the η_p trace appropriate to the category of ILS service (I, II, III) is selected and placed over the η_{p+75} trace with the runway threshold markings in alignment. The overlay is then shifted in the $\pm \mu\text{A}$ direction in such a manner as to center the η_{p+75} trace within the $\pm 2\sigma$ limits (or in such a manner as to equalize the total time that $+2\sigma$ limit and -2σ limit are each exceeded). The location of the $0 \mu\text{A}$ reference mark on the overlay is then transferred to the η_{p+75} oscillograph record. The separation in μA between the reference line previously drawn on the oscillograph record and the transferred $0 \mu\text{A}$ mark is designated v_{+75} . This distance is positive if the mark lies below the reference line and negative if the mark lies above. This procedure is repeated for the η_{p-75} trace. The corresponding distance in this case is designated v_{-75} . The sign of v_{-75} is determined by the same convention.

*In obtaining these records, the $0 \mu\text{A}$ RTT reference is elevated or depressed by 0.35 deg with respect to the commissioned or desired angle.

The sensitivity factor increment and nonlinearity metric are then computed according to the following equations.

$$(\text{Sensitivity factor increment}) = (v_{-75} - v_{+75}) / (150 + v_{+75} - v_{-75}) \quad (13)$$

$$(\text{Nonlinearity metric}) = \left| \frac{v_{+75} + v_{-75}}{150 + v_{+75} - v_{-75}} \right| \quad (14)$$

The sensitivity factor increment magnitude must be less than 0.2. A zero value is desirable and indicates the ILS Glide Slope guidance sensitivity is equal to the nominal value of 214.3 $\mu\text{A}/\text{deg}$. A negative value of the sensitivity factor increment indicates a lower than nominal sensitivity (i.e., a wider than nominal mean path). A positive value indicates a higher than nominal sensitivity. The nonlinearity metric should be less than 0.2. A zero value is desirable and indicates complete linearity of the ILS Glide Slope guidance.

Tolerance on the Differential Trace

A tolerance on the differential trace is redundant with respect to those listed previously. However, it provides an important tie-in with the existing procedure for flight inspection data analysis. Its use should probably be required during the introductory period for revised standards, and later its use might be made optional.

The location of the 0 μA reference mark of the overlay with respect to the 0 μA line on the η_p trace (resulting from application of the tolerance on actual path angle and typical aircraft path response) is located with respect to the 0 μA line on the η_r oscillograph record. A reference line is then drawn at this constant μA value on the η_r record.

The overlay providing the $\pm 2\sigma$ limits for the η_r trace appropriate to the category of ILS service (I, II, III) is selected and placed over the η_r trace with the runway threshold markings in alignment. The overlay is then shifted in the $\pm \mu\text{A}$ direction in such a manner as to align the 0 μA line on the overlay with reference line drawn previously on the η_r trace. The total $\pm 2\sigma$ level exceedence time for the η_r oscillograph trace must not exceed 2.5 percent of the total record time for the interval from the outer marker to

ILS Point C for Category I service, or to the runway threshold for Category II and Category III services. Similarly, the total -2σ level exceedence time must not exceed 2.5 percent of the same total record time.

If either or both of the 2σ level exceedence times exceeds 2.5 percent of the total record time, then the ILS Glide Slope structure is excessive as indicated by the η_r trace.

Example Application of the $\pm 2\sigma$ Limit Exceedence Criterion

An illustration of the overlay providing the $\pm 2\sigma$ limits for the η_p trace and the actual path alignment limits for Category II and III ILS Glide Slope service is displayed in Fig. 5. (The specific numerical values for the limits are those determined by $CSF = 1.50$ in Fig. 9 presented subsequently.)

Figure 6 shows the overlay superimposed upon a typical η_p trace in accordance with the instructions given in the subsection "Tolerance on Actual Path Angle and Typical Aircraft Path Response" above. Since the $\pm 2\sigma$ limits are exceeded, the overlay has been shifted in such a manner as to (approximately) equalize the total time that the $+2\sigma$ limit and -2σ limit are each exceeded, i.e., the shift is such that

$$t_1 + t_3 + \dots = t_2 + \dots$$

for the interval T between the outer marker and ILS Point C for Category I facilities and the runway threshold for Category II and III facilities.

Next, one proceeds to determine if the $0 \mu A$ line on the η_p trace falls within the actual path alignment limits, $\pm 48 \mu A$, on the overlay. In the illustration, it does. This indicates acceptable actual path alignment.

Finally, the values of

$$\frac{t_1 + t_3 + \dots}{T} \quad 100\% \quad \text{and} \quad \frac{t_2 + \dots}{T} \quad 100\%$$

are computed. If each computed value is 2.5 percent or less, then the typical aircraft path response is acceptable.

The $\pm 2\sigma$ limit exceedence criterion is applied in a similar manner to the $\dot{\eta}_p$, η_e and η_r traces. In the cases of the $\dot{\eta}_p$ and η_e traces, however,

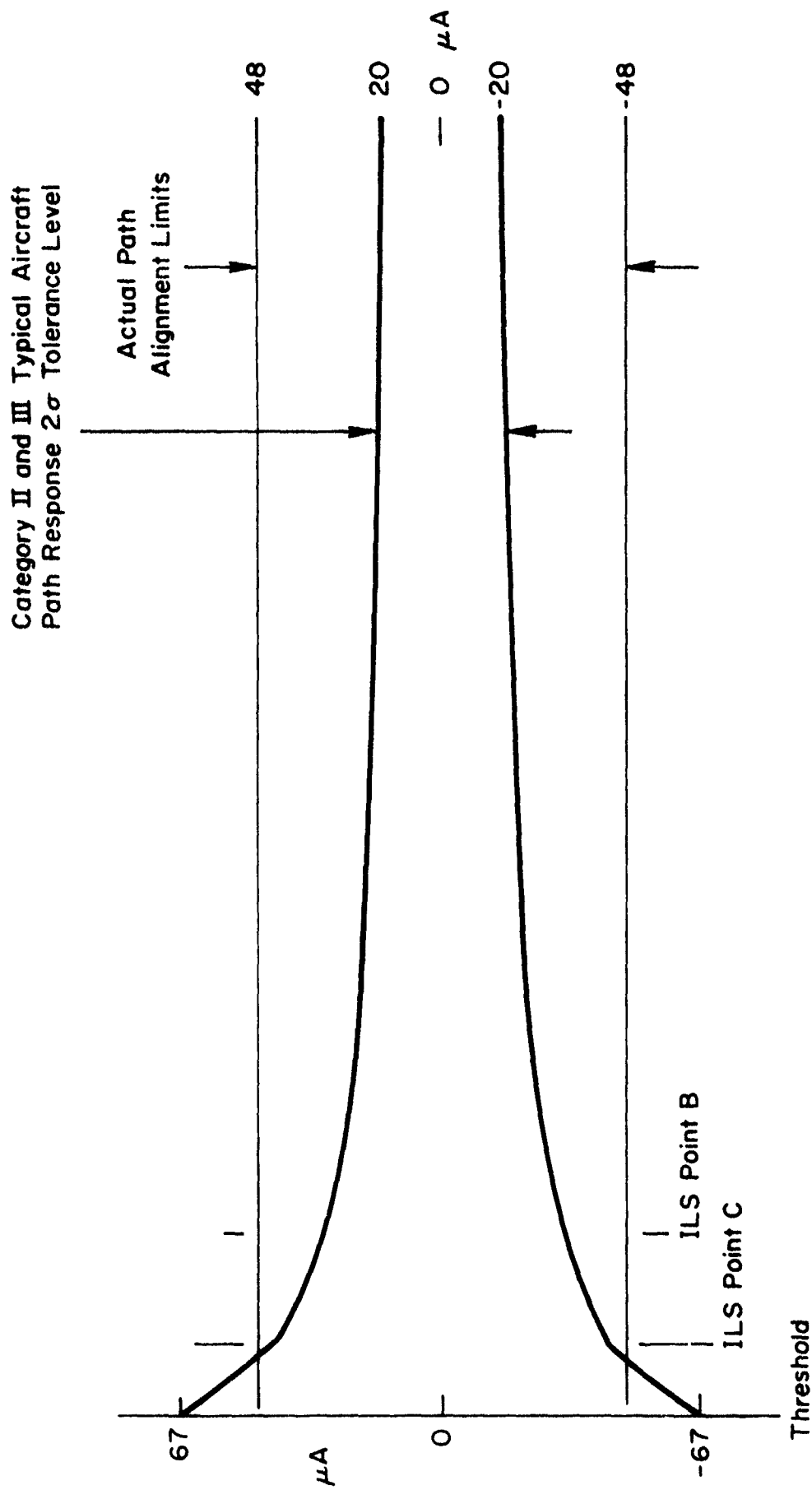


Figure 5. Tolerances for the η_p Trace for Category II and III ILS Glide Slope Service

Category II and III Typical Aircraft
Path Response 2σ Tolerance Level

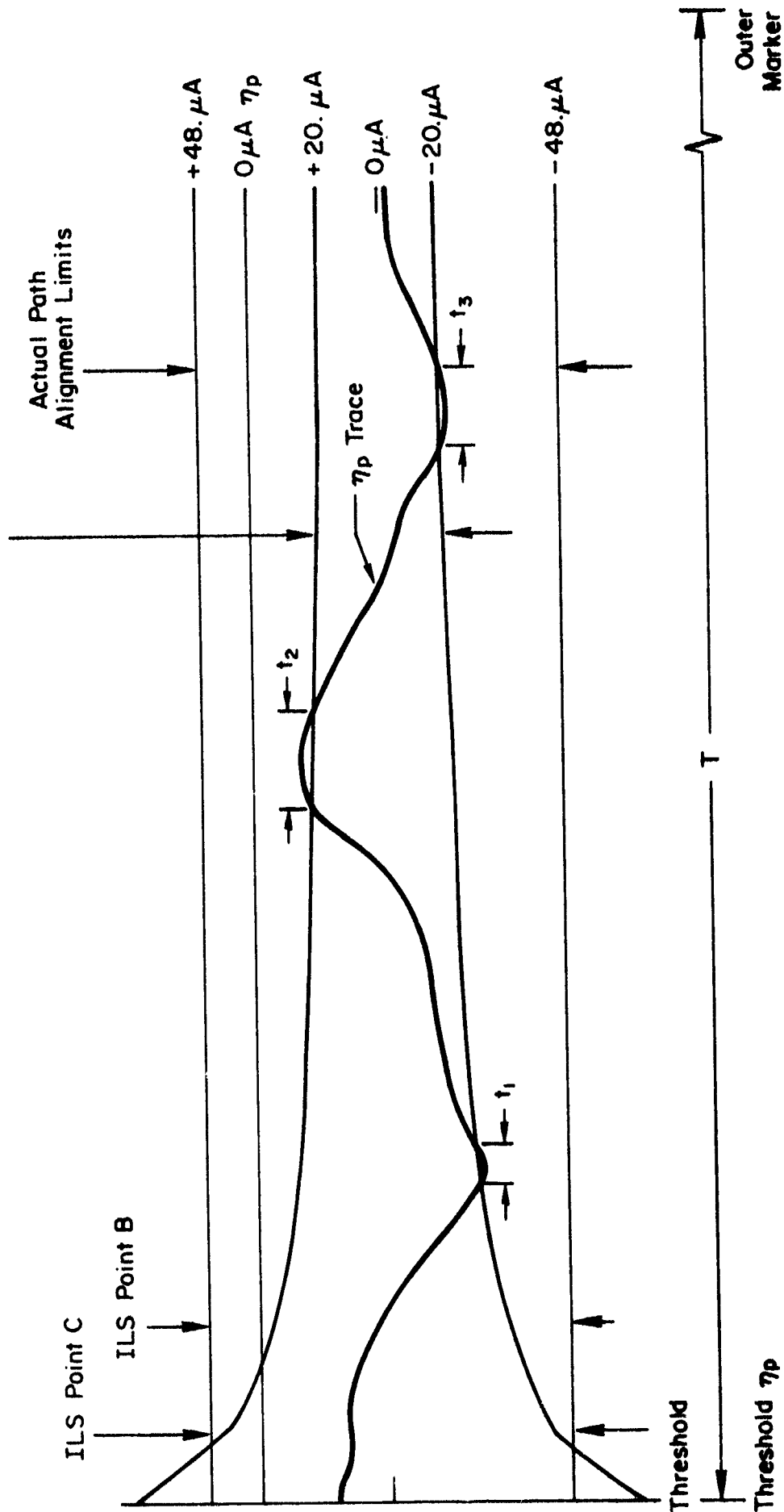


Figure 6. Illustrative Application of Tolerances for the
 η_p Trace for Category II and III ILS Glide Slope Service

the 0 μ A lines on the respective traces and overlays are placed in alignment.

NUMERICAL TOLERANCE VALUES

The overall system performance analysis results provide the key numerical values from which working tolerances for overall system and subsystem performance are developed. There are several steps to this development, and two different types of tolerances are developed. The two types of tolerances respectively are:

- Dynamic
- Static and quasi-static

The steps in working tolerance development involve:

- Adjustment of overall tolerances to allow for errors in the flight inspection measuring system
- Calibration of the filter system which generates typical aircraft responses from the differential trace
- Budget the working overall system tolerance among the various subsystem error sources

Adjustment of Overall Tolerances

The radio telemetering theodolite (RTT), which is part of the flight inspection measuring system, introduces a dynamic measurement error as the result of small imprecisions in manually adjusting the crosshairs to track the reference point on the inspecting aircraft. Dr. Richard H. McFarland has estimated bounds on this tracking error for the elevation axis to be as shown in Table 6. These estimated values are plotted along with the range variation model for ILS Glide Slope structure in Fig. 7. The variations with range (or equivalently, altitude) are seen to be nearly identical. Therefore, since 0.02 deg corresponds to 4.29 μ A,

$$2\sigma_{\eta_{RTT_{dyn}}} = 4.29 \left[1 + 2.48 e^{(X + 1000)/2304} \right] \mu A \quad (15)$$

will be used to model the dynamic RTT tracking error. The dynamic tracking error and the ILS Glide Slope structure are assumed to be uncorrelated.

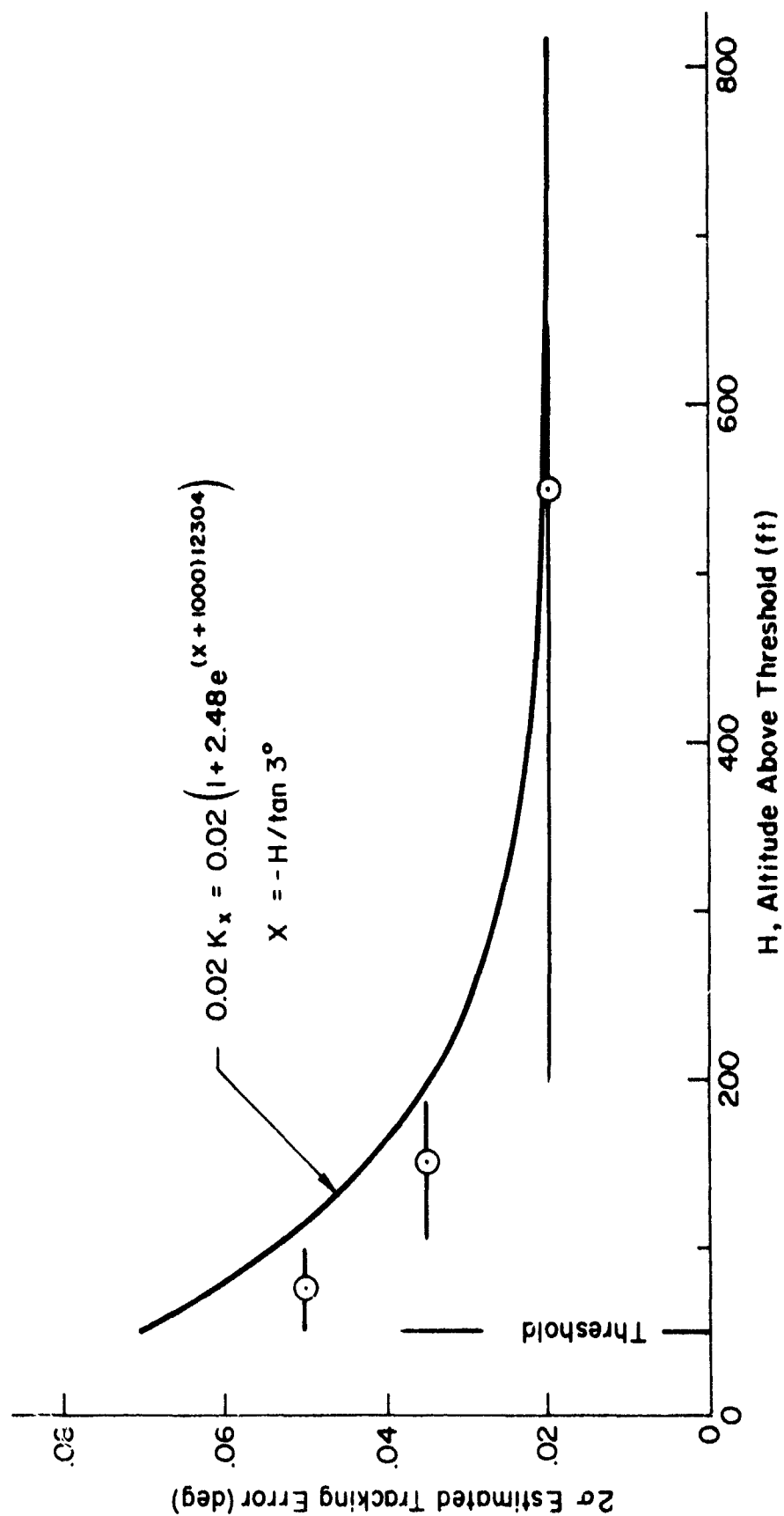


Figure 7. Comparison of Variation of Estimated Tracking Error with ILS Glide Slope Variation Function

TABLE 6
ESTIMATED BOUNDS ON DYNAMIC
TRACKING ERROR IN ELEVATION

Altitude of Approaching Aircraft (ft)	2 σ Value of Tracking Error Estimate (deg)
greater than 200	0.020
200 to 100	0.035
100 to 50	0.050

Dynamic Tolerances

In these circumstances, the dynamic tracking error is in constant ratio with the overall maximum level of ILS Glide Slope structure. For Category I operations this ratio is:

$$r_I = \frac{\sigma_{\eta_{RTT}}_{dyn}}{\sigma_{\eta_r}_{max}} = \frac{4.29/2}{3.00(5.99)} = 0.119 \quad (16)$$

and for Categories II and III this ratio is:

$$r_{II} = \frac{\sigma_{\eta_{RTT}}_{dyn}}{\sigma_{\eta_r}_{max}} = \frac{4.29/2}{1.50(5.99)} = 0.239 \quad (17)$$

The working maximum levels for ILS Glide Slope structure as characterized by an effective value for its scale factor are, for Category I

$$CSF_{IW} = 3.00 \sqrt{1 - r_I^2} = 2.98 \doteq 3.00 \quad (18)$$

and for Categories II and III

$$CSF_{IIW} = 1.50 \sqrt{1 - r_{II}^2} = 1.46 \doteq 1.50 \quad (19)$$

These working levels provide tolerances appropriate for application to the flight inspection data. That is, the working levels allow for the dynamic tracking error attendant to RTT measurement.

The 2σ tolerance level for structure on the differential trace can now be expressed as an equation based upon Eq B-10 and -11 in Appendix B. For Category I service

$$2\sigma_{\eta_{rI}} = 35.7 \left[1 + 2.48e^{(X + 1000)/2304} \right] \quad (20)$$

and for Categories II and III service

$$2\sigma_{\eta_{rII}} = 17.5 \left[1 + 2.48e^{(X + 1000)/2304} \right] \quad (21)$$

where $35.7 = 2 (2.98) 5.99$ and $17.5 = 2 (1.46) 5.99$. The function $2\sigma_{\eta_r}$ is plotted for various values of the scale factor CSF in Fig. 8.

Figures 9, 10 and 11 show the 2σ levels for the typical aircraft filter responses for the same scale factor values. (The block diagram for this filter is Fig. 4. Counterpart figures to Fig. 9, 10 and 11 are given in Appendix E for the alternative filter system presented in that Appendix.) The figures respectively show the actual glide path deviation response, actual glide path deviation rate response, and indicated glide path deviation response 2σ levels. The curves in each case include our recommended 2σ tolerance levels for the respective variables. The recommended Category I tolerances are the $CSF = 2.98 \doteq 3.00$ curves up to ILS Point C. (No tolerances need apply between ILS Point C and the threshold for Category I because the absolute minimum descent altitude using the ILS Glide Slope is 200 ft.) The recommended Category II and III tolerances are the $CSF = 1.46 \doteq 1.50$ curves which extend to the threshold.

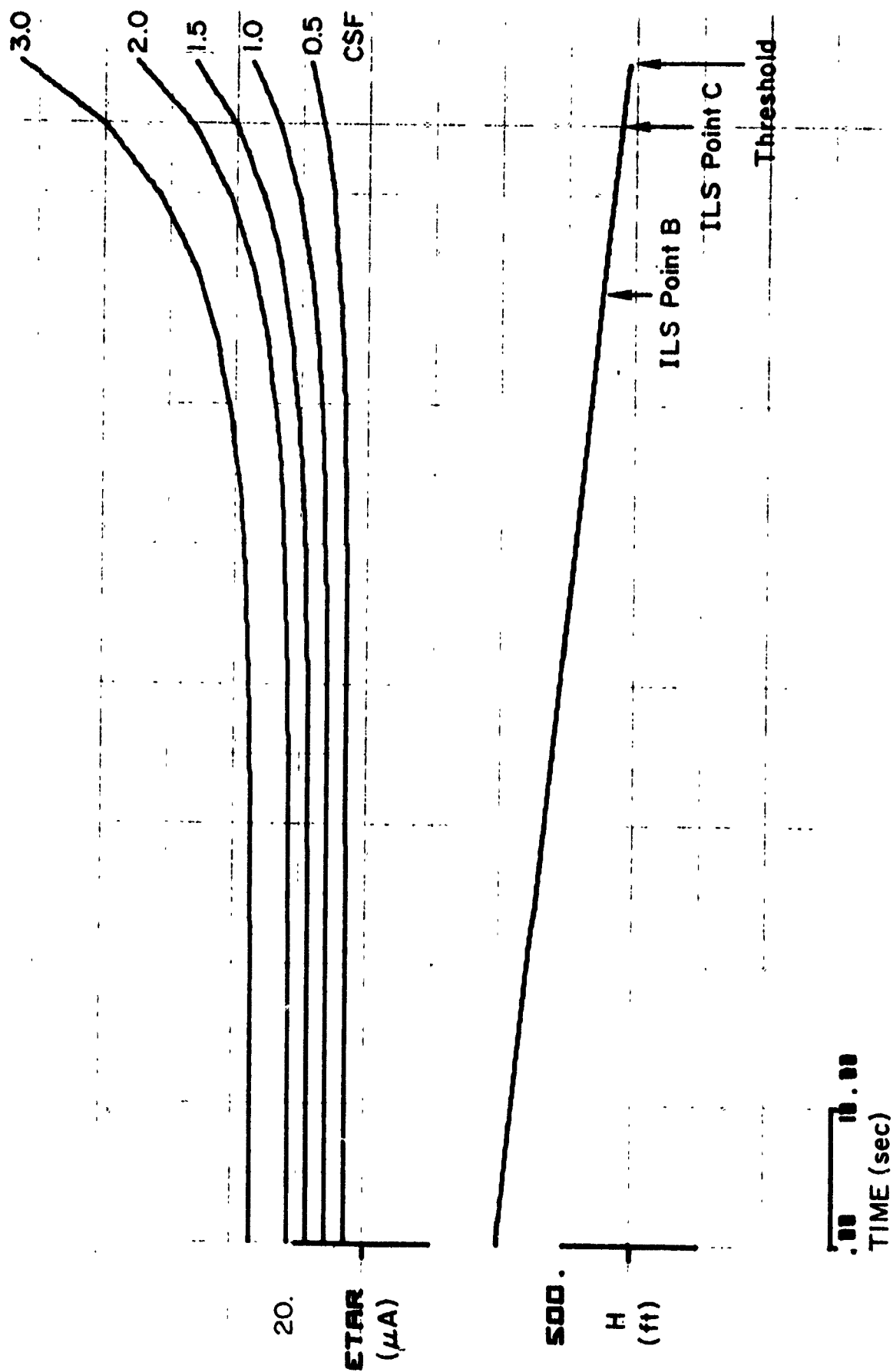


Figure 8. 2 σ Tolerance Level Curves for the Differential Trace

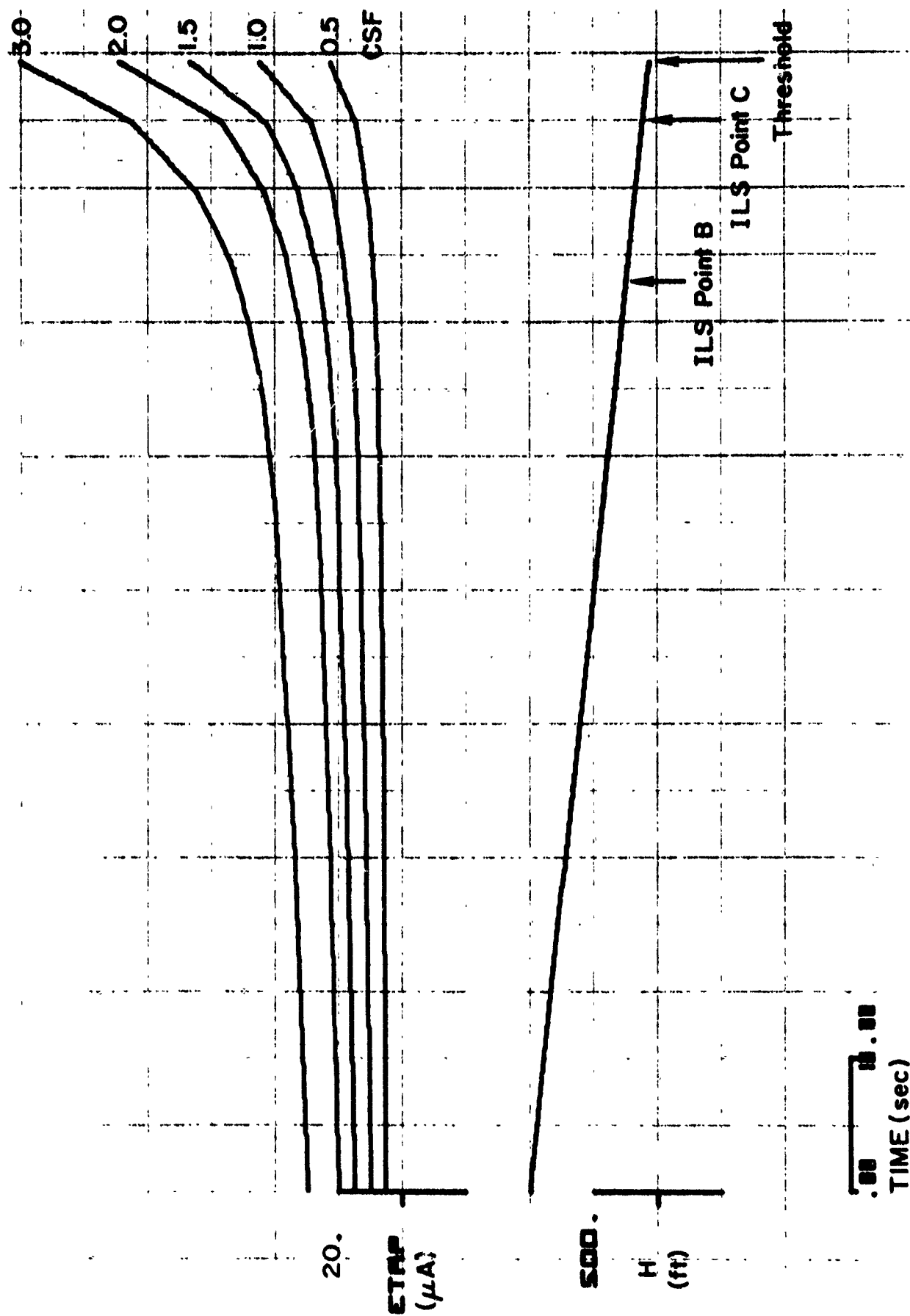


Figure 9. 2σ Tolerance Level Curves for Typical Aircraft Actual Path Deviation Response
(Filter System No. 1)

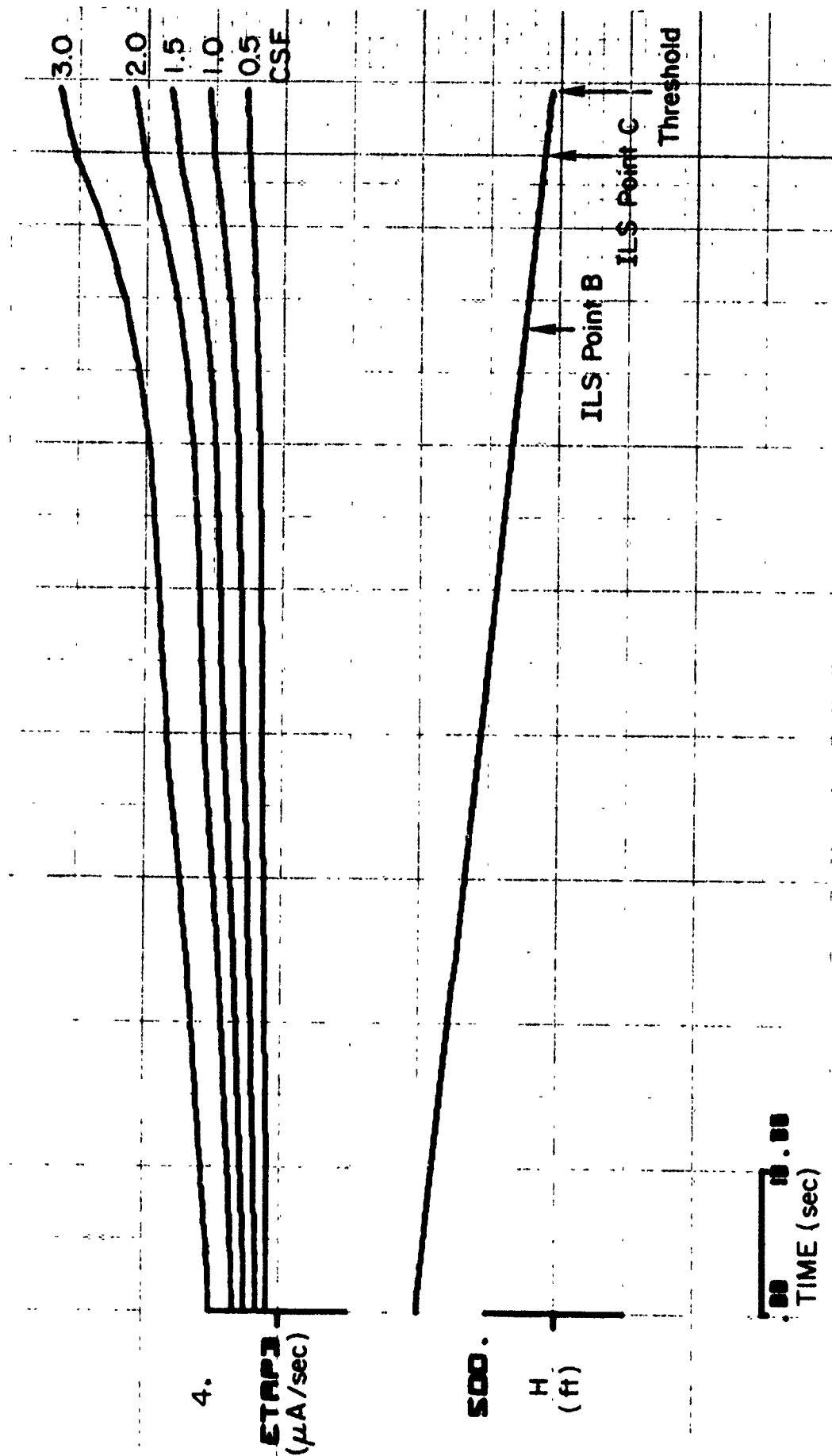


Figure 10. 2σ Tolerance Level Curves for Typical Aircraft Actual Path Deviation Rate Response
(Filter System No. 1)

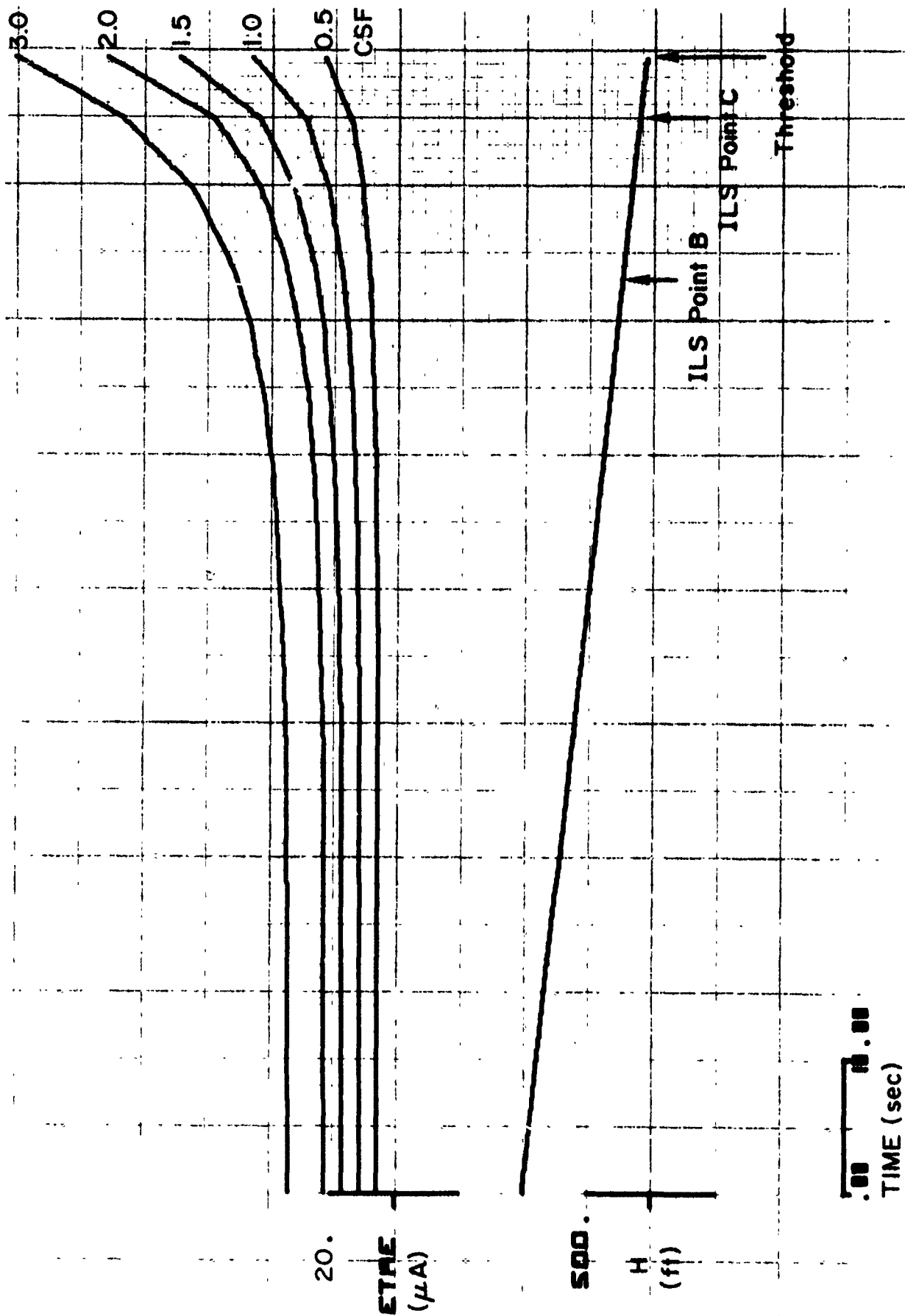


Figure 11. 2σ Tolerance Level Curves for Typical Aircraft
 - Indicated Glide Path Deviation at 500 ft
 - ILS

Static and Quasi-Static Tolerances

Alignment of Actual Path with Commissioned or Desired Angle

Alignment of the actual path with the commissioned angle Θ was not found to affect landing performance in a sensitive way. Current standards require alignment to within $\pm 0.075\Theta$. For $\Theta = 3.0$ deg this corresponds to ± 0.225 deg, ± 48.2 μA , or ± 3.93 ft at the threshold. If the current standard, which is an absolute limit, is interpreted as a 3σ value, then 1σ would correspond to 16.1 μA or 1.31 ft at the threshold.

In exercising the overall system performance analysis model, values for $\sigma_{\Delta\Theta}$ up to 0.262 deg, 56.1 μA or 4.57 ft at the threshold were used (i.e., 3.5 times the current standard) with no observable effect other than a very small increase in the sink rate dispersion at touchdown. This being the case, it would appear that the limitations upon alignment error between the actual path and the commissioned angle are imposed by considerations outside the scope of the overall system performance analysis model. For example, below the commissioned angle, wheel-to-runway threshold clearance may be the key consideration. Above the commissioned angle, the ability to arrest the rate of sink in the flare while maintaining an adequate margin from stall may be the key consideration in so far as landing performance limits are concerned.

However, analysis of data for actual Category II and II training Glide Slopes has resulted in a $\sigma_{\Delta\Theta}$ estimate of 8.01 μA while the 1σ equivalent level of the current standard is 16.1 μA . Thus it appears that alignment with respect to the current standard is easily accomplished in the field. Since this is the case, and because the alignment error has no appreciable effect upon landing performance, our recommendation is for an absolute tolerance of ± 48.0 μA on alignment of the actual path with respect to the commissioned or desired angle for Categories I, II and III.* This recommended tolerance is comparable to the current standard for Category I and II facilities.

If, however, an overall tolerance on alignment error between the actual path and the commissioned or desired angle set by landing performance limitations were known, say $\sigma_{\Delta\Theta}^$, then that value would have to be reduced by the allowable variability in the airborne ILS receiver centering error for both the inspecting aircraft and the operating aircraft, $\sigma_{RX_{insp}}$ and $\sigma_{RX_{res-op}}$

Actual Path Altitude at Threshold Crossing and Related Tolerances

The tolerances related to typical actual path altitude at threshold crossing require careful attention to a wide variety of component parts. Let the minimum typical actual path altitude at threshold crossing in the absence of wind, wind shear and gust effects be denoted by $(PTH)_{min}$, the minimum main gear wheel clearance in normal operation denoted by W_{min} , and the nominal effective altitude difference between the ILS glide path receiver antenna and the lowest point on the landing gear with the aircraft in landing attitude denoted by A_0 . Let any difference between the nominal effective altitude difference between the glide path receiver antenna and the lowest point on landing gear and the actual altitude difference on a particular aircraft be denoted by ΔA . (When $\Delta A > 0$ the altitude difference exceeds A_0 .) All of the above quantities are in units of feet. The equation for testing the performance of the user's aircraft/control system combination against the component tolerances is

$$\begin{aligned} (PTH)_{min} - W_{min} - A_0 - 3 \left[\left(\frac{1000}{12278} \right)^2 \left\{ (\sigma_{RTT_{acc}})^2 + (\sigma_{RTT_{dyn}})^2 + (\sigma_{RX_{insp}})^2 \right. \right. \\ \left. \left. + (\sigma_{RX_{op}})^2 \right\} + (\sigma_{H_{wind}})^2 + (\sigma_{H_{gusts}})^2 \right]^{1/2} \geq \Delta A \end{aligned} \quad (23)$$

THRESHOLD

pectively. $\sigma_{RX_{insp}}$ and $\sigma_{RX_{op}}$ indicate one standard deviation levels. The working absolute tolerance upon alignment error would then be given by:

$$3 \left[(\sigma_{\Delta\theta}^*)^2 - (\sigma_{RX_{insp}})^2 - (\sigma_{RX_{op}})^2 \right]^{1/2} \quad (22)$$

For typical numbers $\sigma_{RX_{insp}} = 5 \mu A$ and $\sigma_{RX_{op}} = 10 \mu A$, $\sigma_{\Delta\theta}^*$ would have to be at least $11.2 \mu A$.

where σ_{RTT}^{acc} is the standard deviation of the certified accuracy of the RTT, $1.43 \mu A$; and σ_{RTT}^{dyn} is the tracking error standard deviation which is $7.56 \mu A$ at the threshold. σ_{RX}^{insp} and σ_{RX}^{op} are the standard deviations of the ILS glide path receiver centering errors for the inspecting aircraft and operating aircraft respectively. $\sigma_{H_{wind}}$ and $\sigma_{H_{gust}}$ are the altitude standard deviation components arising from wind and windshear, and gusts respectively for a particular aircraft/control system combination.

The overall system performance analysis established a typical value for

$$\left[\left(\sigma_{H_{wind}} \right)^2 + \left(\sigma_{H_{gust}} \right)^2 \right]^{1/2} \text{Threshold}$$

of 1.76 ft.

The remaining items on the left hand side of Eq 23 may be selected to have positive values and provide consistency with the inequality for $\Delta A = 0$. Their selection amounts to a budgeting of the allowable error among the error sources.

Consider current typical values for the remaining parameters on the left hand side of Eq 23.

$$(PHT)_{min} = (TCH)_{min} = 47 \text{ ft}$$

$$W_{min} = 10 \text{ ft}$$

$$A_o = 19 \text{ ft}$$

$$\sigma_{RX}^{insp} = 5 \mu A$$

$$\sigma_{RX}^{op} = 8 \mu A$$

The left hand side then calculates out to 11.94 ft which provides a comfortable margin with respect to 2.02 ft for the standard deviation of the total random uncertainty in operation.

In terms of the standard deviation of total random uncertainty in operation,

$$\left\{ \left[\left(\sigma_{H_{wind}} \right)^2 + \left(\sigma_{H_{gust}} \right)^2 \right] + \left(\frac{1000}{12278} \right)^2 \left[\left(\sigma_{RTT_{acc}} \right)^2 + \left(\sigma_{RTT_{dyn}} \right)^2 + \left(\sigma_{RX_{insp}} \right)^2 + \left(\sigma_{RX_{op}} \right)^2 \right] \right\}^{1/2} \text{ Threshold}$$

the margin is 5.91σ .

It is not possible to recommend numerical values for the individual terms in Eq 23 on the basis of system analysis alone. The only requirement that can be definitely established is that the inequality of Eq 23 must be satisfied by the tolerances. The most relaxed tolerances (in the overall sense) will result when Eq 23 is satisfied as a strict equality.

The fact that the typical values result in a considerable margin in the above example indicates that the tolerance can justifiably be relaxed. For example, if

$$(P_{TT})_{min} = 40 \text{ ft}$$

$$W_{min} = 10 \text{ ft}$$

$$A_o = 19 \text{ ft}$$

$$\sigma_{RTT_{acc}} = 3 \mu A$$

$$\sigma_{RTT_{dyn}} = 10 \mu A$$

$$\sigma_{RX_{insp}} = 5 \mu A$$

are the tolerances upon the ILS Glide Slope signal at the threshold and upon the flight inspection process, then every user's airborne systems must satisfy

$$11 - 3 \left[0.89 + \left(\frac{1000}{12278} \right) \left(\sigma_{RX_{op}} \right)^2 + \left(\sigma_{H_{wind}} \right)^2 + \left(\sigma_{H_{gust}} \right)^2 \right]^{1/2} \geq \Delta A \text{ Threshold} \quad (24)$$

which represents the tolerance on the airborne user's system performance. The exact manner in which the user chooses to partition the allowable tolerance between ΔA , $\sigma_{RX_{op}}$, $\sigma_{H_{wind}}$ and $\sigma_{H_{gust}}$ should be at his discretion. For example, if $\Delta A = -1$ ft for the particular aircraft and $\sigma_{RX_{op}} = 10 \mu A$ for the particular ILS glide path receiver, then the aircraft/control system combination must be effective in reducing

$$\left[\left(\sigma_{H_{wind}} \right)^2 + \left(\sigma_{H_{gust}} \right)^2 \right]^{1/2} \text{Threshold}$$

to 3.80 ft or less.

No requirement for a limit upon $(PHT)_{max}$ is indicated by this study. Satisfaction of all other tolerances is sufficient to assure that the typical actual path altitude threshold crossing is not excessive.

COMPARISON OF TOLERANCES WITH CURRENT STANDARDS

The following comparison is presented in order to establish a connecting link between the newly developed tolerances and the current flight inspection standards. This comparison cannot be carried out with ultimate precision, but it can be accomplished in a spirit of reasonable accuracy. The reasons for this are as follows:

- Some of the current standards are in absolute terms, while corresponding, newly developed tolerances are in terms of 2σ levels
- A one-to-one correspondence does not always exist between the ILS Glide Slope features controlled by the current standards and those controlled by the newly developed tolerances
- Quantities such as the "graphical average path" and the "typical aircraft path response" are conceptually closely related but they are not precisely equivalent

Nevertheless, the comparison will be made assuming that:

- Absolute limits and 3σ levels are suitable for comparison
- Comparison of features where a one-to-one correspondence exists will be adequate

- A conceptual equivalence between quantities in lieu of precise equivalence may be accepted

Figures 12 and 13 compare the newly developed 2σ tolerance level and the current 2σ standard for ILS Glide Slope structure for Category I and Category II facilities respectively. (Refer to Para. 217.44 and 217.5 (16)(a) of Ref. 5.) The current structure standard for Category I facilities is conservative with respect to the tolerance level. The current structure 2σ standard for Category II facilities is slightly more permissive than the 2σ tolerance level throughout most of ILS Zone 2. At the end of Zone 2 and throughout Zone 3, the current standard becomes increasingly conservative as the threshold is approached.

Figure 14 compares the current (absolute) standard for ILS Glide Slope change/reversal in slope with the newly developed tolerances for Category I and Category II and III facilities. (Refer to Para. 217.5 (16)(d) of Ref. 5.) The current slope change/reversal standard is quite conservative throughout most of ILS Zones 2 and 3 with respect to the 3σ tolerance level for Category I facilities. For Category II, however, the current slope change/reversal standard is more permissive than the 3σ tolerance level throughout most of ILS Zone 2. At the end of Zone 2, and throughout Zone 3 the current standard becomes increasingly conservative as the threshold is approached.

Figure 15 compares the current average glide path alignment standard with the tolerance for the typical aircraft path response for Category II ILS Glide Slope facilities. (Refer to Ref. 21.) These standards and tolerances are not truly comparable because the standard in actual fact applies to a combination of the alignment error of the actual path with the commissioned or desired angle, and the aircraft path response to structure (as represented by the so-called average path), while the newly developed tolerance applies only to the typical aircraft path response to structure. (Recall that overall system landing performance was found to be insensitive to the alignment error between the actual path and the commissioned or desired angle.) Despite this disparity in the quantities being compared, the current standard is conservative with respect to the 3σ tolerance level throughout ILS Zone 3.

The above comparison illustrates a practice which must be avoided in future revisions of standards. Specifically, the current FAA average path alignment standard is a combined specification on critical and non-critical features of the ILS Glide Slope, i.e., aircraft response to structure and

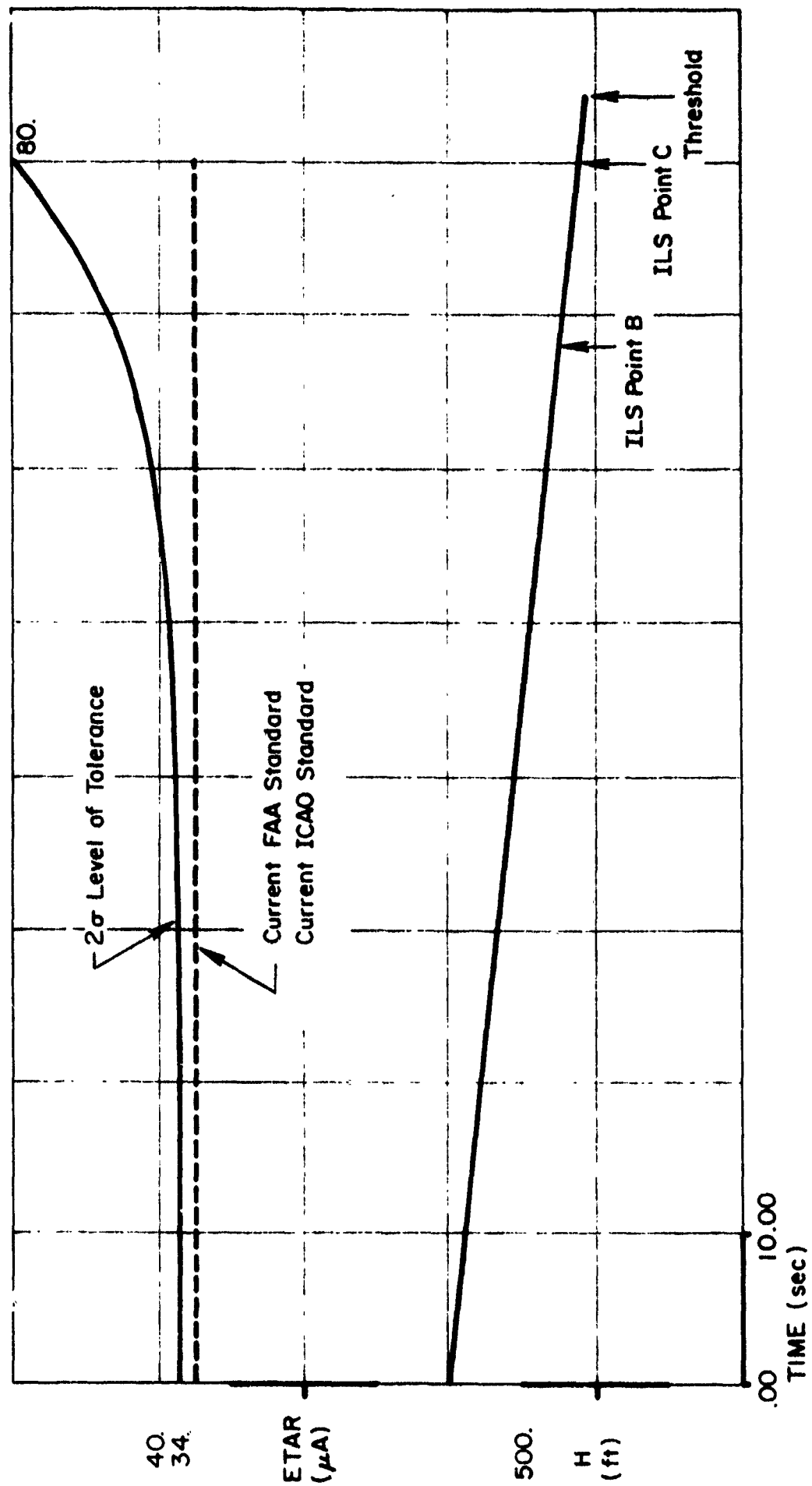


Figure 12. Comparison of Current Structure Standard for Category I with the 2 σ Tolerance Level for the Differential Trace

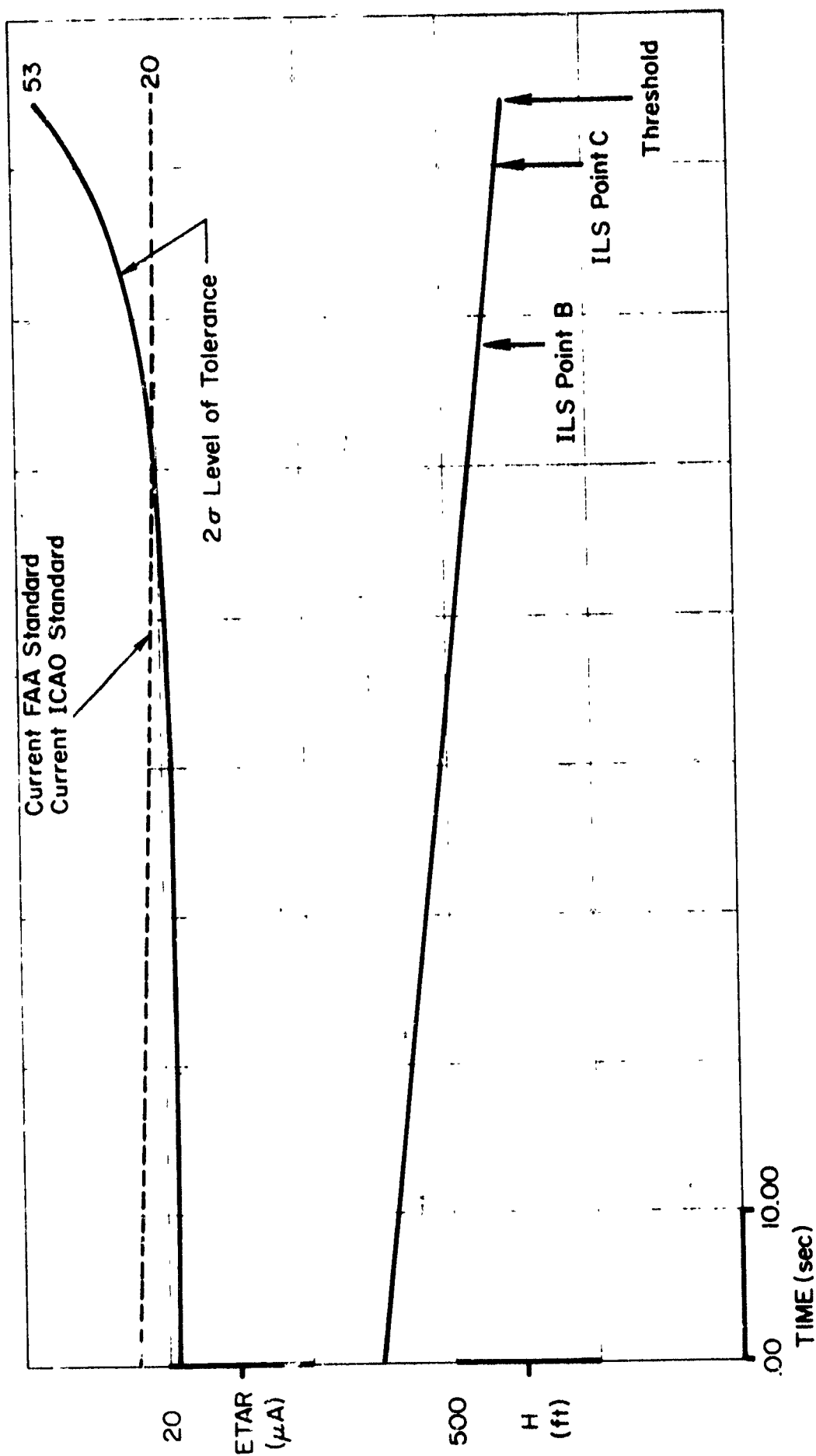


Figure 13. Comparison of Current Structure Standard for Category II with the 2σ Tolerance Level for the Differential Trace

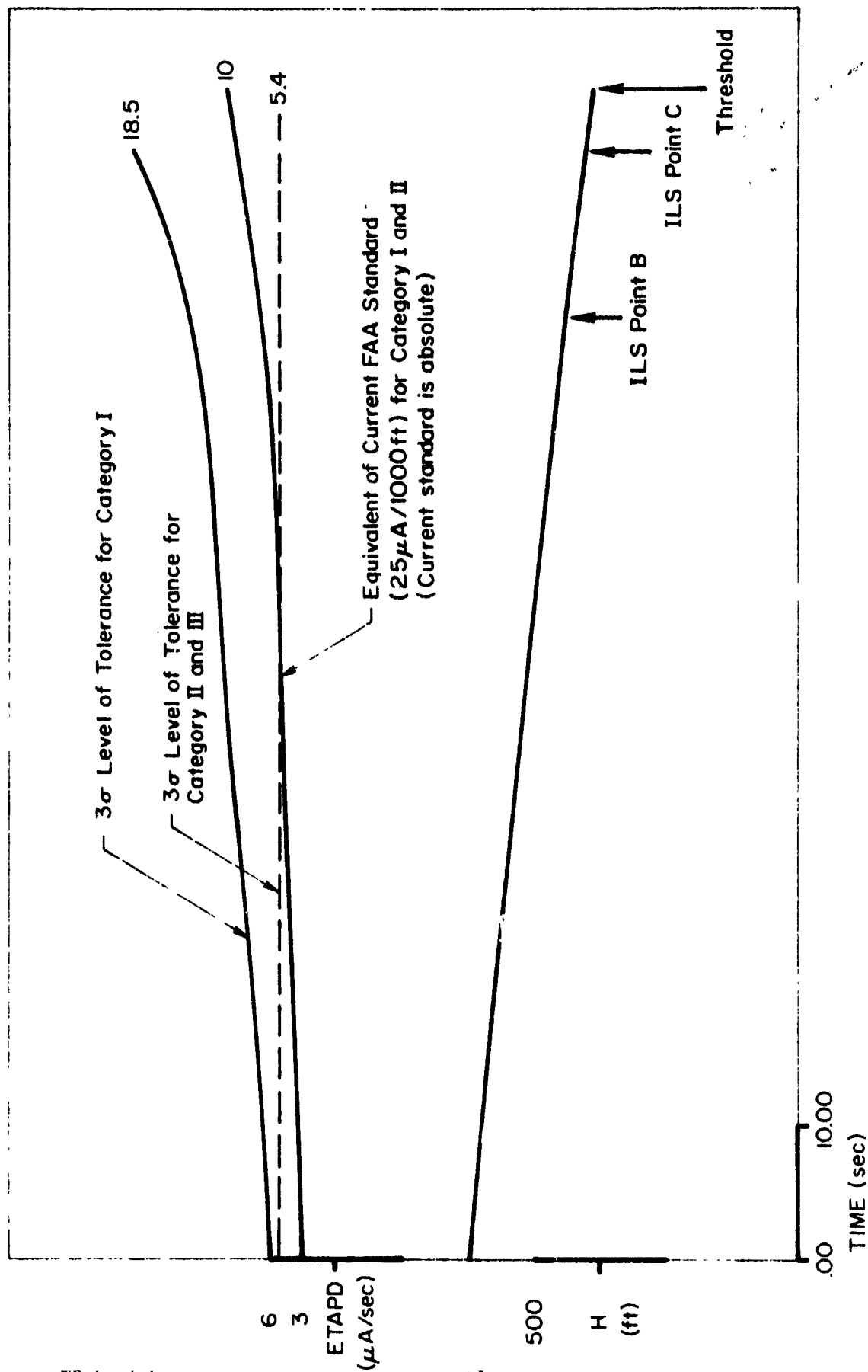


Figure 14. Comparison of Current FAA Climb Change, Reversal Standard with the 3σ Tolerance Level for the Typical Aircraft Path Deviation Rate Response for Category I, II, and III Filter System.

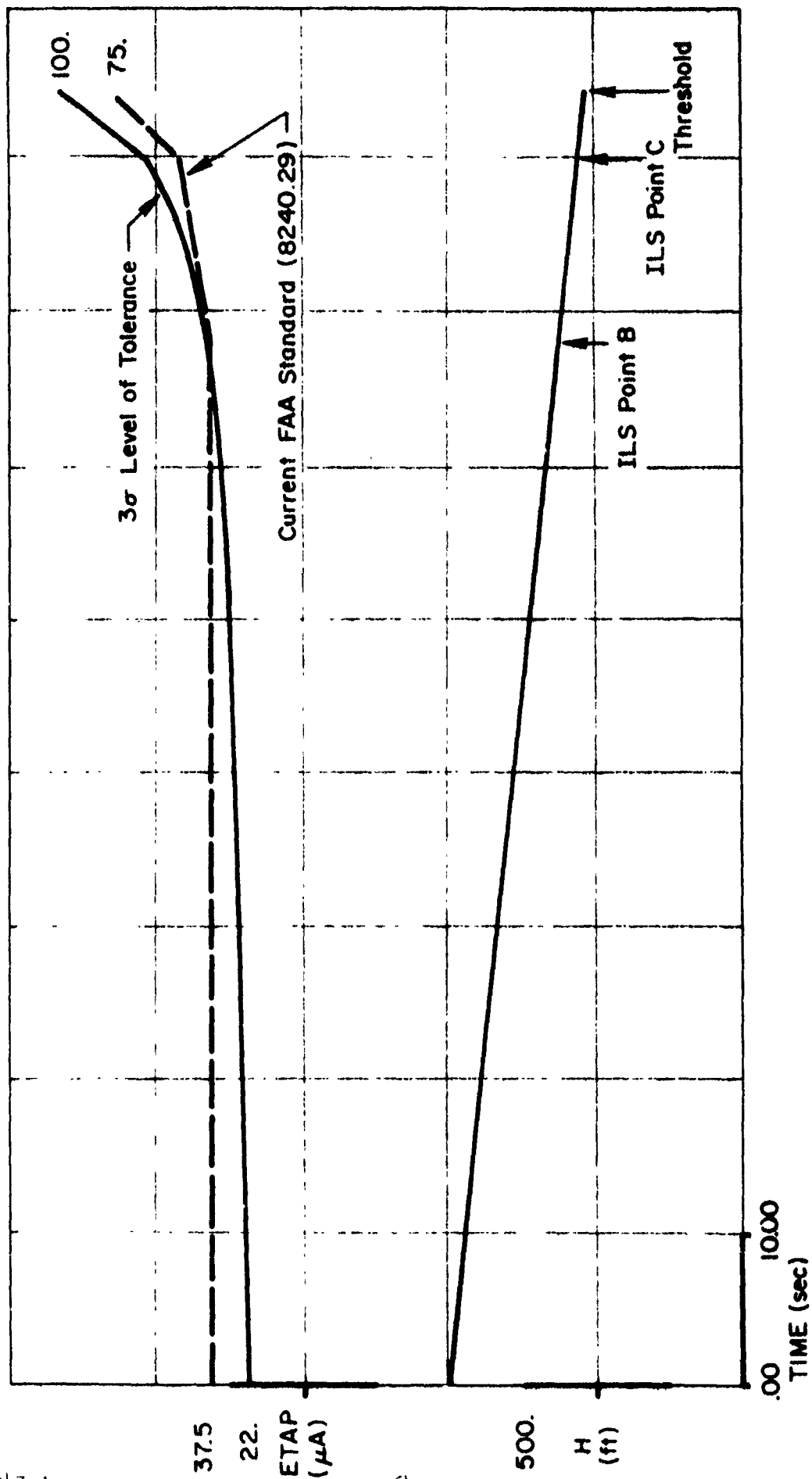


Figure 15. Comparison of Current FAA Average Path Alignment Standard for Category II with the 3σ Tolerance Level for the Typical Aircraft Path Deviation Response (Filter System No. 1)

the alignment of the actual path with the commissioned or desired angle, respectively. While the present standard is conservative because the combined specification on the two features is less than 3σ tolerance level for the critical feature in ILS Zone 3, the standard would have been unconservative had it exceeded the 3σ tolerance level, and landing safety goals would perhaps be compromised. This is because, with a combined specification, a hypothetical situation could exist wherein the (non-critical) alignment error could be very small and the (critical) aircraft response could be large, but still acceptable under the standard, but unacceptable with respect to the 3σ tolerance level. On the other hand, if the combined specification is conservative (as it is at present), the effect is to overly restrict the allowable Glide Slope structure in some cases; specifically in those cases wherein the alignment error consumes a substantial portion of the allowable error.

Care should be exercised to avoid such combinations of specifications upon distinctly different features in a single standard in the future.

IMPACT OF REVISED FLIGHT INSPECTION STANDARDS

The impact expected as the result of applying the proposed revised flight inspection standards will affect the Flight Standards Service, Flight Inspection National Field Office, the Flight Inspection District Offices, Flight Inspection Groups, the airport facilities operators, and the aircraft operators and crews. Maximum benefits with virtually no burden will accrue to the aircraft operators and crews. At high levels in the organizational pyramid the benefits will be more closely balanced against the burden. The main benefits will be generally increased levels of safety and productivity for airport facilities and aircraft. At the highest level the main benefit will be enhancement of regulatory goals for safety of aircraft operations. This will be through the development and provision of flight inspection standards which are more keenly attuned to actual operational needs for ILS approach and landing.

Flight Standards Service

The Flight Standards Service will bear the economic burden of validating and converting the tolerances proposed as a result of this research effort into flight inspection standards. The principal benefit to the Flight Standards Service will be that of furthering their mission through the promulgation

of flight inspection standards which at the same time enhance the safety of ILS approaches and landings, and encourage more intensive and effective use of existing ILS facilities. Safety will be served by replacing several steps in the flight inspection data analysis procedure now dependent upon human judgment with data processing. However, only those steps which can be better accomplished by data processing than by human judgment (i.e., averaging) will be replaced. In addition, specifications will be placed upon variables derived from the flight inspection data. These derived variables will have direct relevance to the conduct of approach and landing operations. For example, separate specifications will be applied to variables representing typical indicated glide path deviation, actual glide path deviation, and actual glide path deviation rate response. (This is in distinction to current procedures wherein separate specifications are applied to various features of the "differential trace" which has only an indirect relevance to the conduct of approach and landing operations.)

The revised standards will encourage more intensive and effective use of existing ILS facilities because the separate tolerances applied to the derived variables will be more flexible and permissive than the current standards. This will also result in a reduction in the number of so-called "special case" installations.

Proposed revisions include maintenance of a central archive for magnetic tapes containing flight inspection data. Even though data need only be kept for a fixed limited time, the burden of maintaining this data is new. (It is assumed that the current practices for maintaining oscillograph record data will be continued.) The magnetic tape data archive will provide the benefit of a compact permanent record of the basic inspection data. These records will be in a form that may be readily used to reproduce oscillograph records, or which may readily be subjected to more extensive analysis should special investigative or research needs arise.

Furthermore, the revised method for obtaining flight inspection data will require a minimum of new equipment.

Flight Inspection National Field Office, Flight Inspection District Offices, Flight Inspection Groups

Flight Inspection National Field Office and District Offices

Benefits to the Flight Inspection National Field Office and District Offices will be increased ILS facility acceptance rates for Category II and Category III service, increased flight inspection productivity, and a reduction in the number of special case facilities. Increased productivity will result in reduced aircraft operating cost per inspection.

Flight Inspection Groups

Benefits to Flight Inspection Groups will be reduction in flight inspection workload through introduction of data processing and tolerance overlays and a reduction in the amount of judgment which is necessary to interpret the data. This will be accomplished by relatively modest changes to the current flight inspection procedures.

Airport Facility Operators

Airport facility operators will benefit from reduced problems in bringing ILS facilities to commissioned status and maintaining them in that status. Modest reductions in cost should result from a reduced need for site modification and perhaps from installing less sophisticated ILS equipment at some new facilities. The number of facilities requiring special case treatment will be reduced.

Burdens upon airport operators will include installation, maintenance and protection of benchmarks for the RTT and the bare possibility of having to recommission a very few ILS installations which meet present standards but will not meet the revised standards.

Aircraft Operators and Crews

Aircraft operators and crews will benefit from greater productivity resulting from more permissive standards. A principal benefit of this integrated development of overall system tolerances is one of enhanced safety. Crew confidence in the airborne and ground facilities will be enhanced as the

result of applying specifications to variables derived from ILS flight inspection measurement which have direct relevance to approach and landing success and pilot acceptance.

SECTION IV

A REVIEW OF CURRENT FAA AND ICAO STANDARDS

APPROACH AND LANDING PERFORMANCE

The current FAA definition of a successful ILS Category II approach is given in Ref. 12 in terms of maximum acceptable airplane dispersions with respect to the indicated center of the guidance beam at an altitude of 100 ft above the runway. (The same definition necessarily applies also to the successful Category III landing as given in Ref. 13, provided that the additional sufficiency requirements on touchdown dispersion in Ref. 6 are met in Category III. See Table 7 herein.) In essence, the FAA has defined a "window" that an airplane must be within at the 100 ft decision height.

Because a decision height window is at the decision height, it is actually a horizontal window, as shown in Fig. 16. Thus, even though an airplane may be above or below the indicated center of the glide slope beam, the decision height remains the same (100 ft above the runway elevation for ILS Category II). This means that if an airplane is above (or below) the beam, then it must be closer to (or farther from) the runway threshold when it reaches the decision height. In other words, what appears to be a vertical deviation from some point on the beam should really be thought of as a horizontal deviation from a different point on the beam (a point that is at the same altitude as the airplane). The relation between an "apparent" vertical deviation from the beam and the more appropriate horizontal deviation is just the tangent of beam angle. Consequently, the ILS Category III window tolerance of ± 12 ft at the decision height transforms into a horizontal dispersion tolerance of between 19 and 23 times the window tolerance or between ± 228 ft and ± 276 ft, depending on the actual Glide Slope angle Θ in Fig. 16. These horizontal dispersion tolerances represent between 30 and 37 per cent of the 2σ longitudinal touchdown dispersion (1500 ft) for Category III performance in Table 7. However, this dispersion will be reduced to some extent by the action of the coupler and control system between the decision height and the flare initiation altitude at which point typical modern systems cease to use ILS Glide Slope guidance. The remainder of the maximum allowable longitudinal 2σ

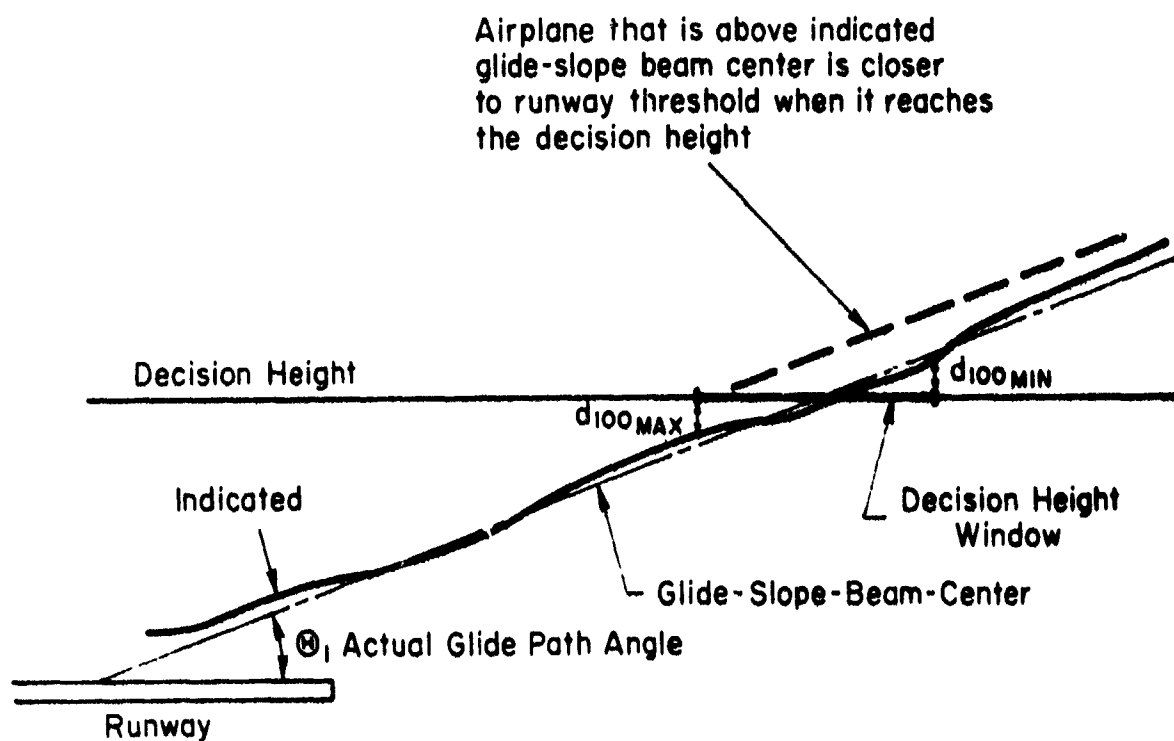


Figure 16. Relation Between Decision Height Window and Maximum Allowable Deviations Above and Below the Glide Slope Beam.

TABLE 7
OVERALL ILS GLIDE SLOPE SYSTEM PERFORMANCE REQUIREMENTS

ILS Performance Category	Overall Flight Tracking Performance Requirement on Glide Slope
I	(No performance standard; only equipment complement, pilot training and proficiency, and operational standards; see AC 120-29 [Ref. 12])
II	From 700 ft altitude to the decision altitude (100 ft), $\pm 35 \mu A$ or ± 12 ft with respect to indicated "on-path" position, whichever is larger, without sustained oscillations (AC 120-29, App. 1 pg. 6)
III	From 700 ft altitude to the flare initiation height [circa 50 ft], $\pm 35 \mu A$ or ± 12 ft with respect to indicated "on-path" position, whichever is larger, without sustained oscillations (AC 120-28A, App. 1, p. 4 [Ref. 13] <u>and</u> repeatable touchdown on the runway within the longitudinal limits 200 ft and 2500* ft from the runway threshold and with a 2σ dispersion of 1500 ft about the nominal touchdown point (AC 20-57A [Ref. 6])

*For a medium large jet transport (e.g., DC-8 Series 60) this distance results from applying the requirement that the pilot be able to see at least four bars of the 3000-ft touchdown zone lights on 100-ft centers.

touchdown footprint dimension must accomodate:

- Errors in aligning the actual mean path with the commissioned or desired angle, and
- Deviation of the indicated center of the Glide Slope from the actual mean path, both of which shift the center of the window horizontally with respect to the runway without the pilot's knowledge, and
- Additional wind, wind shear and turbulence induced dispersion.

The effect of the first item on system landing tends to be minimal since the mean glide path asymptote remains focussed upon the GPIIP regardless of the actual mean path angle. This point will be explained further in discussion of Table 9 below. However, the latter two items are genuine concerns.

Figures D-5, 6, 9, 10, 13, 14, 17 and 18 of Appendix D support the " $\pm 35 \mu A$ or ± 12 ft, whichever is larger" Glide Slope tracking error performance requirement. These values should be interpreted as 2σ levels since the probability of missed approach of 5 per cent has been selected to correspond to the ± 12 ft indicated Glide Slope deviation dimension of the window at the decision height.

The requirement for repeatable touchdown on the runway within the longitudinal limits 200 ft and 2500 ft from the runway threshold and with a 2σ dispersion of 1500 ft about the nominal touchdown point is assumed to be a fundamental and absolute performance requirement in this study.

A second dimension of the window that an aircraft must be within at the decision height on a Category II approach is given by a tolerance upon airspeed deviation. The airspeed deviation, exclusive of turbulence effects, must be within ± 5 kts (± 8.45 ft/sec) in order to continue the approach (Ref. 12 and 19).

The results of the system analysis indicated that airspeed deviation, exclusive of turbulence effects, is virtually always within the ± 5 kts tolerance for the autothrottle control laws investigated.

The approach window is the same for all air carrier and general aviation

airplanes and control systems. Presumably the FAA had in mind a typical jet transport when it devised the window. However, given the operational objective, it is easy to imagine an airplane plus controller for which the given window is too restrictive, as well as an airplane plus controller for which it is too permissive. The idea that a single window may not be appropriate for all airplanes and control systems was the motivation behind the study reported in Ref. 7. The primary purpose of that study was to determine how logically to set the decision height window boundaries for any given airplane plus control system.

ILS FLIGHT INSPECTION STANDARDS REVIEW

Current tolerances for ILS Glide Slope structure are based on the desire to restrict aircraft path deviations caused by beam roughness, scalloping, and bends to specific vertical displacements throughout the approach to ILS Point C* for Category I facilities and throughout the approach to runway threshold for Category II and III facilities. (Normally, self-contained airborne flare guidance replaces Glide Slope guidance beyond the runway threshold.)

Table 9 summarizes the salient ILS Glide Slope standards. Part a. of Table 9 gives the ICAO standards, and part b. gives the FAA standards which are subjects for this study.

Several standards in Table 9 are worth comparing with some of the overall system performance standards in Table 7.

The tolerance on deviations of mean path angle with respect to the commissioned glide path angle in Approach Zone (Item 2 in Table 9) is ± 7.5 percent of the commissioned angle for Category I and II and ± 4 percent for Category III.

The rather appreciable tolerances on deviation of the mean path angle in Approach Zones 2 and 3 (by comparison in comparable units with the tolerance on overall Glide Slope tracking performance with respect to the indicated

*Definitions for ICAO and FAA terminology used in the respective standards are given in Table 8.

TABLE 8

ICAO AND FAA DEFINITIONS USED IN CONNECTION WITH
GLIDE SLOPE STANDARDS

ICAO

FAA

Facility Performance Category I - ILS

An ILS which provides guidance information from the coverage limit of the ILS to the point at which the localizer course line intersects the ILS glide path at a height of 60 metres (200 ft) or less above the horizontal plane containing the threshold.

Note. - This definition is not intended to preclude the use of Facility Performance Category I - ILS below the height of 60 metres (200 ft), with visual reference where the quality of the guidance provided permits, and where satisfactory operational procedures have been established.

Facility Performance Category II - ILS

An ILS which provides guidance information from the coverage limit of the ILS to the point at which the localizer course line intersects the ILS glide path at a height of 15 metres (50 feet) or less above the horizontal plane containing the threshold.

Facility Performance Category III - ILS

An ILS which, with the aid of ancillary equipment where necessary, provides guidance information from the coverage limit of the facility to, and along, the surface of the runway.

ILS Point "A"

A point on the ILS glide path measured along the extended runway centre line in the approach direction a distance of 4 nautical miles from the threshold.

Performance Category I - ILS

An ILS which provides acceptable guidance information from the coverage limits of the ILS to the point at which the localizer course line intersects the glide path at a height of 100 feet above the horizontal plane containing the runway threshold.

Performance Category II - ILS

An ILS which provides acceptable guidance information from the coverage limits of the ILS to the point at which the localizer course line intersects the glide path at a point above the runway threshold.

Category II Training - ILS

A Category I operational use facility with performance within the standards for Category II and which is advertised as acceptable for Category II qualification training.

ILS Point "A"

An imaginary point on the glide path/localizer course measured along the runway centerline extended, in the approach direction, 4 nautical miles from the runway threshold.

TABLE 8 (CONT'D.)

ICAO

ILS Point "B"

A point on the ILS glide path measured along the extended runway centre line in the approach direction a distance of 1050 metres (3500 feet) from the threshold.

ILS Point "C"

A point through which the downward extended straight portion of the nominal ILS glide path passes at a height of 30 metres (100 feet) above the horizontal plane containing the threshold.

ILS Glide Path Angle

The angle between a straight line which represents the mean of the ILS glide path and the horizontal.

ILS Reference Datum

A point at a specified height located vertically above the intersection of the runway centre line and the threshold and through which the downward extended straight portion of the ILS glide path passes.

Half Glide Path Sector

The sector in the vertical plane containing the ILS glide path and limited by the loci of points nearest to the glide path at which the DDM is 0.0875.

ILS Glide Path Sector

The sector in the vertical plane containing the ILS glide path and limited by the loci of points nearest to the glide path at which the DDM is 0.175.

(see on next page)

FAA

ILS Point "B"

An imaginary point on the glide path/localizer course measured along the runway centerline extended, in the approach direction, 3500 feet from the runway threshold.

ILS Point "C"

A point through which the downward extended straight portion of the glide path (at the commissioned angle) passes at a height of 100 feet above the horizontal plane containing the runway threshold.

Actual Glide Path Angle

The straight line arithmetic mean of all deviations of the differential trace occurring in ILS Approach Zone 2.

Desired Path Angle

During site, commissioning or commissioning-type inspections, the angle required for the procedural use of the facility.

Threshold Crossing Height

The height of the straight line extension of the glide path above the runway centerline at the threshold.

Glide Path Sector Width

(Normal Approach Envelope)

The width of a sector in the vertical plane containing the glide path and limited by the loci of points above and below the path at which a reading of 75 microamperes is obtained. (Nominally, 150 microamperes corresponds to 0.175 DDM).

TABLE 8 (CONT'D.)

ICAO

FAA

Note - The ILS glide path sector is located in the vertical plane containing the runway centre line, and is divided by the radiated glide path in two parts called upper sector and lower sector, referring respectively to the sectors above and below the glide path.

Angular Displacement Sensitivity

The ratio of measured DDM to the corresponding angular displacement from the appropriate reference line.

DDM - Difference in Depth of Modulation

The percentage modulation depth of the larger signal minus the percentage modulation depth of the smaller signal, divided by 100.

ILS Glide Path

That locus of points in the vertical plane containing the runway centre line at which the DDM is zero, which, of all such loci, is the closest to the horizontal plane.

ILS Approach Zone 1

The distance from the coverage limit of the localizer/glide path to Point "A" (four miles from the runway threshold).

ILS Approach Zone 2

The distance from Point "A" to Point "B".

ILS Approach Zone 3

The distance from Point "B" to Point "C" for evaluations of Category I and Category II training systems. The distance from Point "B" to the runway threshold for evaluations of Category II operational systems.

TABLE 8 (CONCLUDED)

ICAO

FAA

**Change/Reversal in Slope of the
Glide Path**

A long term (1500 feet or more) change in the direction of the "on path" position as determined by the graphic averaging of the short term (roughness, high frequency scalloping) deviations of the differential trace.

Graphical Average Path

The average path described by a line drawn through the mean of all deviations in the differential trace; i.e., deviations are balanced about the graphical average path. This will usually be a curved line which follows long term trends (1500 feet or greater) and averages shorter term deviations in the differential trace.

Trend

The general direction or incline of a segment of the glide path which persists for a distance of 1500 feet or more along the approach course.

Differential Trace

The trace on the recording which is the algebraic sum of the Radio Telemetering Theodolite (RTT) crosspointer (DDM) and the aircraft receiver crosspointer (DDM) and which is produced by the differential amplifier within the airborne Theodolite Recording System (TRS).

Categorization

A "special" comprehensive evaluation of the quality of a commissioned Category I facility in order to determine if its performance is within Category II standards.

TABLE 9a. SALIENT ICAO CLITE PATH STANDARDS FOR
THE SIGNAL IN SPACE (Ref. 4)

ICAO ILS PERFORMANCE CATEGORY			
		II	
		I	III
1.	Commissioned Angle, θ ; Operationally Permitted Angle, $2.5 \leq \theta \leq 3 \text{ deg}$ (Para. 3.1.4.1.2.1, Att. C Para. 2.4.2) Exceptional Angle, $3 < \theta \text{ deg}$	No Tolerance	No Tolerance
2.	Tolerance on deviations of mean path angle with respect to θ between ILS Point A and ILS Point B (Att. C Para. 2.4.12)	$\pm 0.075 \theta$	$\pm 0.04 \theta$
3.	ILS reference datum (runway threshold crossing height) (Para. 3.1.4.14, Att. C Para. 2.4.10)	$50 \pm 10 \text{ ft}$	$50 \pm 10 \text{ ft}$
4.	Tolerance on deviations of mean path angle with respect to θ between ILS Point B and ILS Point C (Cat. I) or the runway threshold (Cat. II and III)	No Limits	No Limits
5.	Tolerance on deviations with respect to mean path. At a ground speed of $100 \pm 5 \text{ kts}$, if the path deviation within each mutually exclusive 40-sec time interval "window" centered about a region where the tol- erance is exceeded is out of tolerance for an interval of time ≤ 5 percent of the total time window, the path deviation is acceptable. (At other ground speeds, the total time window will be prorated to provide the equivalent of a $700 \pm 338 \text{ ft}$ distance window.) (Para. 3.1.4.4, Att. C Para. 2.1.5 and 2.1.6)	$\pm 30 \mu\text{A}$ ($\pm 0.035 \text{ DDM}$) to ILS Point C from outer limits of coverage	Limits for Category II apply with the additional requirement that trans- mitter signal fluctuations will not exceed $\pm 17 \mu\text{A}$ (0.02 DDM) peak-to-peak frequency band from 2.01 Hz (0.0628 rad/sec) to 10 Hz (62.8 rad/sec). (Para. 3.1.4.2.3)
6.	Nominal angular displacement sensitivity for the facility should be selected so that $70 \mu\text{A}$ (0.07 DDM) above or below path corresponds to 0.12θ within the tolerances given at the right (Para. 3.1.4.6.1, 2, 3 and 4)	Above and below path $\pm 0.02 \theta$, -0.05θ ($\pm 0.02 \theta$ recommended)	Above Path $\pm 0.02 \theta$, -0.05θ Below Path $\pm 0.02 \theta$
7.	Tolerance on angular displacement sensitivity with respect to the nominal value for the facility.	$\pm 25 \text{ percent}$ (Para. 3.1.4.6.6)	$\pm 15 \text{ percent}$ (Para. 3.1.4.6.5)

TABLE 9b. SALIENT FAA GLIDE PATH STANDARDS FOR
THE SIGNAL IN SPACE (Ref. 5)

FAA ILS PERFORMANCE CATEGORY			
	I	II	
		No Tolerance	.TIA
1. Commissioned Angle, θ Operationally Preferred Angle, $2.5 \leq \theta \leq 3$ deg Exceptional Angle, $2 < \theta < 2.5$ deg (AC 120-29, Chg. 1, App. 2, p. 12)	No Tolerance	No Tolerance	No Tolerance
2. Tolerance on deviations of mean path angle with respect to θ in Approach Zone 2 (OA P 8200.1, Chg. 17, Para. 217.5 (14) (b) (5) and (4))	$\pm 0.075 \theta$	$\pm 0.075 \theta$	(Not yet published)
3. Runway threshold crossing height (AC 120-29, App. 2, p. 12)	50 ft nominal; no tolerance	50 ± 10 ft	(Not yet published)
4. Tolerance on deviations of mean path angle with respect to θ in Approach Zone 3 (OA 8200.1, Chg. 17, Para. 217.5 (14)(b)(5)) $\pm 20 \mu A$ about the actual (mean) path at ILS Point B to the values listed at Point C; thereafter constant from Point C to the threshold. The tolerance at ILS Point C to the threshold is determined with respect to the commissioned angle.	No limits other than the "departure of the graphical average path shall be smooth and continuous within the rate of change tolerance" of 5. below.	Below the Commissioned Angle Threshold Crossing Limit at Point C Height 55'-60' 54' 53' 50'-52' 47'-49' Above the Commissioned Angle 58'-59' 56'-57' 55'-55' 47'-52' 10 μA 20 μA 30 μA 40 μA	(Not yet published)
5. Maximum allowable deviations with respect to mean path and change/reversal in the slope (OA P 8200.1, Chg. 17, Para. 217.5 (16)(a)). At a ground speed of 105 ± 5 kts, if the path deviation within each mutually exclusive 40-sec time interval "window" centered about a region where the tolerance is exceeded is out of tolerance for an interval of time ≤ 5 per cent of the total time window, the path deviation is acceptable.	$\pm 30 \mu A$ Change in Slope $\leq 25 \mu A/kft$ from OM or Point A, whichever is further, to Point C	$\pm 30 \mu A$ in Approach Zone 1 $\pm 30 \mu A$ decreasing linearly to $\pm 20 \mu A$ at Point B in Approach Zone 2 $\pm 20 \mu A$ in Approach Zone 3 Change in Slope same as for Cat. I	(Not yet published)
6. 75 μA half-width of glide path, $W/2$: $1.5 \leq W \leq 0.9$ deg; Optimum $W = 0.7$ deg Tolerance on symmetry of distribution of W above/below "on path" position (OA P 8200.1, Chg. 17, Para. 217.5 (14)(a))	$40\% \leq$ above $\leq 60\%$ $40\% \leq$ below $\leq 60\%$	$45\% \leq$ above $\leq 55\%$ $45\% \leq$ below $\leq 55\%$	(Not yet published)
7. Nominal angular displacement sensitivity: $0.0875 \text{ NM} = 75 \mu A = W/2$. Tolerance on angular displacement sensitivity (OA 8200.1, Chg. 17, Para. 217.5(14)(3)).	No Tolerance	No Tolerance	(Not yet published)

on-path position) might seem to result in a position reference in space which may vary considerably with respect to the runway. Furthermore, variability of the mean position of the path in space is unknown to the pilot under IFR conditions. However, the results of the system analysis indicate touchdown dispersion is relatively insensitive to variability of the mean path angle. This is because all mean paths emanate from the same point. This being the case, the major contribution to touchdown dispersion from this source is the result of inconsistency of the approach speed (because it is based upon commissioned angle rather than the actual mean path angle) for use with a given flare control law.

The mean touchdown point, which depends upon GPIIP location along the runway centerline, has a significant influence on the ability of the overall system to meet the requirement that the longitudinal 2σ touchdown footprint be contained in the interval from 200 ft to 2500 ft from the runway threshold. (Refer to Table 7.) This, in turn, requires that the GPIIP be located in the interval from 900 ft to 1200 ft assuming the flare results in a mean touchdown point at least 50 ft, but no more than 550 ft, beyond the GPIIP. Furthermore, the combination of GPIIP location, elevation of the GPIIP with respect to the runway threshold, and commissioned or desired angle must result in a threshold crossing height which equals or exceeds $(TCH)_{min}$. The GPIIP, in turn, is determined by the effective pedestal height of the runway, the commissioned or desired angle and the longitudinal displacement of the Glide Slope antenna mast from the runway threshold, and is therefore controlled by the antenna siting.

The tolerance on beam deviations with respect to the mean path has been previously compared with the system analysis results in Fig. 12 and 13. The current Category I structure standard is conservative with respect to the system analysis result in Approach Zones 2 and 3. The current Category II structure standard is slightly more permissive than the system analysis result throughout most of Approach Zone 2. At the end of Zone 2 and throughout Approach Zone 3, the current standard becomes increasingly conservative (restrictive) as the runway threshold is approached.

Some of the tolerances upon glide path alignment in paragraph 217.5 (14) b of Ref. 5 have been superseded by Change Order 8240.29, Ref. 21. Table 9b has been constructed on the basis of paragraph 217.5 (14) b. A summary and

comparison of the revised standards with their predecessors is given in Table 10.

This standard has been previously compared with a roughly equivalent result from the system analysis in Fig. 15. The standard is conservative throughout Approach Zone 3 with respect to the system analysis result. Since the system analysis indicates landing performance is insensitive to variability in the mean path, the limits of the standard in Approach Zone 2 are not crucial.

GLIDE PATH RECEIVER STANDARDS

The salient airborne glide path receiver standards are given in Table 11. The tolerance which is the primary concern is the one on centering error. The centering error tolerance affects the apparent mean glide path as perceived by the airborne system. Its effect upon system performance is therefore analogous to the effect of deviations of the mean path angle with respect to the commissioned angle in Zone 2.

The current glide path receiver centering error standard is conservative. (Refer to the discussion accompanying Eq 23 in Section III.) The suggestion is made in Section III in connection with Eq 24 that the glide path receiver centering error be incorporated as a component of an overall tolerance upon airborne system performance as reflected in requirements for a minimum threshold crossing height.

Glide path receiver centering error does not otherwise affect landing performance in a sensitive way. This is because receiver centering error is similar in its effects to error in aligning the beam with the commissioned angle.

TABLE 10

SUMMARY OF RECENT CHANGES ON CATEGORY II
 ILS GLIDE PATH TOLERANCES RESULTING
 FROM CHANGE ORDER 8240.29 (Ref. 21)

<u>Item</u>	<u>8240.29</u>	<u>Superceded Standard</u>
Tolerance on deviations of mean path angle with respect to Θ in Approach Zone 2	$\pm 37.5 \mu A$	$\pm 0.075 \Theta$ (approximately $\pm 48.2 \mu A$)
Tolerance at Runway threshold crossing	$\pm 75 \mu A$	See Table 9b, Item 4, Category II.
Tolerance on deviations of mean path angle with respect to Θ in Approach Zone 3	$\pm 37.5 \mu A$ at ILS Point B increasing linearly to $\pm 48.75 \mu A$ at ILS Point C, thence increasing linearly to $\pm 75 \mu A$ at the runway threshold	$\pm 20 \mu A$ <u>with respect to mean path</u> at ILS Point B, increasing linearly to values given in Table 9b, Item 4, Category II.

TABLE 11

SALIENT AIRBORNE GLIDE PATH RECEIVER STANDARDS
(RTCA DO-132 [Ref. 22] and FAA AC 20-57A [Ref. 6])

Centering Error (2σ)

A/C Stall Speed (V_{SO})	Cat I	Cat II	Cat III
$V_{SO} < 55$ kts	20 μ A	16 μ A	10 μ A
$55 \leq V_{SO} \leq 95$ kts	16 μ A	13 μ A	↓
$95 \text{ kts} < V_{SO}$	13 μ A	10 μ A	

Standard Deflection (75 μ A at 700 μ V input signal level) Deviation
 $\pm 11 \mu$ A over an input signal range from 100 to 10,000 μ V

Deflection Balance (Polarity Reversal) Error $< 3 \mu$ A

Visual Glide Slope Deviation Indication

Range $\pm \frac{5}{8}$ inch = 150 μ A

Linearity over the range $\pm 150 \mu$ A : < 10 per cent of signal
or $< 3.75 \mu$ A, whichever is greater; monotonic beyond the range
 $\pm 150 \mu$ A to a value of 0.8 DDM; and over an input signal range
from 100 to 10,000 μ V

Step response from 0 to any |value| $< 150 \mu$ A: $T = 2$ sec with
overshoot < 5 per cent of final value

Autopilot/Coupler Glide Slope Deviation Output

Linearity same as above

Step response from 0 to any |value| $< 150 \mu$ A : $T = 0.6$ sec
with overshoot < 2 per cent of final value

SECTION V

CONCLUSIONS

This Section provides an outline summary of the major conclusions reached as a result of the research and system study reported here.

Standards of Concern in this Research

Overall System Approach and Landing Performance

- Pilot acceptance of pitch attitude and normal acceleration variability on approach
- Glide Slope tracking precision for Category II and III approaches
- Longitudinal touchdown dispersion and location limits

IIS Glide Slope Siting

- Minimum and maximum threshold crossing height

Flight Inspection of the IIS Glide Slope

- Theodolite placement
- Mean beam alignment
- Beam structure
- Beam slope changes/reversals
- Beam off-path sensitivity/linearity

Airborne Glide Path Receiver

- Centering accuracy
- Off-path sensitivity/linearity

Results of System Analysis to Establish Most Permissive Tolerances Upon IIS Glide Slope Characteristics

Category I Facilities

- Pitch attitude excursions during final approach limit relaxation of IIS Glide Slope standards for jet transport Category I operations

Category II and III Facilities

- Category II and III requirements upon ILS Glide Slope alignment and structure are identical
- ILS Glide Slope beam alignment is critical (for clearance in the "low" direction and for sink rate arrest in flare in the "high" direction) only for values beyond those investigated
- Category II and III approaches which would result in excessive touchdown dispersion are converted to missed approaches at the Category II Decision Height
- Missed approach probability in excess of 5 per cent limits relaxation of the ILS Glide Slope specification for jet transport Category II and III operations
- Landing performance for jet transport Category II operations is similar for automatic or manual flight director approach and landing, and for direct or inertially smoothed coupling to the Glide Slope
- Inertial smoothing gives a reduction in touchdown dispersion
- Manual landing gives a small reduction in touchdown dispersion
- Touchdown dispersion limits Category II landing performance for low wing-loading straight-wing aircraft
- Missed approaches and touchdown dispersion for low wing-loading, straight-wing aircraft arise almost entirely from wind, wind shear and gusts
- The existing Category II Glide Slope tracking accuracy requirement is probably inappropriate for low wing-loading straight-wing aircraft

Recommended Changes for Flight Inspection

Data Collection and Processing

- Place theodolite to minimize deviations arising from the "pedestal effect"
- All signals currently oscillograph recorded plus barometric altitude should be recorded directly onto magnetic tape
- Three additional signals representing typical aircraft glide path indicated deviation, actual deviation, and deviation rate responses should be generated by filtering the "differential trace"

Data Analysis

- Standards evolved from the system performance analysis and based upon 2σ statistics appropriate to safe landing should be used
- Standards should be applied to the typical aircraft actual glide path deviation and deviation rate traces as well as to the typical indicated glide path deviation trace
- Separate ILS Glide Slope standards are not necessary to determine beam suitability for different user airborne system configurations
- Analysis of beam characteristics should be based upon a 5 per cent criterion: The $\pm 2\sigma$ level for each trace shall not be exceeded for more than 5 per cent of the critical trace interval
- $\pm 2\sigma$ levels appropriate to each trace should be inscribed on transparent overlays to facilitate application of the 5 per cent criterion to the oscillograph traces

Tolerance on ILS Glide Slope

Structure, Slope Changes/Reversals

- Existing Glide Slope standards for Category I and II facilities may be relaxed considerably between ILS Point B and ILS Point C for Category I facilities, or the runway threshold for Category II facilities
- Category I standards may be relaxed slightly in Zone 2
- Category II standards may need to be slightly tightened in Zone 2
- Additional standards should be placed upon filtered versions of the "differential trace" which represent typical aircraft glide path indicated deviation, actual deviation and deviation rate responses
- Category II and III standards should be identical

Tolerance on ILS Glide Slope Alignment

- Existing Glide Slope alignment standards may be relaxed to the extent that they are not clearance related and do not produce excessive sink rate at flare initiation

IIS Glide Slope Siting

- A standard specifying limits for GPIF location should replace the use of limits upon threshold crossing height for this purpose. (Specification of a minimum threshold crossing height should be retained to provide adequate wheel clearance, however.)

APPENDIX A

ANALYSIS OF THE COLLINS RADIO CO.

GLIDE SLOPE DATA

This Appendix describes the objectives of the analysis, the approach followed, and the technical details for the individual steps of the approach as well as the results.

OBJECTIVES OF ANALYSIS

The objectives of the nonstationary statistical analysis of the Collins Radio Co. Glide Slope data are as follows:

- Extract the mean and variance for each segment of each record. Compute ensemble average mean and variance for corresponding segments of the records
- Extract the power spectral density for each segment of each record. Compute the ensemble average power spectral density for corresponding segments of the records.

APPROACH FOR ANALYSIS OF DATA

The planned approach has two main facets. The first facet involves estimating means and variances; the second involves estimating the power spectral densities.

Estimation of Means and Variances

Editing and segmenting extant data records

- i. The existing records will be edited so that samples subsequent to runway threshold crossing are eliminated. If the data does not extend to runway threshold crossing (as in Trace No. 4, Fig. 4 of Ref. 9), the data will be reflected about the existing endpoint to fill the void.
- ii. The existing records will be edited to a uniform even number of samples corresponding to a 160 second interval. The number of samples is 1120 based upon a nominal sampling rate of 7 samples per second (Ref. 9). If the data does not extend backward from the runway threshold crossing for 1120 samples (as in Trace No. 20, Fig. 6, and Trace No. 24, Fig. 7, of Ref. 9), the data will be reflected about the existing endpoint in order to fill the void.

iii. The individual data records are culled to assure face validity. The culling process eliminates records for which theodolite placement was not according to current standard procedure, or in which there are significant voids, significant error in aircraft tracking of the ILS Glide Slope or significant error in theodolite tracking of the aircraft. Seventeen records survive the culling process. These are record numbers 2 through 7, 12, 15 through 18, and 20 through 25 of Fig. 4 through 6 in Ref. 9.

iv. Each record is stored in a file with a name embodying codes enabling programmed calls for operation upon that file by various statistical subroutines. Necessary arguments in the file name will indicate

D A time record data file (in distinction to, say, a Fourier Transform file)

NR Source record number

NI Inter-record set identifier

ND Record set identifier (All records analyzed belong to a single set.)

via D(NR, NI, ND) or similar. The variable, time, is regarded as zero at the runway threshold end of the edited record, and increases in the direction of the outer marker. That is, "time" is "time to go until runway threshold crossing." The data file is a sequence of samples stored in this order. Actual segmenting is as follows.

<u>Segment Length (sec)</u>	<u>Segment Center Time (sec)</u>	<u>Segment Order Number</u>	<u>First Point At Time (sec)</u>	<u>Last Point Before Time (sec)</u>
64	32	1	0	64
↓	64	2	32	96
↓	96	3	64	128
↓	128	4	96	160
8	4	1	0	8
↓	8	2	4	12
↓	12	3	8	16
↓	16	4	12	20
↓	20	5	16	24
↓	24	6	20	28
↓	28	7	24	32
↓	32	8	28	36
↓	36	9	32	40
↓	40	10	36	44
↓	44	11	40	48
↓	48	12	42	52

Computation of means and variances for individual records

- i. The estimate of the mean for each record segment is computed according to

$$\hat{\mu}_r(NS, NC, NI, ND) = \frac{1}{7NS} \sum_{i=NF}^{NT} D_i(NR, NI, ND) \quad (A-1)$$

where:

$$NF = 7(NC - NS/2) + 1$$

$$NT = 7(NC + NS/2)$$

$$NC = \text{Record segment center time (sec)}$$

$$NS = \text{Record segment length (sec)}$$

- ii. The estimate of the variance for each record segment is computed according to:

$$\hat{\sigma}_r^2(NS, NC, NI, ND) = \frac{1}{7NS-1} \sum_{i=NF}^{NT} [D_i(NR, \dots) - \hat{\mu}_r(NS, \dots)]^2 \quad (A-2)$$

- iii. The data for $\hat{\mu}_r$ and $\hat{\sigma}_r$ are listed for each record in the following format.

GLIDE SLOPE		NR	MEAN AND VARIANCE	
		NS	8 Sec Window	
Time (Sec)	Mean (MU A)		Standard Deviation	Variance (MU A)**2
4	$\hat{\mu}_r(NR, 8, NC, ND)$		$\hat{\sigma}_r(NR, 8, NC, ND)$	$\hat{\sigma}_r^2(NR, 8, NC, ND)$
8	↓		↓	↓
12				
.				
.				
.				
NC				
.				
.				
.				
40				
44				
48	$\hat{\mu}_r(NR, 8, NC, ND)$		$\hat{\sigma}_r(NR, 8, NC, ND)$	$\hat{\sigma}_r^2(NR, 8, NC, ND)$

GLIDE SLOPE

NR

MEAN AND VARIANCE

 $\frac{NS}{64}$ Sec Window

Time (Sec)	Mean (MU A)	Standard Deviation	Variance (MU A)**2
32	$\hat{\mu}_r(NR, 64, NC, ND)$	$\hat{\sigma}_r(NR, 64, NC, ND)$	$\hat{\sigma}_r^2(NR, 64, NC, ND)$
.	↓	↓	↓
.			
NC			
.			
.			
128	$\hat{\mu}_r(NR, 64, NC, ND)$	$\hat{\sigma}_r(NR, 64, NC, ND)$	$\hat{\sigma}_r^2(NR, 64, NC, ND)$

ESTIMATED VARIABILITY FOR $\frac{NS}{64}$ SEC WINDOW

Time (Sec)	0.95 Confidence ± Variability About Mean (MU A)	0.95 Confidence Variability About Standard Deviation (MU A)
32	$0.52\hat{\sigma}_r(NR, 64, NC, ND)$	$(\sqrt{2.4}-1)\hat{\sigma}_r(NR, 64, NC, ND)$
.	↓	↓
.		
NC		
.		
.		
128	$0.52\hat{\sigma}_r(NR, 64, NC, ND)$	$(\sqrt{2.4}-1)\hat{\sigma}_r(NR, 64, NC, ND)$

Number of Ensemble Members = 1

Degrees of Freedom = 15.3

Based Upon WE = 0.25*PI

There is no estimated variability for the 8 second window results because there are only 1.33 degrees of freedom for each of these computed statistics. Hence the variability is very large.

Computation of means and variances for ensembles of records

- i. The estimate of the ensemble mean for corresponding record segments is computed according to:

$$\hat{\mu}(NS, NC, ND) = \frac{1}{NND} \sum_{NI=1}^{NND} \hat{\mu}_r(NS, NC, NI, ND) \quad (A-3)$$

where NND is the number of records in the set designated by ND.
(NND = 17)

- ii. The estimate of the ensemble variance for corresponding record segments is computed according to:

$$\hat{\sigma}^2(NS, NC, ND) = \frac{1}{7 NS NND - 1} \sum_{NI=1}^{NND} \sum_{i=1}^{NT} [D_i(NR, NI, ND) - \hat{\mu}(NS, \dots)]^2 \quad (A-4)$$

The variance is also equal to:

$$\begin{aligned} & \frac{1}{7 NS NND - 1} \left[(7 NS - 1) \sum_{NI=1}^{NND} \hat{\sigma}_r^2(NS, \dots) \right] \\ & + \frac{7 NS}{7 NS NND - 1} \left[(NND - 1) \hat{\sigma}_{\bar{\mu}_r}^2(NS, \dots) \right] \quad (A-5) \end{aligned}$$

This may be used to compute the variance, over the record set, of the individual means for each segment, $\hat{\sigma}_{\bar{\mu}_r}^2(NS, NC, ND)$, where:

$$\hat{\sigma}_{\bar{\mu}_r}^2(NS, NC, ND) = \frac{1}{NND - 1} \sum_{r=1}^{NND} [\hat{\mu}_r(NS, \dots) - \hat{\mu}(NS, \dots)]^2 \quad (A-6)$$

iii. The data for $\hat{\mu}$ and $\hat{\sigma}$ is listed in the following format.

GLIDE SLOPE SET $\hat{\mu}$ ENSEMBLE MEAN AND VARIANCE

Time (Sec)	8 NS Sec Window		
	Mean (MU A)	Standard Deviation	Variance (MU A)**2
4	$\hat{\mu}(8, NC, ND)$	$\hat{\sigma}(8, NC, ND)$	$\hat{\sigma}^2(8, NC, ND)$
16	↓	↓	↓
20			
.			
.			
NC			
.	↓	↓	↓
.			
40			
44	↓	↓	↓
48			
	$\hat{\mu}(8, NC, ND)$	$\hat{\sigma}(8, NC, ND)$	$\hat{\sigma}^2(8, NC, ND)$

Time (Sec)	64 NS Sec Window		
	Mean (MU A)	Standard Deviation	Variance (MU A)**2
32	$\hat{\mu}(64, NC, ND)$	$\hat{\sigma}(64, NC, ND)$	$\hat{\sigma}^2(64, NC, ND)$
.	↓	↓	↓
.			
.			
NC			
.			
.	↓	↓	↓
128			
	$\hat{\mu}(64, NC, ND)$	$\hat{\sigma}(64, NC, ND)$	$\hat{\sigma}^2(64, NC, ND)$

ESTIMATED VARIABILITY FOR ^{NS} 8 SEC WINDOW

Time (Sec)	0.95 Confidence ± Variability About Mean (MU A)	0.95 Confidence Variability About Standard Deviation (MU A)
4	$0.32\hat{\sigma}(8, NC, ND)$	$(\sqrt{1.7}-1)\hat{\sigma}(8, NC, ND)$ $(\sqrt{0.67}-1)\hat{\sigma}(8, NC, ND)$
8		
12		
.		
.		
NC		
.		
.		
40		
44		
48	$0.32\hat{\sigma}(8, NC, ND)$	$(\sqrt{1.7}-1)\hat{\sigma}(8, NC, ND)$ $(\sqrt{0.67}-1)\hat{\sigma}(8, NC, ND)$

Number of Ensemble Members = 17

Degrees of Freedom = 38.66

Based Upon WE = $0.25 \cdot \pi$ (rad/sec)

ESTIMATED VARIABILITY FOR ^{NS} 64 SEC WINDOW

Time (Sec)	0.95 Confidence ± Variability About Mean (MU A)	0.95 Confidence Variability About Standard Deviation (MU A)
32	$0.12\hat{\sigma}(64, NC, ND)$	$(\sqrt{1.17}-1)\hat{\sigma}(64, NC, ND)$ $(\sqrt{0.84}-1)\hat{\sigma}(64, NC, ND)$
.		
.		
NC		
.		
.		
128	$0.12\hat{\sigma}(64, NC, ND)$	$(\sqrt{1.17}-1)\hat{\sigma}(64, NC, ND)$ $(\sqrt{0.84}-1)\hat{\sigma}(64, NC, ND)$

Number of Ensemble Members = 17

Degrees of Freedom = 276.66

Based Upon WE = $0.25 \cdot \pi$ (rad/sec)

Estimation of Power Spectral Densities

Editing and prewhitening extant data records

- i, ii, and iii. Items i, ii, and iii under "Editing and segmenting extant data records" apply here also.
- iv. Each record is prewhitened based upon a form of the power spectral density assumed to be representative of the original continuous data. This is accomplished using the second order difference equation, initial conditions and coefficient values given by Eq A-18.

The prewhitening is accomplished with increasing values of i' in the difference equation corresponding to decreasing distance to the runway threshold. Thus i' corresponds to

$$i' = 1121 - i$$

where i is the sample index used previously. The prewhitened data records are stored in files designated P and have the same arguments as the D files. The sequence of the samples in the P file is the same as for the D files.

Segmenting, mean removal and Fourier Transformation of prewhitened data records

1. Segmenting of the prewhitened records is best accomplished by creating conditioned data files, or C files, which are in a form directly usable by a Fast Fourier Transform (FFT) subroutine. FFT subroutines typically require that the mean of each segment to be transformed be zero (or very nearly zero).

The actual segmenting is as follows.

Segment Length (Sec)	Segment Center Time (Sec)	Segment Order No.	First Point At Time (Sec)	Last Point Before Time (Sec)
128	96	1	32	160
64	32	1	0	64
↓	64	2	32	96
	96	3	64	128
32	16	1	0	32
↓	32	2	16	48
	48	3	32	64
	64	4	48	80
↓	80	5	64	96

"Time" in the above table is in the sense of "time to go before runway threshold crossing."

- ii. The mean for each prewhitened segment is computed according to:

$$m(NS, NC, NI, ND) = \frac{1}{7NS} \sum_{i=NF}^{NT} P_i(NR, NI, ND) \quad (A-7)$$

The conditioned data file then consists of sequential entries

$$C_{i''}(NS, NC, NI, ND) = P_i(NR, NI, ND) - m(NS, NC, NI, ND) \quad (A-8)$$

for

$$\begin{aligned} NF &\leq i \leq NT \\ i'' &= i - NF + 1 \end{aligned}$$

Each C file contains exactly 7 NS samples.

Creation of the C files, in effect, executes the prewhitened data record segmenting plan.

- iii. Fourier Transformation of the conditioned data files is accomplished by an algorithm which is equivalent to

$$F_k(NS, NC, NI, ND) = \frac{1}{7} \sum_{i=NF}^{NT} C_i(NS, NC, NI, ND) e^{-j \frac{2\pi k}{7NS} (i - 7NC)} \quad (A-9)$$

for $k = 1, 2, \dots, 7 NS/2$, where $F_k(NS, NC, NI, ND)$ is the complex number in the sequence stored in the F file which corresponds to the angular frequency $2\pi k/NS$. The result of the computation is a Fourier Transform file (the F file). The sequence of entries in this file are the $7 NS/2$ real parts of the Fourier Transform in order of increasing frequency, followed by $7 NS/2$ imaginary parts of the Fourier Transform in order of decreasing frequency. Each F file contains exactly 7 NS points.

c. Forming estimates of the power spectral densities.

i. The double-sided raw power spectral density estimate is given by:

$$\tilde{R}\left(\frac{k}{NS/2\pi}, NS, NC, ND\right) = \frac{1}{NS \text{ NND}} \sum_{NI=1}^{\text{NND}} |\tilde{r}_n(NS, NC, NI, ND)|^2 \quad (\text{A-10})$$

The argument, $k/(NS/2\pi)$, represents discrete angular frequency as the index, k , ranges over:

$$1 \leq k \leq 7NS/2$$

ii. Weighted averaging of the raw power spectral density is used to form estimates of the power spectral density which approximate the deconvolution of the raw power spectral density which itself is a convolution of the effective analysis filter frequency resolution with the true power spectral density. The computations used are

$$\begin{aligned} \tilde{G}\left(\frac{1}{NS/2\pi}, NS, NC, ND\right) &= \frac{2}{3} \tilde{R}\left(\frac{1}{NS/2\pi}, NS, NC, ND\right) \\ &+ \frac{1}{3} \tilde{R}\left(\frac{2}{NS/2\pi}, NS, NC, ND\right) \quad (\text{A-11a}) \end{aligned}$$

$$\begin{aligned} \tilde{G}\left(\frac{k}{NS/2\pi}, NS, NC, ND\right) &= \frac{1}{4} \tilde{R}\left(\frac{k-1}{NS/2\pi}, NS, NC, ND\right) \\ &+ \frac{1}{2} \tilde{R}\left(\frac{k}{NS/2\pi}, NS, NC, ND\right) \\ &+ \frac{1}{4} \tilde{R}\left(\frac{k+1}{NS/2\pi}, NS, NC, ND\right) \quad (\text{A-11b}) \end{aligned}$$

for

$$2 \leq k \leq 7NS/2 - 1$$

and

$$\begin{aligned} \tilde{G}\left(\frac{7NS/2}{NS/2\pi}, NS, NC, ND\right) &= \frac{1}{3} \tilde{R}\left(\frac{7NS/2-1}{NS/2\pi}, NS, NC, ND\right) \\ &+ \frac{2}{3} \tilde{R}\left(\frac{7NS/2}{NS/2\pi}, NS, NC, ND\right) \quad (\text{A-11c}) \end{aligned}$$

- iii. Power spectral density estimates are of most interest when \log_{10} of the power per Hertz is presented as a function of \log_{10} of the angular frequency. Under these circumstances, equally spaced data points are desirable and are used. At high frequencies this allows several points at adjacent frequencies to be averaged with the result that the averaged value is characterized by a greater effective number of degrees of freedom and therefore has lower variability.

This average is computed according to

$$\hat{G}\left(\frac{2^M}{NS/2\pi}, NS, NC, ND\right) = \frac{1}{NTS} \sum_k G\left(\frac{k}{NS/2\pi}, NS, NC, ND\right) \quad (A-12a)$$

for

$$2^{(2M-1)} \leq k^2 \leq 2^{(2M+1)}$$

$$M = 0, 1, 2, \dots, NX$$

$$NS = 2^{NX} - 1$$

where NTS is the number of values in the indicated summation over k. At intermediate points, this average is computed according to

$$\begin{aligned} \hat{G}\left(\frac{\sqrt{2} 2^M}{NS/2\pi}, NS, NC, ND\right) &= \frac{1}{NTS} \left\{ \frac{1}{2} \left[\tilde{G}\left(\frac{2^M}{NS/2\pi}, NS, NC, ND\right) \right. \right. \\ &\quad \left. \left. + \tilde{G}\left(\frac{2^{M+1}}{NS/2\pi}, NS, NC, ND\right) \right] + \sum_k \tilde{G}\left(\frac{k}{NS/2\pi}, NS, NC, ND\right) \right\} \quad (A-12b) \end{aligned}$$

for

$$2^M < k < 2^{M+1}$$

where NTS is one plus the number of values in the indicated summation over k. The effect of frequency averaging is to reduce variability in the power spectral density estimate as the average is extended over increasing numbers frequency points.

- iv. Post-darkening is necessary for removal of the prewhitening effects. The computation for removal of the prewhitening is

$$10 \log_{10} \hat{\phi}(W, NS, NC, ND) = 10 \log_{10} \left\{ \frac{[W^2 + (6.8)^2]^2}{(185.6)^2 [W^2 + (0.25)^2]} \right\} + 10 \log_{10} \hat{G}(W, NS, NC, ND) \quad (A-13)$$

where:

$$W = \frac{1}{NS/2\pi}, \frac{\sqrt{2}}{NS/2\pi}, \dots, \frac{2^M}{NS/2\pi}, \frac{\sqrt{2} 2^M}{NS/2\pi}, \dots$$

W, of course, denotes the angular frequency in radians per second. The data point spacing is shown in Fig. A-1 for NS = 128, 64, 32 seconds.

- v. The data for $\hat{\phi}$ is listed for each of the 9 possible combinations of data window length and data window center time in the following format.

GLIDE SLOPE SET $\hat{\phi}$ POWER SPECTRAL DENSITY

NS 32 Sec Window		NC 48 Sec Window Center Time	
Angular Freq. (Rad/Sec)	PSD (μA)**2/Hz	10*Log(PSD)	
0.196 ...	$\hat{\phi}(W, NS, NC, ND)$	$10 \log_{10} \hat{\phi}(W, NS, NC, ND)$	
:	↓	↓	
W			
:			
17.65	$\hat{\phi}(W, NS, NC, ND)$	$10 \log_{10} \hat{\phi}(W, NS, NC, ND)$	

The power spectral densities are listed for the frequencies at the tick marks in Fig. A-1.

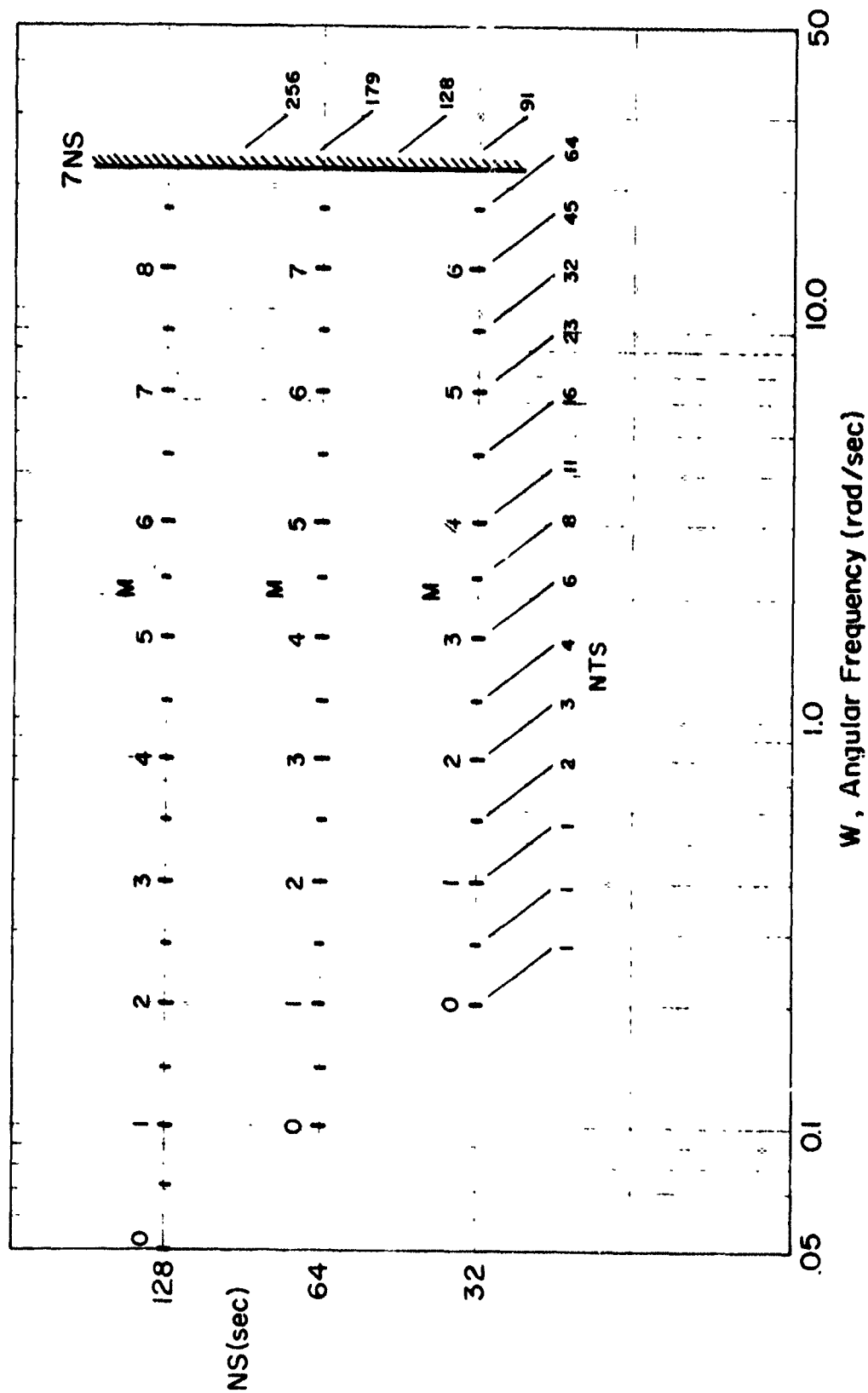


Figure A-1. Frequency Points at Which $\hat{\phi}$ (W, NS, NC, ND) Is Evaluated

TECHNICAL CONSIDERATIONS

A number of technical considerations are involved with various elements of the nonstationary statistical analysis described in the previous section.

Considerations in Computing Estimates of the Mean and Variance

Determination of variability for estimates of the mean and variance

- i. The effective statistical bandwidth, W_e , of a random process is given by (Refs. 24 and 25)

$$W_e = \frac{\left[\int_0^\infty \phi \, d\omega \right]^2}{\int_0^\infty \phi^2 \, d\omega} = WE \quad (A-14)$$

where ϕ is the actual power spectral density of the random process, WE is in angular frequency units, and the mean square value for the process is given by:

$$\sigma^2 = \frac{1}{2\pi} \int_{-\infty}^{\infty} \phi \, d\omega$$

The effective statistical bandwidth plays a key role in establishing the effective number of (measurement) degrees of freedom in a sample of that random process which is T seconds long.

- ii. The effective number of degrees of freedom, κ' , in a sample of the random process characterized by ϕ which is T seconds long is approximated by (Ref. 24)

$$\kappa' = \frac{3TW_e - 2\pi}{3\pi} \quad (A-15)$$

- iii. The total effective number of degrees of freedom, κ , in an ensemble of N members, each of which is characterized by ϕ and each of which is T seconds long is approximated by

$$\kappa = N(\kappa' + 1) - 1 = N \frac{3TW_e - 2\pi}{3\pi} + N - 1 \quad (\text{A-16})$$

The above expression results from the fact that the effective number of degrees of freedom in any single record is one less than the effective number of independent data points in that single record and, in general, the fact that the number of degrees of freedom is one less than the number of independent measurements.

- iv. Confidence intervals for estimates of the mean and variance depend in a key way upon the total effective number of degrees of freedom, κ , for the ensemble under analysis.

The variability in the estimate of the mean is quantified in the following way. The true mean of the process characterized by Φ can be expected to lie within the interval

$$\hat{\mu} \pm \frac{\hat{\sigma} t_{\kappa; \beta/2}}{\sqrt{\kappa + 1}}$$

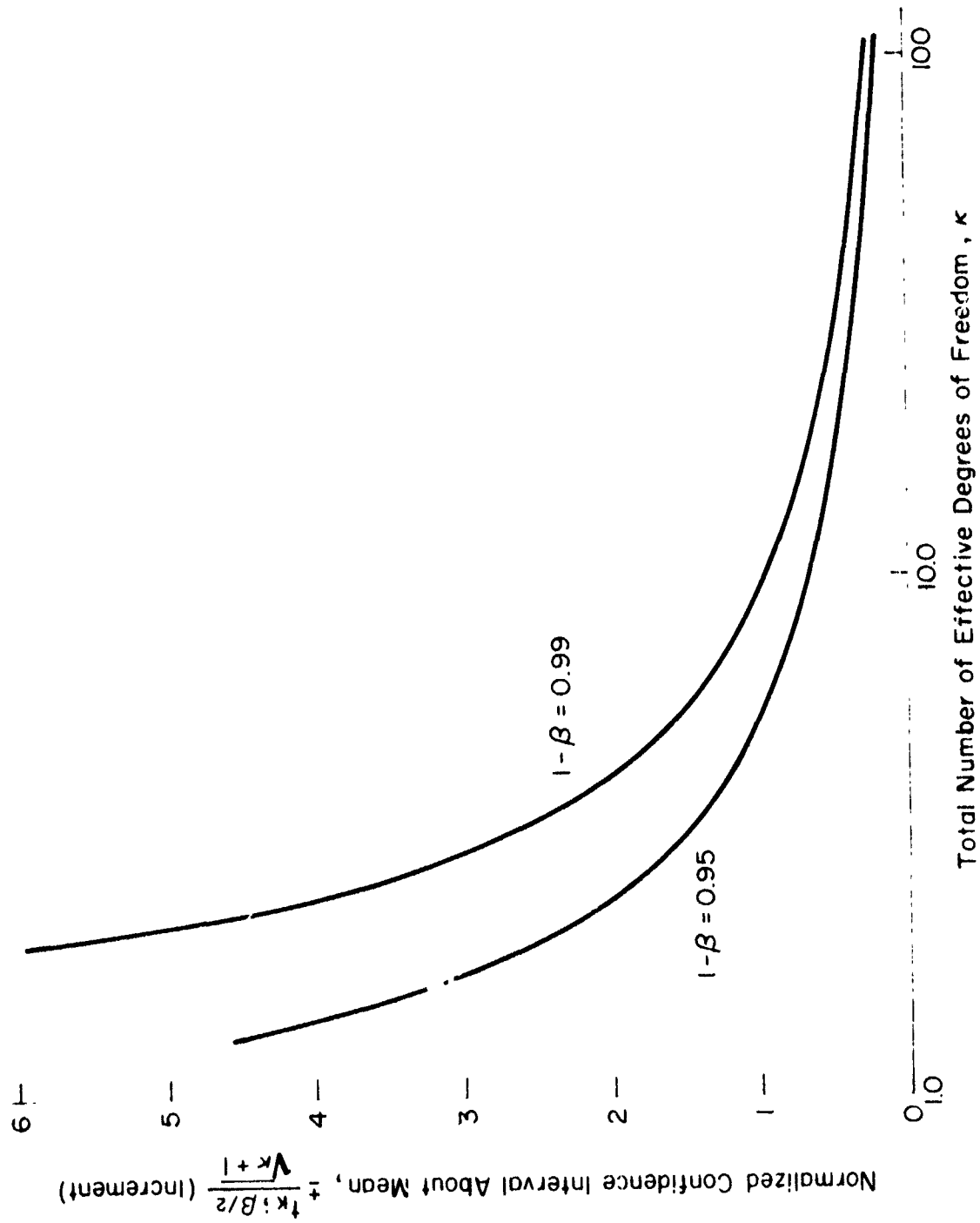
with probability (or confidence level) $1 - \beta$. $t_{\kappa; \alpha}$ is the value of t in the student t -distribution corresponding to the 100 α percentile for κ degrees of freedom.

The variability in the estimate of the variance is quantified in the following way. The true variance of the process characterized by Φ can be expected to lie between the values

$$\frac{\kappa \hat{\sigma}^2}{\chi^2_{\kappa; \beta/2}} \quad \text{and} \quad \frac{\kappa \hat{\sigma}^2}{\chi^2_{\kappa; 1 - \beta/2}}$$

with probability (or confidence level) $1 - \beta$. $\chi^2_{\kappa; \alpha}$ is the value χ^2 in the χ^2 -distribution corresponding to the 100 α percentile for κ degrees of freedom.

Figure A-2 is a plot of the normalized confidence interval increment about the estimated mean for confidence intervals of 0.99 and 0.95. Figure A-3 is a plot of the normalized confidence interval factor for the estimated variance.



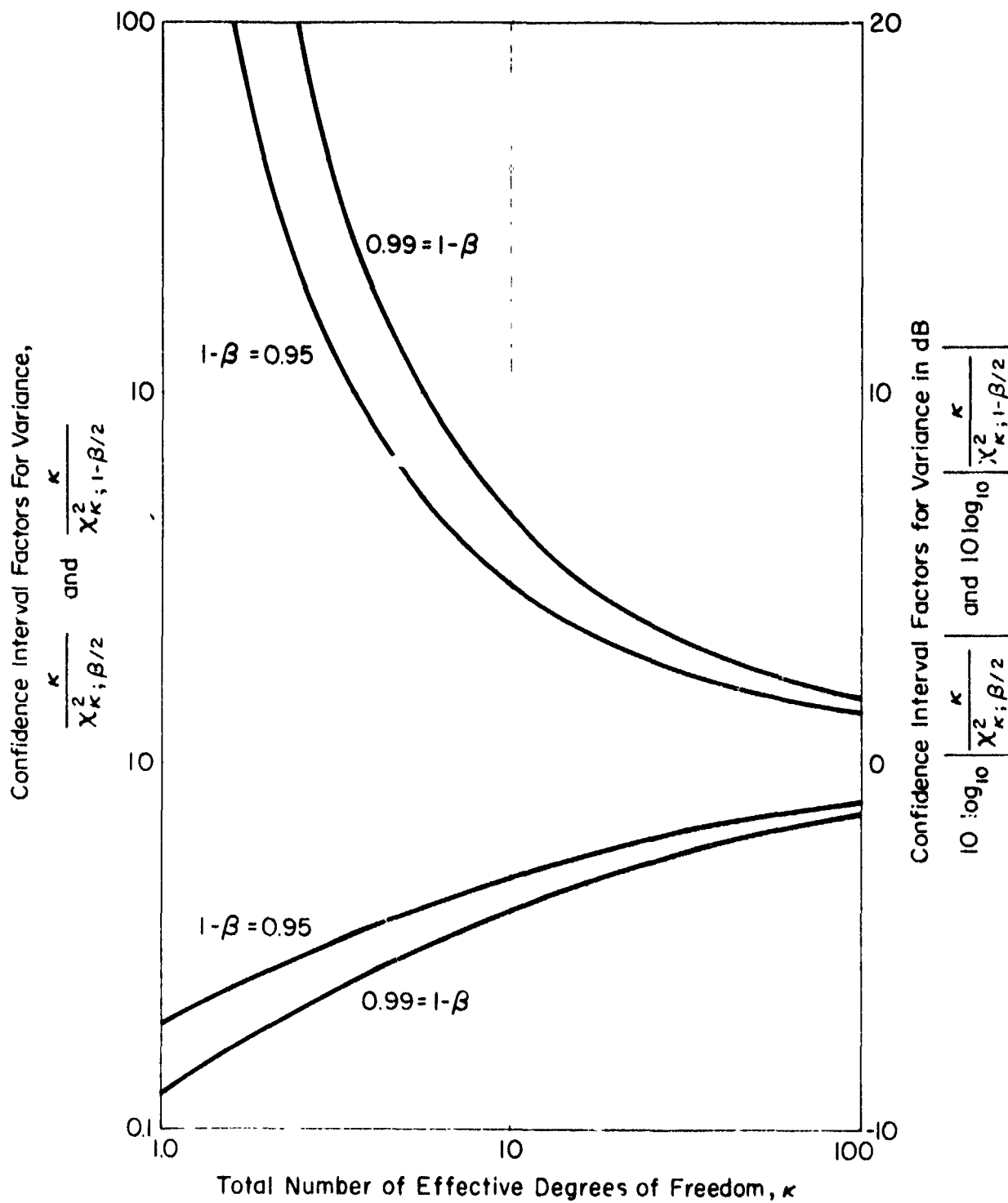


Figure 4-5. Normalized Confidence Interval for Variance as a Function of Total Effective Number of Degrees of Freedom

Considerations in Computing the Power Spectral Density Estimates

Prewhitening of data records

Filtering of time series data records to produce a "prewhitened" record having a nearly constant power density spectrum in the frequency range of interest is necessary in order to form accurate power spectral density estimates. (The final power spectral density estimate must, of course, be "post-darkened" by the inverse of this filtering in order to obtain the estimate of the actual power spectral density.) Prewhitening is required in order to minimize the effects of the non-ideal characteristics of the effective spectral windows. A graphic illustration of the effects prewhitening tends to overcome is given in Fig. 10 of Ref. 24, while a mathematical development which makes the need for prewhitening clear results in Eqs. 15-56 of Ref. 26.

Prewhitening is best applied to the continuous data record. However, in the present case only the sampled records are in hand. Since the Nyquist frequency for the sampled records is well above the frequency range of interest in the analysis, we will apply the prewhitening by means of the difference equation analog to the continuous filter we would have used for the continuous data record.

Reference 11 recommends first order filtered white noise with the filter break frequency set to 0.25 rad/sec as a model for the Glide Slope beam. The prewhitening filter will accordingly be chosen to have the transfer function:

$$185.6 \frac{s + 0.25}{(s + 6.8)^2} = K \frac{(s + b)}{(s + a)^2} \quad (A-17)$$

This will cause the prewhitened data to have an approximately flat power spectral density out to 1/0.6 rad/sec, the break frequency of the ILS receiver filter.

which corresponds to a rectangular data window T seconds long. Q_1 is also the Fourier transform of the effective lag window, D_1 , in the autocorrelation function domain. D_1 , in turn, is the convolution of the rectangular time domain data window with itself. Plots of Q_1 and D_1 are shown in Fig. A-4 which has been reproduced from Ref. 24. The rectangular data window would correspond to the plot of D_0 in Fig. A-4 if τ on the abscissa were replaced by $2(t - NC)$. These relationships are more thoroughly treated on pages 93 through 100 in Ref. 24.

If $\Phi(\omega_1)$ is white noise, then $\Phi(\omega_1) = (\text{const})$, and the fact that $\tilde{R}(\omega)$ results from the convolution of $\Phi(\omega_1)$ with $Q_1(\omega - \omega_1)$ is of little consequence since

$$R(\omega) = (\text{const}) \quad (\text{A-22})$$

because

$$2 \int_{-\infty}^{\infty} Q(\omega - \omega_1) d\omega_1 = 1 \quad (\text{A-23})$$

However, if $\Phi(\omega_1)$ is not white noise, but rather is a function which varies with ω_1 , this convolution distorts the measurement of $\Phi(\omega_1)$ by means of $\tilde{R}(\omega)$, and it may be worthwhile to perform an approximate deconvolution upon $\tilde{R}(\omega)$ in order to form an estimate of $\Phi(\omega_1)$ which is an improvement upon $\tilde{R}(\omega)$. We have selected an averaging process for deconvolution given by

$$y_k = 0.25x_{k-1} + 0.5x_k + 0.25x_{k+1} \quad (\text{A-24})$$

for all points in the sequence x except for the first and last. Figure A-4 shows clearly that a portion of the power which would be included in an ideal spectral window $1/T$ Hz wide is lost, and in its place there appears a portion of the power from the neighboring frequency bands. It is also evident in Fig. A-4 that most of the power from the neighboring frequency bands comes from the adjacent frequency bands.

This argument can be turned around in order to arrive at the rationale for the averaging process. Only a portion (let us say 0.5) of the power in any band $1/T$ Hz wide actually arises in that band, while most of the remaining

The extant data record is a sampled record at 7 samples a second. Prewhitening will be applied to the sampled data record using the difference equation analog of the above transfer function

$$y(i') = C_1 y(i'-1) + C_2 y(i'-2) + D_1 x(i'-1) + D_2 x(i'-2) \quad (A-18a)$$

$$C_1 = 2e^{-a\tau} \quad (A-18b)$$

$$C_2 = -e^{-2a\tau} \quad (A-18c)$$

$$D_1 = K \left[\frac{b}{a^2} + e^{-a\tau} \left(\frac{a-b}{a} \tau - \frac{b}{a^2} \right) \right] \quad (A-18c)$$

$$D_2 = K \left[\frac{b}{a^2} (e^{-a\tau} - 1) - \frac{a-b}{a} \tau \right] e^{-a\tau} \quad (A-18e)$$

$$\tau = \text{sampling interval} = 1/7 \text{ sec}$$

The initial conditions on the filter variables are given by

$$y(0) = y(-1) = x(0) = x(-1) = x(1)$$

where $y(i')$ is the prewhitened sample sequence (for $1 \leq i' \leq 1120$), $x(i')$ is the data record sequence (for $1 \leq i' \leq 1120$) and $x(1)$ is the first data record sample. The choice of $b = 0.25$ rad/sec compensates for the dominant break frequency in the raw record power spectral density. The double lag with $a = 6.8$ rad/sec serves to wash out the lead factor at frequencies well above 1.67 rad/sec where the ILS receiver filter break frequency is located, yet well below the Nyquist frequency, 3.5 Hz or 22 rad/sec, so that additional smoothing is supplied beyond the frequencies of interest in the power spectral density determination.

Post-darkening is applied to the computed, hanned and averaged power spectral density for the prewhitened process. The post-darkening is the square of the inverse of the amplitude ratio as a function of angular frequency for the transfer function given above, namely:

$$\left(\frac{1}{185.6} \right)^2 \frac{[\omega^2 + (6.8)^2]^2}{\omega^2 + (0.25)^2} \quad (A-19)$$

Confidence intervals, when expressed in dB intervals (refer to Fig. A-3), are the same before and after post-darkening since the interval is the product of a constant factor and the power spectral density estimate in either case.

Confidence intervals for power spectral density estimates

- i. The effective statistical measurement bandwidth associated with any single point in the raw power spectral estimate is $2\pi/T$ rad/sec where $T = NS$ is the data window length in seconds.

This determination of the effective statistical bandwidth can be used to determine the total effective number of degrees of freedom per frequency point in the raw power spectral density estimate as was done above for the estimates of the mean and variance.

- ii. Confidence intervals for single frequency points in the raw power spectral density estimate are computed in the same way as for the variance, but using $2\pi/T$ as the effective statistical bandwidth.

For a single record ($N = 1$), the total effective number of degrees of freedom, K , per frequency point in the power spectral density estimate is 1.33; for a nine-record ensemble ($N = 9$) it is 20; while for a seventeen-record ($N = 17$) ensemble it is 38.66. One may refer to Fig. A-3 to determine the corresponding confidence interval. As an example, for $K = 20$, and a 0.95 confidence level, this interval is +3.25 dB, -2.35 dB.

Frequency averaging, which is discussed later, can be used to increase the total effective number of degrees of freedom and hence reduce the confidence interval. However, this is at the expense of resolution in frequency.

Interpretation of the raw power spectral density estimate

It is shown in Ref. 26, page 237, for the case of a continuous record of length T , that the power spectral density estimate is given by

$$\hat{R}(\omega) = 2 \int_{-\infty}^{\infty} \Phi(\omega_1) Q_1(\omega - \omega_1) d\omega_1 \quad (\text{A-20})$$

where $\Phi(\omega_1)$ is the non-ideally prewhitened signal under analysis and Q_1 is the effective spectral window in the frequency domain

$$Q_1(\omega) = \frac{\sin^2 \omega T/2}{\omega^2 T/2} \quad (\text{A-21})$$

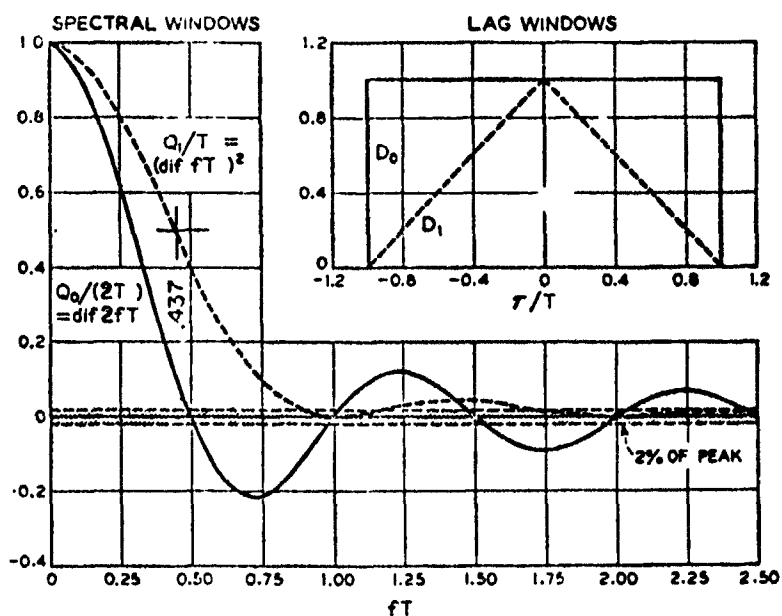


Figure A-4. Lag Windows D_0 and D_1 ; Spectral Windows Q_0 and Q_1 (From Ref. 24)

power (let us say 0.5) which should be in that band is approximately evenly distributed among the two adjacent bands of width $1/T$ Hz.

Frequency averaging of points in the power spectral density estimate

1. When the finite Fourier transform of a sample sequence is used to obtain a power spectral density estimate, calculated values of the estimate occur at equal intervals in frequency. Usually, the interesting characteristics of the power spectral density require its presentation as a function of the logarithm of the frequency. Therefore, calculated values of the estimate tend to be required at equal intervals in the logarithm of the frequency. This fact enables averaging over increasing numbers of calculated values of the estimate with increasing frequency. The result is reduction in the confidence interval for the average as more frequency points are included in the average.

For the above reason, a frequency averaging algorithm has been included which averages all calculated values of the power spectral density estimate which fall within an octave centered on the frequency of interest. The center frequencies chosen start with the lowest frequency point in the power spectral density estimate for a given data window, and occur at every one-half octave frequency interval thereafter until the Nyquist frequency is encountered. This is shown in Fig. A-1.

When the average is computed in this way, every second point in

the averaged power spectral density is independent by virtue of being the average of values in non-overlapping frequency intervals. Half the values in the averages for adjacent points in the power spectral density are common to both, hence adjacent points are not independent.

- ii. The manner in which frequency averaging affects the confidence intervals for the power spectral density estimate is presented below as a function of the number of frequency points, NTS, in the average.

<u>Number of Points in Average, NTS</u>	<u>Total Effective Number of Degrees of Freedom, K</u>	<u>dB Variability for 95% Confidence (From Fig. A-3)</u>
1	38.67	+2.2 - 1.6
2	78.33	+1.5 - 1.3
3	118.00	+1.1 - 1.0
4	157.67	.
6	237.00	.
8	.	.
11	.	.
16	.	.
23	.	.
32		
45		
64		
91		
128		
179		
256		

Computations are based upon $W_e = 2\pi \text{ NTS}/T$, $N = 17$, and the expression for the total effective number of degrees of freedom. The effect of frequency averaging is incorporated by means of NTS in the expression for W_e .

The values of NTS listed above correspond to specific center frequencies for a given data window length. This correspondence has been indicated on Fig. A-1 which gives the center frequencies for each data window length.

RESULTS OF NONSTATIONARY STATISTICAL ANALYSIS FOR SEVENTEEN CATEGORY II AND II-TRAINING GLIDE SLOPE BEAMS

Pages 35 through 85 include the data for estimates of the mean and variance and the variability in those two estimates in some cases for each of the 17 beams. Pages 86 through 88 include similar data for the ensemble average for all 17 beams. Pages 89 through the end include estimates of the power spectral density for the ensemble average of all 17 beams.

Time traces for the 17 differential traces analyzed are available in Ref. 9.

The data in this section of the Appendix was produced by David Hemmel and Bryon Wiscons of the Collins Radio Co. under the direction of Elmer Schultz.

SUMMARY OF THE DATA AND ITS INTERPRETATION

Selected portions of the data resulting from the Collins Radio Co. analysis of 17 Category II and II-training quality Glide Slopes are plotted in Fig. A-5 through -9.

Mean Beam Alignment

Estimates of the mean beam alignment formed using 64 second and 8 second data windows and ensemble averaging over all 17 Glide Slopes are plotted in Fig. A-5. A small systematic deviation which does not depend upon range (or time) from the runway threshold is evident. This systematic alignment error of $-2.5 \mu A$ indicates that the actual beam mean lies above the ideal C DDM locus.

Beam Total Standard Deviation

Estimates of the beam total standard deviation (with respect to the mean) formed using 64 second and 8 second data windows and ensemble averaging over all 17 Glide Slopes are plotted in Fig. A-6. The total standard deviation, $\hat{\sigma}_t$, consists of the root-sum-square of components arising from the Glide Slope-to-Glide Slope variability of the mean $\hat{\sigma}_{\Delta\Theta}$, and from the ensemble averaged variability of each Glide Slope over the data window time

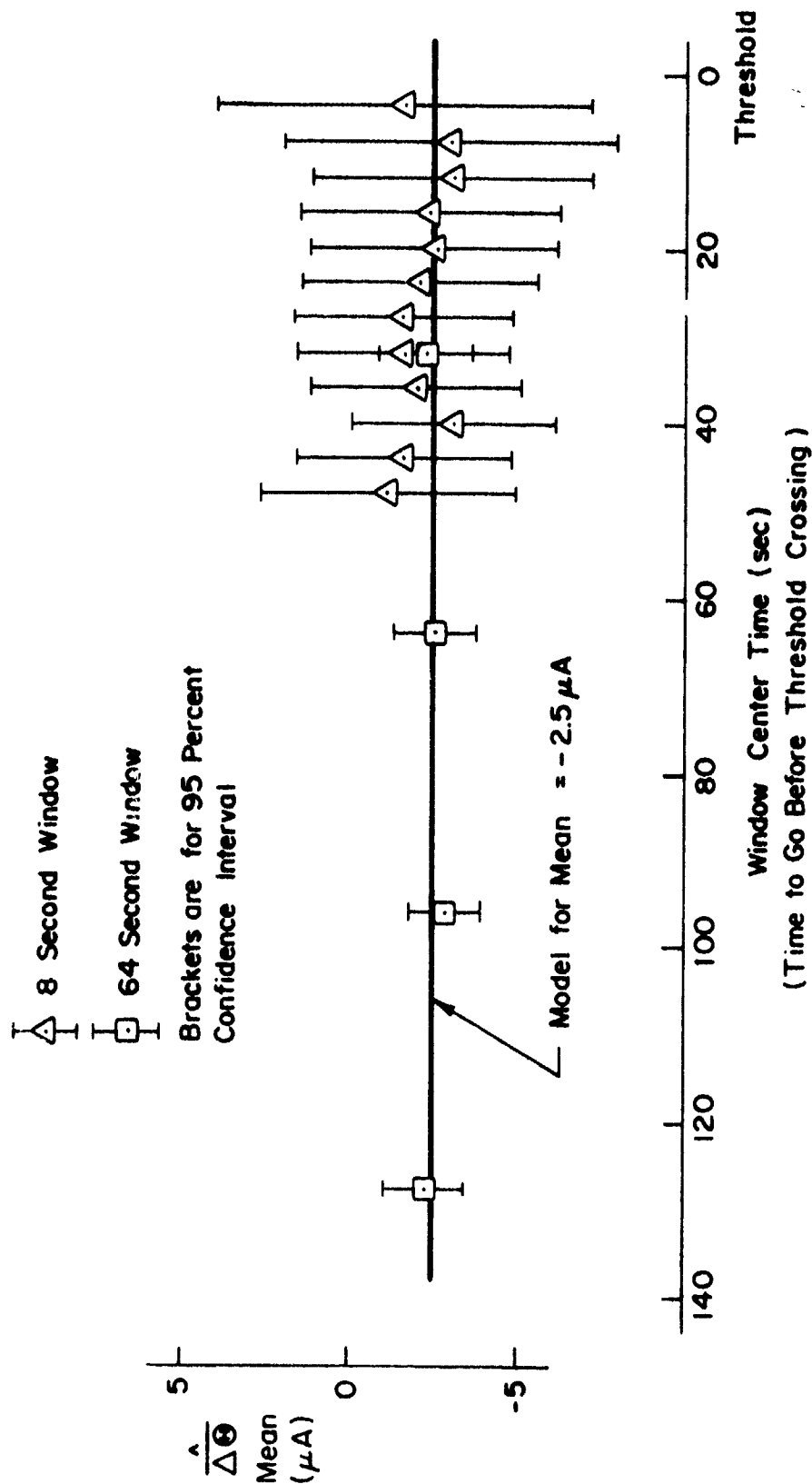


Figure A-5. Estimates of Differential Trace Mean Values

interval, $\hat{\sigma}_\eta$. The $\hat{\sigma}_\eta$ component therefore corresponds to beam structure.

An estimate of the stationary power spectral density for a 128 second data window extending from 32 seconds to 160 seconds and which is an ensemble average over all 17 Glide Slopes is plotted in Fig. A-7. The data points are nicely fitted by a power spectral density model

$$\frac{(128,96)}{\Phi(\omega)} = \frac{12.90}{\omega^2 + (.18)^2} \quad (A-25)$$

This power spectral density model may be integrated to obtain an estimate of $\hat{\sigma}_\eta$ for $32 \leq t \leq 160$ seconds.

$$\hat{\sigma}_\eta = \frac{1}{2\pi} \int_{-\infty}^{\infty} \frac{(128,96)}{\Phi(\omega)} d\omega = (5.99)^2 \quad (A-26)$$

This in turn enables calculation of an estimate for $\hat{\sigma}_{\Delta\theta}$ over the same time interval since $\hat{\sigma}_t = 10 \mu A$ over that time interval.

$$\hat{\sigma}_{\Delta\theta} = \sqrt{\hat{\sigma}_t^2 - \hat{\sigma}_\eta^2} = 8.01 \mu A, \quad 32 \leq t \leq 160 \text{ sec} \quad (27)$$

Since the mean alignment error does not depend upon range, it is reasonable to assume that the standard deviation of the alignment error is also independent of range so that $\hat{\sigma}_{\Delta\theta} = 8.01 \mu A$ for $0 \leq t \leq 160$ seconds.

The total standard deviation, $\hat{\sigma}_t$, is plainly dependent upon range in Fig. A-6. It will be assumed that this dependency arises solely in $\hat{\sigma}_\eta$ for $t \leq 64$ seconds.

Beam Range-Varying Power Spectral Density

The range-variation of the total standard deviation has been attributed above to the variability of the Glide Slopes over the data window interval. This variability is expressed in terms of a power spectral density. It has already been indicated that $\hat{\sigma} = 5.99 \mu A$ for $32 \leq t \leq 160$ seconds. In order

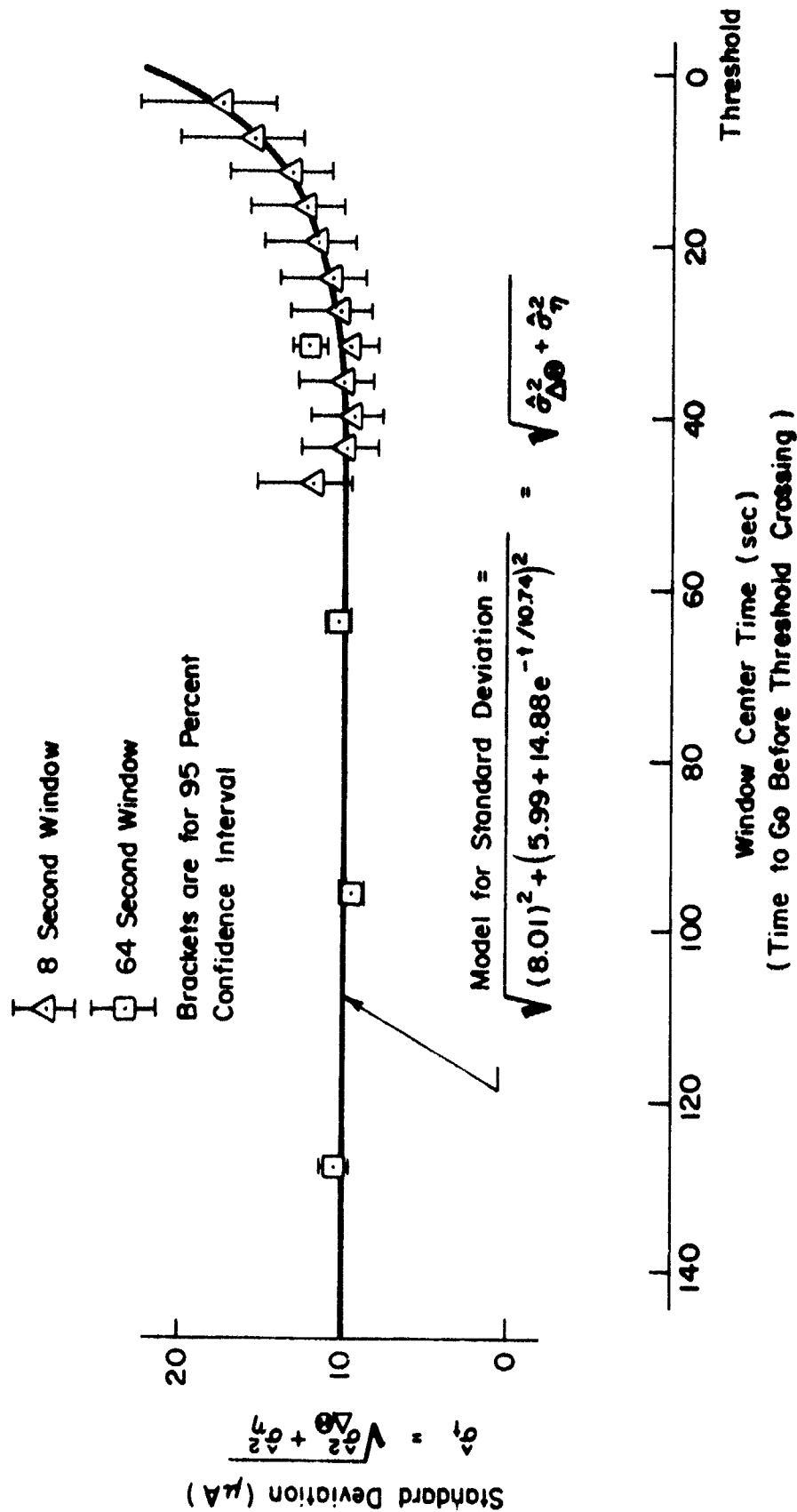


Figure A-6. Estimates of Differential Trace Total Standard Deviation

to obtain a curve fit for the interval $0 \leq t \leq 160$ seconds, the residual* has been plotted versus t in Fig. A-8. The time function

$$\hat{\sigma}_{\eta} = 5.99 + 14.88 e^{-t/10.74} \mu A \quad (A-28)$$

provides an excellent fit to the data in both Fig. A-6 and A-8.

The range-varying power spectral density must be such that it has the standard deviation $\hat{\sigma}_{\eta}$. It would be desirable to fit appropriate power spectral density models to data for an 8 second data window. However, the lowest frequency point in that power spectral density data would occur at 0.785 rad/sec which is at the upper end of the frequency range of interest. The power spectral density model could not be fitted to the data with reasonable confidence in the absence of data at lower frequencies.

As a substitute, the 64 second data window power spectral density data at 32 second window center time is used. The appropriate standard deviation in this case is:

$$\hat{\sigma}_{\eta}(64, 32) = \sqrt{(\hat{\sigma}_t(64, 32))^2 - \hat{\sigma}_{\Delta\theta}^2} = 9.177 \mu A \quad (A-29)$$

It is shown in Fig. A-9a that a power spectral density model

$$\hat{\Phi}_{\eta}^{(64, 32)}(\omega) = \frac{30.32}{\omega^2 + (.18)^2} \quad (A-30)$$

fits the data rather well. (Notice that the half-power frequency, $\hat{\omega}_{\eta} = 0.18$ rad/sec, has not been changed from the value in $\hat{\Phi}_{\eta}^{(128, 96)}(\omega)$.)

The power spectral density model, $\hat{\Phi}_{\eta}^{(128, 96)}(\omega)$, has also been superimposed in Fig. A-9b and A-9c upon the power spectral data for the 64 second data window at the 64 and 96 second center times to show the good quality of

*Actually, the natural logarithm of the residual is used for analytical convenience in determining the time function

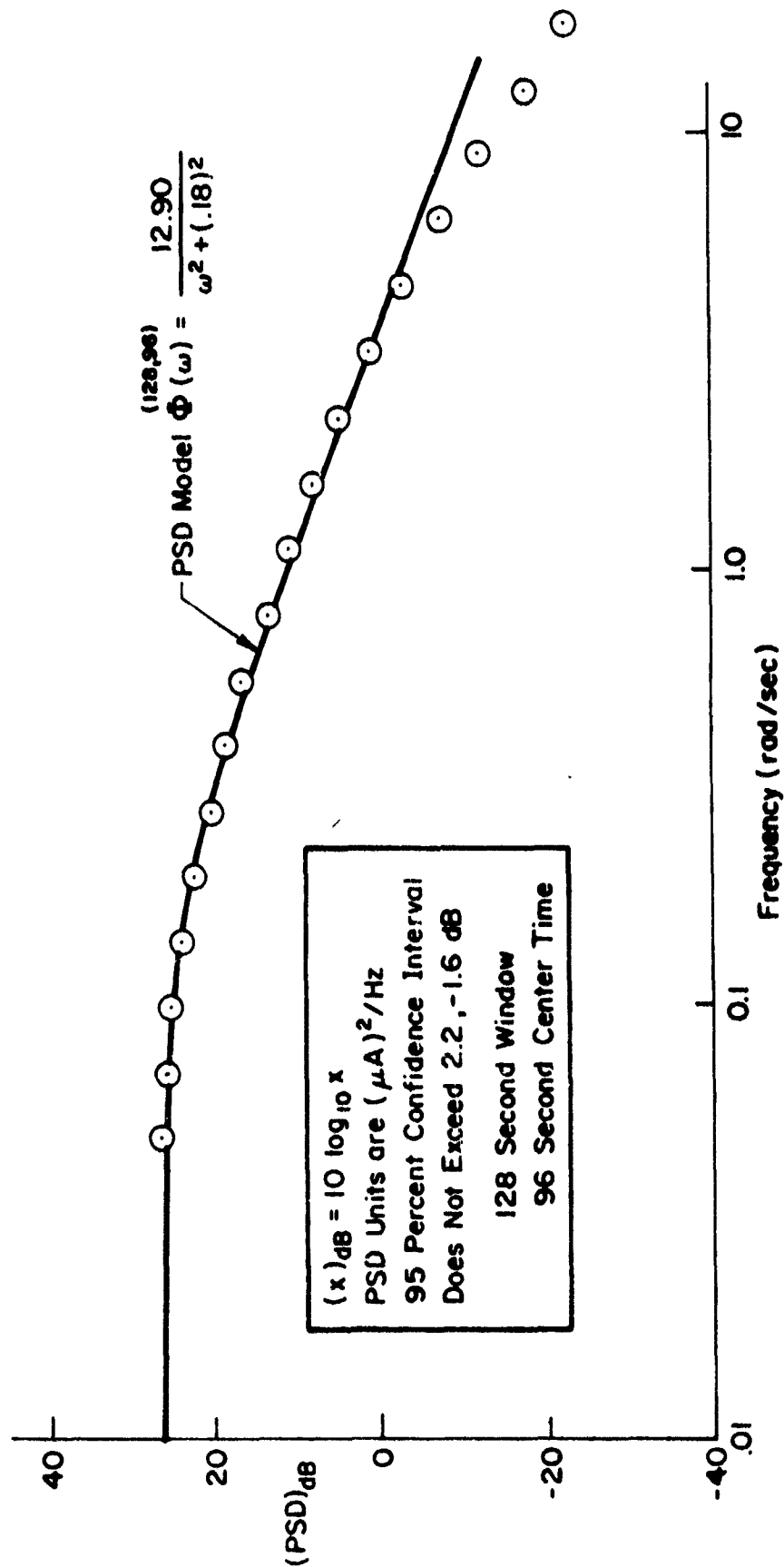


Figure A-7. Estimate for Differential Trace Stationary Power Spectral Density

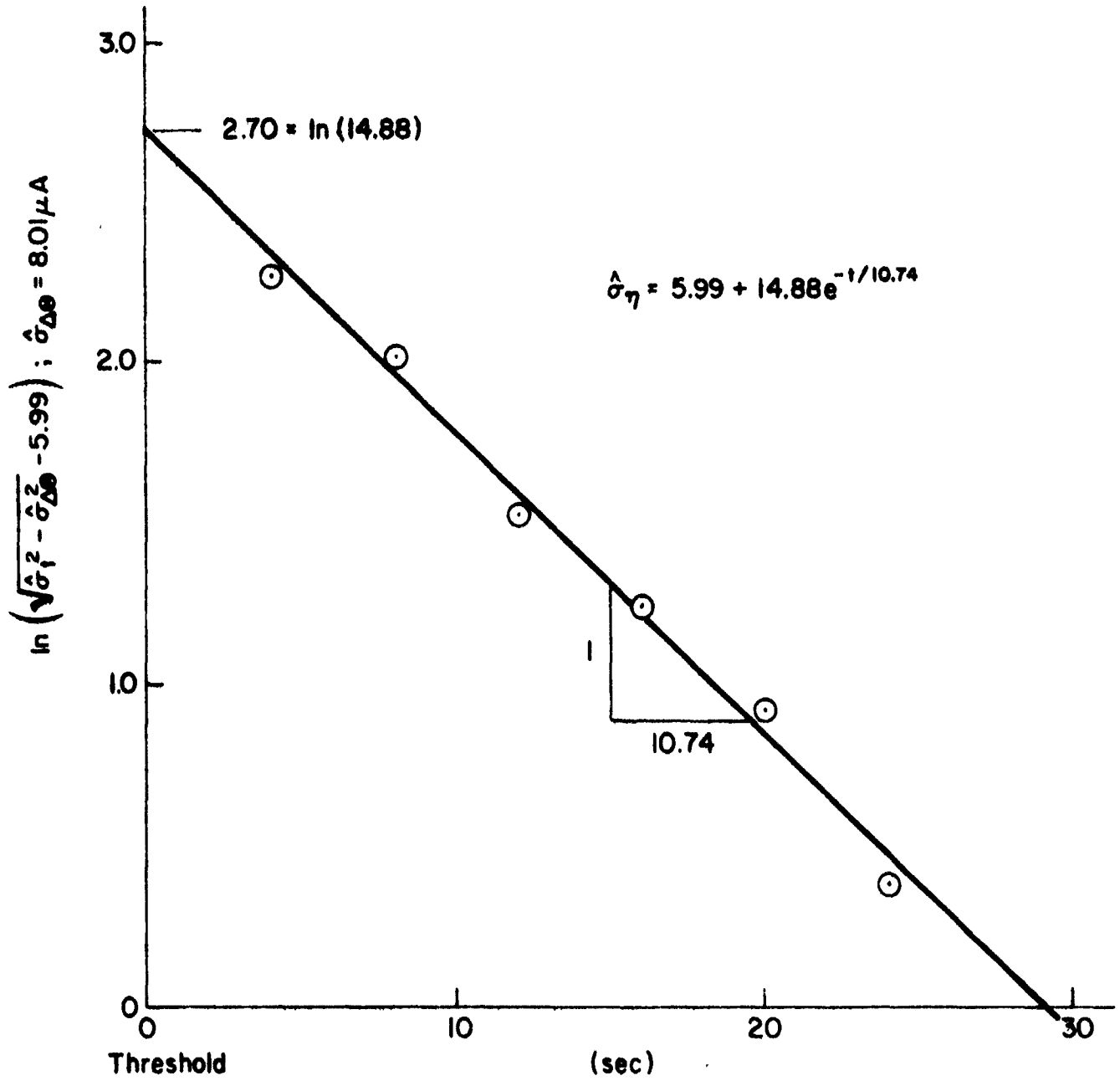


Figure A-8. Obtaining a Model for $\hat{\sigma}_\eta$

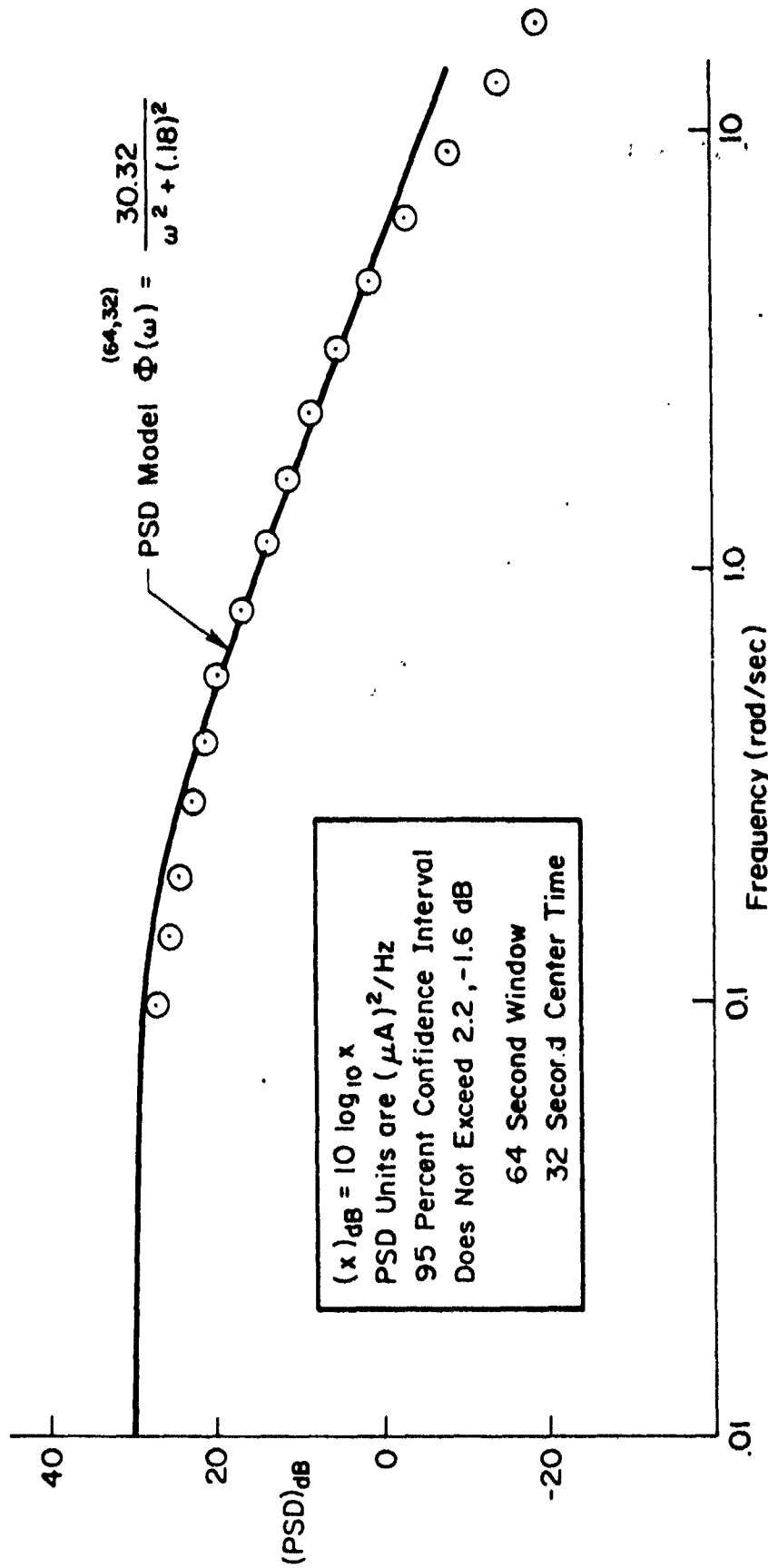


Figure A-9a. Estimate of Differential Trace Power Spectral Density

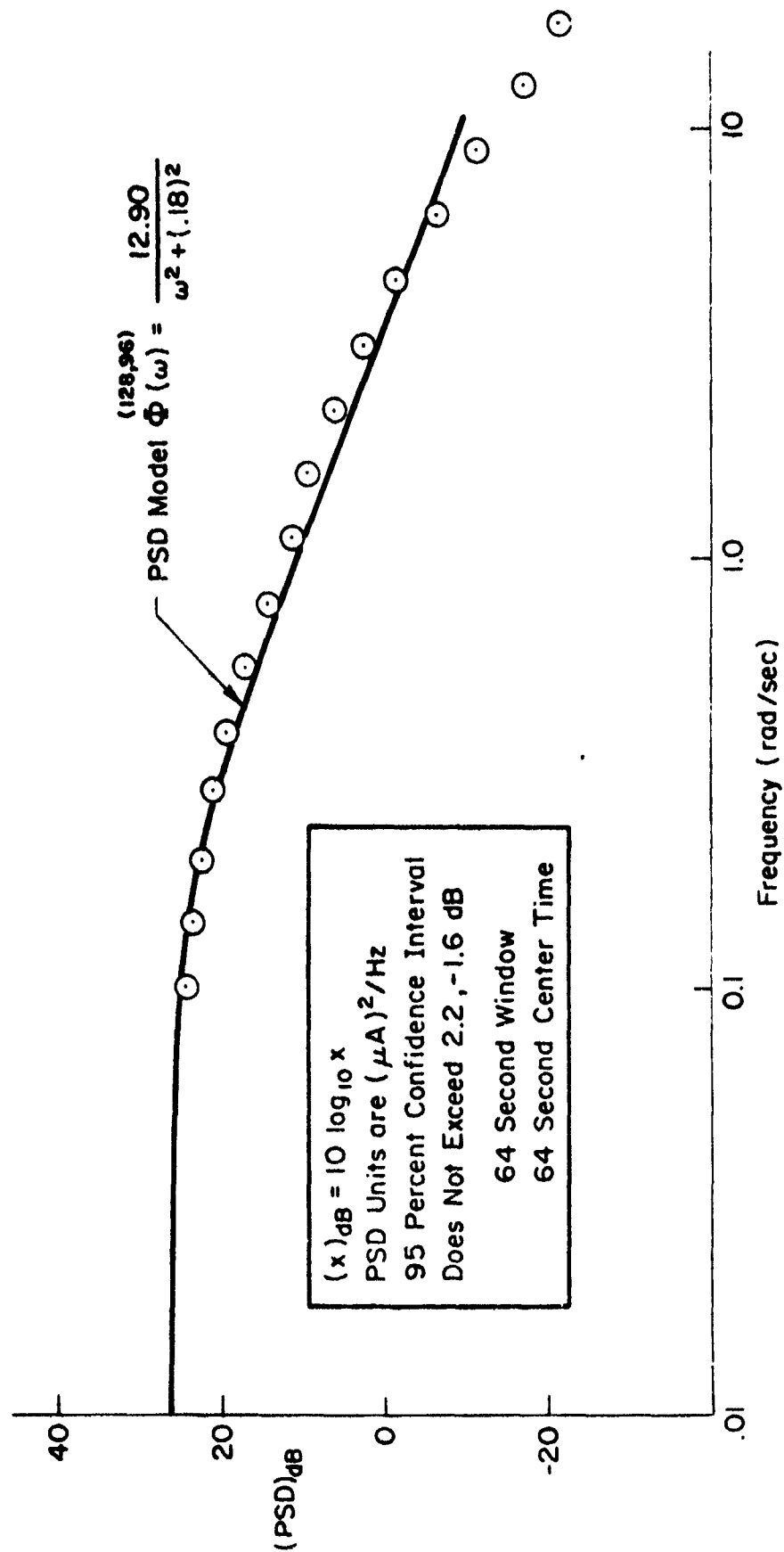


Figure A-9b

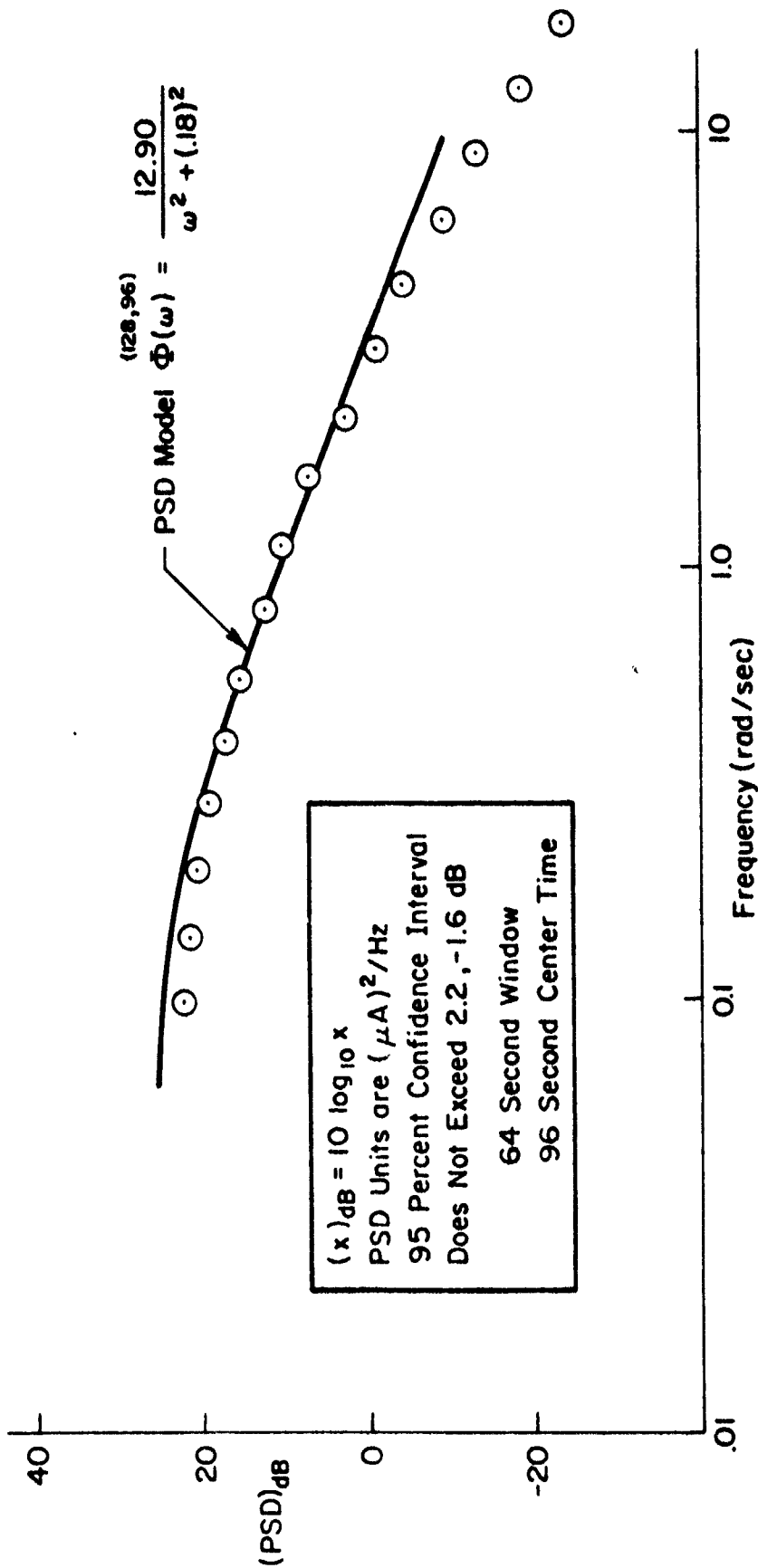


Figure A-9c

fit. The conclusion to be drawn is that $\hat{\omega}_\eta = 0.18$ rad/sec is a good estimate of the half-power frequency for the power spectral density for $0 \leq t \leq 160$ seconds.

Given the above fact that the half-power frequency of the power spectral density, $\hat{\omega}_\eta$ is independent of range (or time), and the standard deviation, $\hat{\sigma}_\eta$, as a function of range (or equivalently, time), the final power spectral density model for the interval $0 \leq t \leq 160$ seconds is:

$$\Phi(\omega) = \frac{0.3595(5.99 + 14.88 e^{-t/10.74})^2}{\omega^2 + (.18)^2} \quad (\text{A-31})$$

MINNEAPOLIS (3-21-69) GLIDE-SLOPE

MINIMUM= -.957

MAXIMUM= .941

ZERO REF.= -.0016

FIRST DATA POINT NUMBER= 156

NUMBER OF VALID POINTS=1629

OVERALL SIGNAL MEAN= -9.057

OVERALL SIGNAL SIGMA= 6.117

AVG FOR THE 1120 SAMPLES = -8.275

SIGMA = 6.441

GLIDE SLOPE . 2 MEAN-AND-VARIANCE

6 SECOND WINDOW

TIME (SEC)	MEAN (MU A)	STD DEV (MU A)	VARIANCE (MU A)**2
4	-4.8153	6.9711	48.5958
8	-4.2874	5.9702	35.6434
12	-4.1627	4.1650	17.3470
16	-6.6974	2.5350	6.4265
20	-7.5653	2.9902	8.9411
24	-5.0784	6.7156	45.0999
28	-3.6267	7.0689	49.9689
32	-6.5784	6.4246	41.2760
36	-10.9175	4.8918	23.9302
40	-7.5005	4.5013	20.2613
44	-2.9686	4.0838	16.6776
48	.4196	3.3652	11.3244

64 SECOND WINDOW

TIME (SEC)	MEAN (MU A)	STD DEV (MU A)	VARIANCE (MU A)**2
32	-4.1833	6.5153	42.4489
64	-8.8239	8.1857	67.0060
96	-11.5259	5.1514	26.5366
128	-9.3540	3.6849	13.5783

ESTIMATED VARIABILITY FOR 64 SEC WINDOW

TIME (SEC)	0.95 CONFIDENCE +,- VARIABILITY ABOUT MEAN (MU A)	0.95 CONFIDENCE VARIABILITY ABOUT STD DEV (MU A)	
32	3.3879	3.5782	-1.7275
64	4.2566	4.4955	-2.1705
96	2.6787	2.8291	-1.3659
128	1.9161	2.0237	-.9771

NUMBER OF ENSEMBLE MEMBERS = 1

DEGREES OF FREEDOM = 15.3

BASED UPON WE = 0.25*PI

SIOUX FALLS (10-30-68) GLIDE SLOPE

MINIMUM= -.963

MAXIMUM= .925

ZERO REF.= -.0045

FIRST DATA POINT NUMBER= 173

NUMBER OF VALID POINTS=1159

OVERALL SIGNAL MEAN= -.921

OVERALL SIGNAL SIGMA= 10.966

AVG FOR THE 1120 SAMPLES = -.513

SIGMA = 10.450

GLIDE SLOPE 3 MEAN AND VARIANCE

8 SECOND WINDOW

TIME (SEC)	MEAN (MU A)	STD DEV (MU A)	VARIANCE (MU A)**2
4	8.3537	4.4170	19.5098
8	-1.9732	8.4921	72.1150
12	-7.9136	5.8882	34.6705
16	-4.6364	5.9568	35.4833
20	-1.6404	4.2504	18.0660
24	-1.8779	3.9641	15.7144
28	-.9172	4.7211	22.2887
32	.5216	4.5039	20.2850
36	1.3284	5.0196	25.1985
40	-4.4173	6.3967	70.5052
44	-6.7498	6.4602	41.7336
48	-.4628	4.1019	16.8258

64 SECOND WINDOW

TIME (SEC)	MEAN (MU A)	STD DEV (MU A)	VARIANCE (MU A)**2
32	-2.9869	7.9837	63.7388
64	-3.2776	9.5927	92.0205
96	.5720	9.0774	82.3999
128	2.7971	11.5890	134.3041

SIoux FALLS (9-30-69)

GLIDE SLOPE

MINIMUM= -.938

MAXIMUM= .894

ZERO REF.= -.0460

FIRST DATA POINT NUMBER= 155

NUMBER OF VALID POINTS=1321

OVERALL SIGNAL MEAN= -10.684

OVERALL SIGNAL SIGMA= 9.985

AVG FOR THE 1120 SAMPLES = -13.531

SIGMA = 8.520

ESTIMATED VARIABILITY FOR 64 SEC WINDOW

TIME (SEC)	0.95 CONFIDENCE +,- VARIABILITY ABOUT MEAN (MU A)	0.95 CONFIDENCE VARIABILITY ABOUT STD DEV (MU A)	
32	4.1515	4.3846	-2.1169
64	4.9882	5.2683	-2.5435
96	4.7203	4.9853	-2.4069
128	6.0263	6.3646	-3.0728

NUMBER OF ENSEMBLE MEMBERS = 1

DEGREES OF FREEDOM = 15.3

BASED UPON WE = 0.25*PI

GLIDE SLOPE 4 MEAN AND VARIANCE

8 SECOND WINDOW

TIME (SEC)	MEAN (MU A)	STD DEV (MU A)	VARIANCE (MU A)**2
4	-11.6112	3.9642	15.7151
8	-12.5592	4.5931	21.0968
12	-17.0657	5.6284	31.6789
16	-13.0528	5.4463	29.6617
20	-17.2613	9.9900	99.8002
24	-7.5330	6.1078	37.3054
28	-5.3325	5.9224	35.0752
32	-8.1971	7.7954	60.7686
36	-11.6626	6.3162	39.8941
40	-10.5814	4.1011	16.8189
44	-9.5151	3.6378	13.2338
48	-23.7867	16.9265	286.5058

64 SECOND WINDOW

TIME (SEC)	MEAN (MU A)	STD DEV (MU A)	VARIANCE (MU A)**2
32	-15.6505	10.6244	112.8773
64	-14.4891	10.1455	102.9311
96	-10.0864	6.6128	43.7294
128	-12.8882	6.5460	42.8506

ESTIMATED VARIABILITY FOR 64 SEC WINDOW

TIME (SEC)	0.95 CONFIDENCE +,- VARIABILITY ABOUT MEAN (MU A)	0.95 CONFIDENCE VARIABILITY ABOUT STD DEV (MU A)	
32	5.5247	5.8348	-2.6171
64	5.2757	5.5718	-2.6901
96	5.4387	5.6317	-1.7534
128	5.4059	5.5950	-1.7357

NUMBER OF ENSEMBLE MEMBERS = 1

DEGREES OF FREEDOM = 15.3

BASED UPON WE = 0.25*P1

FARGO, ND (8-27-69)

GLIDE SLOPE

MINIMUM= -.970

MAXIMUM= .877

ZERO REF.= -.0125

FIRST DATA POINT NUMBER= 144

NUMBER OF VALID POINTS=1134

OVERALL SIGNAL MEAN= -14.320

OVERALL SIGNAL SIGMA= 4.282

AVG FOR THE 1120 SAMPLES = -14.298

SIGMA = 4.193

GLIDE SLOPE 5 MEAN AND VARIANCE

8 SECOND WINDOW

TIME (SEC)	MEAN (MU A)	STD DEV (MU A)	VARIANCE (MU A)**2
4	-26.4636	4.9230	24.2356
8	-23.5646	4.5466	20.6717
12	-21.6258	1.5529	2.4114
16	-21.2238	1.6419	2.6959
20	-18.4447	2.5797	6.6547
24	-14.2878	3.3354	11.1252
28	-14.2218	3.2660	10.6666
32	-15.1388	2.4353	5.9306
36	-15.6488	1.7646	3.1137
40	-15.9160	1.8520	3.4299
44	-12.8426	1.8290	3.3454
48	-12.8671	1.7937	3.2174

64 SECOND WINDOW

TIME (SEC)	MEAN (MU A)	STD DEV (MU A)	VARIANCE (MU A)**2
32	-16.5454	5.4935	30.1788
64	-12.8701	1.4601	2.1320
96	-12.0922	1.8089	3.2721
128	-12.7480	2.1452	4.6019

ESTIMATED VARIABILITY FOR 64 SEC WINDOW

TIME (SEC)	0.95 CONFIDENCE		0.95 CONFIDENCE	
	+,- VARIABILITY ABOUT		VARIABILITY ABOUT	
	MEAN (MU A)		STD DEV (MU A)	
32	2.8566		0.0170	-1.4566
64	.7593		.8019	-.3872
96	.9406		.9934	-.4796
128	1.1155		1.1781	-.5688

NUMBER OF ENSEMBLE MEMBERS = 1

DEGREES OF FREEDOM = 15.3

BASED UPON WE = 0.25*PI

DFNVER 26L (11-19-68)

GLIDE SLOPE

MINIMUM= -1.039

MAXIMUM= .969

ZERO REF.= -.0301

FIRST DATA POINT NUMBER= 144

NUMBER OF VALID POINTS=1089

OVERALL SIGNAL MEAN= 7.869

OVERALL SIGNAL SIGMA= 4.770

AVG FOR THE 1120 SAMPLES = 7.647

SIGMA = 4.903

GLIDE SLOPE 6 MEAN AND VARIANCE

8 SECOND WINDOW

TIME (SEC)	MEAN (MU A)	STD DEV (MU A)	VARIANCE (MU A)**2
4	13.1110	4.5972	21.1346
8	10.3310	5.0084	25.0842
12	7.5451	3.7569	14.1144
16	12.5415	5.7598	33.1751
20	13.9255	5.7303	32.8358
24	6.0605	6.4814	42.0083
28	2.7825	4.2846	18.3582
32	4.7548	4.0946	16.7657
36	1.7408	5.0310	25.3112
40	-1.0054	3.0157	9.0944
44	2.1329	4.2096	17.7210
48	5.1614	1.6864	2.8439

64 SECOND WINDOW

TIME (SEC)	MEAN (MU A)	STD DEV (MU A)	VARIANCE (MU A)**2
32	6.1924	6.2780	39.4128
64	5.5791	4.5658	20.8465
96	7.4259	3.2895	10.8211
128	6.8495	3.3640	11.3166

ESTIMATED VARIABILITY FOR 64 SEC WINDOW

TIME (SEC)	0.95 CONFIDENCE	0.95 CONFIDENCE	
	+,- VARIABILITY ABOUT MEAN (MU A)	VARIABILITY ABOUT STD. DEV (MU A)	
32	3.2645	3.4478	-1.6646
64	2.5742	2.5075	-1.2106
96	1.7106	1.8066	-.8722
128	1.7493	1.8475	-.8920

NUMBER OF ENSEMBLE MEMBERS = 1

DEGREES OF FREEDOM = 15.3

BASED UPON WE = 0.25*PI

DENVER 35 (1-2-69)

GLIDE SLOPE

MINIMUM= -1.080

MAXIMUM= .941

ZERO REF.= -.0371

FIRST DATA POINT NUMBER= 144

NUMBER OF VALID POINTS=1323

OVERALL SIGNAL MEAN= 7.596

OVERALL SIGNAL SIGMA= 10.111

AVG FOR THE 1120 SAMPLES = 5.241

SIGMA = 8.107

GLIDE SLOPE 7 MEAN AND VARIANCE

8 SECOND WINDOW

TIME (SEC)	MEAN (MU A)	STD DEV (MU A)	VARIANCE (MU A)**2
4	10.0401	5.7648	33.2329
8	10.4513	3.6824	13.5603
12	8.6458	4.0889	16.7190
16	8.0447	3.6937	13.6431
20	-8.6603	8.5683	73.4166
24	-5.3594	4.9646	24.6474
28	-3.9720	2.4720	6.1108
32	-5.7895	3.2643	10.7868
36	-8.1007	4.5289	20.5113
40	-6.9752	4.4585	19.8776
44	-8.6278	9.1142	83.0685
48	2.6138	6.3209	39.9532

64 SECOND WINDOW

TIME (SEC)	MEAN (MU A)	STD DEV (MU A)	VARIANCE (MU A)**2
32	1.5006	8.5763	73.5527
64	2.9387	7.5409	56.8650
96	5.0194	5.7444	32.9976
128	7.9726	7.4089	54.8912

ESTIMATED VARIABILITY FOR 64 SEC WINDOW

TIME (SEC)	0.95 CONFIDENCE +,- VARIABILITY ABOUT MEAN (MU A)		0.95 CONFIDENCE VARIABILITY ABOUT STD DEV (MU A)	
32	4.4597		4.7100	-2.2740
64	3.9213		4.1414	-1.9995
96	2.9871		3.1548	-1.5231
128	3.8526		4.0689	-1.9645

NUMBER OF ENSEMBLE MEMBERS = 1

DEGREES OF FREEDOM = 15.3

BASED UPON WE = 0.25*PI

CHICAGO ORD TX-1 (10-14 69) GLIDE SLOPE

MINIMUM= -1.194

MAXIMUM= 1.048

ZERO REF.= -.0681

FIRST DATA POINT NUMBER= 135

NUMBER OF VALID POINTS=1035

OVERALL SIGNAL MEAN= 7.734

OVERALL SIGNAL SIGMA= 3.932

AVG FOR THE 1120 SAMPLES = 7.792

SIGMA = 3.911

GLIDE SLOPE 12 MEAN AND VARIANCE

8 SECOND WINDOW

TIME (SEC)	MEAN (MU A)	STD DEV (MU A)	VARIANCE (MU A)**2
4	9.5285	5.4397	29.5905
8	6.7307	2.9651	8.7916
12	10.6825	3.4865	12.1557
16	13.3320	1.1139	1.2407
20	14.3388	2.0659	4.2676
24	16.1397	2.2899	5.2437
28	14.8656	3.2095	10.3010
32	11.3950	2.9123	8.4815
36	9.5126	1.8517	3.4287
40	7.6591	2.0298	4.1201
44	5.9893	.9749	.9505
48	6.4338	2.2957	5.2704

64 SECOND WINDOW

TIME (SEC)	MEAN (MU A)	STD DEV (MU A)	VARIANCE (MU A)**2
32	10.0409	4.2882	18.3889
64	6.8430	2.6031	6.7759
96	5.2072	2.4573	6.0386
128	6.4389	2.9651	8.7919

CHICAGO OHA TX-1 (5-26-69) GLIDE SLOPE

MINIMUM= -1.197

MAXIMUM= 1.048

ZERO REF.= -.0571

FIRST DATA POINT NUMBER= 126

NUMBER OF VALID POINTS=1017

OVERALL SIGNAL MEAN= -6.082

OVERALL SIGNAL SIGMA= 7.637

AVG FOR THE 1120 SAMPLES = -5.095

SIGMA = 7.510

ESTIMATED VARIABILITY FOR 64 SEC WINDOW

TIME (SEC)	0.95 CONFIDENCE		0.95 CONFIDENCE	
	+,- VARIABILITY ABOUT		VARIABILITY ABOUT	
	MEAN (MU A)		STD. DEV. (MU A)	
32	2.2299		2.3551	-1.1370
64	1.3536		1.4296	-.6902
96	1.2778		1.3496	-.6516
128	1.5419		1.6284	-.7862

NUMBER OF ENSEMBLE MEMBERS = 1

DEGREES OF FREEDOM = 15.3

BASED UPON WE = 0.25*PI

GLIDE SLOPE 15 MEAN AND VARIANCE

8 SECOND WINDOW

TIME (SEC)	MEAN (MU A)	STD DEV (MU A)	VARIANCE (MU A)**2
4	-5.0995	7.3685	54.2948
8	-5.5431	6.7247	45.2210
12	2.4739	3.8105	14.5197
16	3.7293	1.2901	1.6643
20	3.3642	2.5842	6.6781
24	3.7621	3.3202	11.0240
28	1.4995	4.1971	17.6155
32	1.9722	4.3102	18.5774
36	3.0058	3.7310	13.9202
40	-0.0568	4.2557	18.1113
44	4.6442	7.9244	62.7960
48	7.0379	5.3828	28.9742

64 SECOND WINDOW

TIME (SEC)	MEAN (MU A)	STD DEV (MU A)	VARIANCE (MU A)**2
32	.5211	6.3484	40.3020
64	-2.0071	7.6696	58.8234
96	-0.8667	6.5541	42.9559
128	-10.3080	3.9769	15.8159

ESTIMATED VARIABILITY FOR 64 SEC WINDOW

TIME (SEC)	0.95 CONFIDENCE +,- VARIABILITY ABOUT MEAN (MU A)		0.95 CONFIDENCE VARIABILITY ABOUT STD DEV (MU A)	
32	3.3012		3.4865	-1.6833
64	3.9882		4.2121	-2.0336
96	3.4081		3.5995	-1.7378
128	2.0680		2.1841	-1.0545

NUMBER OF ENSEMBLE MEMBERS = 1

DEGREES OF FREEDOM = 15.3

BASED UPON WE = 0.25*PI

CHICAGO OHA TX-2 (5-26-69) GLIDE SLOPE

MINIMUM= -1.166

MAXIMUM= 1.076

ZERO REF.= -.0324

FIRST DATA POINT NUMBER= 126

NUMBER OF VALID POINTS= 981

OVERALL SIGNAL MEAN= -8.359

OVERALL SIGNAL SIGMA= 7.140

AVG FOR THE 1120 SAMPLES = -8.189

SIGMA = 7.280

GLIDE SLOPE 16 MEAN AND VARIANCE

6 SECOND WINDOW

TIME (SEC)	MEAN (MU A)	STD DEV (MU A)	VARIANCE (MU A)**2
4	-6.3650	4.7693	22.7466
8	-6.6145	4.4087	19.4364
12	-7.1842	3.8203	14.5945
16	-8.4870	3.8697	14.9746
20	-4.9484	5.9256	35.1142
24	1.1117	3.5376	12.5146
28	1.2839	3.2081	10.2920
32	.7699	2.7654	7.6475
36	-1.5170	5.0898	25.9057
40	.6467	6.7051	44.9584
44	3.5201	4.0086	16.0690
48	1.1022	2.9152	8.4986

64 SECOND WINDOW

TIME (SEC)	MEAN (MU A)	STD DEV (MU A)	VARIANCE (MU A)**2
32	-2.5925	5.6955	32.4385
64	-3.5189	5.5792	31.1269
96	-9.6005	5.2214	27.2626
128	-14.7741	3.5959	12.9302

ESTIMATED VARIABILITY FOR 64 SEC WINDOW

TIME (SLC)	0.95 CONFIDENCE		0.95 CONFIDENCE	
	+,- VARIABILITY ABOUT		VARIABILITY ABOUT	
	MEAN (MU A)		STD DEV (MU A)	
32	2.9616		5.1279	-1.5102
64	2.9012		5.0640	-1.4793
96	2.7151		2.8675	-1.3845
128	1.8698		1.9748	-.9535

NUMBER OF ENSEMBLE MEMBERS = 1

DEGREES OF FREEDOM = 15.3

BASED UPON WE = 0.25*PI

BATILL CREEK TX-2 (5-16-69) GLIDE SLOPE

MINIMUM= -1.149

MAXIMUM= 1.075

ZERO REF.= -.0105

FIRST DATA POINT NUMBER= 135

NUMBER OF VALID POINTS=1548

OVERALL SIGNAL MEAN= -11.994

OVERALL SIGNAL SIGMA= 4.340

AVG FOR THE 1120 SAMPLES = -12.709

SIGMA = 4.496

GLIDE SLOPE 17 MEAN AND VARIANCE

8 SECOND WINDOW

TIME (SEC)	MEAN (MU A)	STD DEV (MU A)	VARIANCE (MU A)**2
4	-17.9093	3.6793	13.5375
8	-17.4860	2.7908	7.7888
12	-16.7046	3.8750	15.0153
16	-17.6615	6.0133	36.1600
20	-16.5727	5.2800	27.8767
24	-16.2071	4.7608	22.6656
28	-12.5169	3.3608	11.2951
32	-12.3093	2.2434	5.0328
36	-14.8537	3.4805	12.1137
40	-17.7397	1.9582	3.8344
44	-16.1960	2.0319	4.1286
48	-16.6582	2.6983	7.2809

64 SECOND WINDOW

TIME (SEC)	MEAN (MU A)	STD DEV (MU A)	VARIANCE (MU A)**2
32	-15.6433	4.0575	16.4634
64	-13.7867	3.4443	11.8633
96	-11.1844	3.1593	9.9811
128	-9.7469	3.2783	10.7475

ESTIMATED VARIABILITY FOR 64 SEC WINDOW

TIME (SEC)	0.95 CONFIDENCE +,- VARIABILITY ABOUT MEAN (MU A)		0.95 CONFIDENCE VARIABILITY ABOUT STD DEV (MU A)	
32	2.1099		2.2284	-1.0759
64	1.7910		1.8916	-.9143
96	1.6428		1.7351	-.8377
128	1.7047		1.8004	-.8693

NUMBER OF ENSEMBLE MEMBERS = 1

DEGREES OF FREEDOM = 15.3

BASED UPON $WE = 0.25 \cdot \pi$

BATILL CREEK TX-1 (5-16-69) GLIDE SLOPE

MINIMUM= -1.147

MAXIMUM= 1.073

ZERO REF.= -.0457

FIRST DATA POINT NUMBER= 135

NUMBER OF VALID POINTS=1449

OVERALL SIGNAL MEAN= -13.321

OVERALL SIGNAL SIGMA= 5.608

AVG FOR THE 1120 SAMPLES = -13.562

SIGMA = 6.192

GLIDE SLOPE 18 MEAN AND VARIANCE

8 SECOND WINDOW

TIME (SEC)	MEAN (MU A)	STD DEV (MU A)	VARIANCE (MU A)**2
4	-27.0657	11.6988	136.8616
8	-23.7743	6.5855	43.3683
12	-19.6289	7.5547	57.0736
16	-16.2035	4.8072	23.1095
20	-10.8901	3.5719	12.7586
24	-19.0523	2.9969	8.9816
28	-17.7924	3.1353	9.8301
32	-14.5674	2.9225	8.5413
36	-13.0908	2.8298	8.0080
40	-14.4103	2.8813	8.3047
44	-16.6576	2.5053	6.2764
48	-15.3473	3.3340	11.1154

64 SECOND WINDOW

TIME (SEC)	MEAN (MU A)	STD DEV (MU A)	VARIANCE (MU A)**2
32	-17.0764	7.0836	50.1769
64	-13.5557	2.8193	7.9484
96	-11.0025	3.2179	10.3552
128	-9.8173	3.3592	11.2842

ESTIMATED VARIABILITY FOR 64 SEC WINDOW

TIME (SEC)	0.95 CONFIDENCE	0.95 CONFIDENCE	
	+,- VARIABILITY ABOUT MEAN (MU A)	VARIABILITY ABOUT STD DEV (MU A)	
32	3.6835	3.8902	-1.6782
64	1.4660	1.5483	-.7475
96	1.6733	1.7673	-.8532
128	1.7468	1.8449	-.8907

NUMBER OF ENSEMBLE MEMBERS = 1

DEGREES OF FREEDOM = 15.3

BASED UPON WE = 0.25*PI

BEAUMONT, TEX (2-12-69) GLIDE SLOPE
MINIMUM= -1.158
MAXIMUM= 1.080
ZERO REF.= -.0407
FIRST DATA POINT NUMBER= 126
NUMBER OF VALID POINTS= 657

OVERALL SIGNAL MEAN= 7.089
OVERALL SIGNAL SIGMA= 7.608
AVG FOR THE 1120 SAMPLES = 8.160
SIGMA = 6.872

GLIDE SLOPE 20 MEAN AND VARIANCE

8 SECOND WINDOW

TIME (SEC)	MEAN (MU A)	STD DEV (MU A)	VARIANCE (MU A)**2
4	0.9850	13.2621	175.8846
8	.2766	6.5723	43.1958
12	6.9637	6.5398	42.7693
16	0.2487	5.1645	26.6722
20	3.8178	2.2207	4.9316
24	10.5056	8.2195	67.5594
28	13.3200	7.7170	59.5524
32	11.2544	5.7756	33.3576
36	11.2998	5.5506	30.8087
40	4.7168	7.6235	58.1182
44	7.1467	8.1952	67.1605
48	13.0673	4.3106	18.5808

64 SECOND WINDOW

TIME (SEC)	MEAN (MU A)	STD DEV (MU A)	VARIANCE (MU A)**2
32	9.5208	7.9686	63.4983
64	7.2865	6.9218	47.9119
96	5.9244	5.3148	28.2468
128	8.9717	5.3006	28.0964

ESTIMATED VARIABILITY FOR 64 SEC WINDOW

TIME (SEC)	0.95 CONFIDENCE		0.95 CONFIDENCE	
	+,- VARIABILITY ABOUT MEAN (MU A)		VARIABILITY ABOUT STD. DEV (MU A)	
32	4.1437		4.3763	-2.1129
64	3.5994		3.8014	-1.8353
96	2.7637		2.9188	-1.4092
128	2.7563		2.9111	-1.4055

NUMBER OF ENSEMBLE MEMBERS = 1

DEGREES OF FREEDOM = 15.3

BASED UPON $WE = 0.25 \cdot \pi$

EL PASO TX-1 (11-25-68) GLIDE SLOPE

MINIMUM= -1.146

MAXIMUM= 1.075

ZERO REF.= -.0434

FIRST DATA POINT NUMBER= 135

NUMBER OF VALID POINTS= 954

OVERALL SIGNAL MEAN= -5.524

OVERALL SIGNAL SIGMA= 12.162

AVG FOR THE 1120 SAMPLES = -6.130

SIGMA = 11.277

GLIDE SLOPE 21 MEAN AND VARIANCE

8 SECOND WINDOW

TIME (SEC)	MEAN (MU A)	STD DEV (MU A)	VARIANCE (MU A)**2
4	31.0246	4.6197	21.3418
8	29.1145	6.6050	43.6258
12	16.9584	8.0710	65.1405
16	8.4312	3.9312	15.4541
20	2.2813	5.7055	32.5526
24	-6.1939	5.0572	25.5757
28	-9.7907	1.7218	2.9645
32	-5.5851	4.5776	20.9540
36	-3.0120	2.8332	8.0272
40	-7.9101	4.0260	16.2090
44	-9.2501	2.7967	7.8213
48	-10.6112	4.2598	18.1455

64 SECOND WINDOW

TIME (SEC)	MEAN (MU A)	STD DEV (MU A)	VARIANCE (MU A)**2
32	.2704	15.5613	242.1551
64	-10.7631	3.9787	15.8302
96	-10.8686	2.4659	6.0807
128	-9.6105	1.8912	3.5766

ESTIMATED VARIABILITY FOR 64 SEC WINDOW

TIME (SEC)	0.95 CONFIDENCE +,- VARIABILITY ABOUT MEAN (MU A)	0.95 CONFIDENCE VARIABILITY ABOUT STD DEV (MU A)	
32	0.0919	0.5462	-4.1261
64	2.0689	2.1851	-1.0550
96	1.2823	1.3543	-.6538
128	.9834	1.0386	-.5015

NUMBER OF ENSEMBLE MEMBERS = 1

DEGREES OF FREEDOM = 15.3

BASED UPON WE = 0.25*PI

HOUSTON TX-2 (1-7-70)

GLIDE SLOPE

MINIMUM= -1.162

MAXIMUM= 1.072

ZERO REF.= -.0365

FIRST DATA POINT NUMBER= 135

NUMBER OF VALID POINTS=1080

OVERALL SIGNAL MEAN= -2.583

OVERALL SIGNAL SIGMA= 6.978

AVG FOR THE 1120 SAMPLES = -2.119

SIGMA = 6.580

GLIDE SLOPE 22 MEAN AND VARIANCE

6 SECOND WINDOW

TIME (SLC)	MEAN (MU A)	STD DEV (MU A)	VARIANCE (MU A)**2
4	5.2772	4.8283	23.3125
8	-2.2956	5.1418	26.4377
12	-7.2362	3.4796	12.1077
16	-3.8447	5.2727	27.8010
20	-2.7633	4.4681	19.9637
24	-10.7449	5.5123	30.3850
28	-9.7923	6.4581	41.7072
32	-8.5339	5.2833	27.9129
36	-3.9249	9.7145	94.3724
40	4.7565	3.7069	13.7411
44	5.4088	3.1841	10.1386
48	.7295	6.5871	43.3892

64 SECOND WINDOW

TIME (SEC)	MEAN (MU A)	STD DEV (MU A)	VARIANCE (MU A)**2
32	-1.5756	7.7270	59.7062
64	.6124	6.1146	37.3883
96	-2.5602	5.5729	31.0569
128	-3.2354	6.2368	38.8980

ESTIMATED VARIABILITY FOR 64 SEC WINDOW

TIME (SEC)	0.95 CONFIDENCE +,- VARIABILITY ABOUT MEAN (MU A)		0.95 CONFIDENCE VARIABILITY ABOUT STD DEV (MU A)	
32	4.0180		4.2436	-2.0488
64	3.1796		3.3581	-1.6213
96	2.8979		3.0606	-1.4777
128	3.2451		3.4252	-1.6537

NUMBER OF ENSEMBLE MEMBERS = 1

DEGREES OF FREEDOM = 15.3

BASED UPON $WE = 0.25 \cdot PI$

LAKE CHARLES. LA TX-1 (4-28-69) GLIDE S

MINIMUM= -1.146

MAXIMUM= 1.071

ZERO REF.= -.0185

FIRST DATA POINT NUMBER= 144

NUMBER OF VALID POINTS= 981

OVERALL SIGNAL MEAN= 3.455

OVERALL SIGNAL SIGMA= 11.821

AVG FOR THE 1120 SAMPLES = 4.986

SIGMA = 10.246

GLIDE SLOPE 23 MEAN AND VARIANCE

8 SECOND WINDOW

TIME (SEC)	MEAN (MU A)	STD DEV (MU A)	VARIANCE (MU A)**2
4	-21.8760	9.1491	83.7061
8	-20.6466	9.1511	83.7424
12	-14.4034	13.3434	178.0464
16	-5.5636	3.9803	15.8424
20	-5.2454	3.0103	9.0621
24	-3.0413	4.6066	21.2204
28	.0520	3.1496	9.9199
32	2.9648	5.7402	32.9499
36	4.5615	6.5482	42.8795
40	7.0683	5.5067	30.3240
44	11.4688	3.2680	10.6799
48	10.0573	4.0860	16.6952

64 SECOND WINDOW

TIME (SEC)	MEAN (MU A)	STD DEV (MU A)	VARIANCE (MU A)**2
32	-1.7052	12.5787	158.2225
64	7.1909	4.5519	20.7200
96	0.4819	3.0005	9.0032
128	10.5646	4.7167	22.2473

ESTIMATED VARIABILITY FOR 64 SEC WINDOW

TIME (SEC)	0.95 CONFIDENCE +,- VARIABILITY ABOUT MEAN (MU A)	0.95 CONFIDENCE VARIABILITY ABOUT STD DEV (MU A)	
32	0.5409	0.9081	-3.3353
64	2.3670	2.4999	-1.2070
96	1.5603	1.6479	-0.7956
128	2.4527	2.5904	-1.2506

NUMBER OF ENSEMBLE MEMBERS = 1

DEGREES OF FREEDOM = 15.3

BASED UPON WE = 0.25*PI

LUBBOCK, TEX (2-27-69)

GLIDE SLOPE

MINIMUM= -1.140

MAXIMUM= 1.069

ZERO REF.= -.0164

FIRST DATA POINT NUMBER= 126

NUMBER OF VALID POINTS= 711

OVERALL SIGNAL MEAN= 11.722

OVERALL SIGNAL SIGMA= 5.176

AVG FOR THE 1120 SAMPLES = 11.147

SIGMA = 5.280

GLIDE SLOPE 24 MEAN AND VARIANCE

8 SECOND WINDOW

TIME (SEC)	MEAN (MU A)	STD DEV (MU A)	VARIANCE (MU A)**2
4	16.5040	4.5331	20.5486
8	16.5329	3.6613	13.4049
12	13.5606	3.9884	15.9070
16	11.2051	4.4191	19.5285
20	10.5074	4.4655	19.9407
24	12.4020	4.3673	19.0735
28	12.4665	4.0351	16.2821
32	12.4518	3.9279	15.4282
36	14.0540	3.1262	9.7730
40	9.6114	5.5029	30.2825
44	6.3757	3.0916	9.5581
48	11.2787	4.5307	20.5271

64 SECOND WINDOW

TIME (SEC)	MEAN (MU A)	STD DEV (MU A)	VARIANCE (MU A)**2
32	12.2249	5.2032	27.0738
64	10.7233	5.1864	26.8988
96	10.4256	5.5290	30.5703
128	10.2400	5.0461	25.4633

ESTIMATED VARIABILITY FOR 64 SEC WINDOW

TIME (SEC)	0.95 CONFIDENCE +/- VARIABILITY ABOUT MEAN (MU A)	0.95 CONFIDENCE VARIABILITY ABOUT STD DEV (MU A)	
32	2.7057	2.8576	-1.3797
64	2.6969	2.8483	-1.3752
96	2.6751	2.8365	-1.4660
128	2.6240	2.7713	-1.3380

NUMBER OF ENSEMBLE MEMBERS = 1

DEGREES OF FREEDOM = 15.3

BASED UPON WE = 0.25*PI

MIDLAND TLX TX-1 (3-5-69) GLIDE SLOPE

MINIMUM= -1.143

MAXIMUM= -1.063

ZERO REF.= -.0439

FIRST DATA POINT NUMBER= 128

NUMBER OF VALID POINTS=1276

OVERALL SIGNAL MEAN= -1.145

OVERALL SIGNAL SIGMA= 4.335

AVG FOR THE 1120 SAMPLES = -1.226

SIGMA = 4.718

GLIDE SLOPE 25 MEAN AND VARIANCE

6 SECOND WINDOW

TIME (SEC)	MEAN (MU A)	STD DEV (MU A)	VARIANCE (MU A)**2
4	-11.2933	8.4675	71.6990
8	-5.5013	6.2736	39.3583
12	-2.7288	4.7308	22.3802
16	.5323	5.6222	31.6088
20	3.9607	3.4932	12.2024
24	4.5546	2.7026	7.3042
28	4.5135	1.7594	3.0954
32	4.0352	1.8643	3.4757
36	1.5210	3.5513	12.6115
40	.1783	2.6244	6.8875
44	2.6243	1.5118	2.2855
48	1.5537	2.8403	8.0671

64 SECOND WINDOW

TIME (SEC)	MEAN (MU A)	STD DEV (MU A)	VARIANCE (MU A)**2
32	.3488	6.4399	41.4724
64	.0554	3.6047	12.9936
96	-2.5984	2.3630	5.5840
128	-2.4183	2.3929	5.7258

ESTIMATED VARIABILITY FOR 64 SEC WINDOW

TIME (SEC)	0.95 CONFIDENCE		0.95 CONFIDENCE	
	+,- VARIABILITY ABOUT		VARIABILITY ABOUT	
	MEAN (MU A)		STD. DEV. (MU A)	
32	3.3488		3.5368	-1.7076
64	1.6744		1.9797	-.9558
96	1.2288		1.2978	-.6266
128	1.2443		1.3142	-.6345

NUMBER OF ENSEMBLE MEMBERS = 1

DEGREES OF FREEDOM = 15.3

BASED UPON $W_E = 0.25 \cdot \pi$

GLIDE SLOPE SET 1 ENSEMBLE MEAN AND VARIANCE

8 SECOND WINDOW

TIME (SEC)	MEAN (MU A)	STD DEV (MU A)	VARIANCE (MU A)**2
4	-1.6515	17.6209	310.4740
8	-3.0299	15.6810	245.8944
12	-3.0426	13.2820	176.4115
16	-2.4474	12.3976	153.7059
20	-2.5645	11.6865	136.5748
24	-2.0612	10.9369	119.6168
28	-1.5517	10.2965	106.0185
32	-1.6694	9.7603	95.2637
36	-1.9944	10.0106	100.2113
40	-3.1103	9.4353	89.0247
44	-1.6175	9.8888	97.7877
48	-1.1211	11.9714	143.3143

64 SECOND WINDOW

TIME (SEC)	MEAN (MU A)	STD DEV (MU A)	VARIANCE (MU A)**2
32	-2.2553	12.1810	148.3756
64	-2.5332	10.2593	105.2535
96	-2.8023	9.4737	89.7516
128	-2.3098	10.5114	110.4889

ESTIMATED VARIABILITY FOR 8 SEC WINDOW

TIME (SEC)	0.95 CONFIDENCE +,- VARIABILITY ABOUT MEAN (MU A)		0.95 CONFIDENCE VARIABILITY ABOUT STD. DEV. (MU A)	
4	5.6385		5.0134	-3.2514
8	5.0179		4.4616	-2.8935
12	4.2502		3.7790	-2.4509
16	3.9673		3.5275	-2.2877
20	3.7397		3.3251	-2.1565
24	3.4998		3.1118	-2.0181
28	3.2949		2.9296	-1.9000
32	3.1253		2.7770	-1.6010
36	3.2034		2.8482	-1.8472
40	3.0193		2.6846	-1.7410
44	3.1644		2.8136	-1.8247
48	3.8408		3.4061	-2.2090

NUMBER OF ENSEMBLE MEMBERS = 17

DEGREES OF FREEDOM = 38.66

BASED UPON $W_E = 0.25 \cdot P_1$ (RAD/SEC)

ESTIMATED VARIABILITY FOR 64 SEC WINDOW

TIME (SEC)	0.95 CONFIDENCE +,- VARIABILITY ABOUT MEAN (MU A)		0.95 CONFIDENCE VARIABILITY ABOUT STD DEV (MU A)	
32	1.4313		.9835	-.9904
64	1.2055		.8283	-.8341
96	1.1132		.7649	-.7703
128	1.2351		.8487	-.8546

NUMBER OF ENSEMBLE MEMBERS = 17

DEGREES OF FREEDOM = 176.66

BASED UPON $\omega_e = 0.25 \cdot \pi$ (RAD/SEC)

GLIDE SLOPE SET 1 POWER SPECTRAL DENSITY

128 SEC WINDOW

96 SEC WINDOW CENTER TIME

ANGULAR FREQ (RAD/SEC)	PSD (UA)**2/HZ	10*LCG(PSD)
.049	436.4413	26.3993
.069	385.8447	25.8641
.090	327.4576	25.1516
.139	237.8094	23.7623
.190	160.8171	22.0633
.270	101.0458	20.0452
.393	73.0742	18.6376
.555	43.5598	16.3909
.785	20.6415	13.1474
1.111	11.8677	10.7437
1.571	6.2458	7.9559
2.221	2.6953	4.3061
3.142	1.2201	.8638
4.443	.4944	-3.0589
6.263	.1621	-7.9033
8.686	.0544	-12.6440
12.566	.0158	-18.0245
17.772	.0052	-22.8536

GLIDE SLOPE SET 1 POWER SPECTRAL DENSITY

64 SEC WINDOW

32 SEC WINDOW CENTER TIME

ANGULAR FREQ (RAD/SEC)	PSD (UA)**2/HZ	10*LOG(PSD)
.090	487.1191	26.8764
.139	377.8467	25.7732
.196	263.8774	24.2140
.270	174.9361	22.4288
.393	121.1564	20.8335
.555	81.6952	19.1220
.785	44.4350	16.4773
1.111	24.0716	13.8150
1.571	12.3700	10.9237
2.221	6.4606	8.1027
3.142	3.1503	4.9835
4.443	1.2539	.9827
6.283	.4404	-3.5611
8.866	.1451	-8.3842
12.560	.0380	-14.1981
17.772	.0123	-19.0678

GLIDE SLOPE SLT 1 POWER SPECTRAL DENSITY

64 SEC WINDOW

64 SEC WINDOW CENTER TIME

ANGULAR FREQ (RAD/SEC)	PSD (UA)**2/HZ	10*LOG(PSD)
.096	271.8988	24.3441
.139	223.9166	23.5009
.196	168.3663	22.2626
.270	131.9711	21.2048
.393	92.3205	19.6530
.555	53.7274	17.3020
.785	26.6173	14.2516
1.111	14.9952	11.7595
1.571	8.6112	9.3506
2.221	5.9859	6.0053
3.142	1.7773	2.4976
4.443	.7009	-1.5432
6.283	.2165	-6.6459
8.886	.0693	-11.5936
12.566	.0200	-16.9924
17.772	.0068	-21.6723

GLIDE SLOPE SLT 1 POWER SPECTRAL DENSITY

64 SEC WINDOW	96 SEC WINDOW CENTER TIME	
ANGULAR FREQ (RAD/SEC)	PSD (UA)**2/HZ	10*LOG(PSD)
.098	168.5995	22.2686
.139	145.2800	21.6221
.190	114.8220	20.6003
.270	89.0015	19.4940
.393	54.4886	17.3631
.555	31.2345	14.9463
.785	18.4199	12.6529
1.111	11.4436	10.5856
1.571	5.1193	7.0921
2.221	1.8921	2.7694
3.142	.8368	-.7740
4.445	.3470	-4.5971
6.283	.1221	-9.1325
8.886	.0421	-13.7535
12.566	.0137	-18.6212
17.772	.0043	-23.6360

GLIDE SLOPE SET 1 POWER SPECTRAL DENSITY

32 SEC WINDOW

16 SEC WINDOW CENTER TIME

ANGULAR FREQ (RAD/SEC)	PSD (UA) ² /HZ	10*LOG(PSD)
.196	313.8047	24.9666
.278	215.6320	23.3371
.393	131.6866	21.1954
.555	86.8715	19.3888
.785	54.4184	17.3575
1.111	29.7495	14.7348
1.571	14.3811	11.5779
2.221	7.6180	8.8184
3.142	3.7046	5.6875
4.443	1.5369	1.8664
6.283	.5967	-2.2426
8.686	.1992	-7.0080
12.566	.0509	-12.9314
17.772	.0162	-17.9110

GLIDE SLOPE SLT 1 POWER SPECTRAL DENSITY

32 SEC WINDOW

32 SEC WINDOW CENTER TIME

ANGULAR FREQ (RAD/SEC)	PSD (GA)**2/HZ	10*LOG(PSD)
.196	168.7147	22.2715
.276	136.3499	21.3465
.396	97.1932	19.8764
.556	61.8296	17.9120
.786	33.1708	15.2076
1.111	17.3497	12.3929
1.571	10.4501	10.1912
2.221	6.6004	8.1957
3.142	3.7052	5.6858
4.443	1.5065	1.7796
6.283	.5020	-2.9926
8.886	.1684	-7.7364
12.566	.0410	-13.8686
17.772	.0143	-18.4524

GLIDE SLOPE SLT 1 POWER SPECTRAL DENSITY

32 SEC WINDOW

48 SEC WINDOW CENTER TIME

ANGULAR FREQ (RAD/SEC)	PSD (UA)**2/HZ	10*LOG(PSD)
.190	186.0454	22.6962
.270	159.0480	22.0153
.390	118.4131	20.7340
.555	68.2645	18.3420
.765	33.9390	15.3070
1.111	17.9695	12.5454
1.571	11.2098	10.4960
2.221	5.6038	7.4249
3.142	2.4854	3.9540
4.443	.9563	-.1939
6.283	.2909	-5.3620
8.880	.0921	-10.3585
12.566	.0253	-15.9603
17.772	.0098	-20.1098

GLIDE SLOPE SET 1 POWER SPECTRAL DENSITY

32 SEC WINDOW

64 SEC WINDOW CENTER TIME

ANGULAR FREQ (RAD/SEC)	PSD (UA)**2/HZ	10*LOG(PSD)
.198	267.8210	24.2784
.278	177.3919	22.4893
.393	103.8033	20.1621
.558	50.3496	17.0200
.785	26.8474	14.2890
1.111	10.0310	12.0496
1.571	9.0705	9.5763
2.221	3.6935	5.9034
3.142	1.4846	1.7161
4.443	.5800	-2.3658
6.283	.1980	-7.0339
8.886	.0685	-11.6400
12.566	.0200	-16.9882
17.772	.0071	-21.4779

GLIDE SLOPE SET 1 POWER SPECTRAL DENSITY

32 SEC WINDOW

80 SEC WINDOW CENTER TIME

ANGULAR FREQ (RAD/SEC)	PSD (UA)**2/HZ	10*LOG(PSD)
.190	130.2294	21.1471
.270	91.6360	19.6207
.390	57.4273	17.5912
.555	31.6499	15.0037
.780	19.2543	12.8453
1.111	11.8895	10.7516
1.571	5.6743	7.5391
2.221	2.5400	4.0463
3.142	1.1069	.4413
4.443	.4319	-3.6466
6.283	.1512	-8.2031
8.880	.0487	-13.1224
12.560	.0154	-18.1375
17.772	.0052	-22.8630

APPENDIX B

MODELS USED FOR ILS GLIDE SLOPE; WIND, WIND SHEAR AND TURBULENCE; AIRCRAFT; APPROACH COUPLERS AND FLIGHT CONTROL SYSTEMS

The equations and numerical parameter values actually used in the overall system performance model are summarized in this Appendix.

GLIDE SLOPE BEAM ALIGNMENT AND STRUCTURE MODEL

This subsection documents the model of the ILS Glide Slope signal used in the system performance analysis. The model represents the received signal in the aircraft (in distinction to representing the ILS signal in space). Consequently, only the deterministic portion of the received signal model is a function of the receiving antenna location for a given range.

The model of the received signal consists of four components:

- The far-field straight line asymptote as determined in the vertical plane containing the runway centerline.
- The deviation of the ideal 0 DDM locus for the commissioned angle from the above asymptote as measured in the vertical plane containing the runway centerline.
- The deviation of the mean alignment for the actual beam from the ideal 0 DDM locus above.
- The deviation arising from actual beam structure with respect to the mean alignment of the beam.

The first two of the above components are deterministic in nature, and are derived by reference to the basic geometric characteristics of the idealized ILS Glide Slope guidance signal. The parameters characterizing their deterministic functions vary over relatively narrow ranges. Furthermore, those parameters are typically selected within limits to be favorable for each ILS Glide Slope site. Typical parameter values will be used for these components of the model.

The forms for the third and fourth components of the model are based upon analytical curves which have been fitted to the results of the non-stationary statistical analysis of actual ILS Glide Slope data conducted

by the Collins Radio Co. (Refer to Appendix A.) The levels for the third and fourth components are made variable in this study. The maximum permissible levels are the object of the investigation.

The third component of the model is a deterministic bias for any one approach and landing operation. However, from one approach and landing to the next the bias changes in order to simulate a population of ILS facilities. This is done by using a range of values for the random parameter in this component of the model.

The last component of the model is a stochastic disturbance representing Glide Slope beam structure.

The specific details of these model components are summarized in the following subsections.

Basic Geometrical Considerations

The basic, highly idealized, geometry for the ideal Glide Slope O DDM signal in relation to the runway and in relation to the trimmed aircraft approach path (the far-field asymptote) is shown in Fig. B-1. The runway is assumed to be level and the axis of symmetry for the O DDM hyperboloid is assumed to be vertical. Under these circumstances the GPIP is not opposite the antenna mast on the runway centerline unless z_1 is zero. This scenario corresponds to the so-called "pedestal case." If the grade between the runway level and the base of the antenna mast is constant, its effect is to tilt the axis of the O DDM hyperboloid from vertical through the grade angle. In this latter case, the GPIP is approximately opposite the antenna mast on the runway centerline regardless of z_1 . We shall refer to the latter case as the "tilted case." Hybrid combinations of the pedestal and tilted cases usually occur in practice.

The main distinctions between these two cases insofar as the system performance analysis is concerned are:

- For a given positive z_1 , the GPIP and hence the nominal center of the touchdown footprint, will be further down the runway by approximately $z_1/\tan \Theta$ for the "tilted case," all other parameters held constant.
- For a given positive z_1 , the threshold crossing height will be increased by approximately z_1 for the "tilted case," all other parameters held constant.

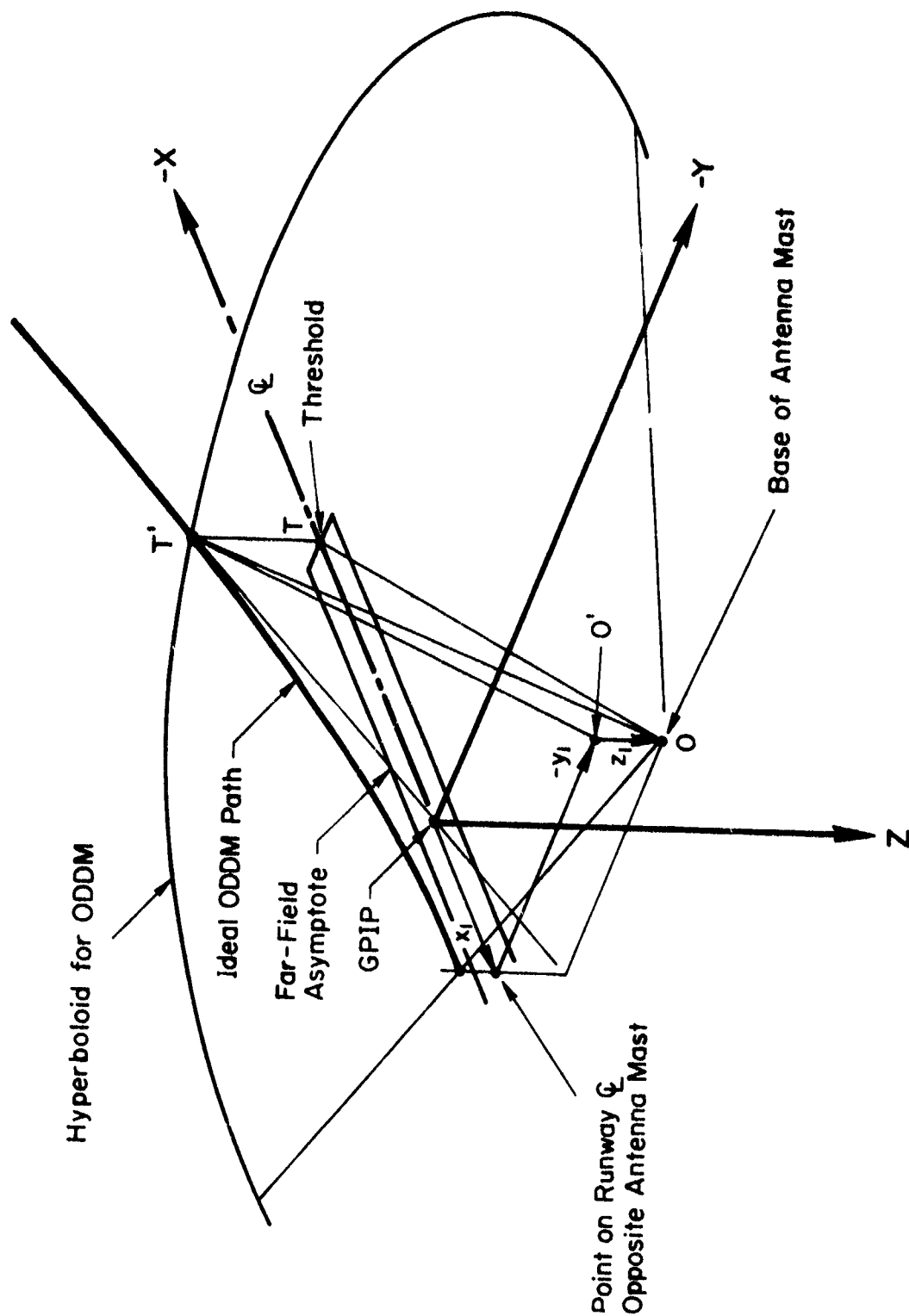


Figure B-1. Basic Geometry Determining Ideal ODDM Path and the Far-Field Asymptote

These two items influence system performance only insofar as the siting of the Glide Slope antenna is concerned. Even then the problem is essentially clearance-related (in distinction to performance-related), and should be dealt with by means of assuring that a minimum threshold crossing altitude is not transgressed.

The "pedestal case" is the basis for the model presented herein. Differences between actual cases and the "pedestal case" are represented by the random components of the model. Threshold crossing height considerations are presumed to be addressed as part of the individual siting specifications.

The equation for the hyperboloid surface representing O DDM in Fig. B-1 is

$$z_h = -\sqrt{c^2 + \tan^2 \Theta_1 [(X - x_1)^2 + (Y - y_1)^2]} + z_1 \quad (B-1)$$

where Θ_1 is the angle that the far-field asymptote makes with the horizontal plane and c is the elevation of the O DDM surface above the antenna mast base. Typical numerical values are:

$$c = 1.5 \text{ ft}$$

$$\Theta_1 = 3.0 \text{ deg}$$

$$z_1 = 2.0 \text{ ft}$$

$$y_1 = \pm 400. \text{ ft}$$

$$x_1 = z_1 / \tan \Theta = 38.2 \text{ ft}$$

Θ_1 is also the angle with respect to horizontal of the asymptote to the curve which is the intersection of the O DDM hyperboloid surface with the vertical plane containing the runway centerline.

The O DDM hyperboloid is well approximated by a cone in the vicinity of the vertical plane containing the runway centerline. The equation for the cone is:

$$z_c = -\tan \Theta_1 \sqrt{(X - x_1)^2 + (Y - y_1)^2} + z_1 \quad (B-2)$$

The equation for the intersection of either the hyperboloid or the cone with the vertical plane through the runway centerline may be obtained by setting $y = 0$ in the appropriate equation above.

The far-field asymptote to either curve is given by:

$$z_a = z_1 + (X - x_1) \tan \Theta_1 = X \tan \Theta_1 \quad (B-3)$$

The origin of the conical reference surface generated by the theodolite is located along the line $O'T'$. The origin of this conical reference surface is nearly always within 100. ft of point O . The exact point of location is typically determined by the vertical distance between the line $O'T'$ and the ambient terrain (approximately represented by the line OT) being 62 inches (Ref. 5). The angle of the line $O'T'$ with respect to horizontal is the commissioned angle Θ . Current practice is to have Θ and Θ_1 nominally equal so the far-field coincides with the conical reference. The theodolite will then be located about 62.6 ft in front of the base of the antenna mast for the typical numbers given above. Other quantities evaluated for the typical parameter values are in Table B-1.

The difference between the curves resulting from the intersection of the conical reference and the C DDM hyperboloid with the vertical plane containing the runway centerline is generally regarded as small at distances greater than the runway threshold from the GPIP. However, the difference at the threshold, 2.0 ft (0.109 deg or 23.4 μA) is appreciable. It should be remarked here that this difference is unique to the "pedestal case." The "tilted case" is not subject to this systematic error which arises in the pedestal case because of $z_1 \neq 0$. That is, the effective pedestal height is not zero.

TABLE B-1 VALUES FOR TYPICAL PARAMETERS

TCH for asymptote	= 52.408 ft
TCH for hyperboloid	= 58.307 -2. = 56.307 ft
TCH for conic reference	= 58.307 ft
Angular difference WRT base of antenna mast	= 0.103 deg
μA difference	= 22.07 μA
Angular difference WRT theodolite	= 0.109 deg
μA difference	= 23.39 μA
Difference in ft	= 2.0 ft

Straight-Line Asymptote Component

The far-field straight-line asymptote at the commissioned angle, Θ , establishes the nominal trimmed flight path for the aircraft equations of motion model. It is in that sense that this component of the Glide Slope signal model is incorporated into the system performance analysis model. The commissioned angle will be treated as a constant ($\Theta = 3. \text{ deg}$) since the effect of the commissioned angle is taken into account in determining the ILS siting. It therefore has no appreciable influence upon landing performance for the narrow range of values which are typically used.

Deviation of the Ideal Path from the Asymptote

The deviation of the ideal O DDM locus for the commissioned angle from the straight-line asymptote as measured in the vertical plane containing the runway centerline is given by $\bar{d}_c \doteq (z_a - z_h) \doteq (z_g - z_c)$. \bar{d}_c is positive when the ideal O DDM locus lies above the straight-line asymptote. For $\Theta = \Theta_1$, this results in

$$\bar{d}_c \doteq \left[\sqrt{(X - x_1)^2 + y_1^2} + (X - x_1) \right] \tan \Theta \quad \text{ft} \quad (\text{B-4})$$

which will serve as the model for this component of Glide Slope signal. The parameter values will be $\Theta_1 = 3. \text{ deg}$, $y_1 = \pm 400. \text{ ft}$ and $x_1 = 38.2 \text{ ft}$. \bar{d}_c may be converted to μA units by multiplying by K_o/R where R is the range to the base of ILS Glide Slope antenna mast and K_o is given by

$$K_o = \frac{150. (57.3)}{0.7} = 12278.6 \mu\text{A/rad} \quad (\text{B-5})$$

The facility-to-facility variation in these parameters is not appreciable in terms of effect upon \bar{d}_c . Therefore the parameters of the model are fixed constants and the variability is modelled by the variability in the $\Delta\Theta$ component described below.

The beam alignment error, $\Delta\Theta$, is modelled by a random selection for each approach and landing, from a Gaussian distribution having mean and standard deviation $\bar{\Delta\Theta}$ and $\sigma_{\Delta\Theta}$ respectively.

$$\dot{\Delta\Theta} = 0, \quad \overline{\Delta\Theta} = 2.5 \text{ CSF } \mu\text{A} \doteq 0. \mu\text{A} \quad (\text{B-6})$$

$$\sigma_{\Delta\Theta} = 8.01 \text{ CSF } \mu\text{A} \quad (\text{B-7})$$

where CSF is a constant scale factor whose maximum value is the object of investigation. $\Theta + \Delta\Theta = \Theta_1$ establishes the trimmed flight path for any one approach and landing. It is in this sense that this component of the Glide Slope signal model is incorporated into the system performance analysis model.

Beam Structure

The nonstationary power spectral density analysis of ILS Glide Slope structure resulted in a model consisting of white noise passed through a first-order low-pass filter. The bandwidth and standard deviation of the filter output are

$$\hat{\omega}_{\eta} = 0.18 \text{ rad/sec} \quad (\text{B-8})$$

$$\hat{\sigma}_{\eta} = 5.99 + 14.88 e^{-t/10.74} \quad (\text{B-9})$$

where t is time-to-go before runway threshold crossing. The data were collected during approaches flown at approximately 135 kt TAS. A headwind component of 8 kt can be assumed, giving a groundspeed of 127 kt (214.6 ft/sec)

The model for the beam structure when generalized to accommodate any arbitrary approach ground speed, is

$$\dot{\eta}_c = -(v_{T_o}^*/L_{\eta})\eta_c + \sigma_{\eta} \sqrt{2v_{T_o}^*/L_{\eta}} \text{ CSF } w_1 \quad (\text{B-10})$$

$$\eta_c^* = K_x \eta_c = (1 + 2.48 e^{(X + 1000)/2304}) \eta_c \quad (\text{B-11})$$

where η_c^* is the variable representing beam structure, η_c is an intermediate variable of convenience and w_1 is an independent unit white noise source. The parameter value for L_{η} is determined from

$$L_{\eta} = \frac{V_{T_0}^*}{\omega_{\eta}} = 1192 \text{ ft} \quad (\text{B-12})$$

and $\sigma_{\eta} = 5.99 \mu\text{A} \quad (\text{B-13})$

The characteristic length, 2304. ft, in the exponential function is determined from

$$L_1 = 10.74 V_{T_0}^* = 2304. \text{ ft} \quad (\text{B-14})$$

while 2.48 is determined from

$$\frac{\hat{\sigma}_{\eta}(0) - \hat{\sigma}_{\eta}(\infty)}{\hat{\sigma}_{\eta}(\infty)} = 2.48 \quad (\text{B-15})$$

CSF is the same constant scale factor used before in connection with Eq B-6 and -7. Its value is the object of investigation. The nominal distance between the GPIP and the runway threshold is taken as 1000 ft.

WIND, WIND SHEAR, AND TURBULENCE MODELS

This subsection documents models for the atmospheric disturbance environment which forms part of the overall system performance model.

The atmospheric disturbance environment model represents disturbances of three types. These are the mean wind, wind shear, and stochastic turbulence. All three types are characterized by parameters which are a function of altitude, and which themselves are possibly random variables.

The mean wind and wind shear are deterministic disturbances for any one approach and landing operation. However, from one approach and landing to the next, the level of the mean wind and wind shear is a random selection from a Gaussian distribution having a particular mean and standard deviation. These disturbances are therefore properly applied to the stochastic portion of the system performance model. The turbulence is a stochastic disturbance.

The turbulence is therefore applied to the stochastic portion of the system performance model.

Mean Wind Model and Wind Shear (Ref. 10 and 27)

The longitudinal component, u_w , of the steady head wind profile of Ref. 27 is used. This results in a profile whose magnitude is determined by a random selection from Gaussian distribution. Thus, for any given approach and landing, the profile is fixed, but from one approach to the next the profile changes. A sample profile is shown in Fig. B-2. To obtain any other profile it is only necessary to scale up (or down) the wind magnitude. Conveniently, any particular profile can be completely determined by specifying the magnitude at a given reference altitude. For the purpose of discussion, a wind reference altitude of 10 ft will be selected. This corresponds to the approximate altitude of the center of gravity for a typical aircraft at the instant of touchdown. At this altitude the wind magnitude varies from a 10 kt tail wind to a 26 kt head wind ($\pm 3\sigma$) and has mean value of 8 kt. These values are consistent with the design values specified by the FAA in Ref. 6.

The probability density function for the mean wind, u_w , is a Gaussian distribution with mean and standard deviation given by:

$$\overline{u_w} = F_w e^{-h^*/H_w} (D_w \log h^* + E_w) / (D_w + E_w) \quad (B-16)$$

$$\sigma_{u_w} = 0.75 \overline{u_w} \text{ CRF} \quad (B-17)$$

$$\text{where } F_w = 13.5 \text{ ft/sec (8 kt)} \quad (B-18)$$

$$D_w = 0.43$$

$$E_w = 0.35$$

$$H_w = 10,000.$$

$$\text{and } h^* = H + h_{ocg}$$

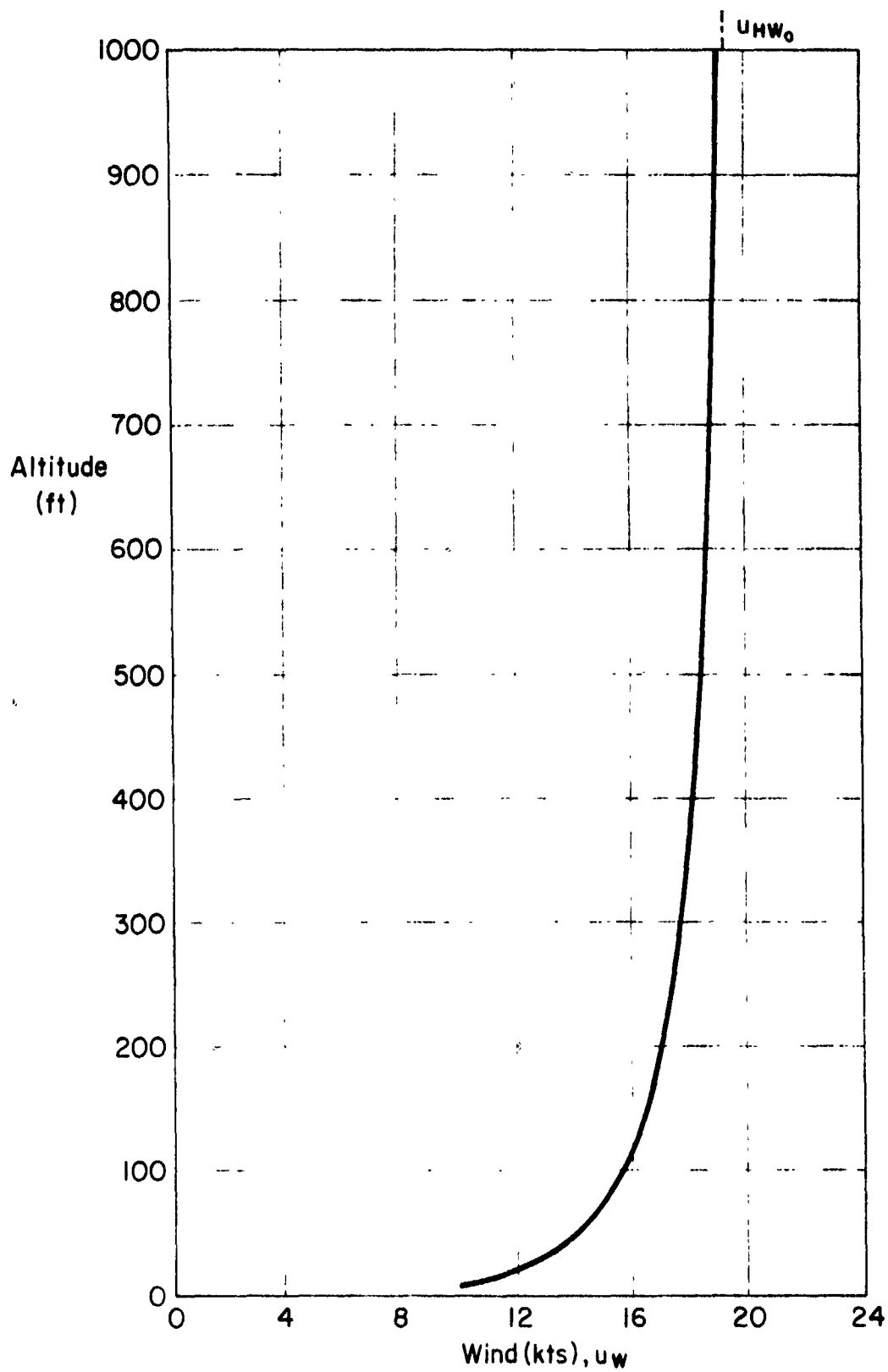


Figure B-2. Wind Profile Associated with
10 kt Wind at 10 ft Altitude (From Ref.10)

H is the altitude of the main landing gear wheels and h_{ocg} is the aircraft cg altitude at touchdown. CRF is a scale factor (having a nominal value of unity) introduced to permit scaling of the variability of the mean wind and wind shear. The nominal value of CRF is used throughout this study. The mean wind \bar{u}_w has the following shear characteristics (Ref. 27).

TABLE B-2 SHEAR CHARACTERISTICS

h^* (ft)	SHEAR	
	FT/SEC/100 ft	KNOTS/100 ft
10	39.2	23.2
100	3.92	2.32
300	1.31	0.77

These characteristics also tend to be consistent with $1/3$ of the 8 kt/100 ft specified by the FAA in Ref. 6 at an altitude of 100 ft. However, the increasing shear with decreasing altitude of the present model poses a more severe but perhaps more realistic environment than does the Ref. 6 model.

Random Turbulence Model (Ref. 28)

The model for random turbulence is a simplified version of that given in Ref. 28. Gradient effects associated with the normal turbulence component are neglected. For any one approach the random turbulence components have Gaussian probability density functions with zero means. The standard deviation σ_{u_g} should be chosen for each approach from a Rayleigh probability density function* having a characteristic speed of σ_{u_g} ft/sec. However, for the sake of simplicity, the mean value of σ_{u_g} , which is σ_{u_g} , is used for all approaches in the overall system performance model.

*The Rayleigh probability density function is for u_g (rather than w_g as stated in Ref. 28). This reinterpretation is based on private communication with NASA-Ames personnel (as well as Cornell) which indicates that a typographical error is the likely explanation.

$$\begin{aligned}\sigma_{u_g} &= 2.79 - 0.245 \log h^* \text{ ft/sec} & h^* > 100 \text{ ft} \\ &= 2.3 \text{ ft/sec} & h^* \leq 100 \text{ ft}\end{aligned}\quad (\text{B-19})$$

The standard deviation σ_{u_g} is a function of σ_{u_g} . The frequency content of the random turbulence and σ_{u_g} are functions of altitude.

The power spectral densities for the longitudinal and normal random turbulence components at a given altitude are respectively:

$$\phi_{u_g} = \frac{\sigma_{u_g}^2 2V_{A_0}/L_u}{\omega^2 + (V_{A_0}/L_u)^2} \quad (\text{B-20})$$

$$\phi_{w_g} = \frac{\sigma_{w_g}^2 2(1.594V_{A_0}/L_w)}{\omega^2 + (1.594V_{A_0}/L_w)^2} \quad (\text{B-21})$$

$$\text{where} \quad \sigma^2 = \frac{1}{2\pi} \int_{-\infty}^{\infty} \phi \, d\omega \quad (\text{B-22})$$

ϕ_{w_g} is a lower order approximation to the power spectral density given in Ref. 28. The approximation is such that the mean-square level and half-power frequency are preserved.

The differential equations for unit-white-noise shaping filters producing output variables u_g and w_g having power spectral densities ϕ_{u_g} and ϕ_{w_g} respectively are:

$$\dot{u}_g = -V_{A_0}/L_u u_g + \sigma_{u_g} \text{CTF} \sqrt{2V_{A_0}/L_u} w_2 \quad (\text{B-23})$$

$$\dot{w}_g = -1.594V_{A_0}/L_w w_g + \sigma_{w_g} \text{CTF} \sqrt{2(1.594V_{A_0}/L_w)} w_3 \quad (\text{B-24})$$

where w_2 and w_3 are independent unit white noises. V_{A_0} is the trim approach airspeed. CTF is a scale factor (having a nominal value of unity) introduced to permit scaling of the turbulence intensity. The nominal value of

CTF is used throughout this study.

The integral scale lengths L_u and L_w are given as functions of altitude h^* by:

$$\begin{aligned} L_u &= 145[n^*]^{1/3} & 100 \leq h^* \leq 1750 \text{ ft} \\ &= 145[100]^{1/3} = 673 & h^* \leq 100 \text{ ft} \end{aligned} \quad (\text{B-25})$$

$$L_w = h^* \quad h^* \leq 1750 \text{ ft} \quad (\text{B-26})$$

The standard deviation for the normal turbulence component σ_{wg} is related to the standard deviation for the longitudinal turbulence component σ_{ug} through the integral scale lengths.

$$\sigma_{wg} = \sqrt{L_w/L_u} \sigma_{ug} \quad (\text{B-27})$$

The random turbulence model is used in the stochastic portion of the system performance model throughout the approach and landing.

AIRCRAFT LONGITUDINAL MOTION MODEL

The method used for system performance analysis requires that equations of motion for the aircraft be in state vector form, include the pertinent kinematic equations, and that appropriate measures be taken to incorporate the deterministic wind effects. All of these considerations force some minor changes upon the customary equations-of-motion model.

The next three subsections cover in turn the kinematic equations, incorporation of deterministic wind effects, and the final set of state equations for the aircraft and kinematics plus auxiliary equations for sensor inputs which are not states.

Kinematic Equations

The scenario for the system performance model is shown in Fig. B-3. A perfectly level runway is assumed. Figure B-4 defines the perturbed

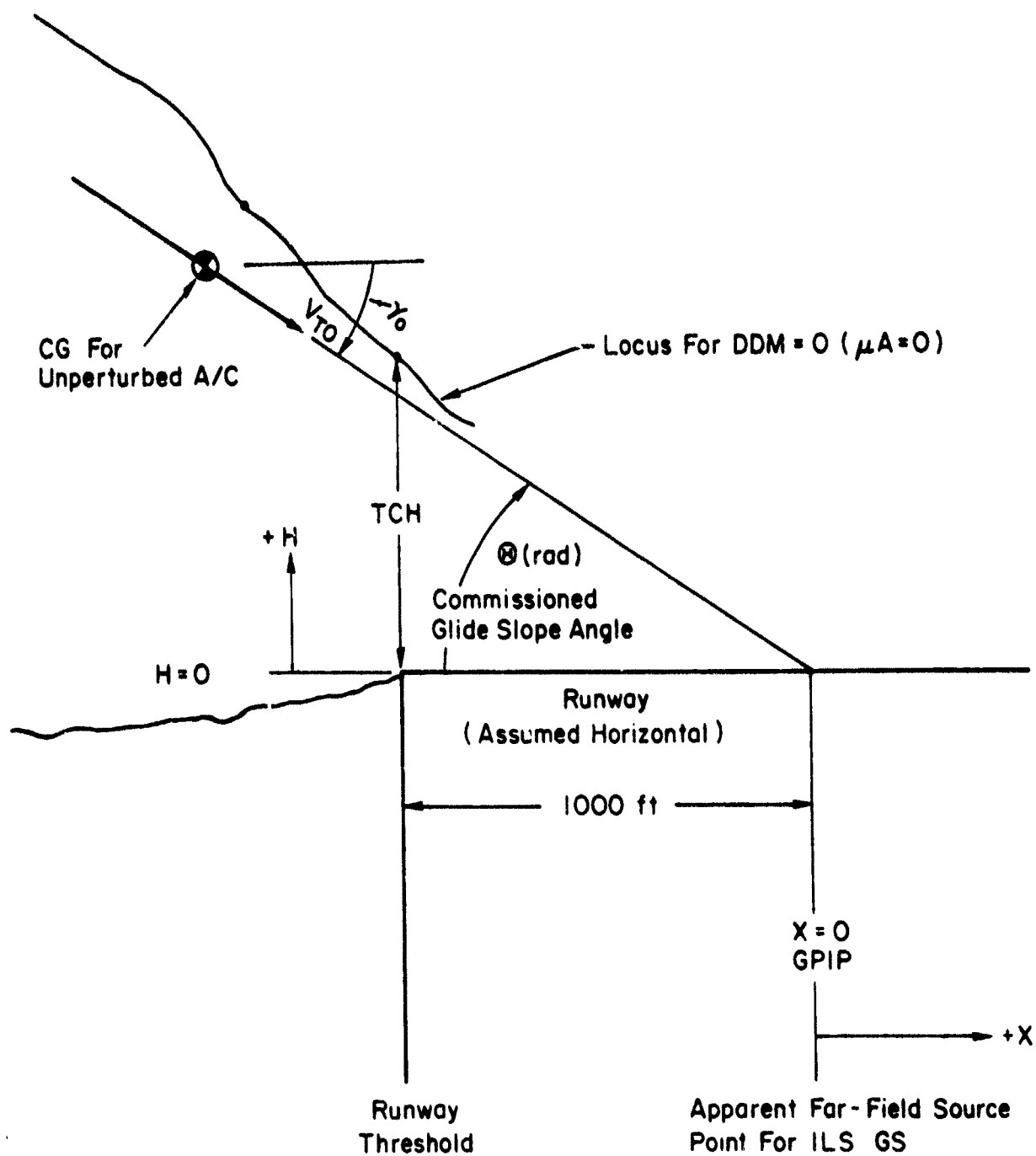


Figure B-3. Scenario for Approach and Landing for System Performance Analysis

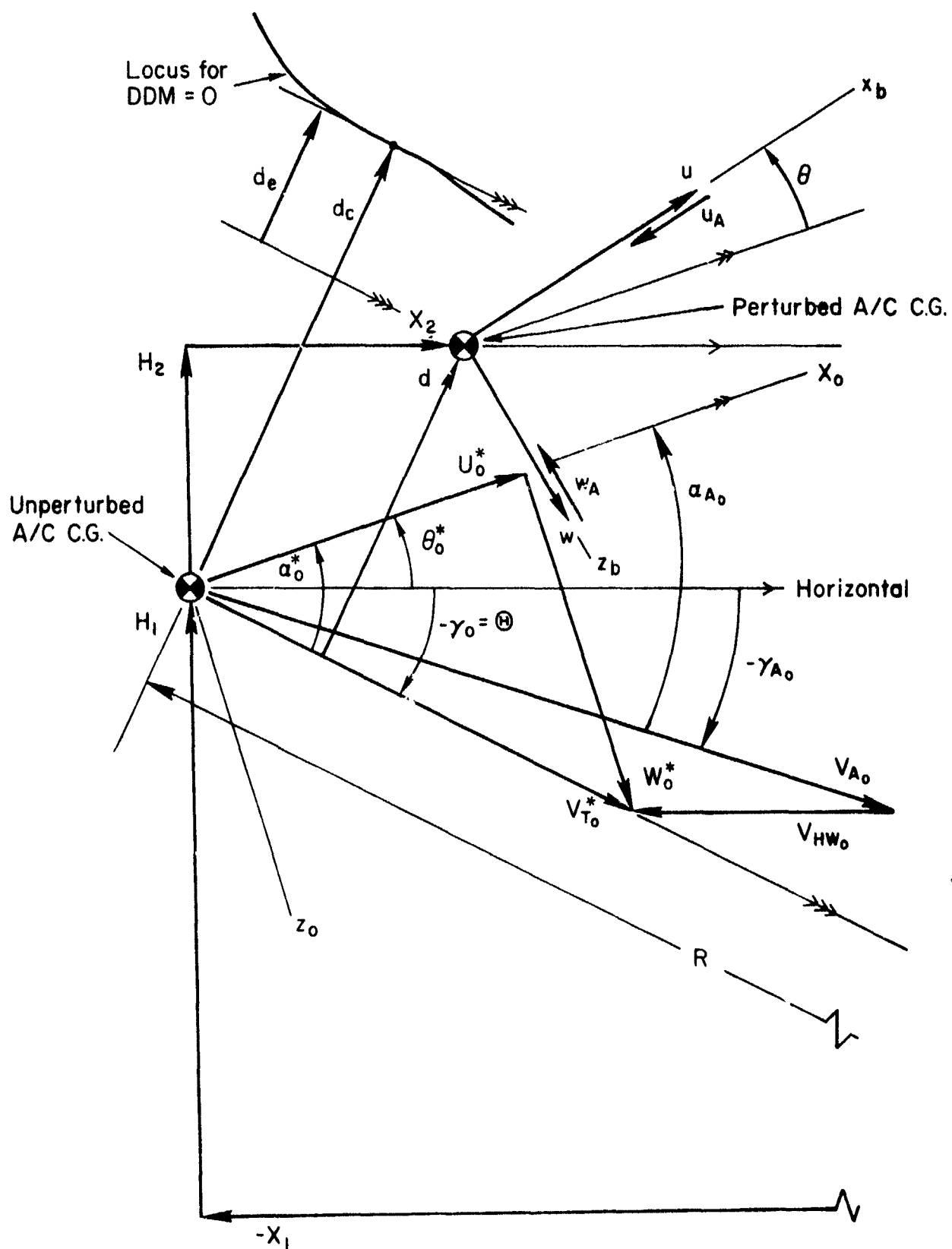


Figure B-4. Perturbed Coordinates Locating the Aircraft

coordinates for the aircraft body axes with respect to the unperturbed (or nominal) coordinates. Kinematic equations locating the aircraft center of gravity with respect to the apparent source of the ILS Glide Slope in the far-field and with respect to the runway are:

$$\dot{X} = \dot{X}_1 + \dot{X}_2 \quad (B-28)$$

$$\dot{X}_1 = V_{T0}^* \cos \gamma_0 \quad (B-29)$$

$$\dot{X}_2 = u \cos \theta_0^* + w \sin \theta_0^* - (U_0^* \sin \theta_0^* - W_0^* \cos \theta_0^*) \theta \quad (B-30)$$

$$\dot{H} = \dot{H}_1 + \dot{H}_2 \quad (B-31)$$

$$\dot{H}_1 = V_{T0}^* \sin \gamma_0 \quad (B-32)$$

$$\dot{H}_2 = \theta (U_0^* \cos \theta_0^* + W_0^* \sin \theta_0^*) + u \sin \theta_0^* - w \cos \theta_0^* \quad (B-33)$$

$$U_0^* = V_{T0}^* \cos (\theta_0^* - \gamma_0) \quad (B-34)$$

$$W_0^* = V_{T0}^* \sin (\theta_0^* - \gamma_0) \quad (B-35)$$

Additional kinematic relationships of interest are:

$$d = H_2 \cos \gamma_0 - X_2 \sin \gamma_0 \quad (B-36)$$

$$d_e = d_c - d \quad (B-37)$$

$$R = (H + z_1)^2 + (X - x_1)^2 + y_1^2 \quad (B-38)$$

R is the distance between the aircraft the the base of the ILS Glide Slope antenna mast. The steady wind* acts in the horizontal direction

*The "steady wind" V_{HW0} is here taken as the initial value of the mean wind u_w in the system performance model. See the second subsection of this Appendix for a description of the mean wind.

only. For a given airspeed, V_{A_0} , $V_{T_0}^*$ is determined by:

$$V_{T_0}^* \cos \gamma_0 = V_{A_0} \cos \gamma_{A_0} - V_{HW_0} \quad (B-39)$$

The difference between the inertial flight path angle and the flight path angle with respect to the steadily translating air mass is usually quite small for CTOL aircraft. Therefore $\gamma_{A_0} \doteq \gamma_0$ and

$$V_{T_0}^* \doteq V_{A_0} - V_{HW_0} / \cos \gamma_0 \quad (B-40)$$

is a valid approximation which also has the advantage of simplicity since power setting and aerodynamic angle of attack are not explicitly involved.

The equilibrium conditions for the perturbation equations of motion may be developed in terms of useful approximations based upon the steady headwind, V_{HW_0} , and the trim inertial flight path angle, γ_0 . Since the equilibrium inertial flight path angle, γ_0 , must be invariant with the steady headwind component which is a horizontal component:

$$\gamma_{A_0} \doteq \sin \gamma_{A_0} \doteq V_{T_0} \sin \gamma_0 / V_{A_0} \doteq V_{T_0}^* \gamma_0 / V_{A_0} \quad (B-41)$$

The lift and drag equilibrium equations are:

$$L = mg \cos \gamma_{A_0} \doteq mg \quad (B-42)$$

$$D = T_0 - mg \sin \gamma_{A_0} \doteq T_0 - mg V_{T_0}^* \gamma_0 / V_{A_0} \quad (B-43)$$

Since the lift must be approximately invariant with γ_{A_0} (i.e., steady headwind), an assumption that equilibrium airspeed, V_{A_0} , is maintained constant regardless of steady headwind results in α_{A_0} and D being independent of the steady headwind. Maintenance of equilibrium, however, then requires that the trim thrust setting T_0 , be adjusted to maintain the right-hand side of the drag equation constant for different values of the steady headwind. Furthermore, the trim values of α_0^* , θ_0^* , U_0^* , and W_0^* are dependent upon the steady headwind.

$$\theta_o^* = \alpha_{A_o} + \gamma_{A_o} + \alpha_{A_o} + V_{T_o}^* \gamma_o / V_{A_o} \quad (B-44)$$

$$\alpha_o^* = \theta_o^* - \gamma_o \doteq \alpha_{A_o} - V_{HW_o} \gamma_o / V_{A_o} \quad (B-45)$$

$$U_o^* = V_{T_o}^* \cos (\theta_o^* - \gamma_o) \quad (B-46)$$

$$W_o^* = V_{T_o}^* \sin (\theta_o^* - \gamma_o) \quad (B-47)$$

When the steady headwind is zero, then $V_{A_o} = V_{T_o}^* = V_{T_o}$, $\theta_o^* = \theta_o$, $\gamma_{A_o} = \gamma_o$, $\alpha_o^* = \alpha_o$, $U_o^* = U_o$, and $W_o^* = W_o$ where the unstarred quantities have the customary definitions. If trim airspeed is constant regardless of the steady headwind, and the approximate expressions given above obtain, then $V_{A_o} = V_{T_o}$ and $V_{T_o}^* = V_{T_o} - V_{HW_o} / \cos \gamma_o$ where V_{T_o} has the customary definition.

Deterministic Wind Effects

The mean wind and wind shear components of the atmospheric disturbance environment act in a horizontal direction and therefore must be resolved into aircraft body-fixed axis coordinates for proper application via the aircraft equations of motion. Let the longitudinal and normal components (with respect to body-fixed axes) of the deterministic atmospheric disturbance environment be designated u_A and w_A respectively.

$$\begin{aligned} u_A &= -u_w \cos (\theta_o^* + \theta) \\ &\doteq -u_w \cos \theta_o^* \end{aligned} \quad (B-48)$$

$$\begin{aligned} w_A &= -u_w \sin (\theta_o^* + \theta) \\ &\doteq -u_w \sin \theta_o^* + \Delta w_{ge} \end{aligned} \quad (B-49)$$

u_w represents the mean wind and wind shear component described in the second subsection of this Appendix. The linearized approximate expressions for u_A and w_A are used in the system performance model. u_A and w_A enter the equations of motion in the manner of u_g and w_g .

TABLE B-3 VARIABLES OF INTEREST

VARIABLE	SENSOR INPUT FOR FEEDBACK TO	REASON FOR INTEREST
u_{AS}	δ_T	Category II window dimension
\dot{H}	δ_e	Touchdown sink rate; defines touchdown event
q	δ_e	
θ	δ_T , sometimes, δ_e	Pilot acceptance
H	*	Defines minimum decision altitude passage and touchdown events
a_z	δ_e	Pilot acceptance
d_e	δ_e	Category II window dimension
X		Touchdown location on runway
d		True measure of Glide Slope tracking performance
d_c		Major variable under investigation
δ_e		Measure of control activity
δ_T		Measure of control activity

*H is used in practice to schedule gains in the d_c to δ_e feedback path. Furthermore, several parameters of the overall system performance model are functions of H. In order to maintain linearity in the model, H must be approximated by a deterministic function of time for the purpose of gain scheduling and for evaluation of these parameters.

Δw_{ge} represents that portion of ground effect which is an apparent change in the angle of attack. This has been identified in Ref. 17 as the only significant facet of ground effect insofar as touchdown related variables are concerned. Δw_{ge} is here treated as a deterministic function of the expected altitude. The details of this function are given later in connection with numerical data for specific aircraft.

State and Output Equations for the Aircraft

Aircraft perturbation equations of motion are customarily expressed in terms of states u , w , q and θ . However, output variables must be obtained which are directly of interest or are inputs to the flight control sensors. For example, rate of climb perturbation \dot{h}_2 is of interest, whereas the plunging velocity w is not of particular interest.

Table B-3 has been constructed to aid selection of appropriate variables for the output vector. It turns out that the number of variables of interest exceeds the dimension of the state vector. For this reason, there is no particular advantage to selecting state variables which are also variables of interest since an output equation is a virtual necessity. This is so because off-diagonal elements of the complete output covariance array are of interest at selected times during the solution.

Assuming $Z_w^* = 0$ and neglecting normal gust gradient effects, the aircraft state equations are (Ref. 15)

$$\begin{aligned} \dot{u} = & X_u u + X_w w - W_o^* q - (g \cos \theta_o^*) \theta \\ & + X_{\delta_e} \delta_e + X_{\delta_T} \delta_T - X_u u_g - X_w w_g \\ & + X_u^* K_w u_{wo} - X_u^* V_{HW_o} - X_w \Delta w_{ge} \end{aligned} \quad (B-50)$$

$$\begin{aligned} \dot{w} = & Z_u u + Z_w w + U_o^* q - (g \sin \theta_o^*) \theta \\ & + Z_{\delta_e} \delta_e + Z_{\delta_T} \delta_T - Z_u u_g - Z_w w_g \\ & + Z_u^* K_w u_{wo} - Z_u^* V_{HW_o} - Z_w \Delta w_{ge} \end{aligned} \quad (B-51)$$

Numerical Data for Example Aircraft and Kinematic Constants

Numerical data for the FAA Convair 880 aircraft is given in Table B-4, and data for a typical light twin-engine aircraft, the Piper PA-30, is given in Table B-5. A model for aerodynamic ground effect is also given.

The selection of the Convair 880 and Piper PA-30 aircraft as representative is justified in Table B-6. Table B-6 compares key parameters which influence glide path control in a significant way for several well-known aircraft. It can be seen that the selected aircraft are indeed representative of the extremes with respect to wing-loading, approach speed, and, most importantly, with respect to the dimensional stability derivative $-Z_w$. ($-Z_w$) is a key parameter because it governs the achievable bandwidth for control of glide path angle and also the response sensitivity to normal gusts.

The kinematic constants of interest are the initial unperturbed altitude above the runway, H_0 , and the Glide Slope angle which is also equal to the negative of trimmed flight path angle, γ_0 . Values for these are:

$$H_0 = 1000 \text{ ft for CV-880, } 750 \text{ ft for PA-30}$$

$$\gamma_0 = -3.0 \text{ deg}$$

Ground effect is usually modeled by correcting the nondimensional lift, drag and moment coefficients as a function of altitude in semi-spans and the coefficient change between no ground effect and full ground effect. This relation is as follows for the Convair 880 (the numerical constants might be slightly different for other aircraft)

$$C_N = C_{N_{OGE}} + K(C_{N_{IGE}} - C_{N_{OGE}}) \quad (B-59)$$

$$K = e^{-2.526(2h^*/b)^{0.891}} \quad (B-60)$$

where C_N is any force or moment derivative or trim angle of attack. The apparent change in angle of attack has been found to be the only significant ground effect insofar as touchdown variables are concerned (Ref. 17). Ground effect produces an apparent increase in the angle of attack which can be

$$\begin{aligned}
\dot{q} = & (M_u + M_w Z_u)u + (M_w + M_w Z_w)w + (M_q + M_w U_o^*)q \\
& + (M_{\delta_e} + M_w Z_{\delta_e})\delta_e + (M_{\delta_T} + M_w Z_{\delta_T})\delta_T \\
& - (M_u + M_w Z_u)u_g - (M_w + M_w Z_w)w_g \\
& + (M_u + M_w Z_u)K_w u_{wo} - (M_u^* + M_w Z_u^*)v_{HW_o} \\
& - (M_w + M_w Z_w) \Delta w_{ge}
\end{aligned} \tag{B-52}$$

$$\dot{\theta} = q \tag{B-53}$$

where:

$$X_u^* = X_u \cos \theta_o^* + X_w \sin \theta_o^* \tag{B-54}$$

$$Z_u^* = Z_u \cos \theta_o^* + Z_w \sin \theta_o^* \tag{B-55}$$

$$M_u^* = M_u \cos \theta_o^* + M_w \sin \theta_o^* \tag{B-56}$$

$$K_w = \frac{(0.43 \log h^* + 0.35)}{(0.43 \log (H_o + h_{ocg}) + 0.35)} e^{-10^{-4}(h^* - H_o - h_{ocg})} \tag{B-57}$$

The airspeed output equation is:

$$u_{AS} = u - u_g + (K_w \cos \theta_o^*)u_{wo} - v_{HW_o} \cos \theta_o^* \tag{B-58}$$

The output equation for \dot{H} is given above with the kinematic equations.

TABLE B-4

CONVAIR 880 NUMERICAL DATA FOR LANDING APPROACH
CONFIGURATION* OUT OF GROUND EFFECT (Ref. 17)

GEOMETRY:

V_{A_0}	α_{A_0}	$\gamma_0(\text{deg})$	l_x	b
265.	.0	-3.000	.0	118.3
a	RHO	MACH	t_j	z_j
1116.4	.002377	.236	-4.20	1.0
s	\bar{c}	WEIGHT (lbs)	I_y	h_{ocg}
2000.0	18.94	155000.	2.63×10^6	11.4

DIMENSIONAL DERIVATIVES:

X_u	X_w	M_q
-0.0375	.0705	-.5144
Z_u	Z_w	Z_w
-.249	.0	-.6238
M_u	M_w	M_w
.0	.000666	-.003952
X_{δ_e}	Z_{δ_e}	M_{δ_e}
.0	-7.4465	-.7685
X_{δ_T}	Z_{δ_T}	M_{δ_T}
2.0748×10^{-4}	.0	$.38 \times 10^{-6}$

*Flaps 50 deg, speed brake 8 deg, landing gear down, CG = .214 MAC.

TABLE B-5

PIPER PA-30 NUMERICAL DATA FOR LANDING APPROACH
CONFIGURATION* OUT OF GROUND EFFECT (Ref. 18)

GEOMETRY:

V_{A_0}	α_{A_0}	γ_0 (deg)	l_x	b
176.0	.0	-3.000	.0	36.0
a	RHO	MACH	l_j	z_j
1116.4	.002377	.1576	2.950	.0
S	\bar{c}	WEIGHT (lbs)	I_y	h_{oog}
178.0	5.000	3600.0	1900.0	3.48

DIMENSIONAL DERIVATIVES:

X_u	X_w	M_q
-.02263	.09151	-6.124
Z_u	Z_w	$Z_{\dot{w}}$
-.3660	-.02505 ± .0	-1.688
M_u	M_w	$M_{\dot{w}}$
.0	-.02025	-1.124
X_{δ_e}	Z_{δ_e}	M_{δ_e}
.0	-61.5	-49.5
X_{δ_T}	Z_{δ_T}	M_{δ_T}
.008925	-.0004599	.0

*Flaps 0 deg, landing gear down, CG = 0.1 MAC.

treated as an angle of attack disturbance entering the problem as a deterministic input, Δw_{ge} , in the manner of w_g

$$\Delta w_{ge} = \left[e^{-2.526(2h^*/b)^{0.891}} \right] (\alpha_{t_{IGE}} - \alpha_{t_{OGE}}) V_{A_0} \quad (B-61)$$

where b = wing span (ft)

h^* = altitude of aircraft c.g. above ground (ft)

$\alpha_t()$ = trim angle of attack in or out of ground effect (rad)

	CV-880	PA-30	
$\alpha_{t_{OGE}}$	0.07330	0.03490*	rad
$\alpha_{t_{IGE}}$	0.04014	0.0*	rad

AIRCRAFT LONGITUDINAL CONTROL SYSTEM MODELS

The longitudinal control systems to be used with the Convair 880 and Piper PA-30 aircraft are specified in this subsection. Three different control systems are used with the Convair 880 in order to illustrate the effects inertial smoothing and manual control may have upon landing performance with respect to a baseline automatic landing system. The control system for the PA-30 (which admittedly is an invented system) will illustrate the effects that vastly different aircraft size, wing-loading and approach speed may have upon landing performance.

*Numbers estimated to provide effective angle of attack change of 2 deg between in full ground effect and out of ground effect.

TABLE B-6

KEY PARAMETERS FOR REPRESENTATIVE AIRCRAFT

AIRCRAFT	WING-LOADING (LB/FT) ²	-Z _w (1/SEC)	APPROACH SPEED	
			(FT/SEC)	(KT)
CV-880	77.5	0.624	265.	157.
B-747	102.	0.512	221.	131.
DC-8	73.1	0.628	244.	144.
PA-30	20.2	1.69	176.	104.
DC-3	23.3	1.24	136.	80.5
JETSTAR	44.1	1.01	224.	133.

Convair 880, Lear-Siegler Automatic Landing System (Baseline System)

The block diagram for this system for Glide Slope final track, flare and touchdown has been adapted from Fig. 3-5 of Ref. 17. It is designated as Fig. B-5 here.

The equations for the approach coupler and flare computer are

$$\eta = S_{\eta} \eta_c^* + K_o (\bar{d}_c - d)/R \quad (\mu A) \quad (B-62)$$

$$\begin{aligned} \dot{\eta}' = & - (1/\tau_R) \eta' + (S_{\eta} K_x / \tau_R) \eta_c + (K_o / [\tau_R R]) \bar{d}_c \\ & - (K_o \cos \gamma_o / [\tau_R R]) H_2 + (K_o \sin \gamma_o / [\tau_R R]) X_2 \end{aligned} \quad (B-63)$$

$$\dot{\eta}'' = K_1 K_o K_{GSI} \eta' \quad , \quad \eta''(0) = V_{T_o}^* \sin \gamma_o \quad (B-64)$$

$$\begin{aligned} \dot{\delta}_e = & - (1/\tau_e) \delta_e + (K_s K_{a_z} Z_u / \tau_e) u + (K_s K_{a_z} Z_w / \tau_e) w \\ & + (K_s K_{a_z} Z_{\delta_e} / \tau_e) \delta_e + (K_s K_{a_z} Z_{\delta_T} / \tau_e) \delta_T \\ & + (-K_s K_{a_z} Z_u / \tau_e) u_g + (-K_s K_{a_z} Z_w / \tau_e) w_g \\ & + (K_s K_{a_z} [Z_u \cos \theta_o^* + Z_w \sin \theta_o^*] / \tau_e) (K_w u_{wo} - V_{HW_o}) \\ & + (-K_s K_{a_z} Z_w / \tau_e) \Delta w_{ge} + (K_s K_{\theta} / \tau_e) q + (K_s K_h \sin \theta_o^* / \tau_e) u \\ & + (-K_s K_h \cos \theta_o^* / \tau_e) w + (K_s K_h [U_o^* \cos \theta_o^* + W_o^* \sin \theta_o^*] / \tau_e) \theta \\ & + (K_s K_h V_{T_o}^* \sin \gamma_o / \tau_e) + (-K_s K_h K_o K_1 K_2 / \tau_e) \eta' + (-K_s K_h K_2 / \tau_e) \eta'' \end{aligned} \quad (B-65)$$

where

$$K_0 = \frac{150 \mu A}{0.7 \text{ deg}} 57.3 \frac{\text{deg}}{\text{rad}} = 12278.6 \frac{\mu A}{\text{rad}}$$

$$K_1 = 1.0, \quad H \geq 600. \text{ ft}$$

$$= (H - 50)/550, \quad 50. < H < 600. \text{ ft}$$

$$= 0.0, \quad H \leq 50. \text{ ft}$$

$$K_2 = 1.0, \quad H \geq 50. \text{ ft}$$

$$= (H + 12.5)/62.5, \quad H < 50. \text{ ft}$$

$$K_\sigma = 0.25 (\text{ft/sec})/\mu A$$

$$K_{GSI} = 0.175 \text{ 1/sec}$$

$$K_s = 0.253$$

$$1/\tau_R = 2. \text{ rad/sec}$$

$$K_{a_z} = -0.0933 \text{ rad}/(\text{ft/sec}^2)$$

$$K_\theta = 15.8 \text{ rad}/(\text{rad/sec})$$

$$K_h = 0.15 \text{ rad}/(\text{ft/sec})$$

$$1/\tau_e = 5.2 \text{ rad/sec}$$

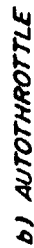


Figure B-5. Lear-Siegler Automatic Landing System for Convair 880 (Ref. 17)

S_η is a switch, which, when open, removes the ILS Glide Slope structure input to the control system. This switch is opened to simulate the continuation of flight under manual control by visual reference to the ground.

$$S_\eta = 1. \quad \begin{array}{l} \text{for Category I approaches if } H \geq 200. \text{ ft} \\ \text{for Category II approaches with manual landing if } H \geq 100 \text{ ft} \\ \text{for Category II or III approaches with automatic landing} \\ \text{if } H \geq 0. \text{ ft} \end{array}$$

$$S_\eta = 0. \quad \begin{array}{l} \text{for Category I approaches if } H < 200. \text{ ft} \\ \text{for Category II approaches with manual landing if } H < 100. \text{ ft} \\ \text{for Category II or III approaches with automatic landing} \\ \text{if } H < 0. \text{ ft} \end{array}$$

The equations for the autothrottle are

$$\dot{\theta}' = - (1/\tau_\theta) \theta' + q \quad (\text{B-66})$$

$$\begin{aligned} \dot{u}' = & - (1/\tau_u) u' + (1/\tau_u) u \\ & - (1/\tau_u) u_g + (\cos \theta_o^* / \tau_u) (K_w u_{wo} - v_{HW_o}) \end{aligned} \quad (\text{B-67})$$

$$\dot{V}' = - K_{IAS} u' + K_{T_\theta} \theta' + K_{IAS} K_{ASC} = V \quad (\text{B-68})$$

$$\begin{aligned} \dot{\delta}_T = & - (1/\tau_E) \delta_T + (- K_T K_{IAS} / \tau_E) u' \\ & + (K_T K_{T_\theta} / \tau_E) \theta' + (K_T K_{IAS} / \tau_E) K_{ASC} \\ & + (K_T / [\tau_E \tau_{IV}]) V' \end{aligned} \quad (\text{B-69})$$

where

$$1/\tau_{\theta} = 0.2 \text{ rad/sec}$$

$$1/\tau_u = 0.714 \text{ rad/sec}$$

$$K_{IAS} = 20. \text{ v/(ft/sec)}$$

$$K_{T_{\theta}} = 2000. \text{ v/rad}$$

$$1/\tau_E = 1.0 \text{ rad/sec}$$

$$1/\tau_{IV} = 0.05 \text{ rad/sec}$$

$$K_T = 48.44 \text{ lb/v}$$

$$K_{ASC} = 0.0 \text{ ft/sec} \quad , \quad H > 50. \text{ ft}$$

$$= 10.14 \text{ ft/sec} \quad , \quad H \leq 50. \text{ ft}$$

Convair 880, Lear-Siegler Automatic Landing System Modified to Incorporate Inertial Smoothing

Only a small modification to the block diagram in Fig. B-5 and Eq B-63 is required to incorporate inertial smoothing of the type represented in Fig. 2.3.4. of Ref. 23. The only quantity affected is η' in Fig. B-5. When inertial smoothing of the ILS Glide Slope signal is used, η' is obtained in the manner shown in Fig. B-6. The inertial smoothing is obtained by complementing the Glide Slope error from the ILS receiver output with the Glide Slope error rate signal obtained from inertial measurements of instantaneous vertical speed and groundspeed. The component of η arising from Glide Slope beam structure and from deviation of the ideal Glide Slope from its far-field asymptote can be heavily filtered because the aircraft deviation information lost in the filtering can be replaced by the complementary inertial measurements

The equations for η' are

$$\dot{\eta} = [\sin(\theta_o^* - \gamma_o)]u - [\cos(\theta_o^* - \gamma_o)]w + v_{T_o}^* \theta \quad (B-70)$$

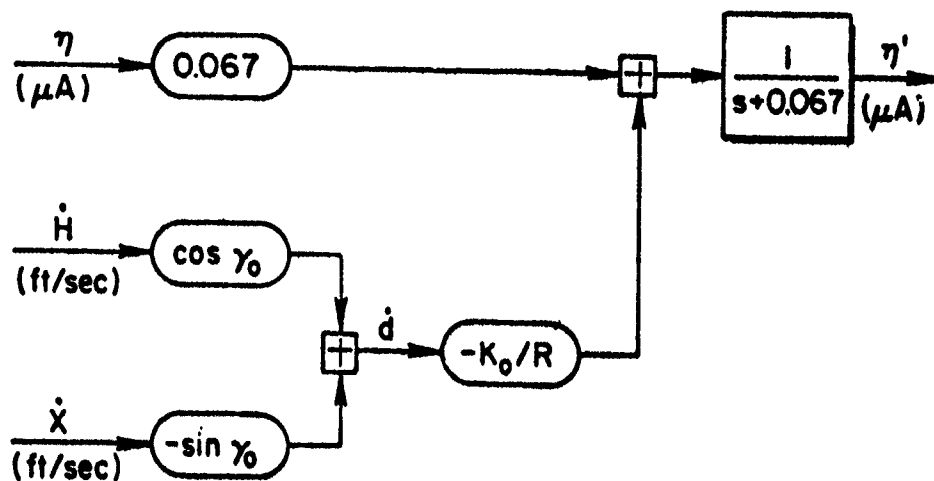


Figure B-6. Inertially Smoothed Glide Slope Deviation

$$\begin{aligned}
 \dot{\eta}' = & -(1/\tau_R)\eta' + (S_{\eta}K_x/\tau_R)\eta_c \\
 & +(K_o/[\tau_R R])\bar{d}_c - (K_o \cos \gamma_o/[\tau_R R])H_2 \\
 & +(K_o \sin \gamma_o/[\tau_R R])X_2 - [K_o \sin (\theta_o^* - \gamma_o)/R]u \\
 & +[K_o \cos (\theta_o^* - \gamma_o)/R]w - [K_o V_{T_o}^*/R]\theta
 \end{aligned} \tag{B-71}$$

where

$$1/\tau_R = 0.067 \text{ rad/sec}$$

The range, R , which enters into the implementation may be obtained inferentially by means of altimetry or directly from DME.

Convair 880, Stability Augmentation, Flight Director System and Autothrottle

The flight director system is configured to give similar performance to the automatic landing system in Fig. B-5a. Feedback loop gains and equalization are the same, however, the loop structure is altered to be appropriate for a flight director computer and the pilot's effective reaction time delay is added. Furthermore, high bandwidth inner loop feedback of normal acceleration and pitch rate are considered to be stability augmentation functions. The autothrottle configuration is the same as shown in Fig. B-5b. (Note

that an automatic throttle system is required for turbojet Category II operations based upon dual flight directors, Ref. 12.)

It will be assumed that the flight director is used down to the Category II decision altitude. From that point on, manual control will be assumed accomplished by visual reference to the ground. Manual control during this latter phase of flight will be simulated by the approach coupler and flare computer shown in Fig. B-5a (with the addition of the pilot's effective delay) operating upon the ideal Glide Slope signal. (That is, η_c will be zero.)

The block diagram for the flight director system is given in Fig. B-7, and equations which are equivalent are given below.

$$\dot{\eta}' = (\text{refer to Eq B-63 for RHS}) \quad (\text{B-72})$$

$$\ddot{\eta}'' = K_1 K_\sigma K_{GSI} \eta', \quad \ddot{\eta}''(0) = V_{T_0}^* \sin \gamma_0 \quad (\text{B-73})$$

$$\begin{aligned} \dot{\delta}_e = & -(1/\tau_e) \delta_e + (K_s K_{a_z} Z_u / \tau_e) u + (K_s K_{a_z} Z_w / \tau_e) w \\ & + (K_s K_{a_z} Z_{\delta_E} / \tau_e) \delta_E + (K_s K_{a_z} Z_{\delta_T} / \tau_e) \delta_T + \\ & + (-K_s K_{a_z} Z_u / \tau_e) u_g + (-K_s K_{a_z} Z_w / \tau_e) w_g + (-K_s K_{a_z} Z_w / \tau_e) \Delta w_{ge} \\ & + (K_s K_{a_z} [Z_u \cos \theta_o^* + Z_w \sin \theta_o^*] / \tau_e) (K_w u_{wo} - V_{HW_o}) \\ & + (K_s K_{\dot{\theta}} / \tau_e) \dot{q} + (-K_s K_{\dot{h}} / \tau_e) \dot{h}_e' \end{aligned} \quad (\text{B-74})$$

$$\begin{aligned} \ddot{h}_e' = & (-1/\tau_p) \dot{h}_e' + (-\sin \theta_o^* / \tau_p) u + (\cos \theta_o^* / \tau_p) w \\ & + (-[U_o^* \cos \theta_o^* + W_o^* \sin \theta_o^*] / \tau_p) \dot{\theta} \\ & + (K_\sigma K_1 K_2 / \tau_p) \eta' + (K_2 / \tau_p) \eta'' - (V_{T_0}^* \sin \gamma_0) / \tau_p \end{aligned} \quad (\text{B-75})$$

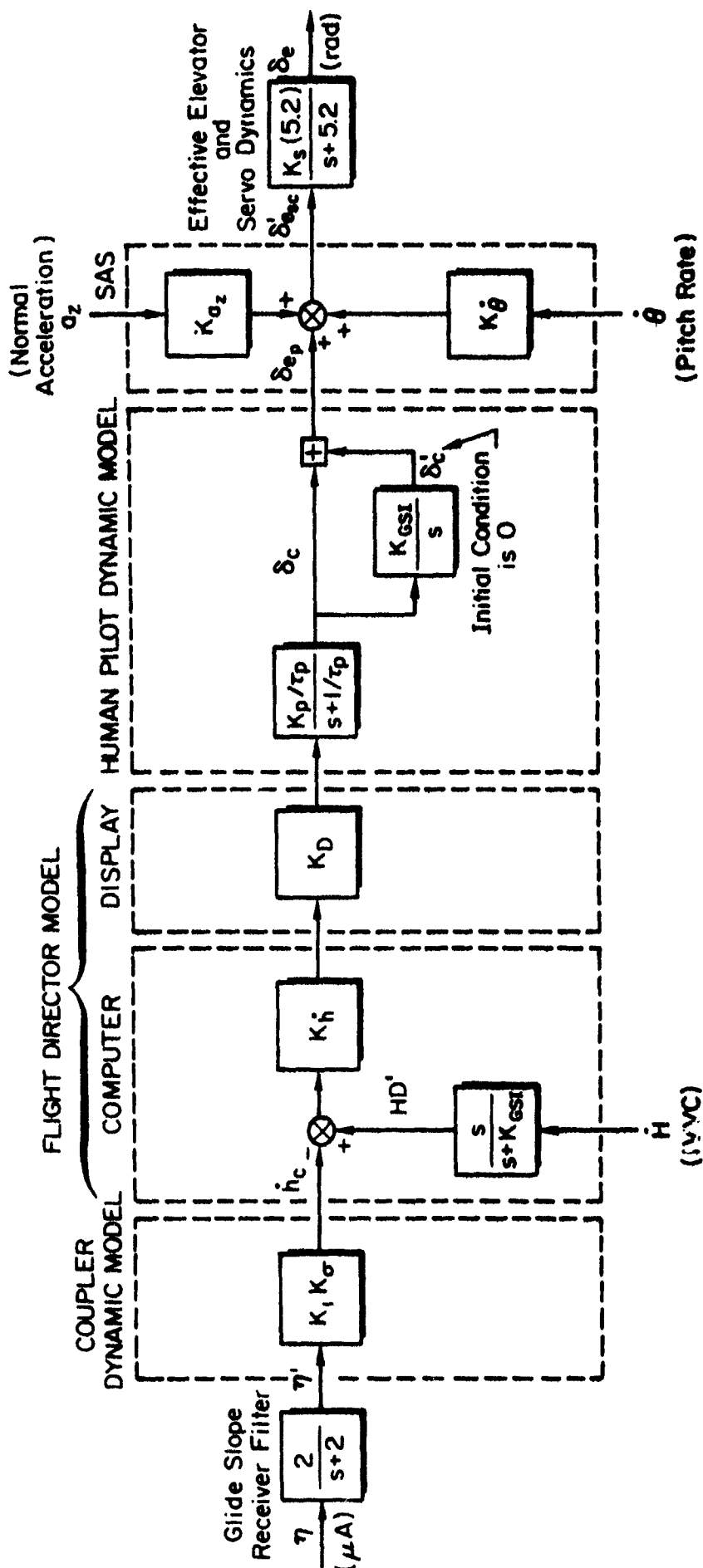


Figure B-7. Flight Director System of Convair 880

$$K_D K_p = 1.0$$

$$K_D = -1.22 \text{ in. FD/rad } \delta'_{esc}$$

$$1/\tau_p = 2.5 \text{ rad/sec}$$

All other parameter values are the same as those used for the Siegler Automatic Landing System.

Piper PA-30, Automatic Coupler, Autothrottle and Manual Landing System

The longitudinal control system model for the Piper PA-30 is similar to that given in Ref. 18. It must be emphasized that the control system is a hypothetical one. It is, however, typical of control systems used in general aviation aircraft. The system loop structure differs from that in Fig. B-5 at altitudes above 100 ft mainly in that pitch attitude feedback is used for path damping in distinction to instantaneous vertical speed. The resulting system is much less effective in coping with shear effects because of this.

The system is used down to 100 ft altitude at which point it is assumed that manual takeover occurs. The Glide Slope signal is ideal from that point on to represent control by means of visual reference to the runway, and the pitch attitude feedback is replaced by visually perceived instantaneous vertical speed. Addition of an altitude scheduled gain in the output path of the Glide Slope integrator provides a model for the manual flare execution.

Block diagrams for the system are given in Fig. B-8 and -9, and the equations are

$$\dot{\eta}' = (\text{refer to Eq B-63}) \text{ for RHS} \quad (\text{B-76})$$

$$\ddot{\eta}'' = K_1 K_o K_{GSI} \eta' , \quad \eta''(0) = V_{T_o}^* \sin \gamma_o \quad (\text{B-77})$$

$$\dot{\delta}_e = -(1/\tau_e) \delta_e + (K_s K_q / \tau_e) q + (K_s S_\theta V_{A_o} / \tau_e) \theta$$

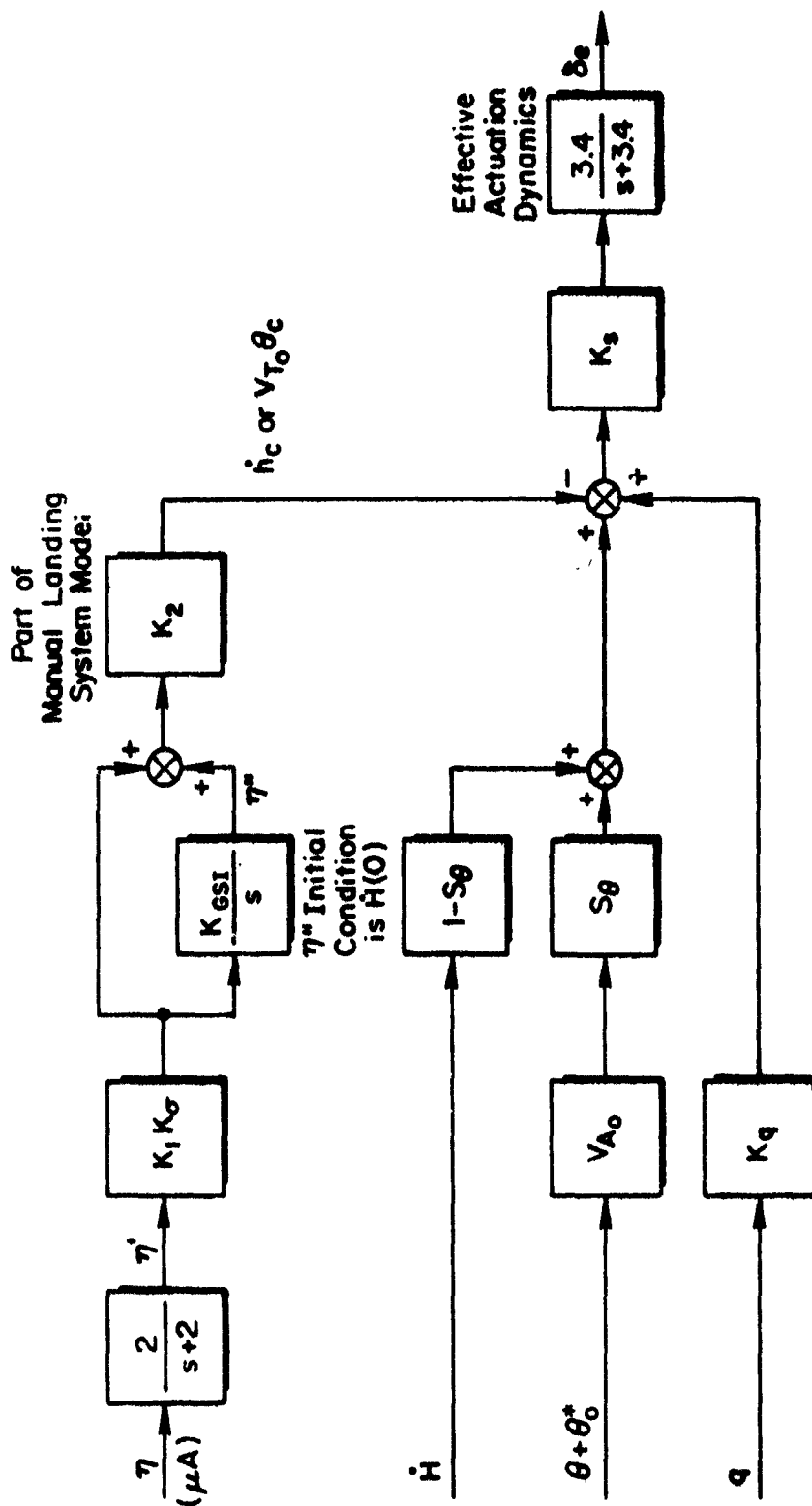


Figure B-8. Automatic Coupler and Manual Landing System Model for Piper PA-30

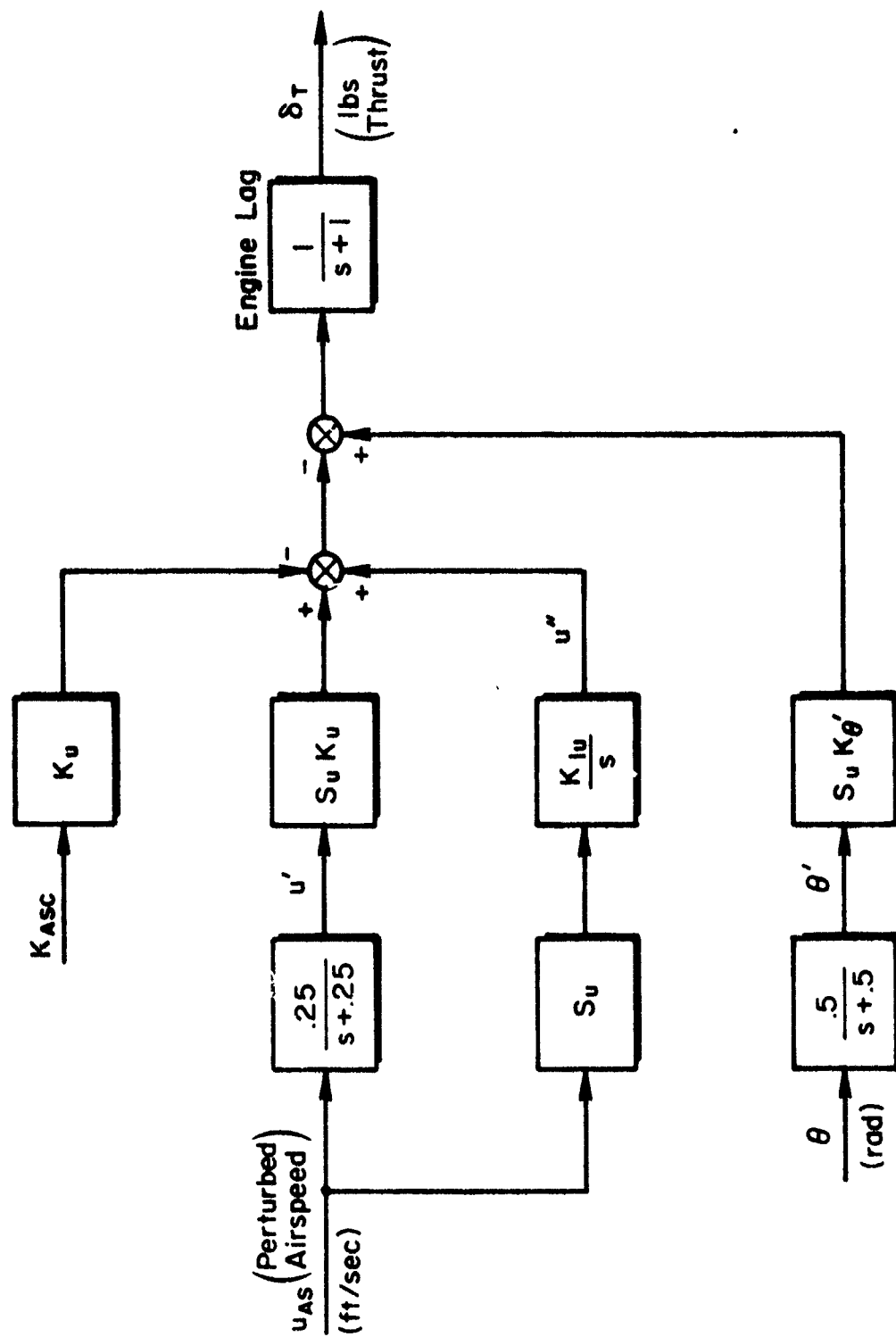


Figure B-9. Autothrottle for Piper PA-30

$$\begin{aligned}
& +(K_s[1 - S_\theta] \sin \theta_o^*/\tau_e)u + (-K_s[1 - S_\theta] \cos \theta_o^*/\tau_e)w \\
& +(K_s[1 - S_\theta][U_o^* \cos \theta_o^* + W_o^* \sin \theta_o^*]\tau_e)\theta + K_s[1 - S_\theta]V_{T_o}^* \sin \gamma_o/\tau_e \\
& +(-K_s K_2/\tau_e)\eta'' + (-K_s K_1 K_2 K_r/\tau_e)\eta' + (K_s S_\theta V_{A_o}/\tau_e)\theta_o^* \quad (B-78)
\end{aligned}$$

where

$$1/\tau_R = 2.0 \text{ rad/sec}$$

$$K_\sigma = 0.43 \text{ (ft/sec)/}\mu\text{A}$$

$$K_{GSI} = 0.084 \text{ (1/sec)}$$

$$K_1 = 1.0, H \geq 1500. \text{ ft}$$

$$= \frac{H - 50}{1450}, 50. < H < 1500. \text{ ft}$$

$$= 0.0, H \leq 50. \text{ ft}$$

$$1/\tau_e = 3.4 \text{ rad/sec}$$

$$K_s = 0.00415 \text{ rad/(ft/sec)}$$

$$K_q = 20.6 \text{ (ft/sec)/(rad/sec)}$$

$$V_{A_o} = 176. \text{ (ft/sec)}$$

$$S_\theta = 1.0, H > 100. \text{ ft}$$

$$= 0.0, H \leq 100. \text{ ft}$$

$$K_2 = 1.0, H \geq 30. \text{ ft}$$

$$= \frac{H + 8.82}{38.82}, H < 30. \text{ ft}$$

$$\dot{u}' = (\text{refer to Eq B-67 for RHS}) \quad (\text{B-79})$$

$$\dot{u}'' = S_u u - S_{u_g} u + (S_u \cos \theta_o^*) [K_w u_{wo} - v_{HW_o}] \quad (\text{B-80})$$

$$\dot{\theta}' = -(1/\tau_\theta) \theta' + (1/\tau_\theta) \theta \quad (\text{B-81})$$

$$\begin{aligned} \dot{\delta}_T = & -(1/\tau_E) \delta_T + (-S_u K_u / \tau_E) u' \\ & + (-K_{Iu} / \tau_E) u'' + (S_u K_{\theta'} / \tau_E) \theta' + (K_u / \tau_E) K_{ASC} \end{aligned} \quad (\text{B-82})$$

$$1/\tau_u = 0.25 \text{ rad/sec}$$

$$K_u = 2.54 \text{ lb-thrust/(ft/sec)}$$

$$K_{Iu} = 0.125 \text{ (lb-thrust/sec)/(ft/sec)}$$

$$1/\tau_\theta = 0.5 \text{ rad/sec}$$

$$K_{\theta'} = 62.9 \text{ lb-thrust/rad}$$

$$1/\tau_E = 1.0 \text{ rad/sec}$$

$$K_{ASC} = 0. \text{ ft/sec} \quad , \quad H > 30. \text{ ft}$$

$$= 0. \text{ ft/sec} \quad , \quad H \leq 30. \text{ ft}$$

*These values are those given in Ref. 18 and used throughout this study. However, the values of K_u and K_{Iu} are too low by a factor of 10 and K_θ is too low by a factor of 30 with respect to values which would produce good auto-throttle performance.

APPENDIX C

STATISTICAL CHARACTERIZATION OF THE TOUCHDOWN EVENT

It is difficult to represent the first touchdown of a landing aircraft within the context of a linear system model. This Appendix explains how such a representation is constructed for use as part of the overall system performance model.

The conceptual basis for the model is to consider the landing aircraft trajectory in the absence of the constraint imposed by the runway surface. The probability of the event $\dot{H} \leq 0$ and $H = 0$ in the interval t to $t + dt$ is then determined and used to eliminate the conditional dependence upon time of the probability of $\left(\dot{H}_{TD}\right)_{\max} \leq \dot{H} \leq 0$ and $X_{TD_1} \leq X \leq X_{TD_2}$ given that $H = 0$. The resulting expression gives the probability density function for all downward crossings of the runway level, $H = 0$. By appropriate normalization to discriminate against multiple downward crossings of $H = 0$ by the same trajectory ensemble member, a result is obtained which approximates the physical touchdown event which is the first downward crossing of $H = 0$.

PROBABILITY OF $\dot{H} \leq 0$ AND $H = 0$

$$P(-\dot{H} \geq 0, H = 0 \text{ in the interval } t \text{ to } t + dt) \triangleq P_1 \quad (C-1)$$

$$P_1 = \int_0^\infty (-\dot{H}) dt \int_0^\infty dH \quad \rho(-\dot{H}, H, t) \quad (C-2)$$

where the two-dimensional Gaussian probability density function $\rho(-\dot{H}, H, t)$ is given by

$$\rho(-\dot{H}, H, t) = \frac{e^{-1/2 \left(\frac{Z_1 - 2\rho_{\dot{H}H} Z_1 Z_2 + Z_2^2}{1 - \rho^2} \right)}}{2\pi \sigma_H \sigma_{\dot{H}} \sqrt{1 - \rho^2}} \quad (C-3)$$

$$Z_1 = \frac{H - \bar{H}}{\sigma_H}$$

$$Z_2 = \frac{(-\dot{H}) - (-\dot{\bar{H}})}{\sigma_{\dot{H}}} \quad (C-4, 5)$$

and ρ is the correlation coefficient for H and $(-\dot{H})$.

Integration over H on the right hand side of Eq C-2 results in:

$$P_1 = dt \int_0^\infty d(-\dot{H}) (-\dot{H}) \rho(-\dot{H}, 0, t) \quad (C-6)$$

Substitution of Eq C-3 into C-6 factoring out $e^{-Z_1^2/2}$, and making the change of variable

$$Y = \frac{(-\dot{H}) - \left[(-\dot{\bar{H}}) + \rho \sigma_{\dot{H}} Z_1 \right]}{\sigma_{\dot{H}} \sqrt{1 - \rho^2}} \quad (C-7)$$

results in

$$dt \frac{\sigma_{\dot{H}} \sqrt{1 - \rho^2} e^{-Z_1^2/2}}{\sqrt{2\pi} \sigma_H} \left[\frac{1}{\sqrt{2\pi}} \int_L^\infty dY Y e^{-Y^2/2} + L \int_L^\infty dY \frac{e^{-Y^2/2}}{\sqrt{2\pi}} \right] \quad (C-8)$$

$$\text{where } L = \frac{(-\dot{\bar{H}}) - \rho \sigma_{\dot{H}} Z_1}{\sigma_{\dot{H}} \sqrt{1 - \rho^2}}$$

Evaluation of the integrals over dY results in:

$$P_1 = dt \frac{\sigma_{\dot{H}} \sqrt{1 - \rho^2} e^{-1/2 \left(\frac{\bar{H}}{\sigma_H} \right)^2}}{2\pi \sigma_H} \left[e^{-L^2/2} - \sqrt{2\pi} L \left\{ 1 - F(L) \right\} \right] \quad (C-9)$$

NORMALIZATION

The probability of the first touchdown occurring in the interval t to $t + dt$ will be approximated by normalizing the probability that $-\dot{H} \geq 0$ and $H = 0$ in the interval t to $t + dt$

$$P(\text{landing in the interval } t \text{ to } t + dt) \triangleq \rho_{TD}(t)dt \quad (C-10)$$

$$\rho_{TD}(t)dt \triangleq P_1 / \int_{-\infty}^{\infty} P_1 \quad (C-11)$$

$\rho_{TD}(t)$ is the probability density function for landings as a function of time.

LONGITUDINAL DIMENSION OF TOUCHDOWN FOOTPRINT

The longitudinal dimension of the 2σ touchdown footprint is given by the minimum longitudinal interval $(X_{TD_2} - X_{TD_1})$ for which the probability of $X_{TD_1} \leq X_{TD} \leq X_{TD_2}$ and $0 \leq (-\dot{H}_{TD}) \leq (-\dot{H}_{TD_{max}})$ given $H = 0$, is equal to the 2σ value, 0.9544.

$$0.9544 = \int_{X_{TD_1}}^{X_{TD_2}} \int_0^{(-\dot{H}_{TD})_{max}} \int_{-\infty}^{\infty} dt \left[\frac{\rho(-\dot{H}, H, X, t)}{\rho(H, t)} \right]_{H=0} \rho_{TD}(t) \quad (C-12)$$

The quantity in the square brackets is the Gaussian probability density function for $(-\dot{H})$ and X given $H = 0$ and t . The integration over t removes the conditional dependence upon time of touchdown.

Evaluation of $(X_{TD_2} - X_{TD_1})$ using the above expression can be a considerable chore. Evaluation can be trivial, however, if some well-founded approximations are made.

- Assume $[\rho(-H, H, X, t) / \rho(H, t)]_{H=0}$ is independent of time in the vicinity of the nominal touchdown time
- Assume $\rho \doteq 0$
- Assume $\int_0^{(-\dot{H}_{TD})_{\max}} d(-\dot{H}) \rho(-\dot{H}) \doteq 1$
- Assume $|\rho_{XH} \bar{H}| \ll |X|$

Then

$$0.9544 \doteq \int_{X_{TD_1}}^{X_{TD_2}} dX \left[\frac{e^{-1/2 \left(\frac{X - \bar{X}}{\sigma_X \sqrt{1 - \rho_{XH}^2}} \right)^2}}{\sqrt{2\pi} \sigma_X \sqrt{1 - \rho_{XH}^2}} \right]_{\bar{H}=0} \quad (C-13)$$

However, because the approximated probability density function is Gaussian:

$$X_{TD_2} - X_{TD_1} \doteq 4 \left[\sigma_X \sqrt{1 - \rho_{XH}^2} \right]_{\bar{H}=0} \quad (C-14)$$

APPENDIX D

TRAJECTORIES FOR MEAN AND STANDARD DEVIATION OF SYSTEM RESPONSE VARIABLES

Trajectories for the mean and standard deviation of several system response variables of interest for the five aircraft/control system combinations listed in Table 3 are contained in this Appendix.

CONVAIR 880, LSI AUTOMATIC LANDING SYSTEM, CATEGORY I OPERATION WITH MANUAL LANDING

Figure D-1 gives the mean system responses from an initial altitude of 1000 ft to touchdown. Figure D-2 gives the three component standard deviation system responses from an initial altitude of 1000 ft to touchdown. The three components arise from wind and wind shear effects (W), ILS Glide Slope Alignment error and structure (ILS), and turbulence (T). The scale factors CRF, CSF, and CTF on the three components are unity.

CONVAIR 880, FLIGHT DIRECTOR SYSTEM, CATEGORY II OPERATION WITH MANUAL LANDING

Figure D-3 gives the mean system responses from an initial altitude of 1000 ft to the decision height, 100 ft. Figure D-4 gives the same responses on an expanded time scale from the decision height, 100 ft, to touchdown. Figure D-5 gives the three component standard deviation system responses from an initial altitude of 1000 ft to the decision height, 100 ft. The scale factors CRF, CSF, and CTF on the three components are unity. Figure D-6 gives the total standard deviation system responses on an expanded time scale from the decision height, 100 ft, to touchdown. The scale factor values are $CSF = 1.50$, $CRF = CTF = 1.0$.

CONVAIR 880, LSI AUTOMATIC LANDING SYSTEM, CATEGORY II OR III OPERATION WITH AUTOMATIC LANDING

Figure D-7 gives the mean system responses from an initial altitude of 1000 ft to the decision height, 100 ft. Figure D-8 gives the same responses on an expanded time scale from the decision height, 100, ft,

to touchdown. Figure D-9 gives the three component standard deviation system responses from an initial altitude of 1000 ft to the decision height, 100 ft. The scale factors CRF, CSF, and CTF on the three components are unity. Figure D-10 gives the total standard deviation system responses on an expanded time scale from the decision height, 100 ft, to touchdown. The scale factor values are $CSF = 1.53$, $CRF = CTF = 1.0$.

**CONVAIR 880, LSI AUTOMATIC LANDING SYSTEM WITH
INERTIALLY SMOOTHED COUPLING, CATEGORY II OR III
OPERATION WITH AUTOMATIC LANDING**

Figure D-11 gives the mean system responses from an initial altitude of 1000 ft to the decision height, 100 ft. Figure D-12 gives the same responses on an expanded time scale from the decision height, 100 ft, to touchdown. Figure D-13 gives the three component standard deviation system responses from an initial altitude of 1000 ft to the decision height, 100 ft. The scale factors CRF, CSF, and CTF on the three components are unity. Figure D-14 gives the total standard deviation system responses on an expanded time scale from the decision height, 100 ft, to touchdown. The scale factor values are $CSF = 1.58$, $CRF = CTF = 1.0$.

**PIPER PA-30, INVENTED FLIGHT CONTROL SYSTEM
AND COUPLER, CATEGORY II OPERATION WITH
MANUAL LANDING**

Figure D-15 gives the mean system responses from an initial altitude of 750 ft to the decision height, 100 ft. Figure D-16 gives the same responses on an expanded time scale from the decision height, 100 ft, to touchdown. Figure D-17 gives the three component standard deviation system responses from an initial altitude of 750 ft to the decision height, 100 ft. The scale factors CRF, CSF, and CTF on the three components are unity. Figure D-18 gives the total standard deviation system responses on an expanded time scale from the decision height, 100 ft, to touchdown. The scale factor values are $CSF = 1.50$, $CRF = CTF = 1.0$.

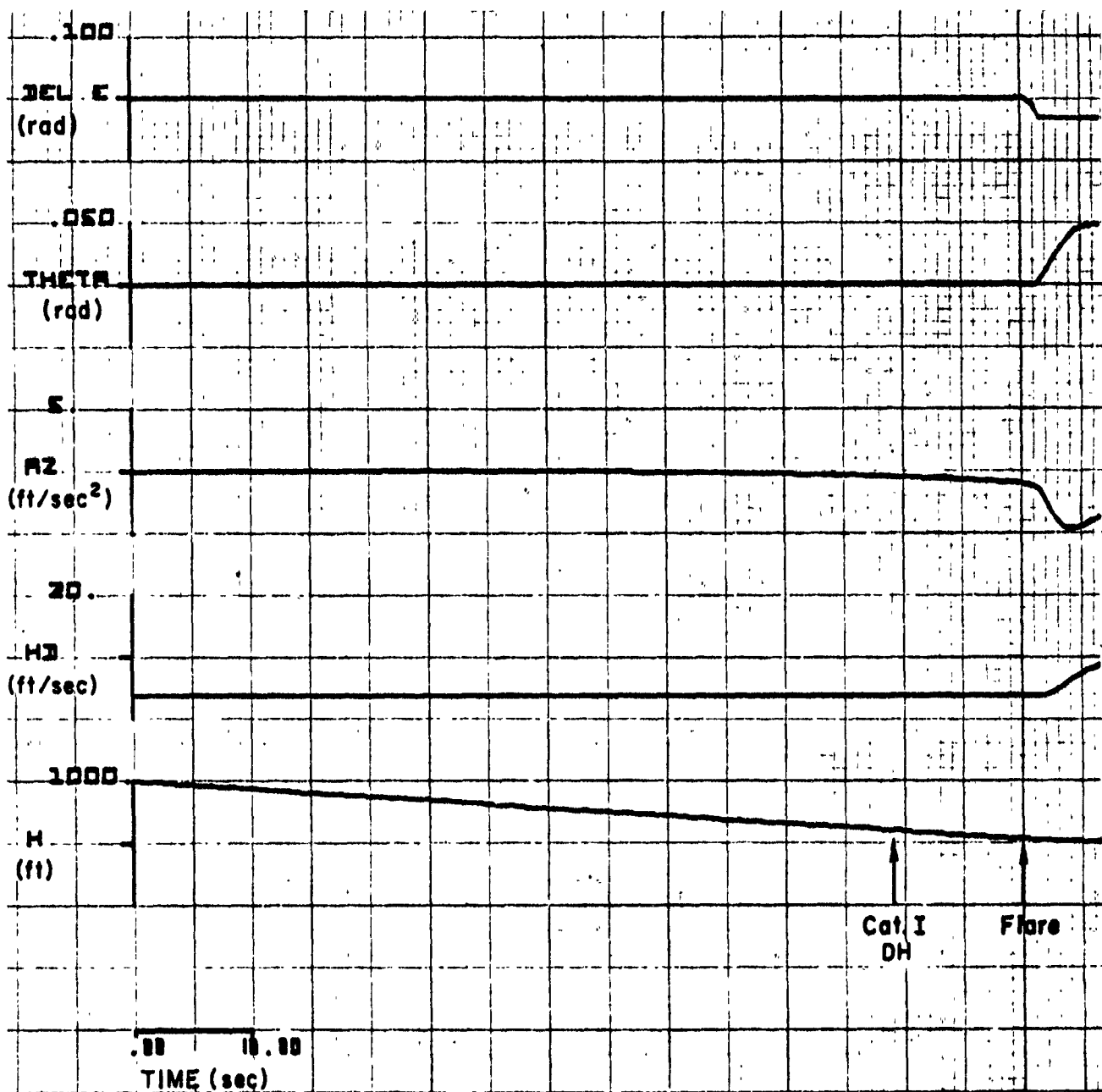


Figure D-1(a). Mean Responses: CV-880, LSI, Cat I, M

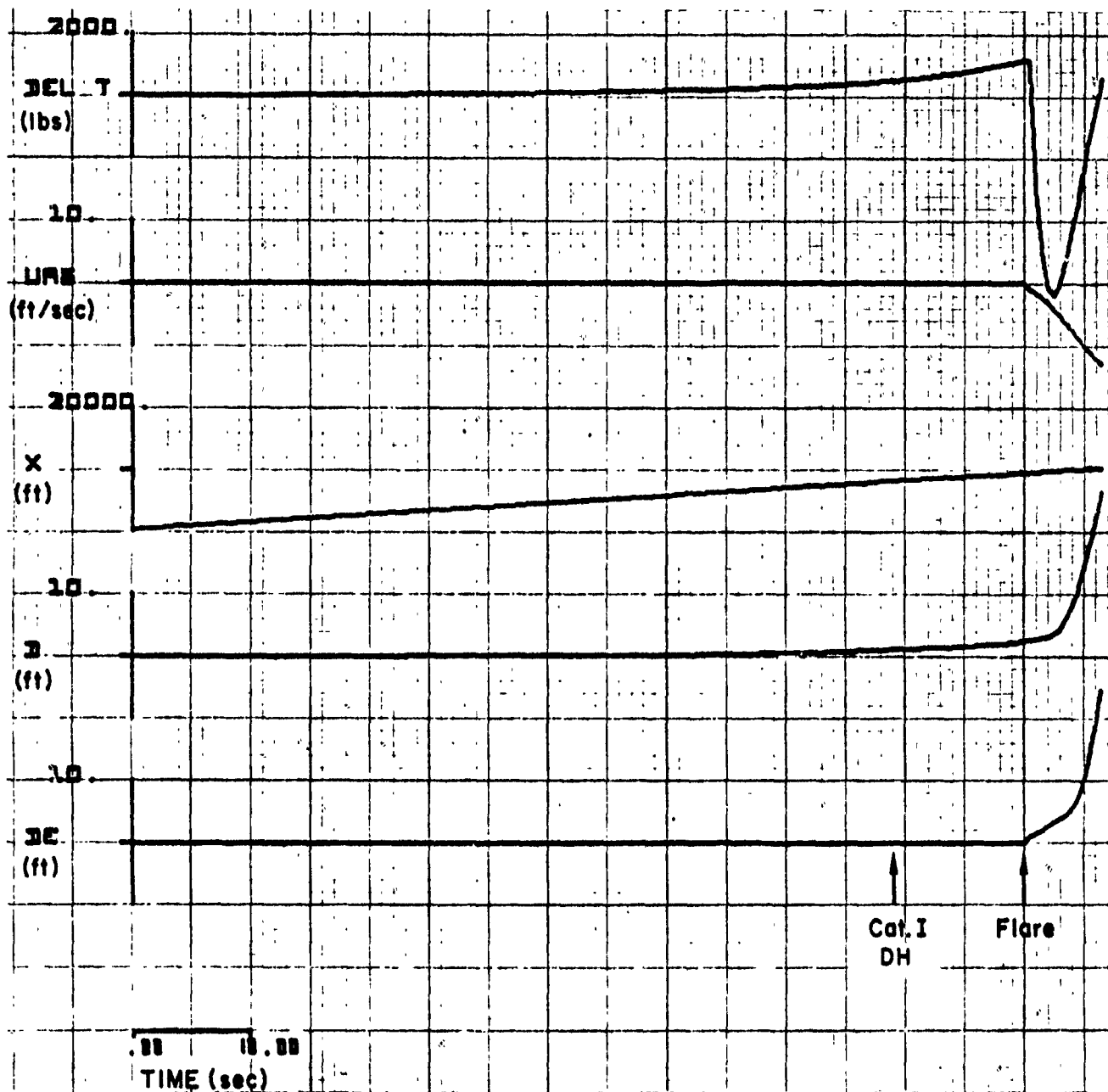


Figure D-1(b)

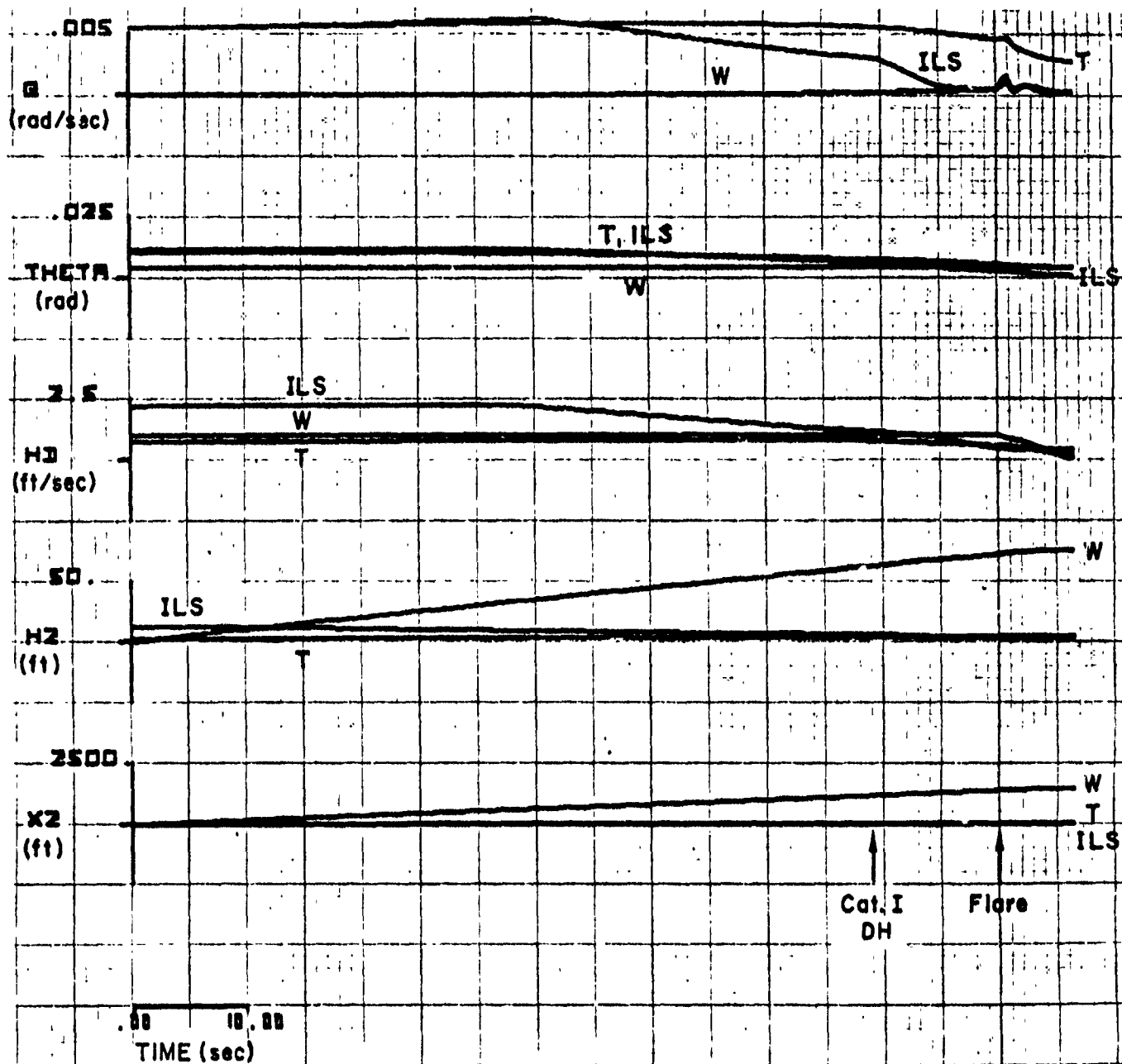


Figure D-2(a). Standard Deviation Responses: CV-880, LSI, Cat I, M

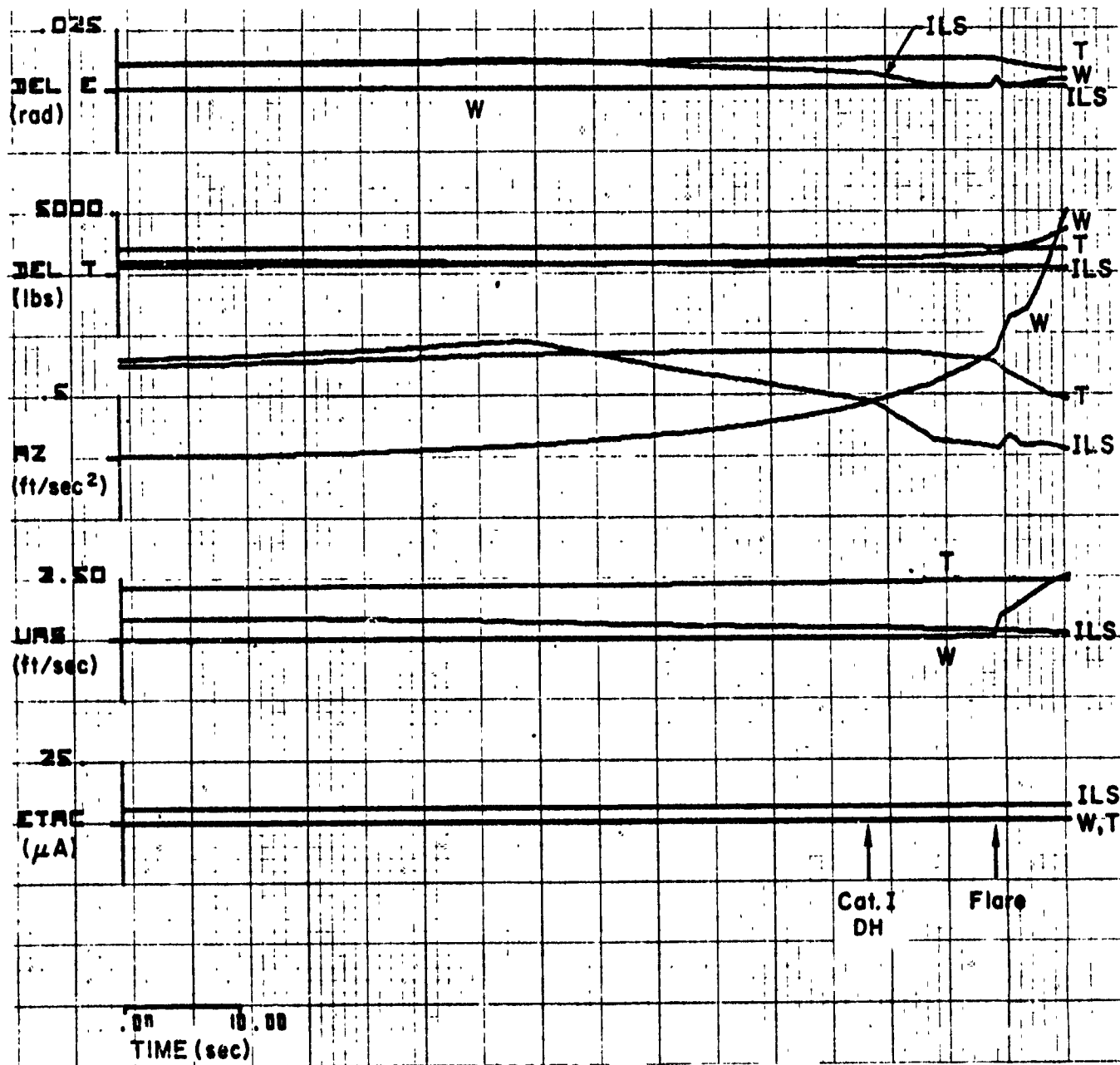


Figure D-2(b)

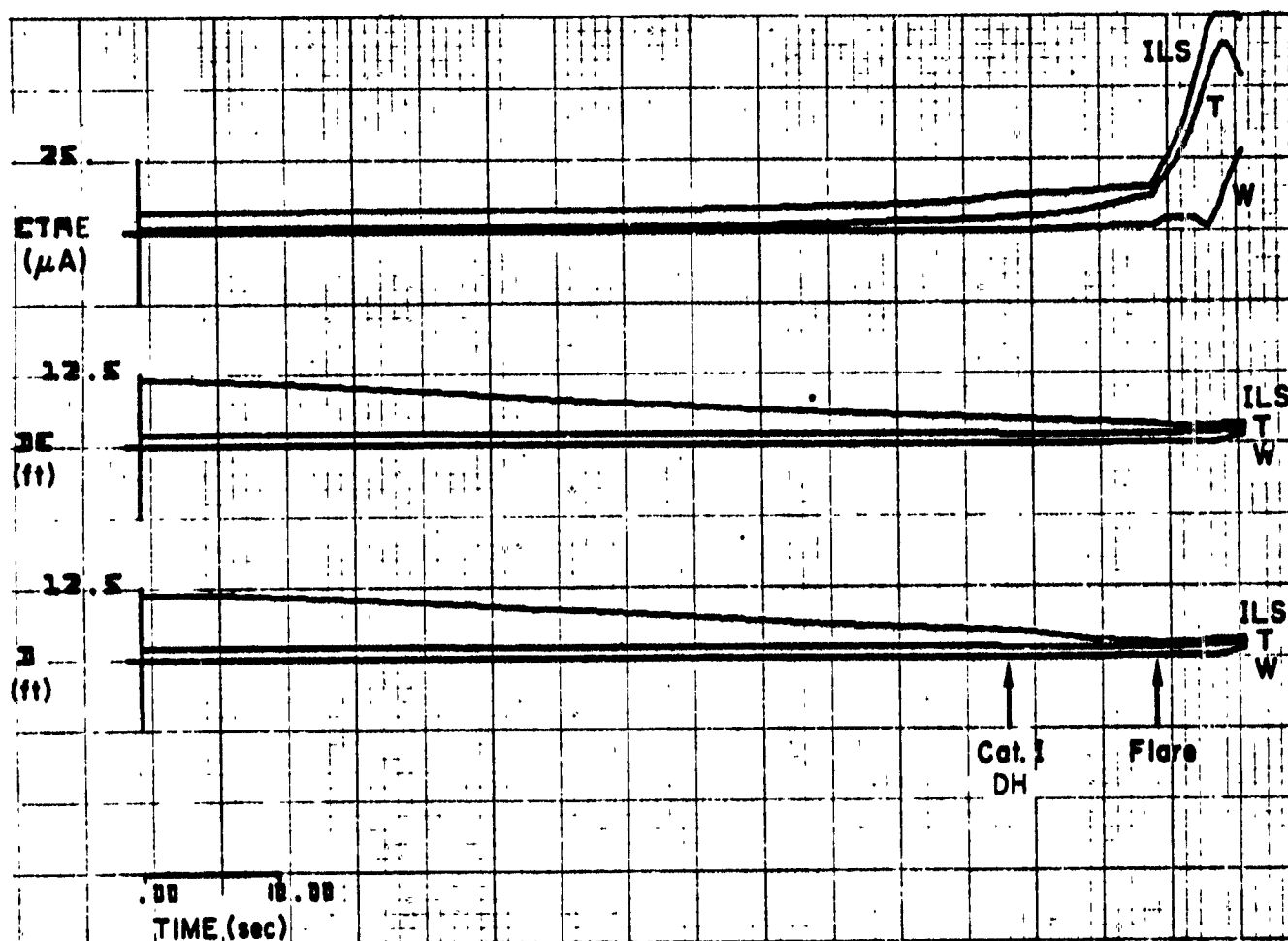


Figure D-2(c)

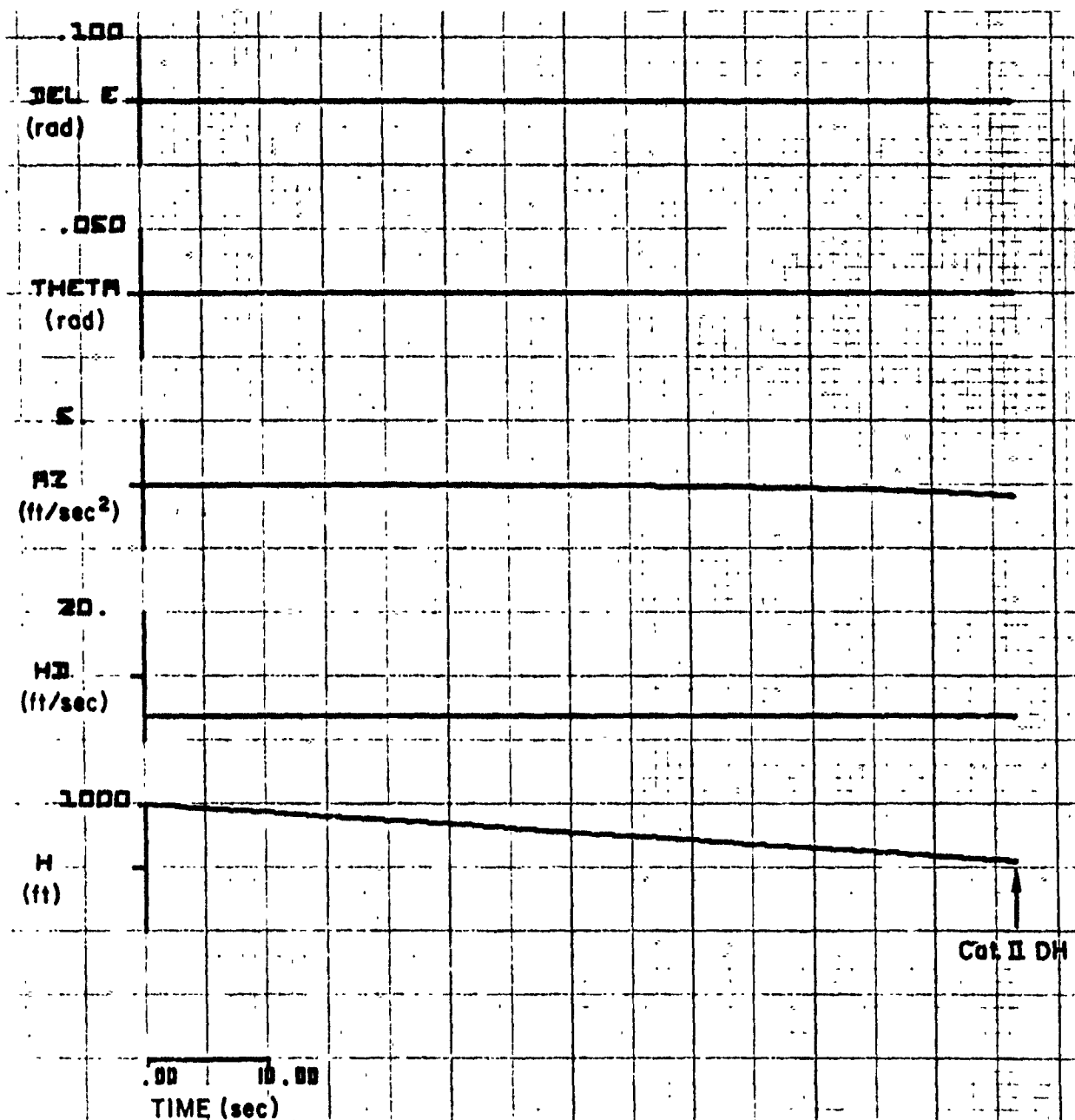


Figure D-3(a). Mean Responses: CV-880, FD, Cat II, M

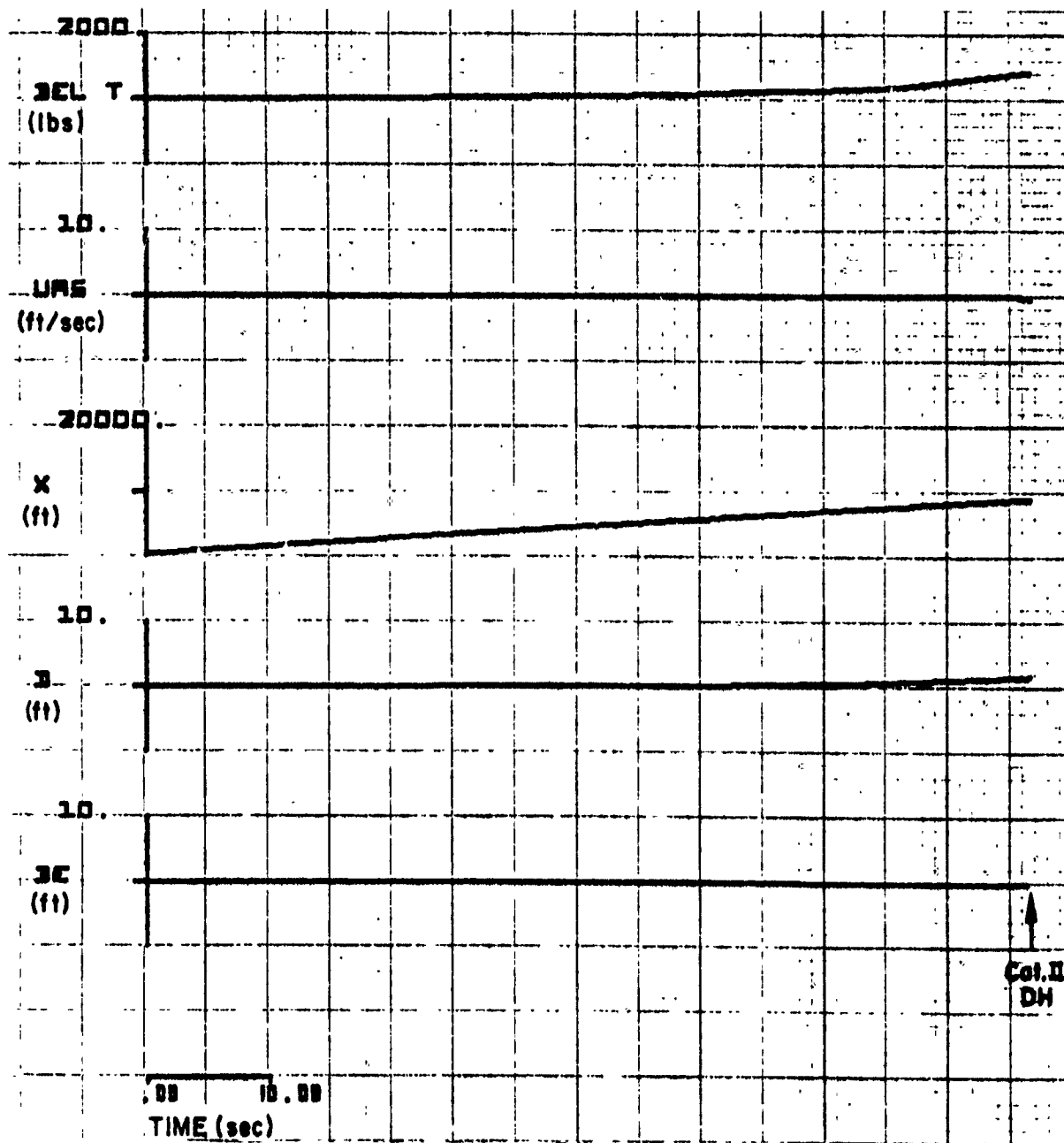


Figure D-3(b)

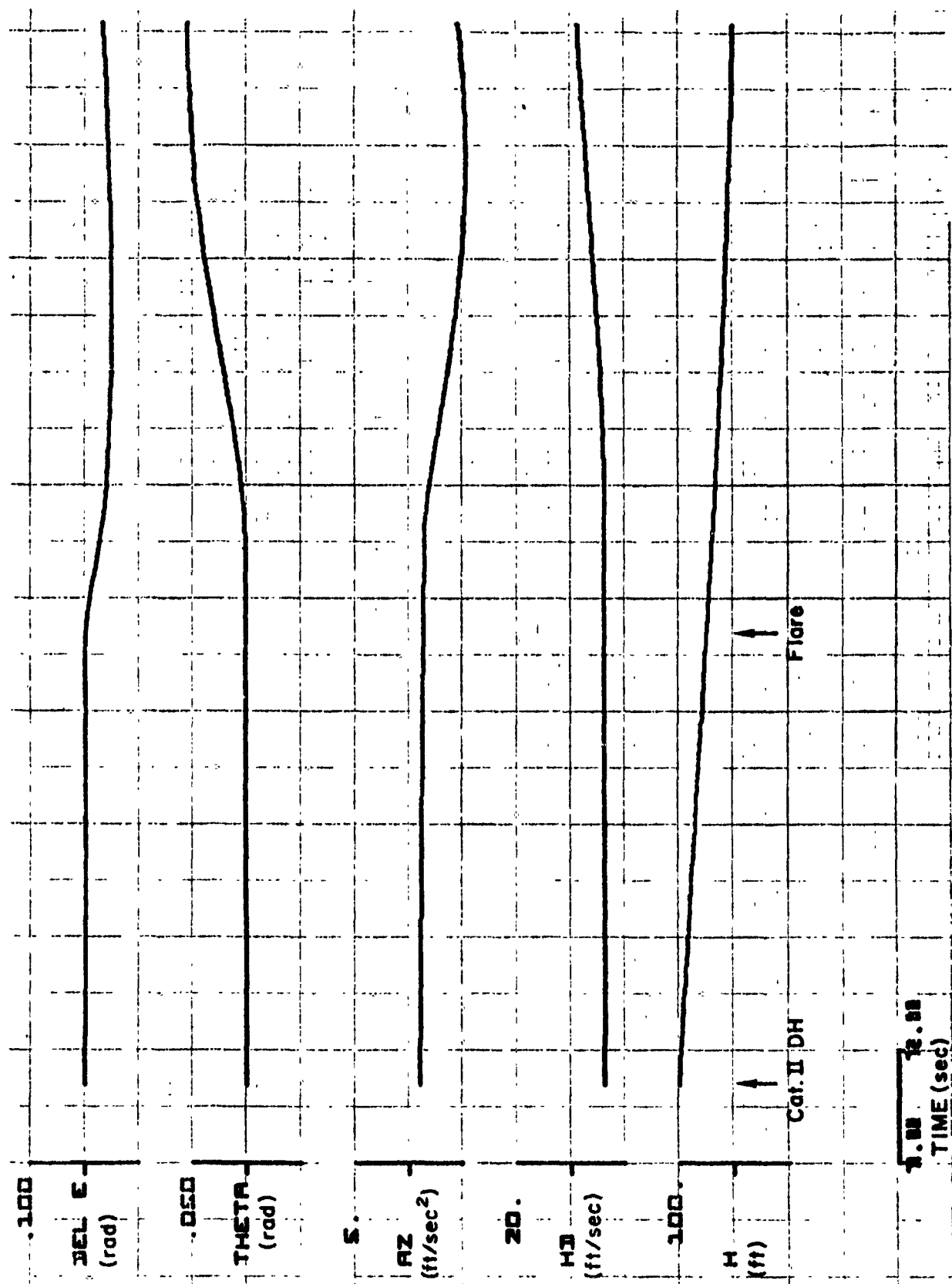


Figure D-4(a). Mean Responses: CV-880, FD, Cat II, M

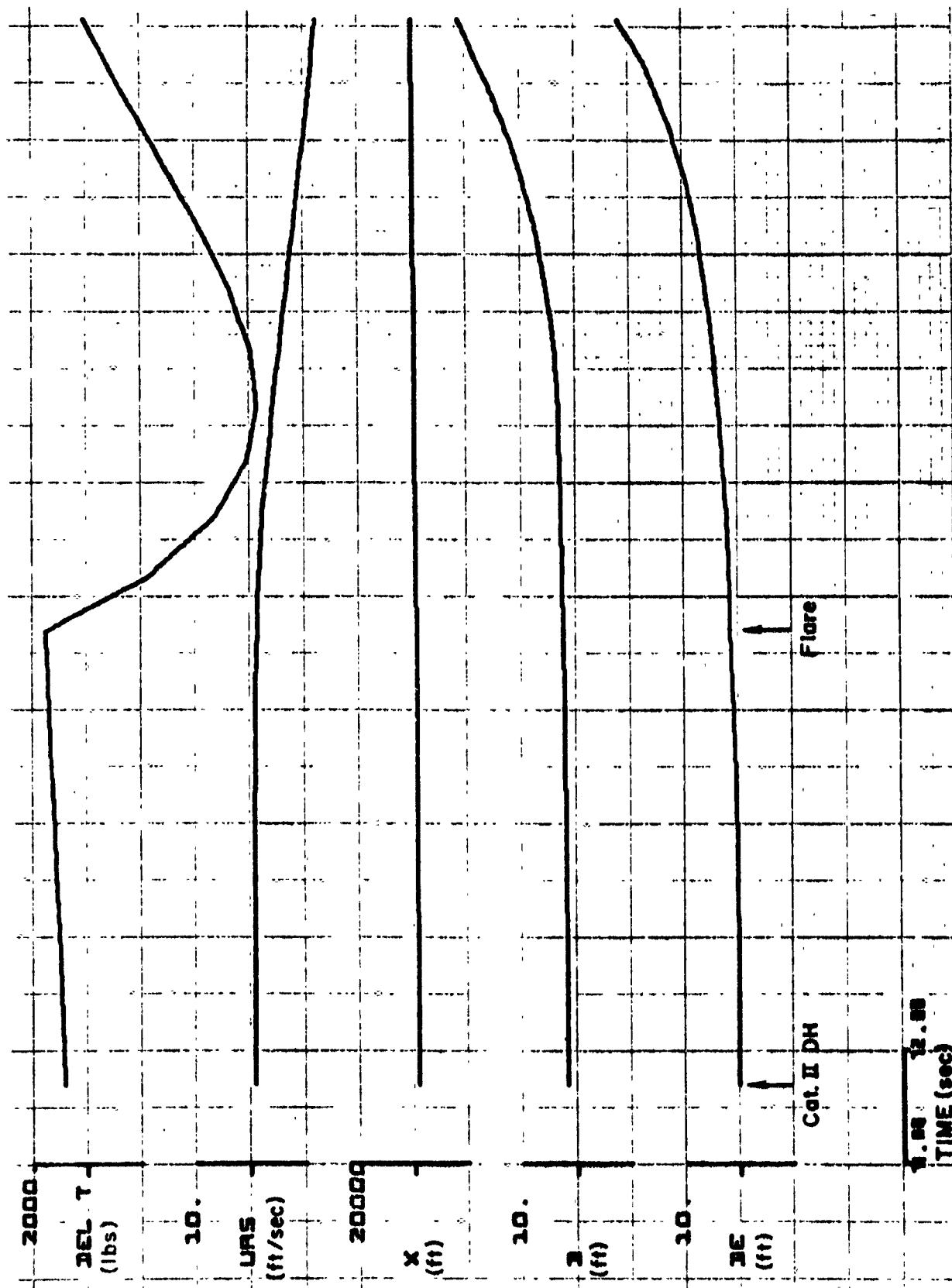


Figure D-4(b)

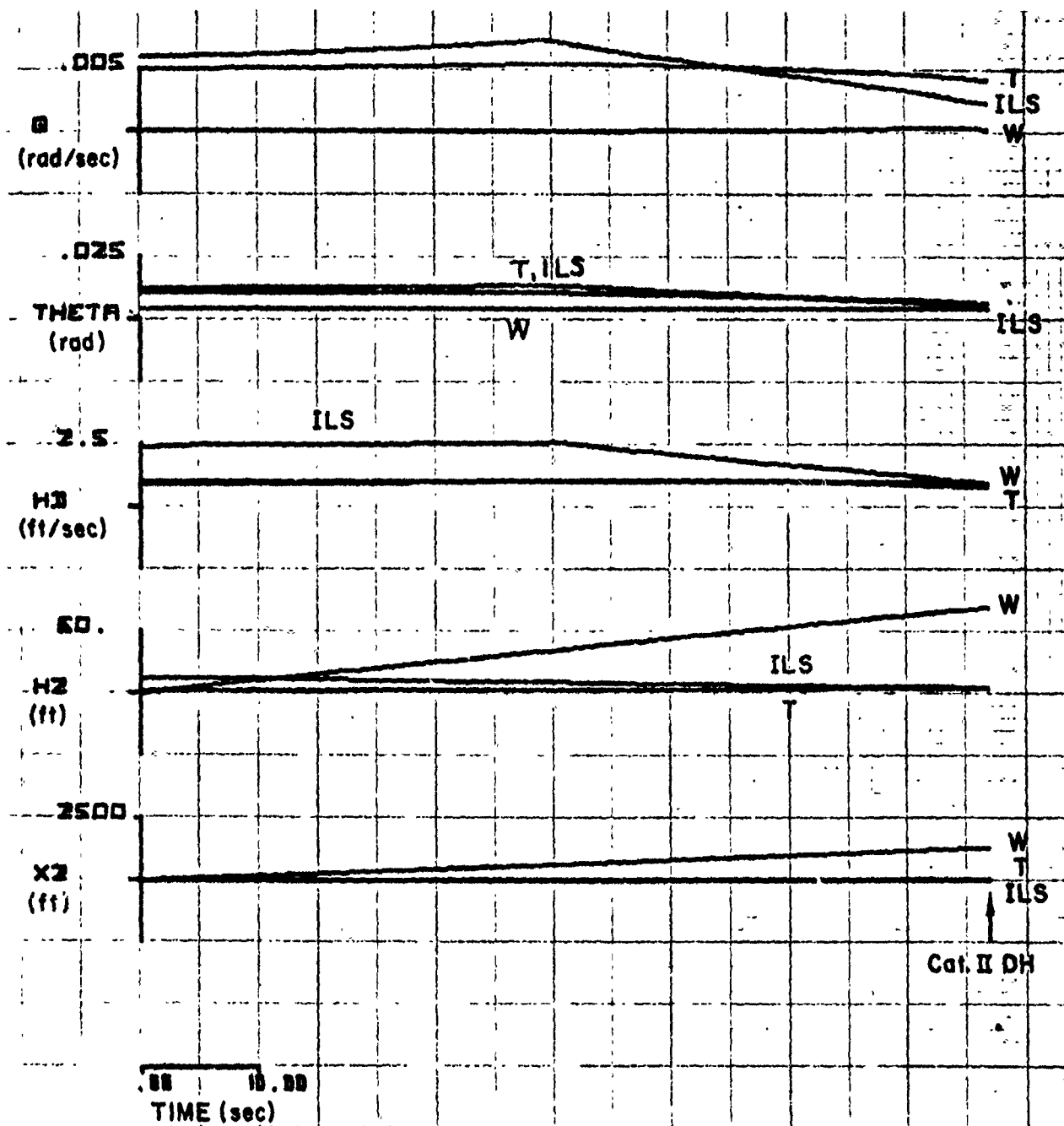


Figure D-5(a). Standard Deviation Responses: CV-880, FD, Cat II, M

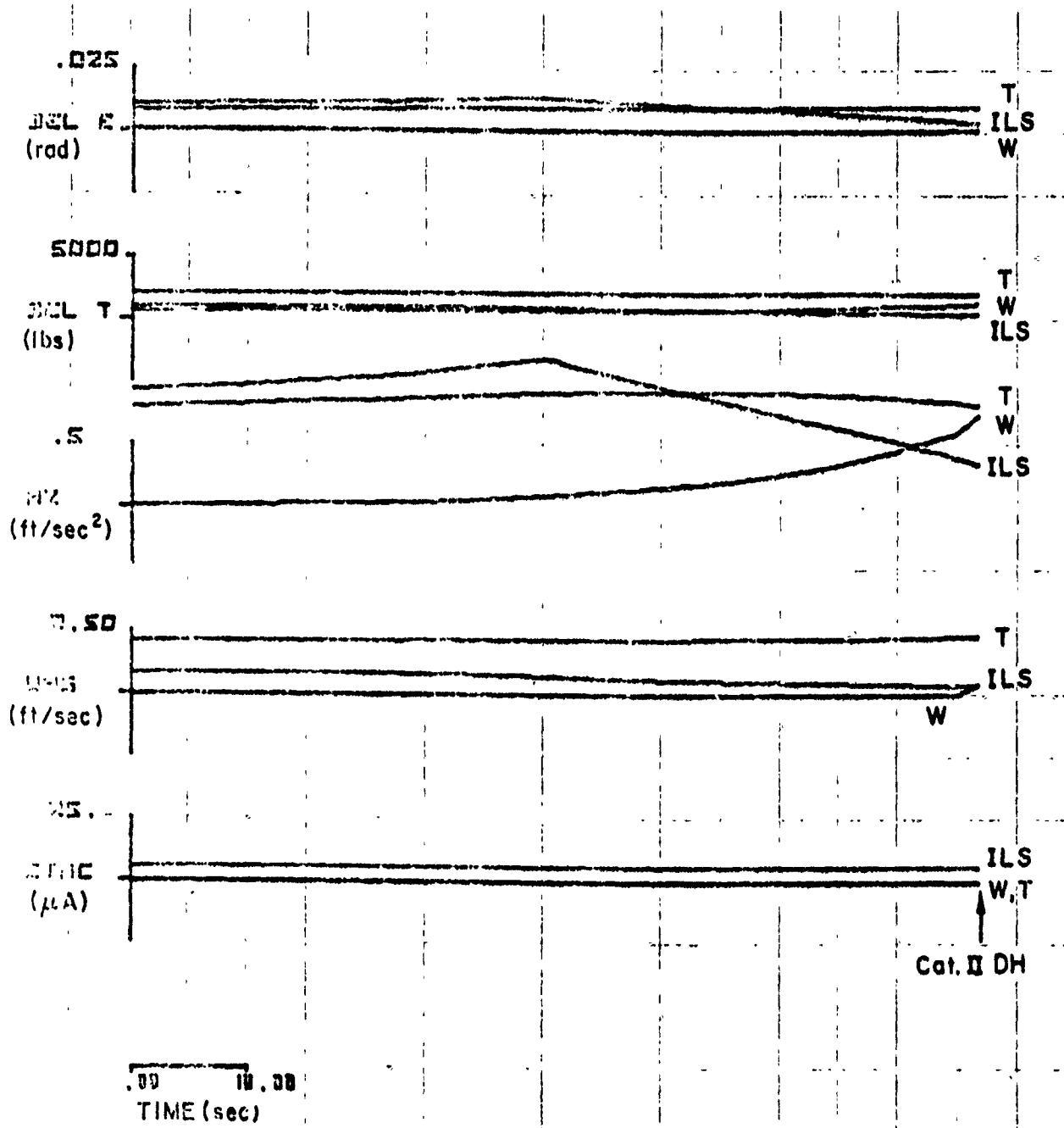


Figure D-5(b)

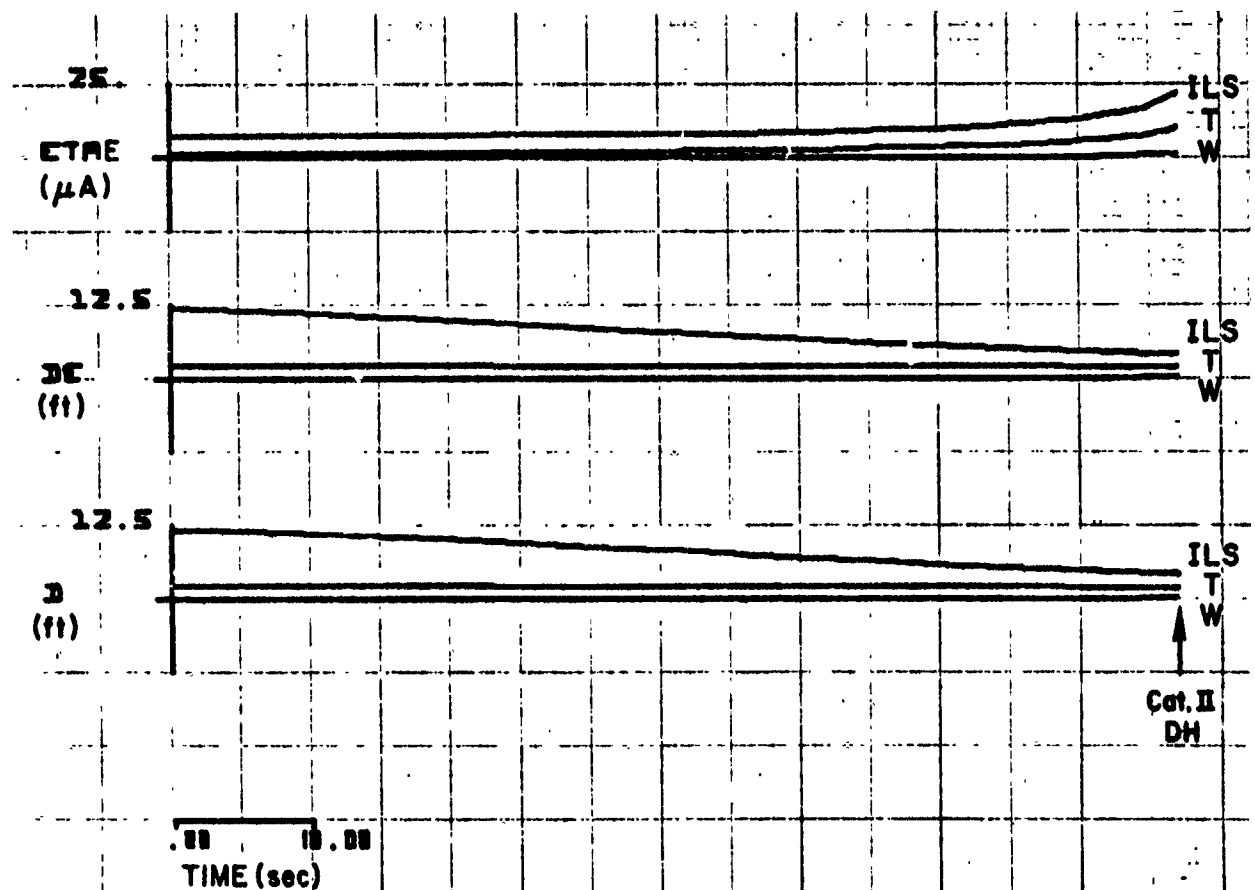


Figure D-5(c)

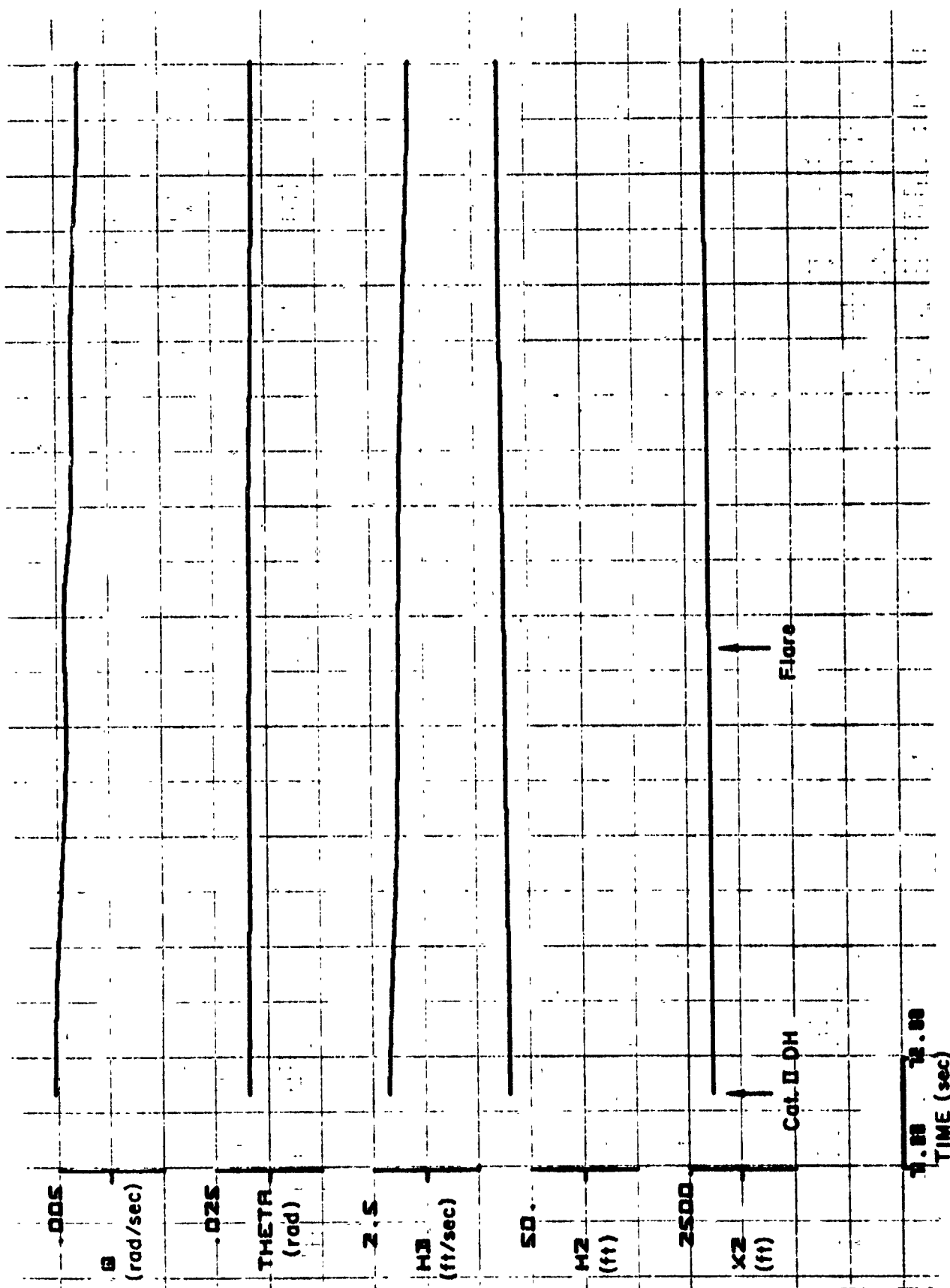


Figure D-6(a). Standard Deviation Responses: CV-890, FD, Cat II, M

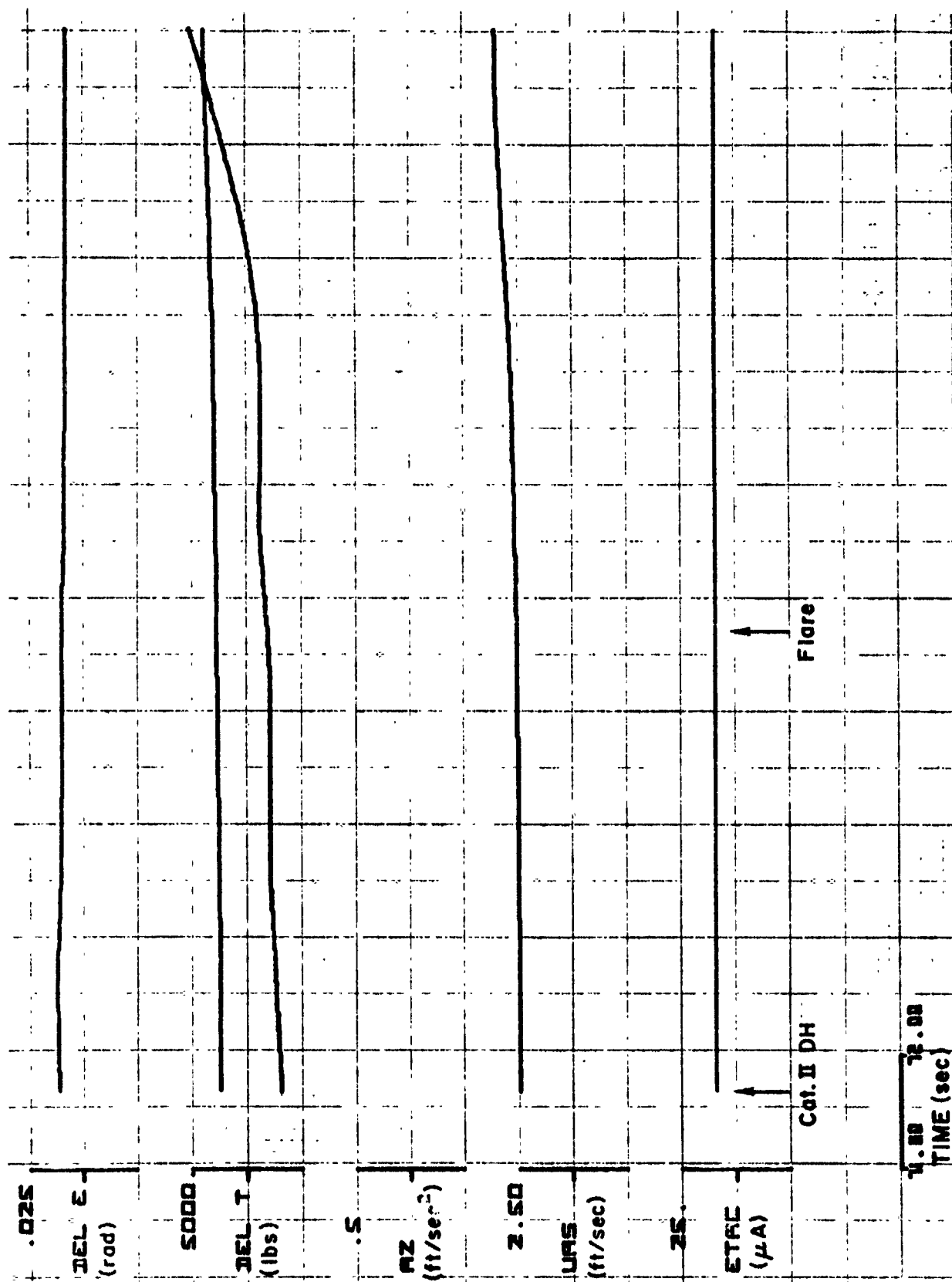


Figure D-6(b)

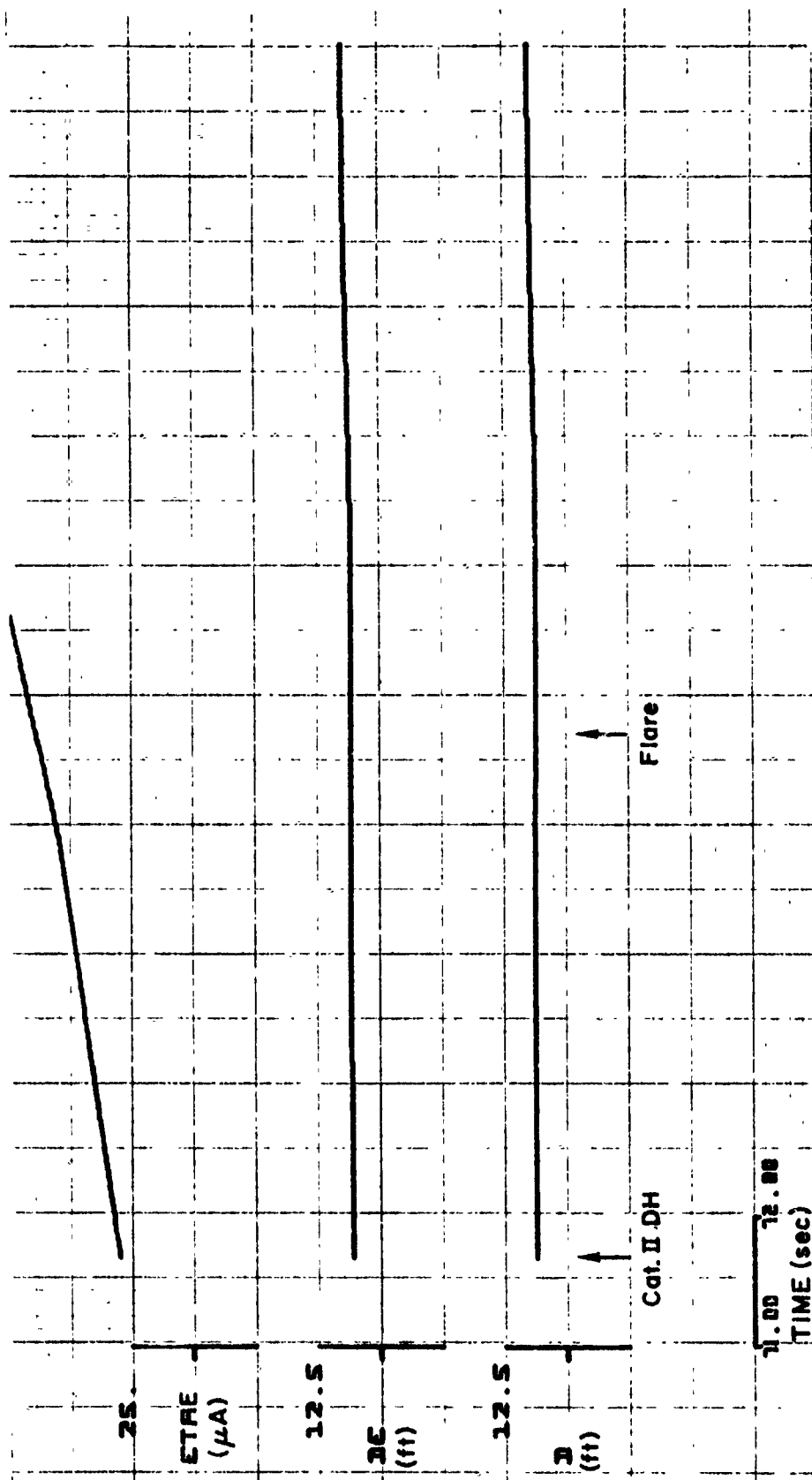


Figure D-6(c)

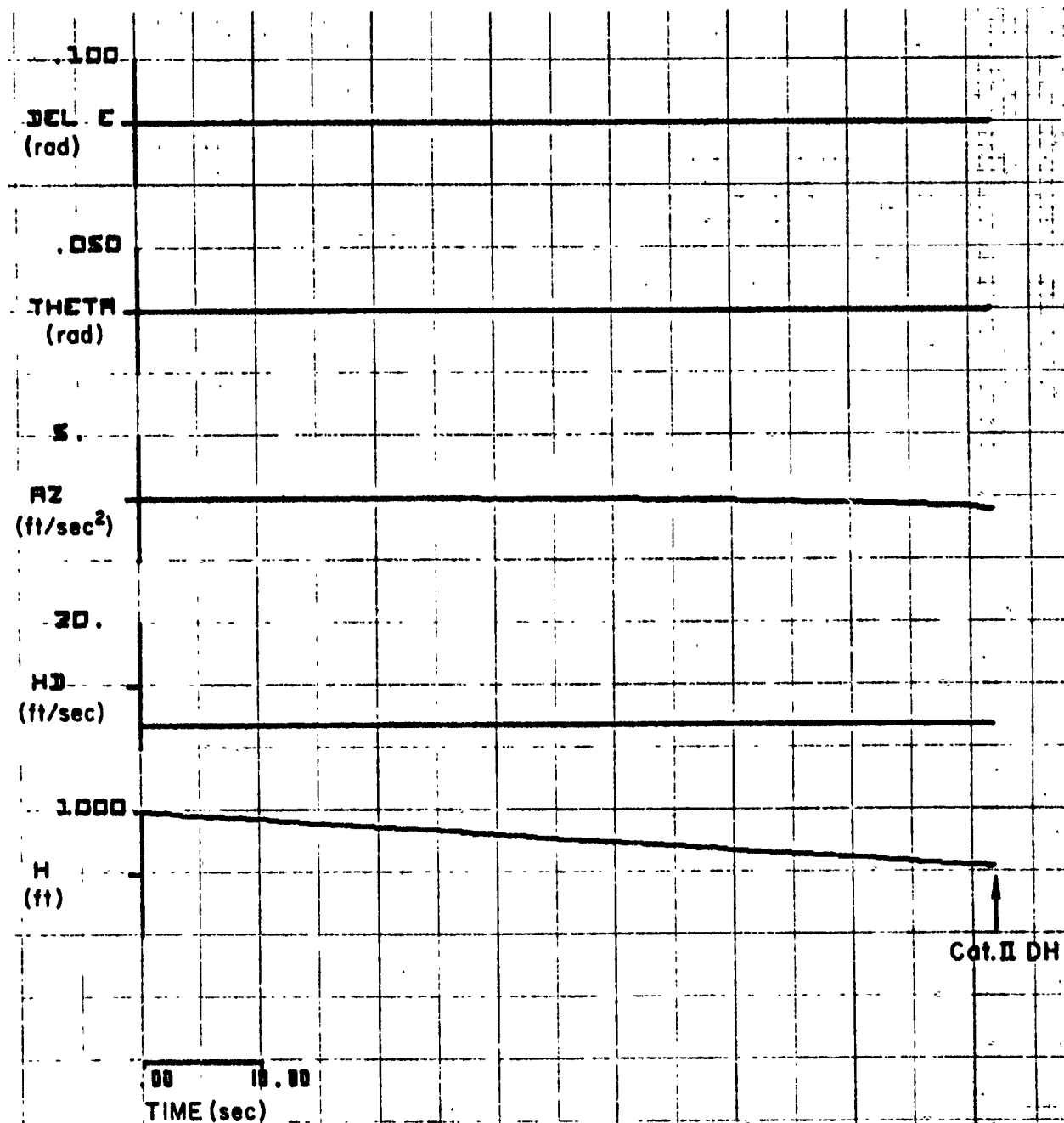


Figure D-7(a). Mean Responses: CV-880, LSI, Cat II, III

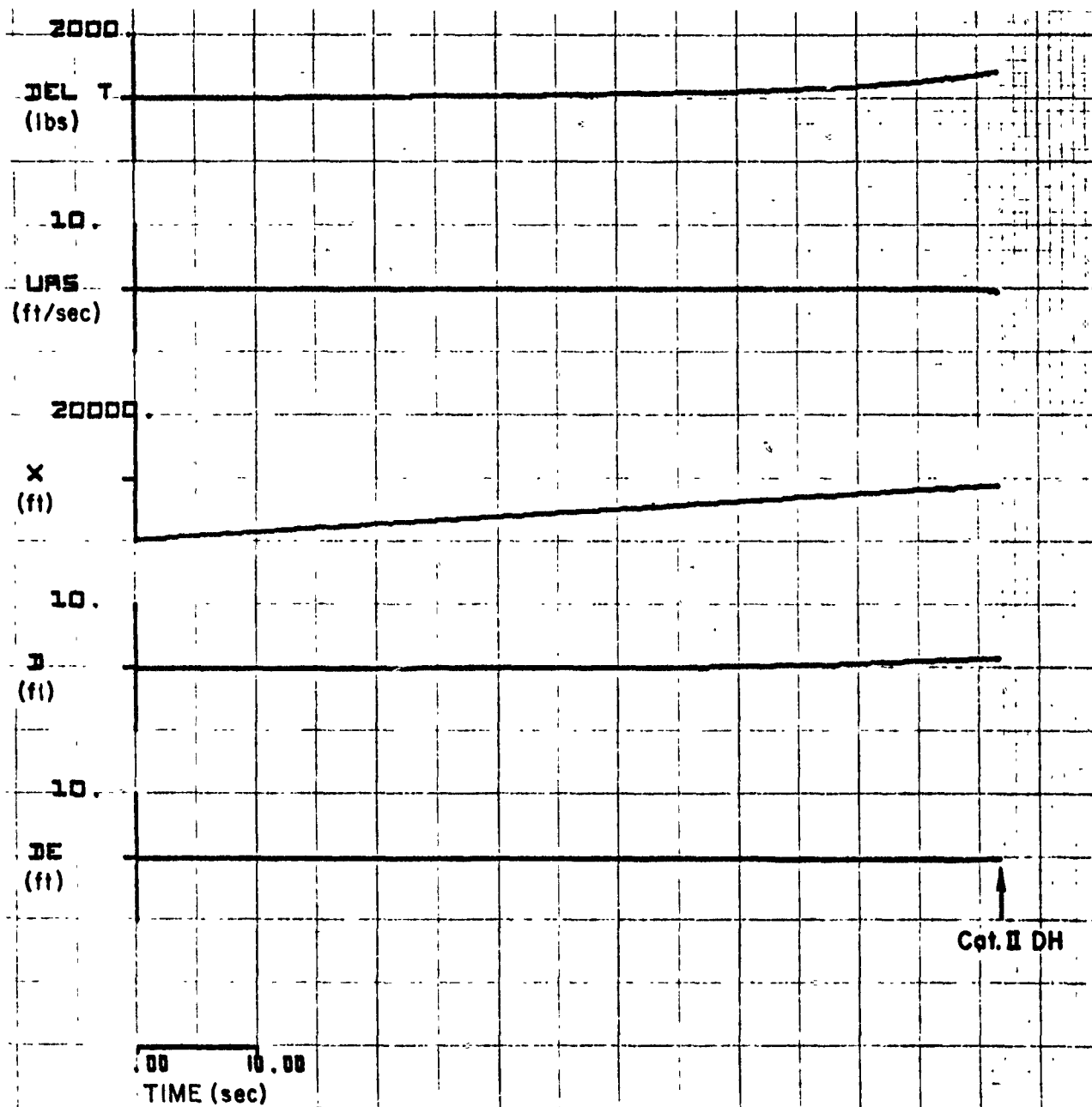


Figure D-7(b)

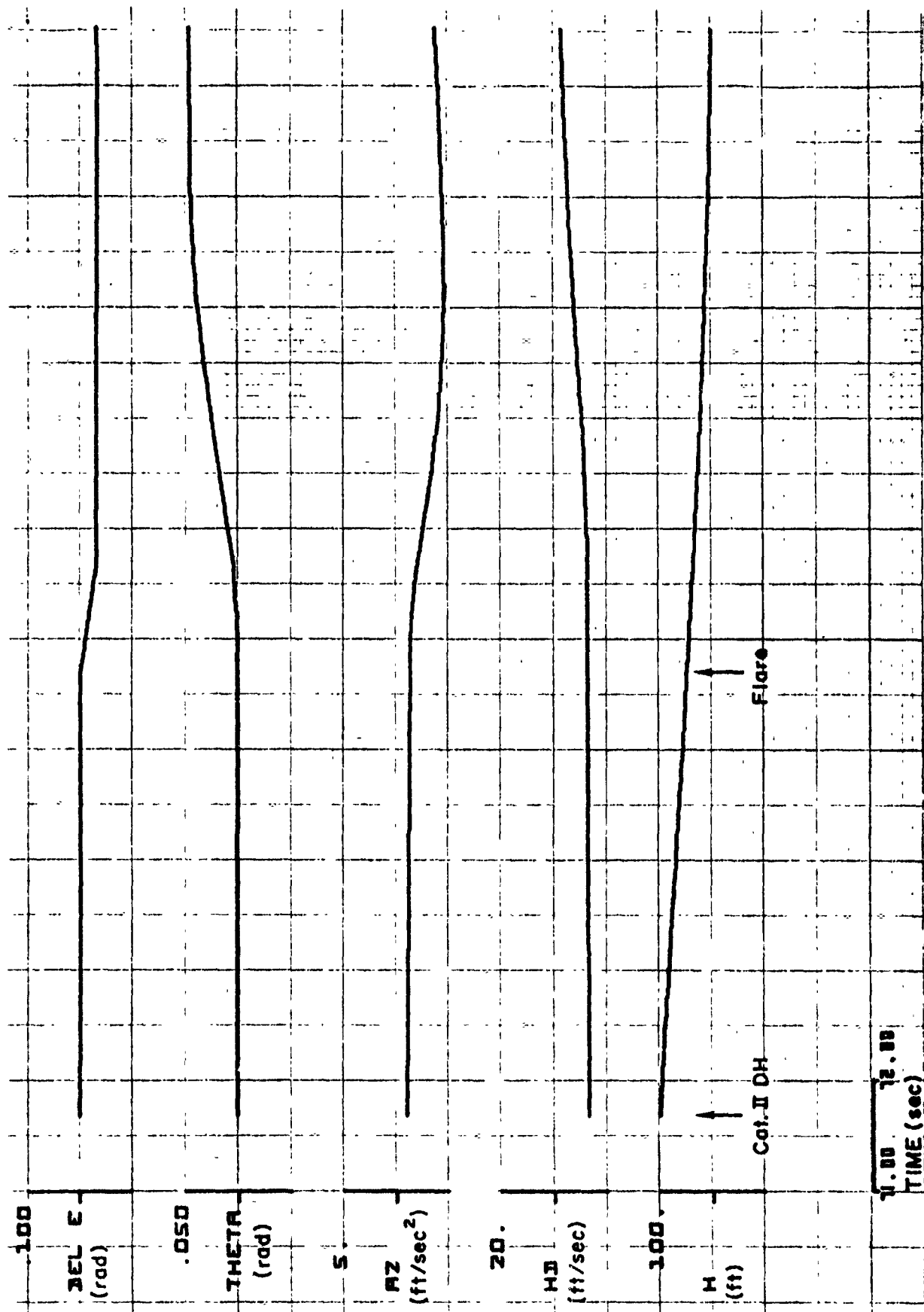


Figure D-8(a). Mean Responses: CV-880, LSI, Cat II, III

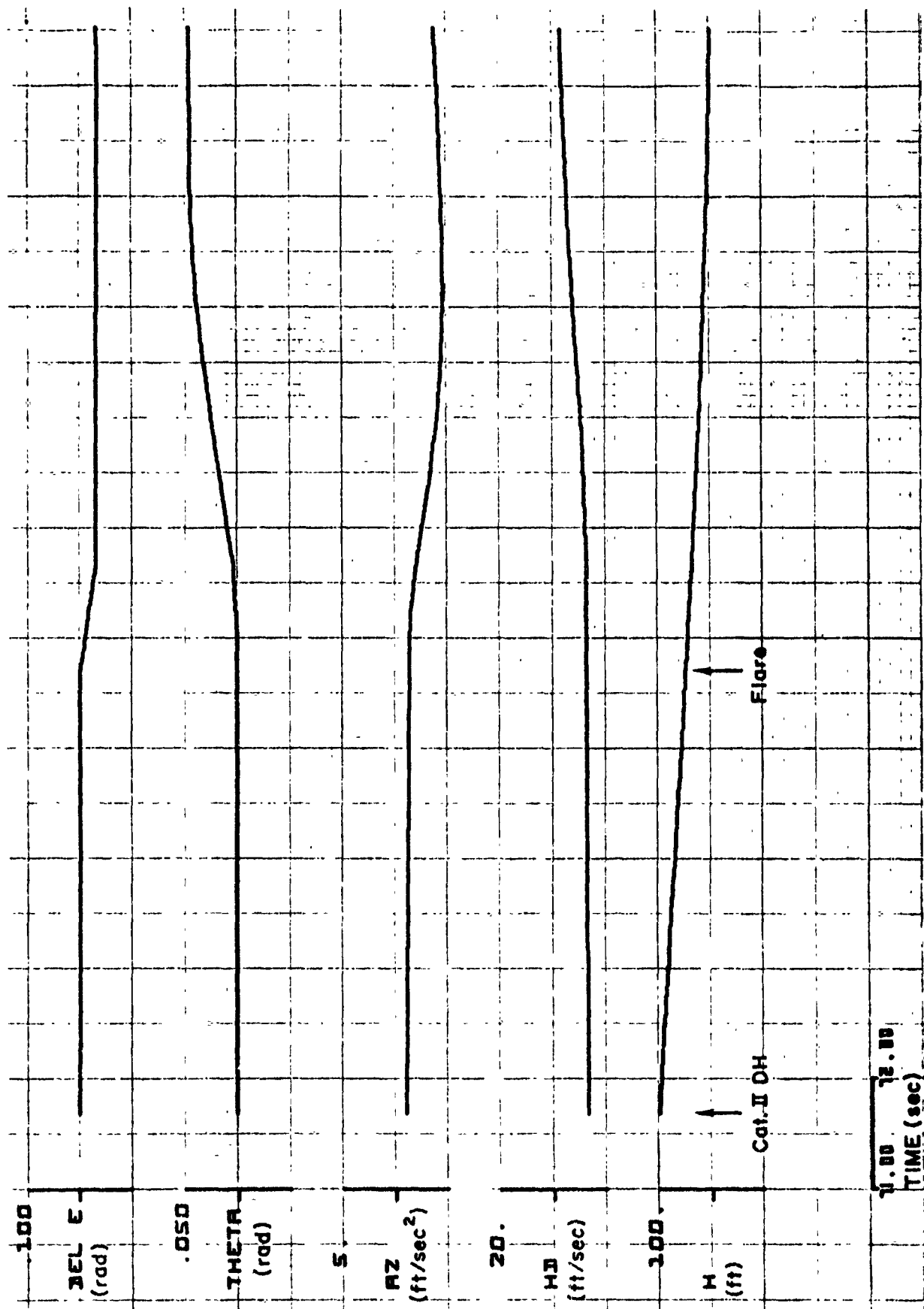


Figure D-8(a). Mean Responses: CV-880, LSI, Cat II, III

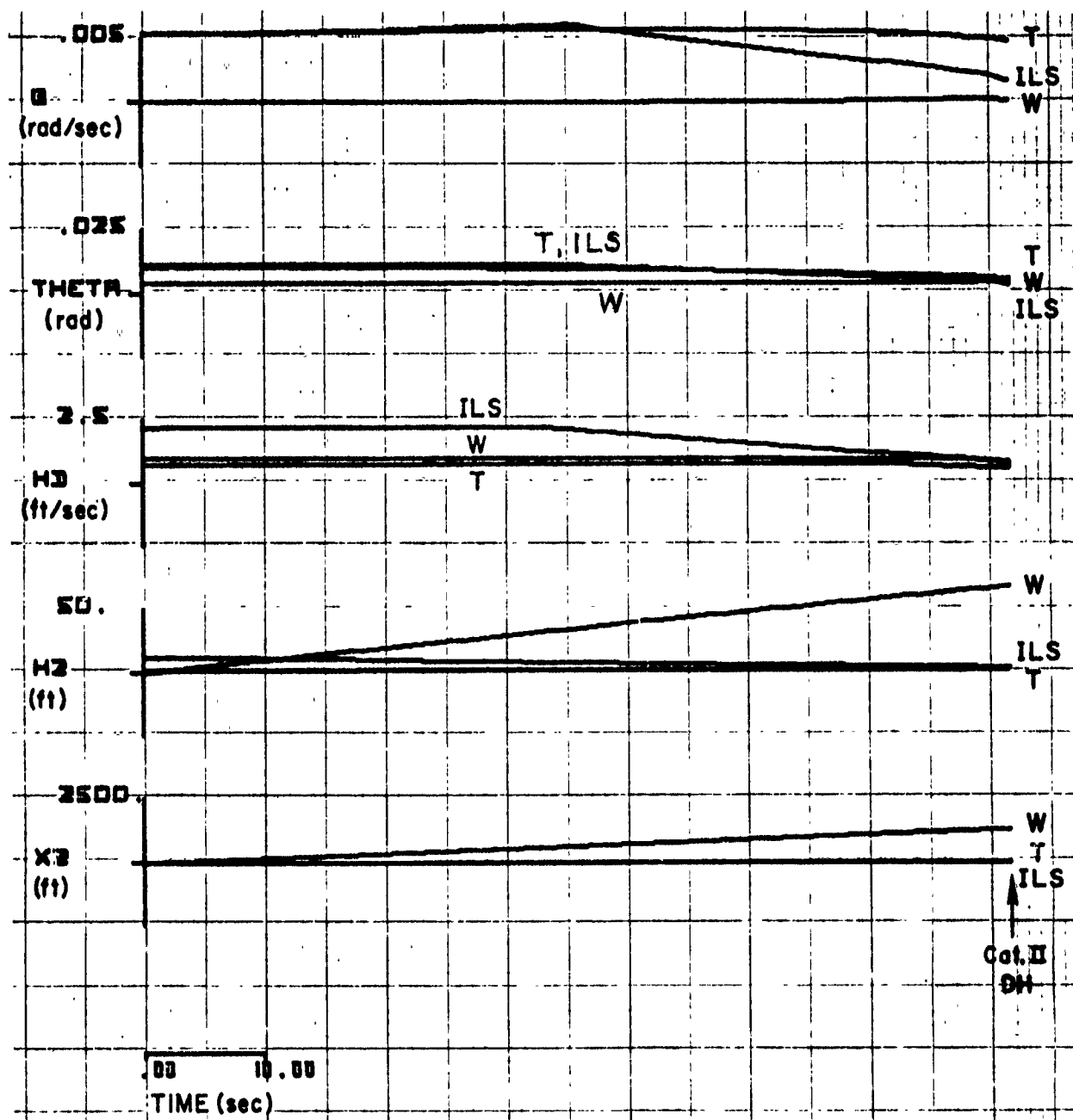


Figure D-9(a). Standard Deviation Responses: CV-880, LSI, Cat II, III

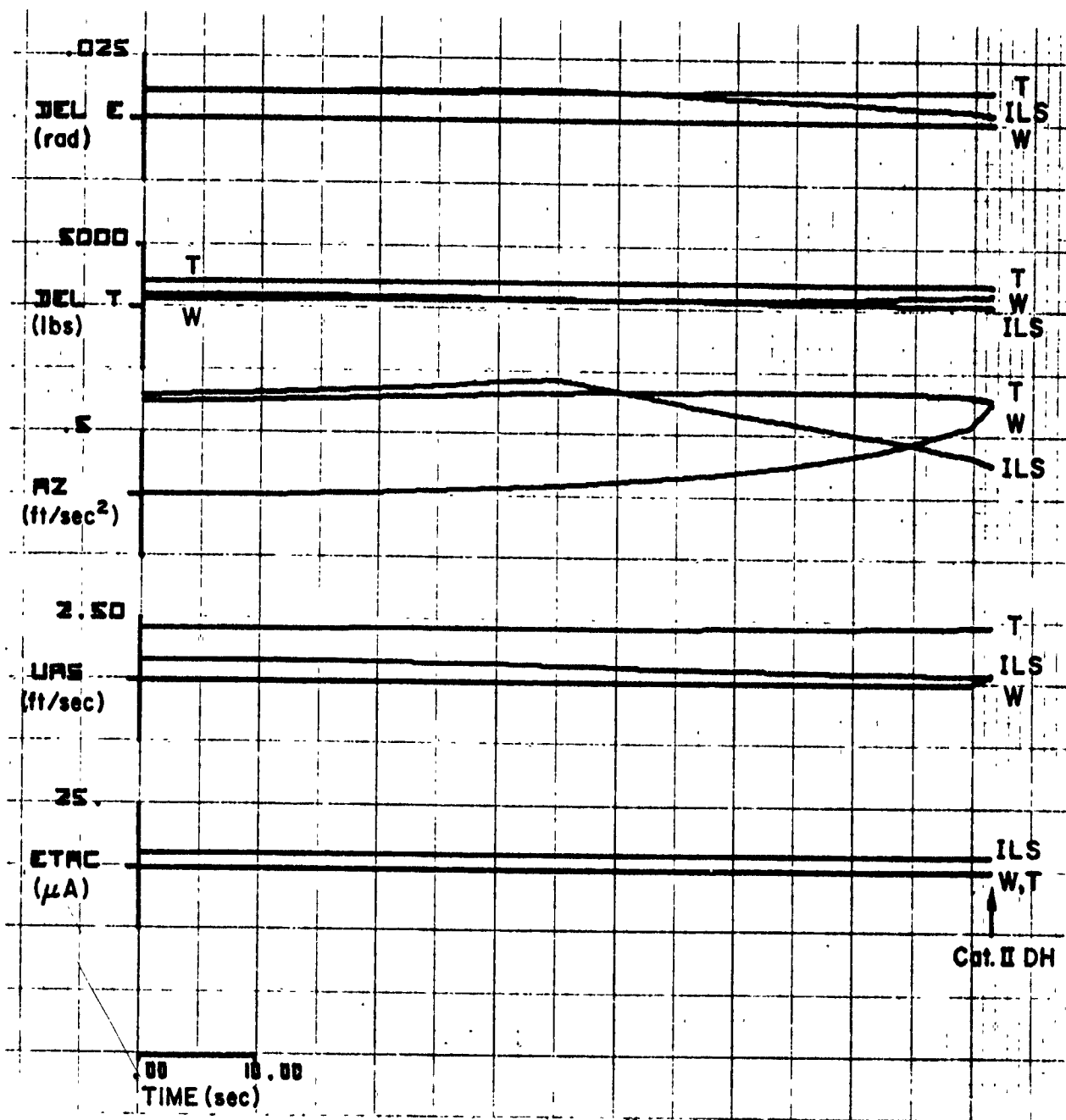


Figure D-9(b)

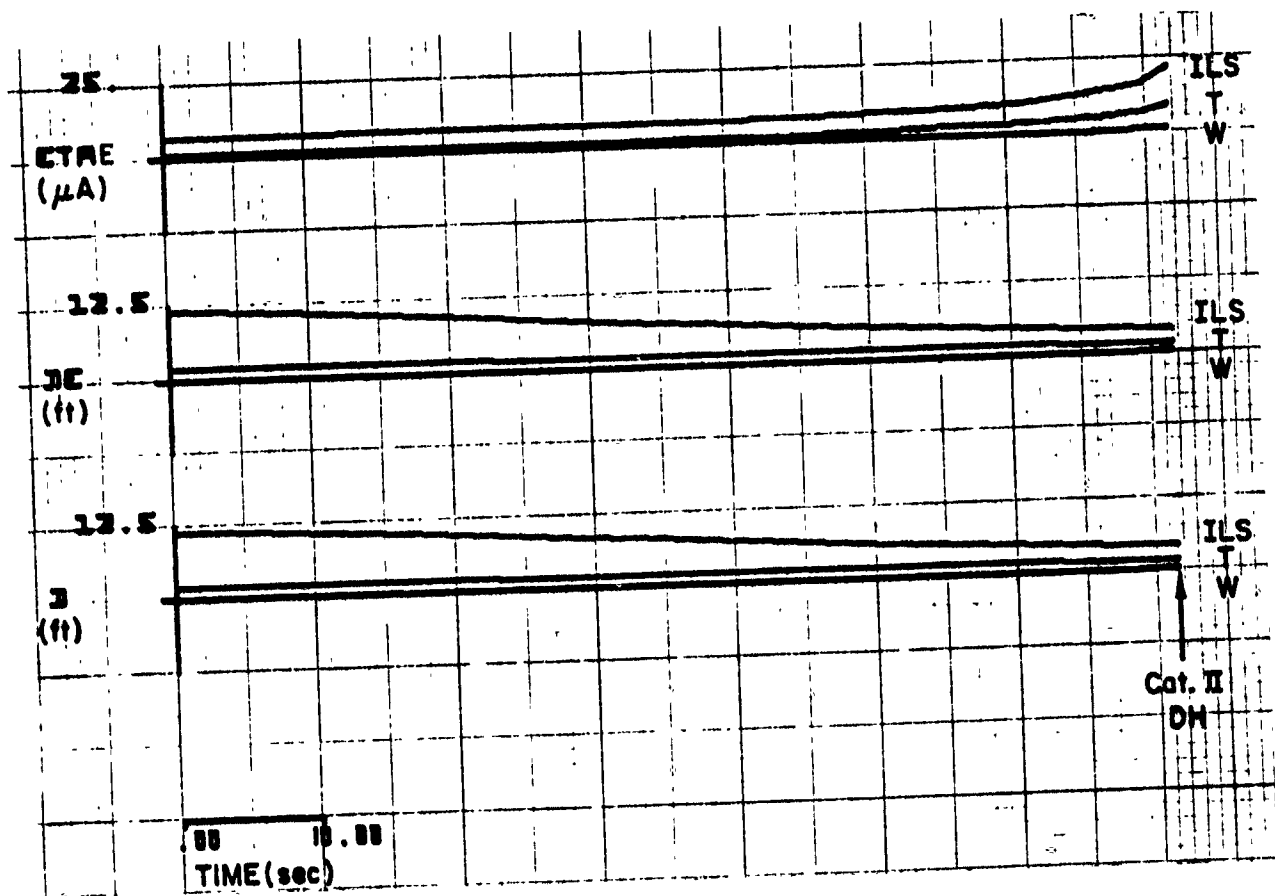


Figure D-9(c)

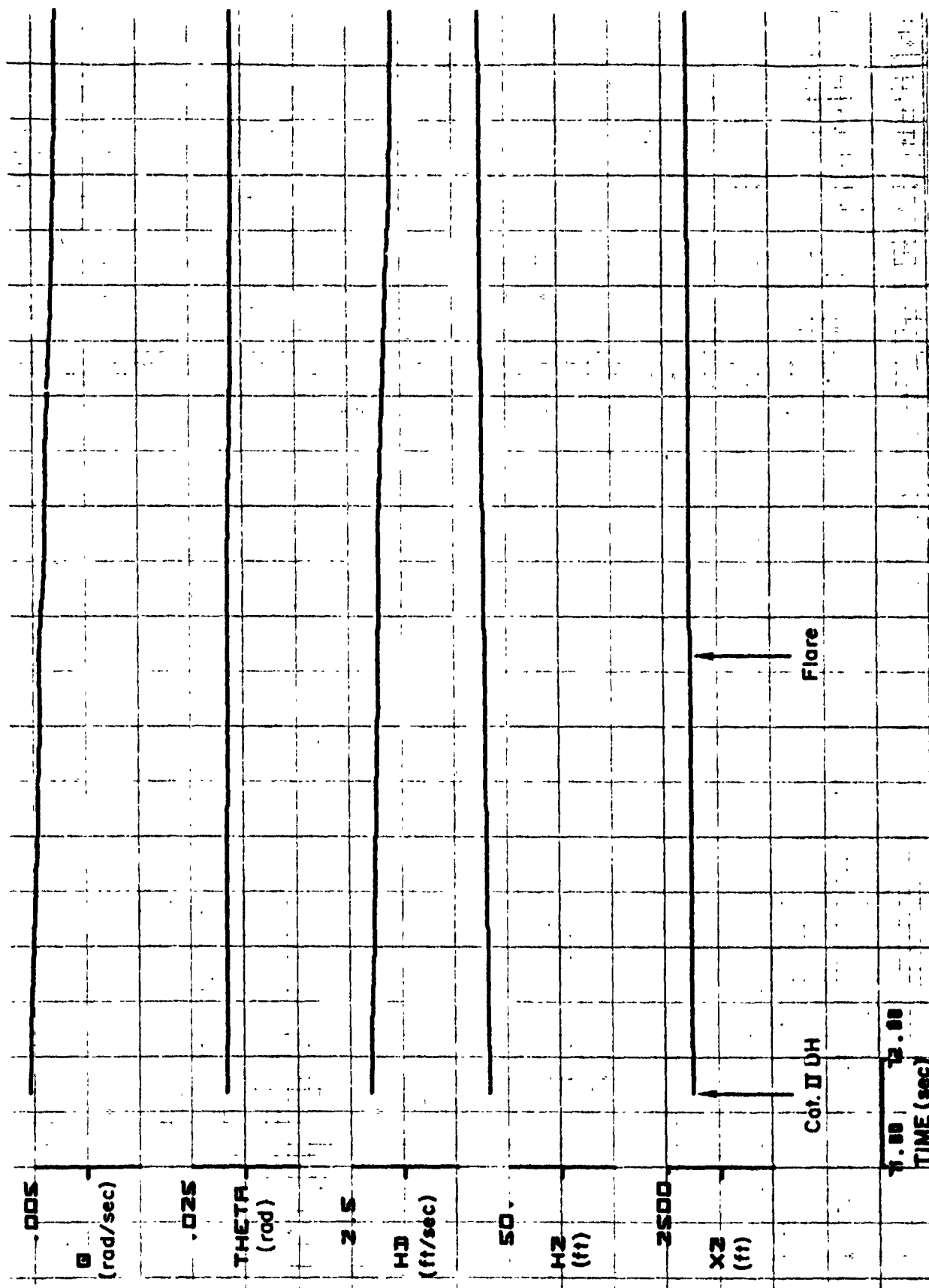
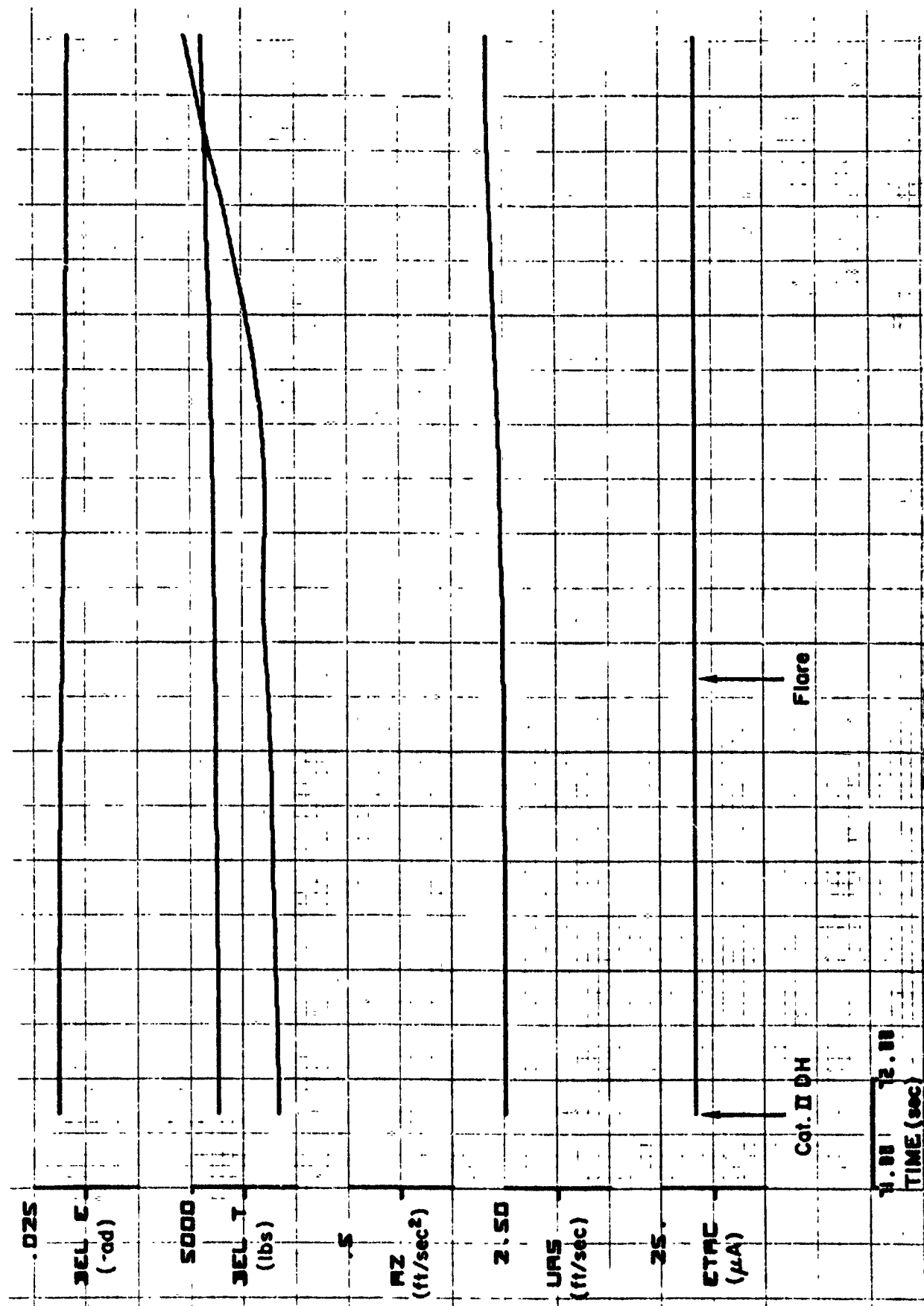


Figure D-10(a). Standard Deviation Responses: CV-880, LSI, Cat II, III



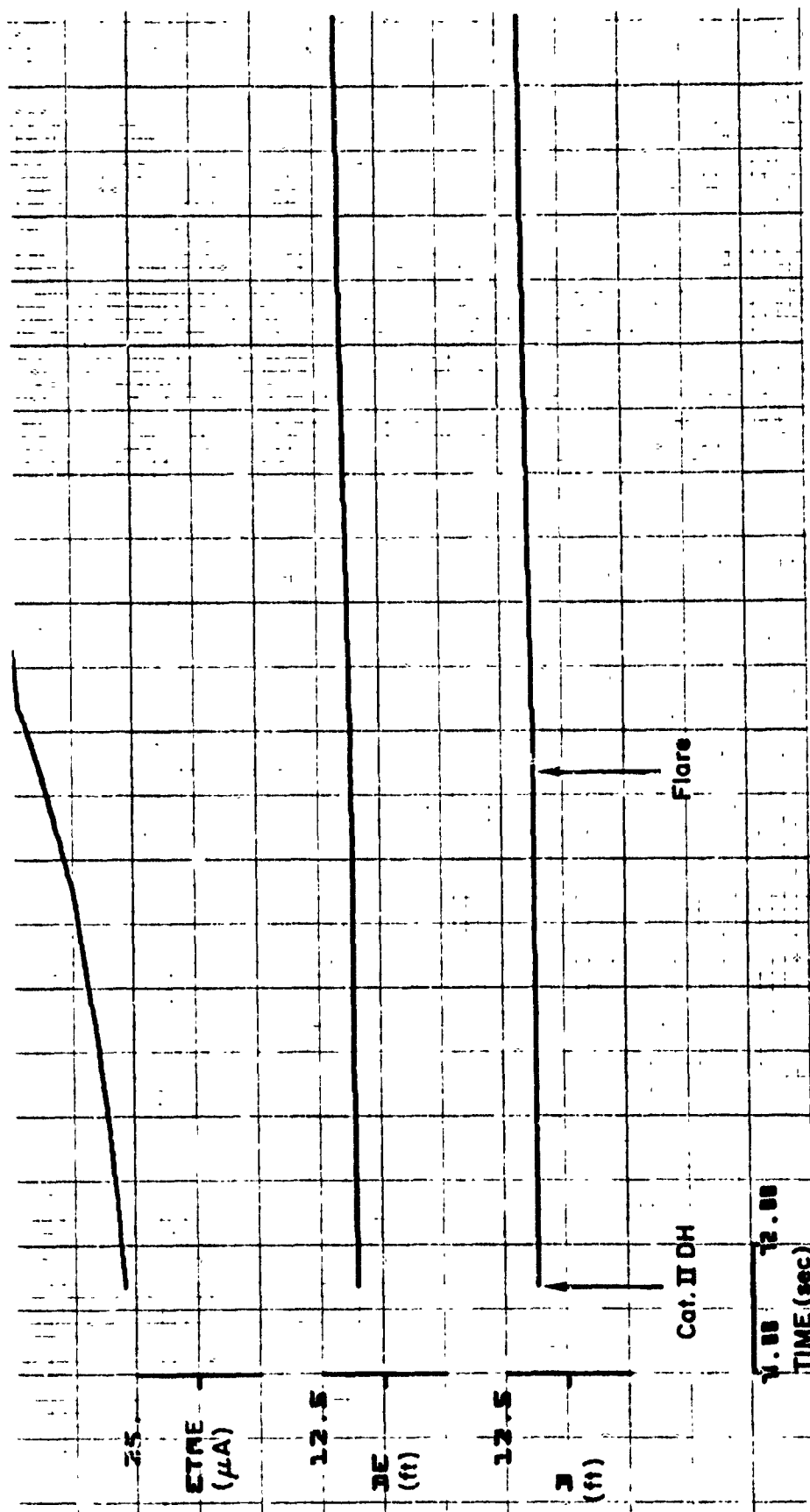


Figure D-10(c)

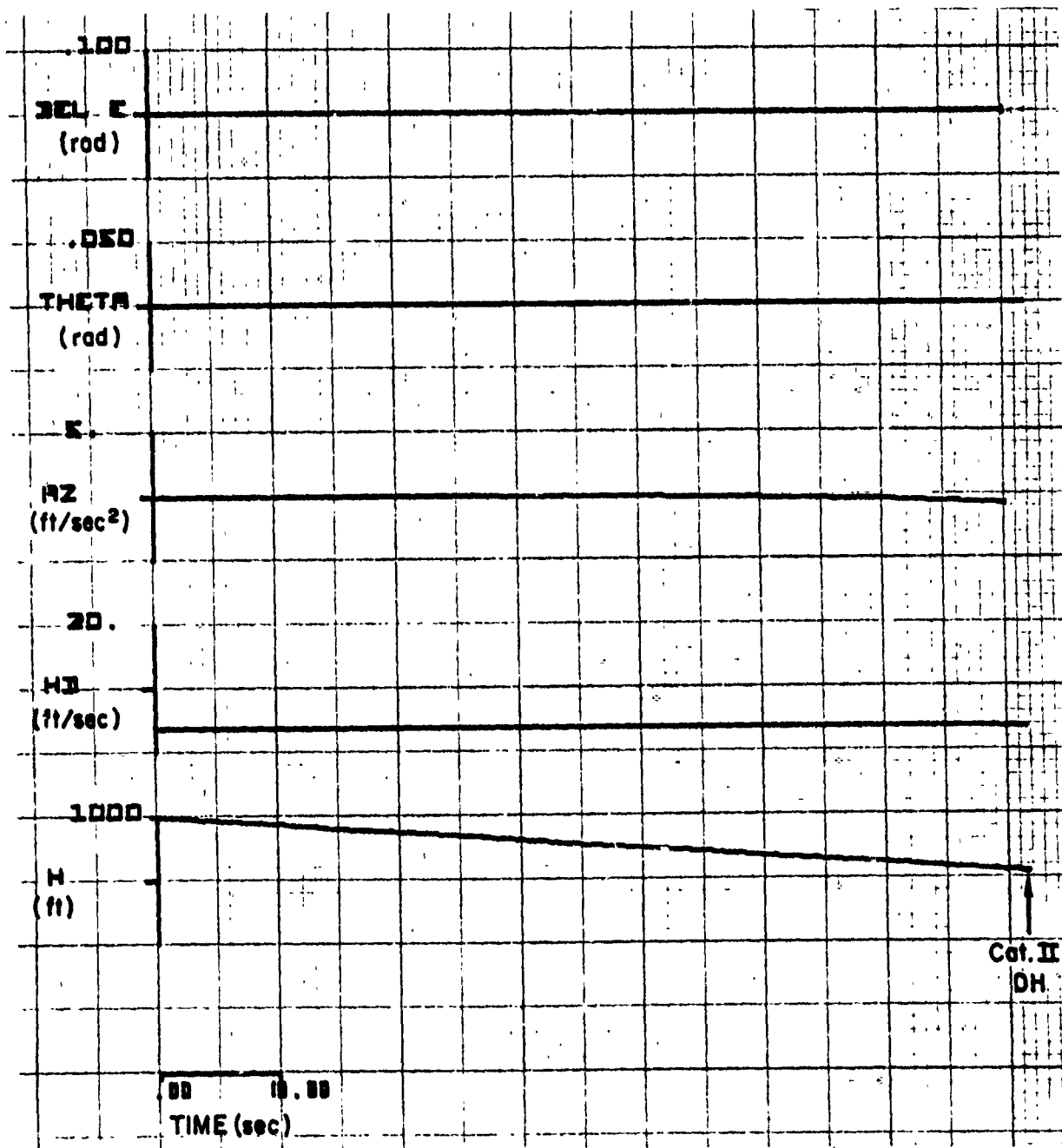


Figure D-11(a). Mean Responses: CV-880, IS, Cat II, III

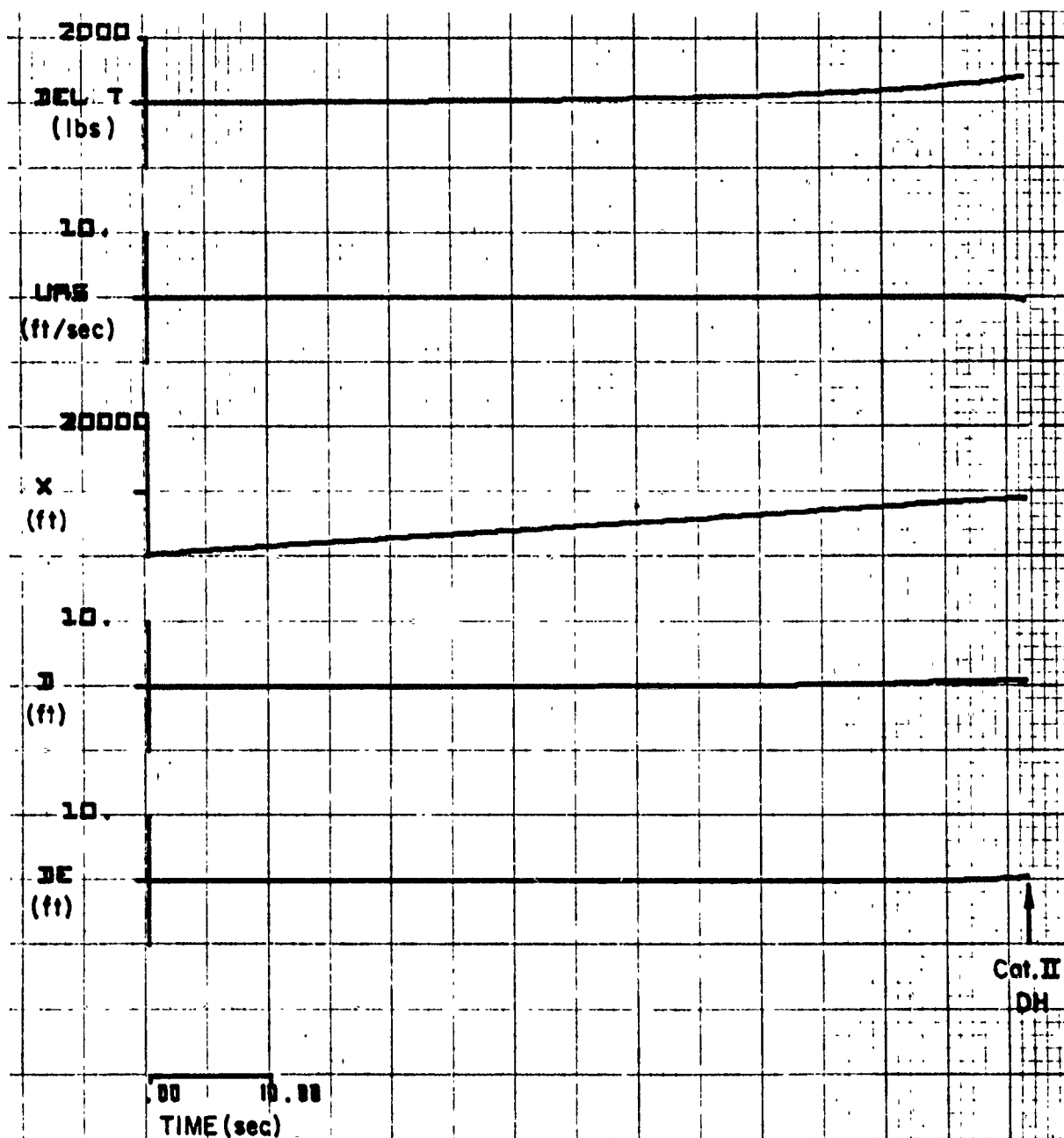


Figure D-11(b)

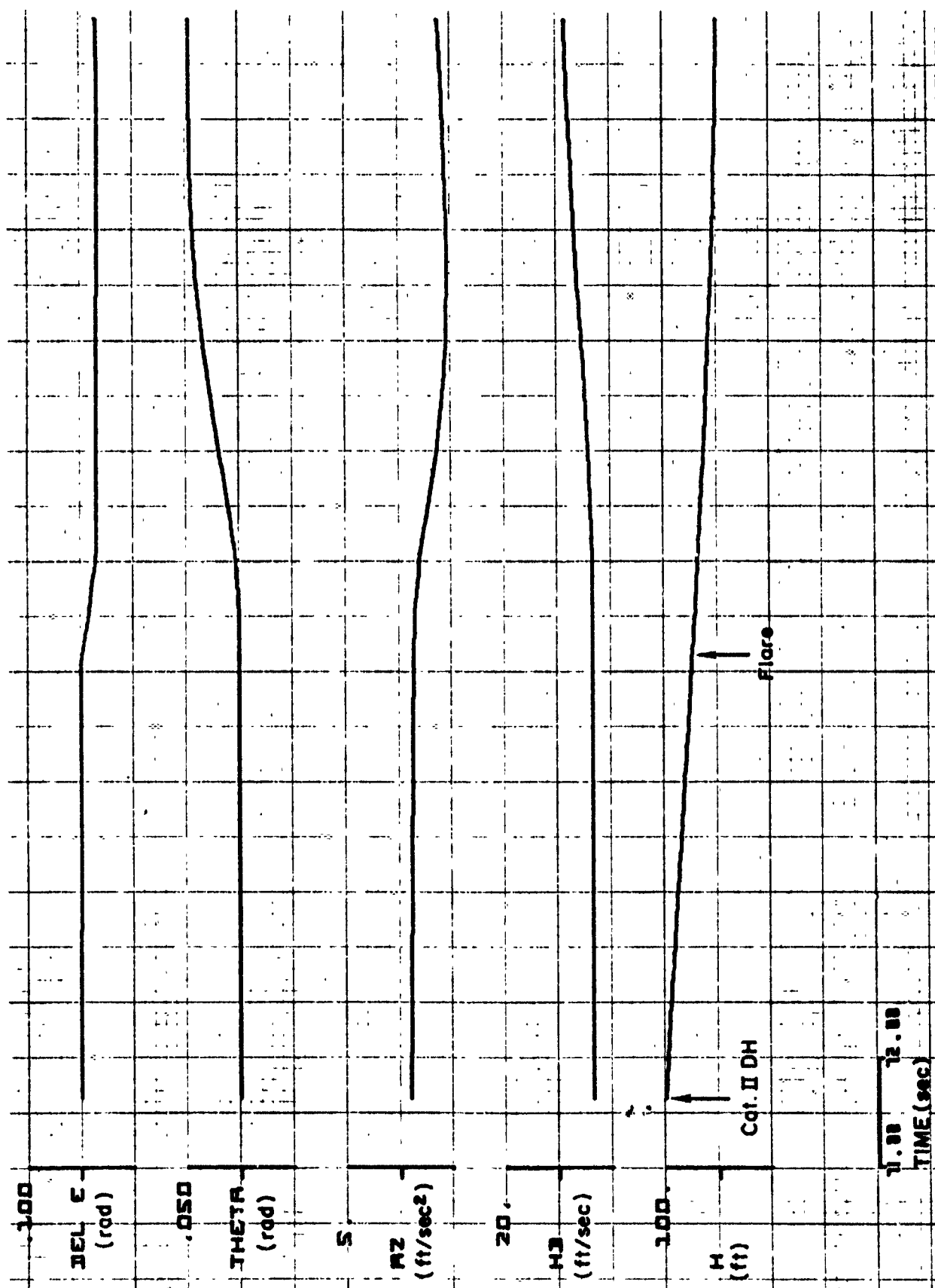


Figure D-12(a). Mean Responses: CV-880, IS, Cat II, III

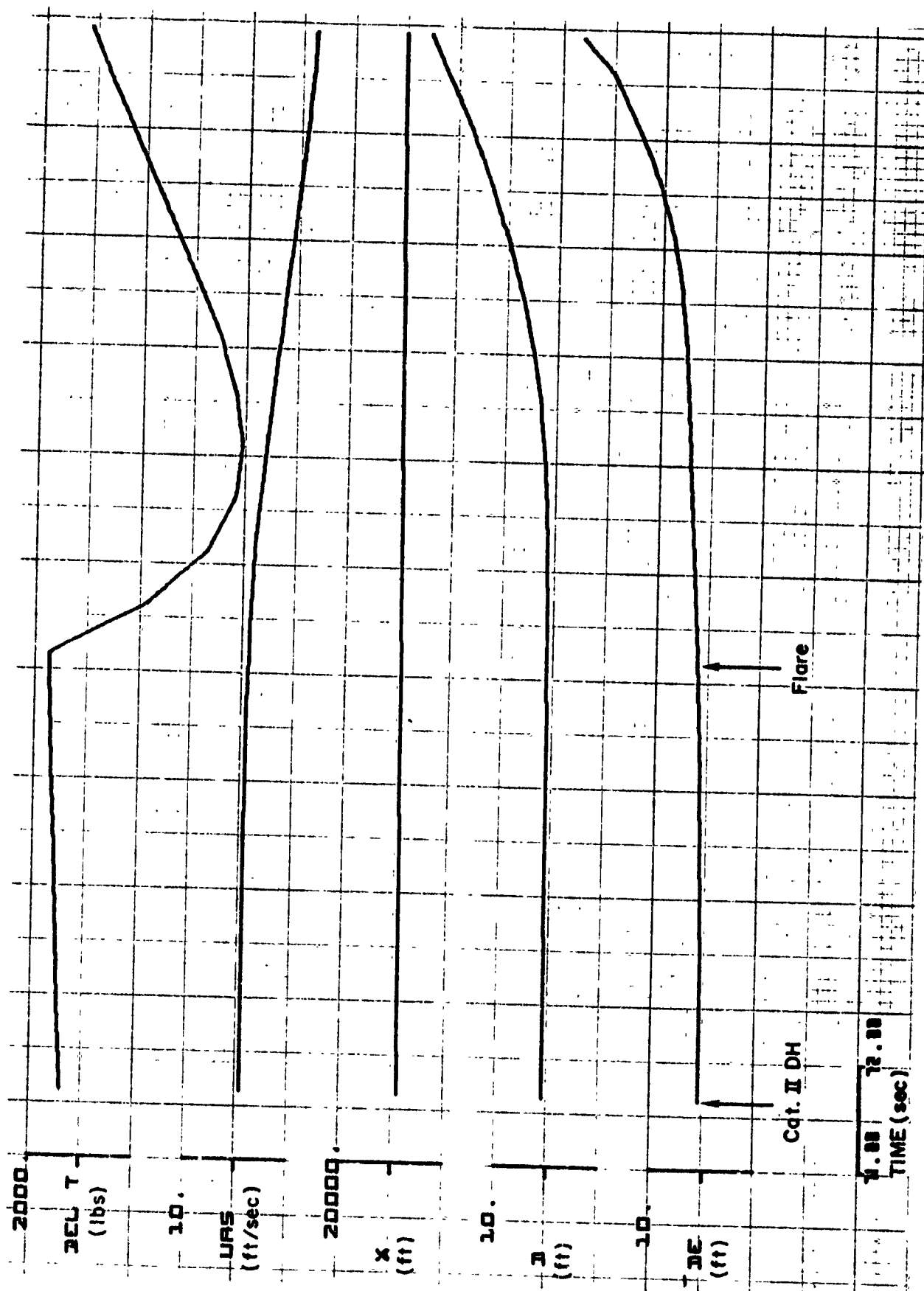


Figure D-12(b)

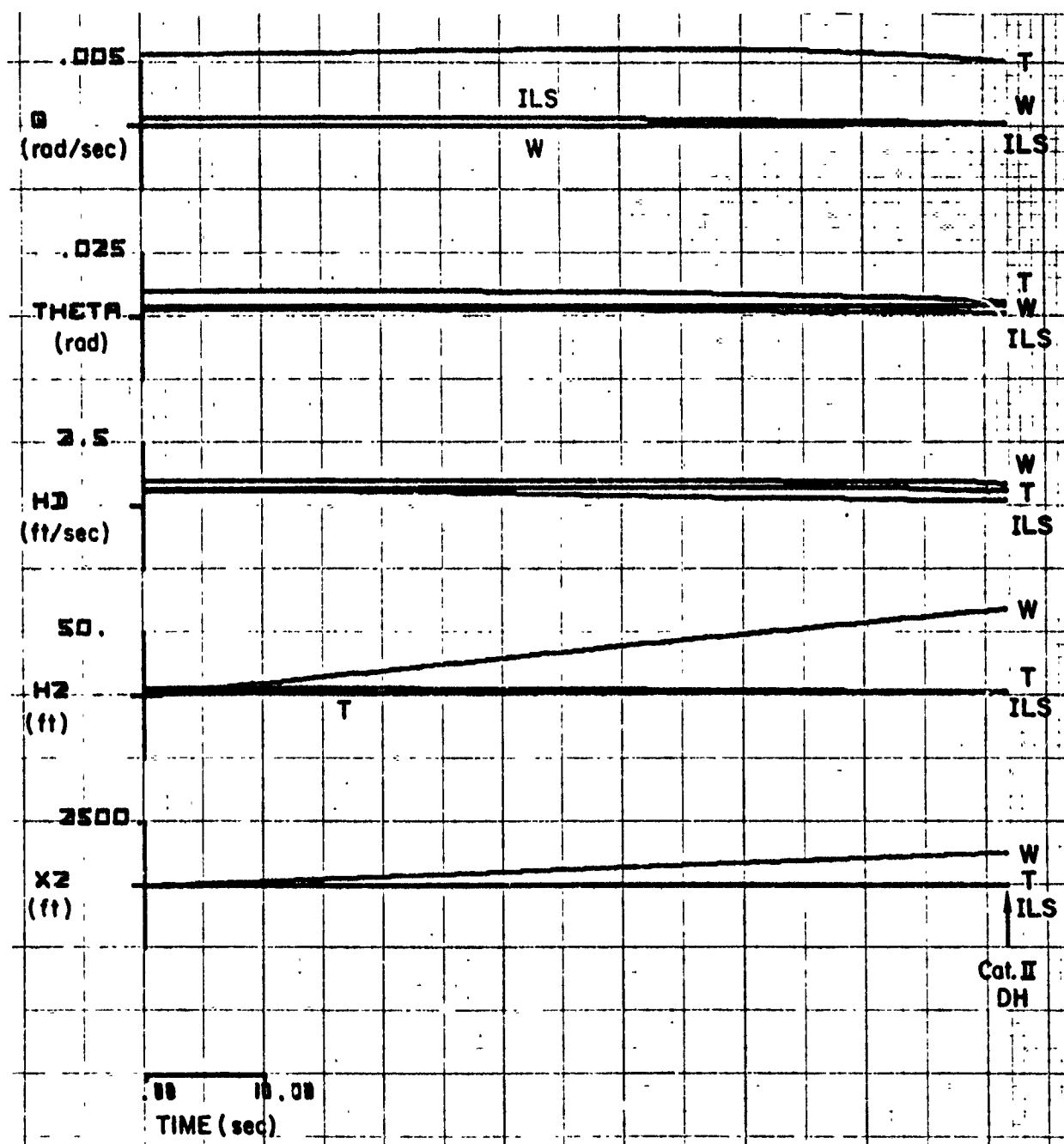


Figure D-13(a). Standard Deviation Responses: CV-880, IS, Cat II, III

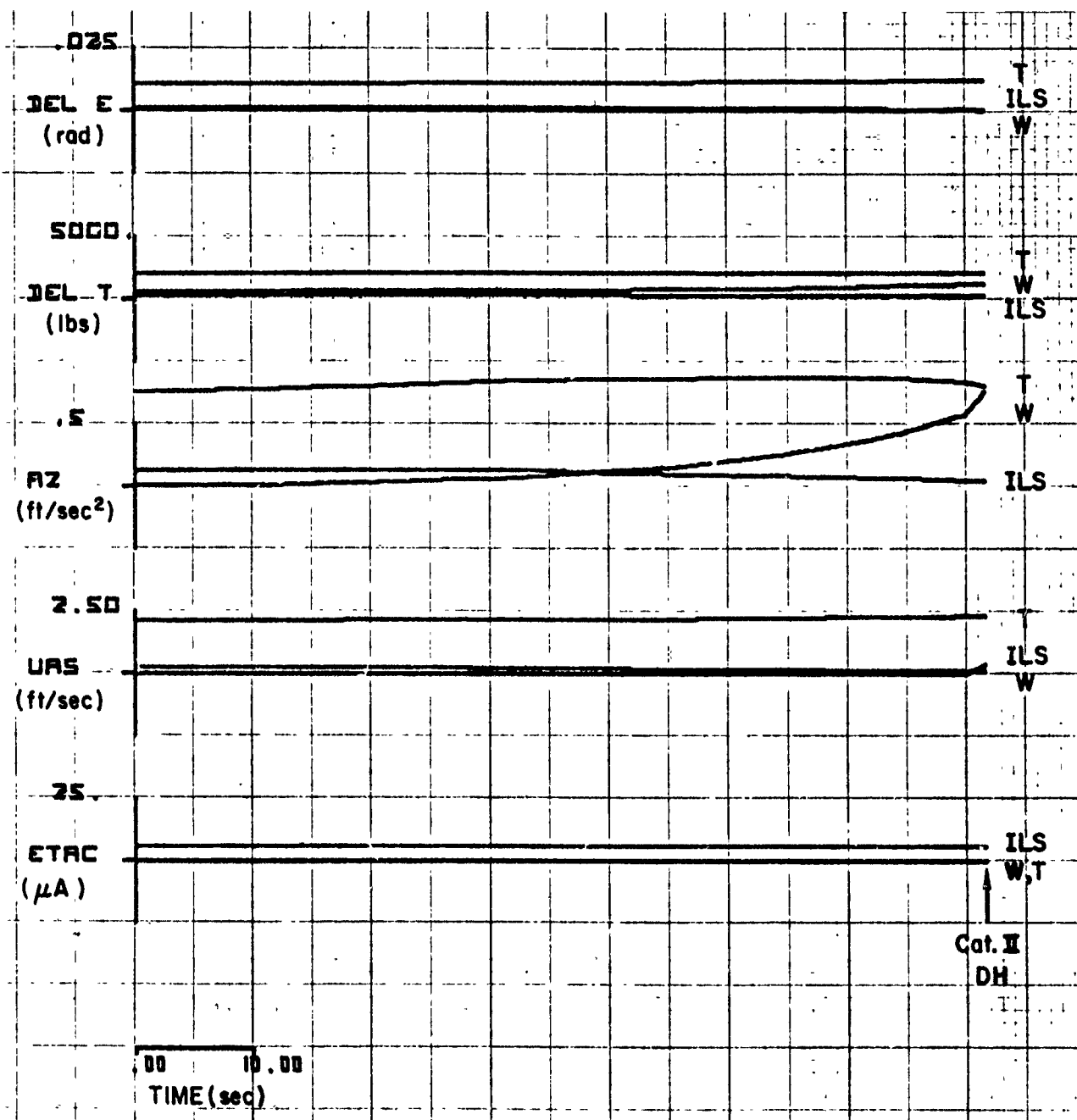


Figure D-13(b)

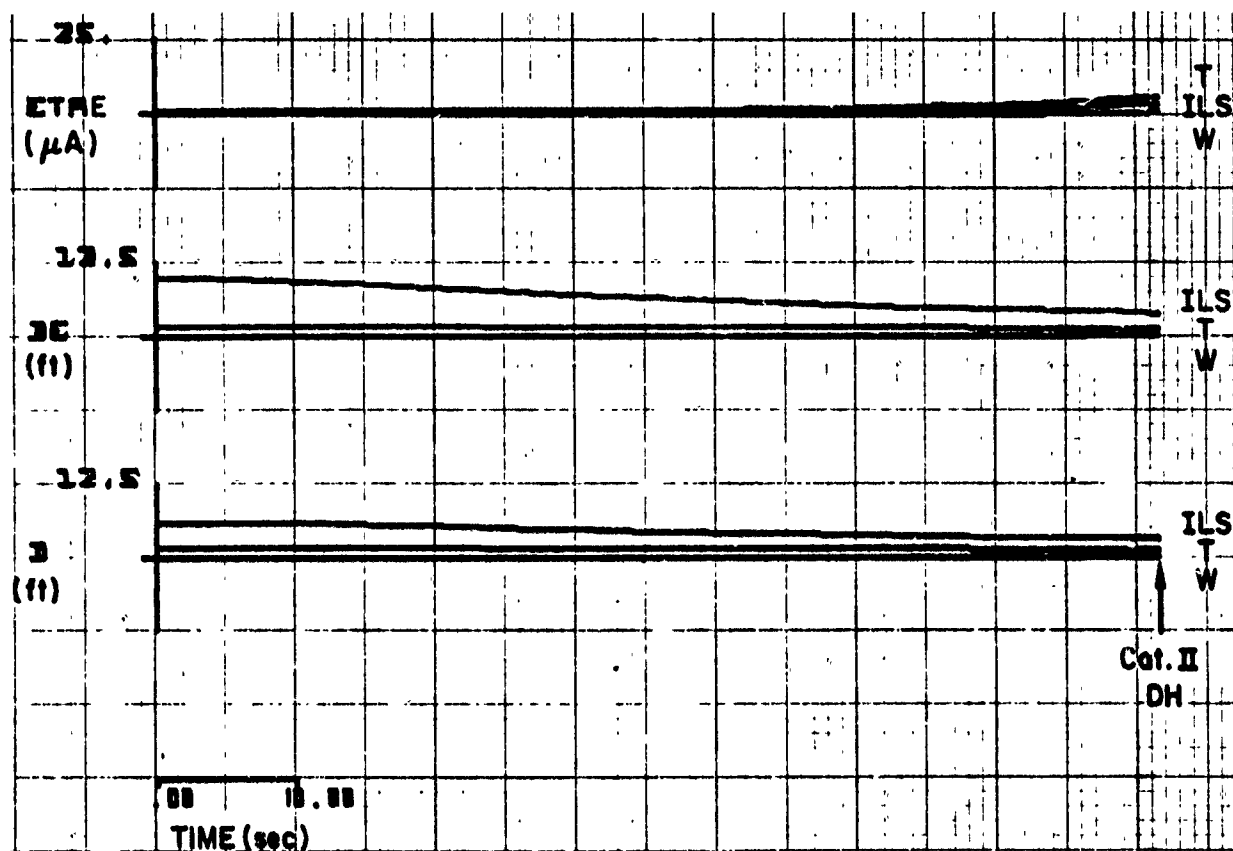


Figure D-13(c)

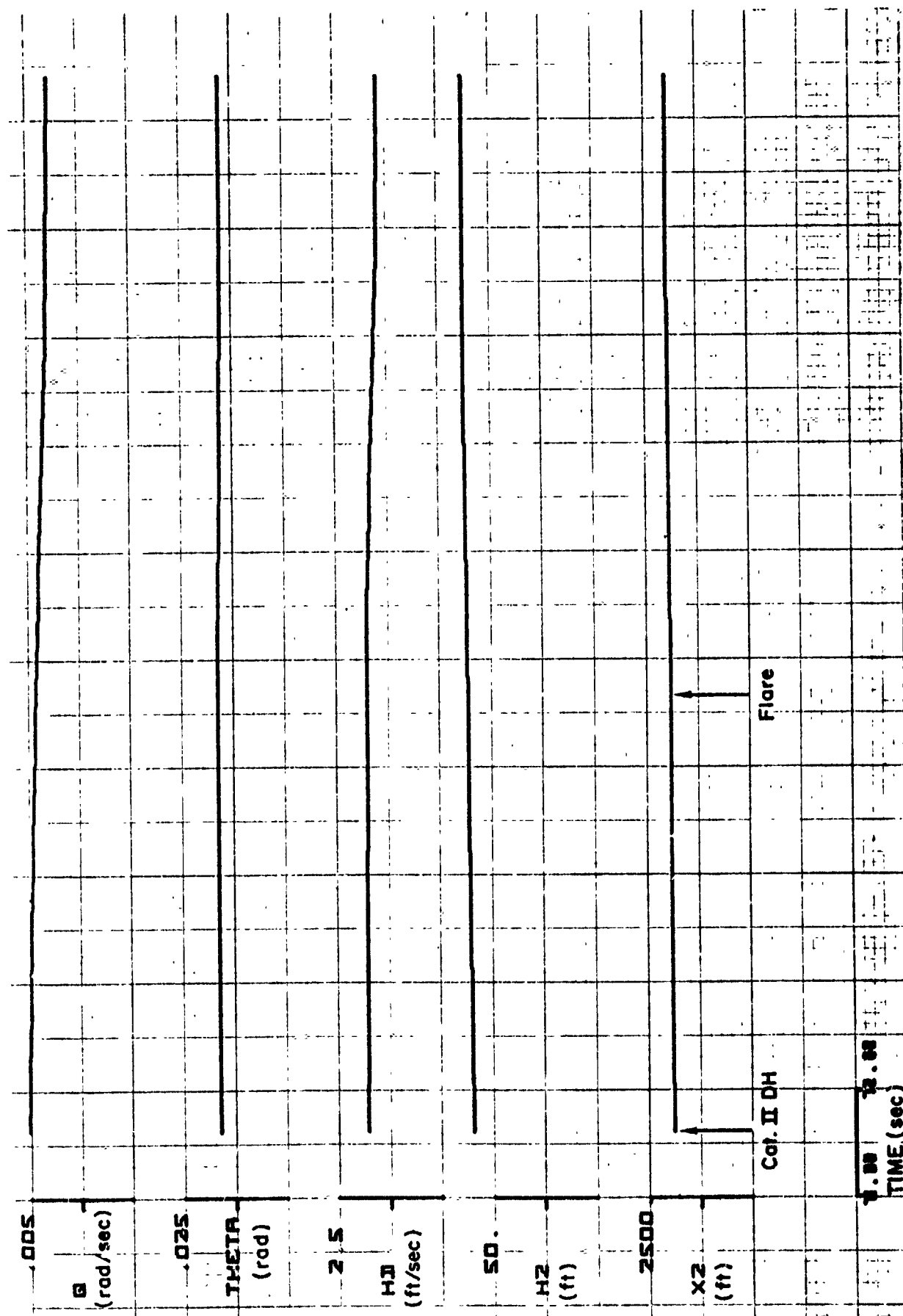


Figure D-14(a). Standard Deviation Responses: CV-880, IS, Cat II, III

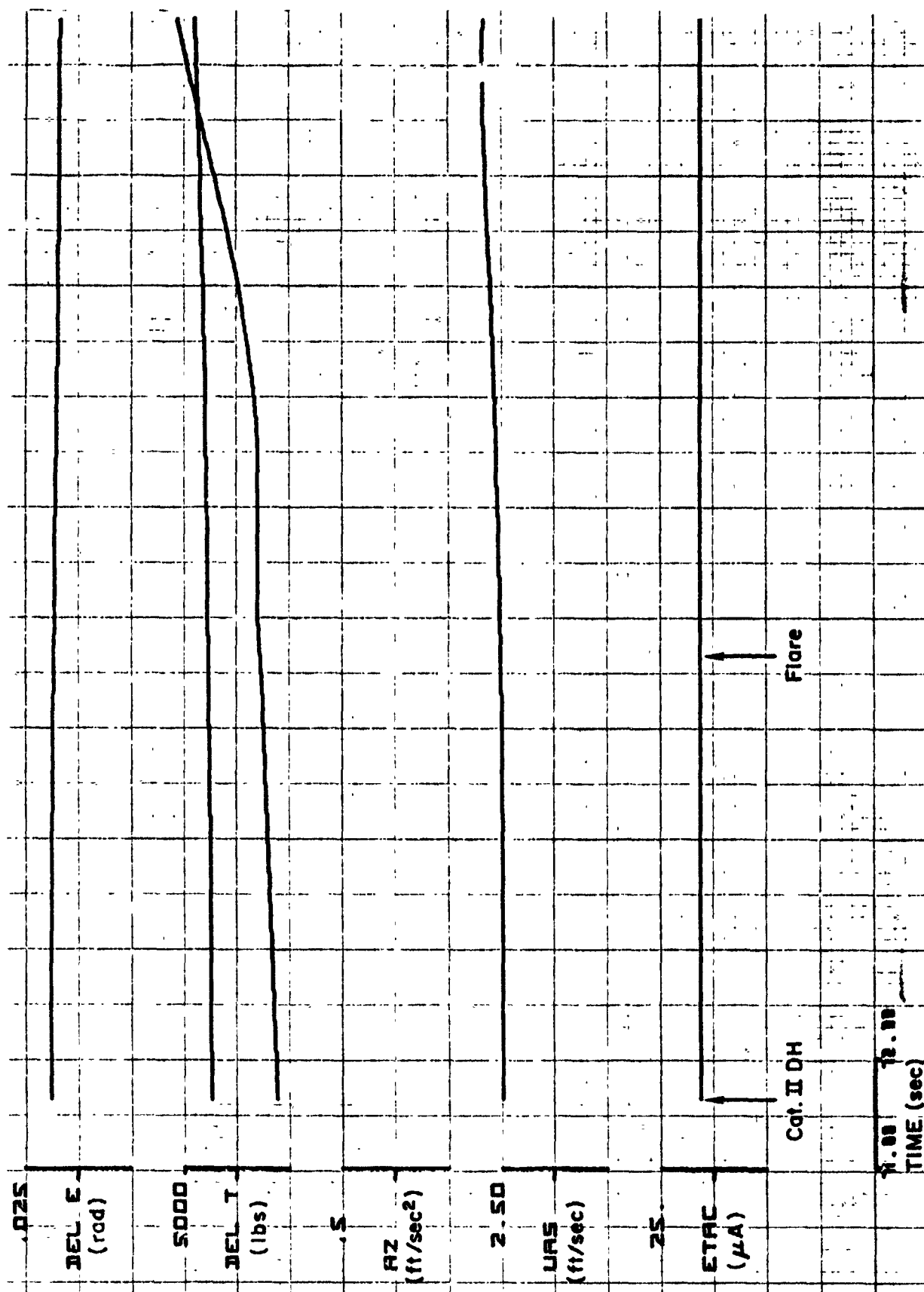


Figure D-14(b)

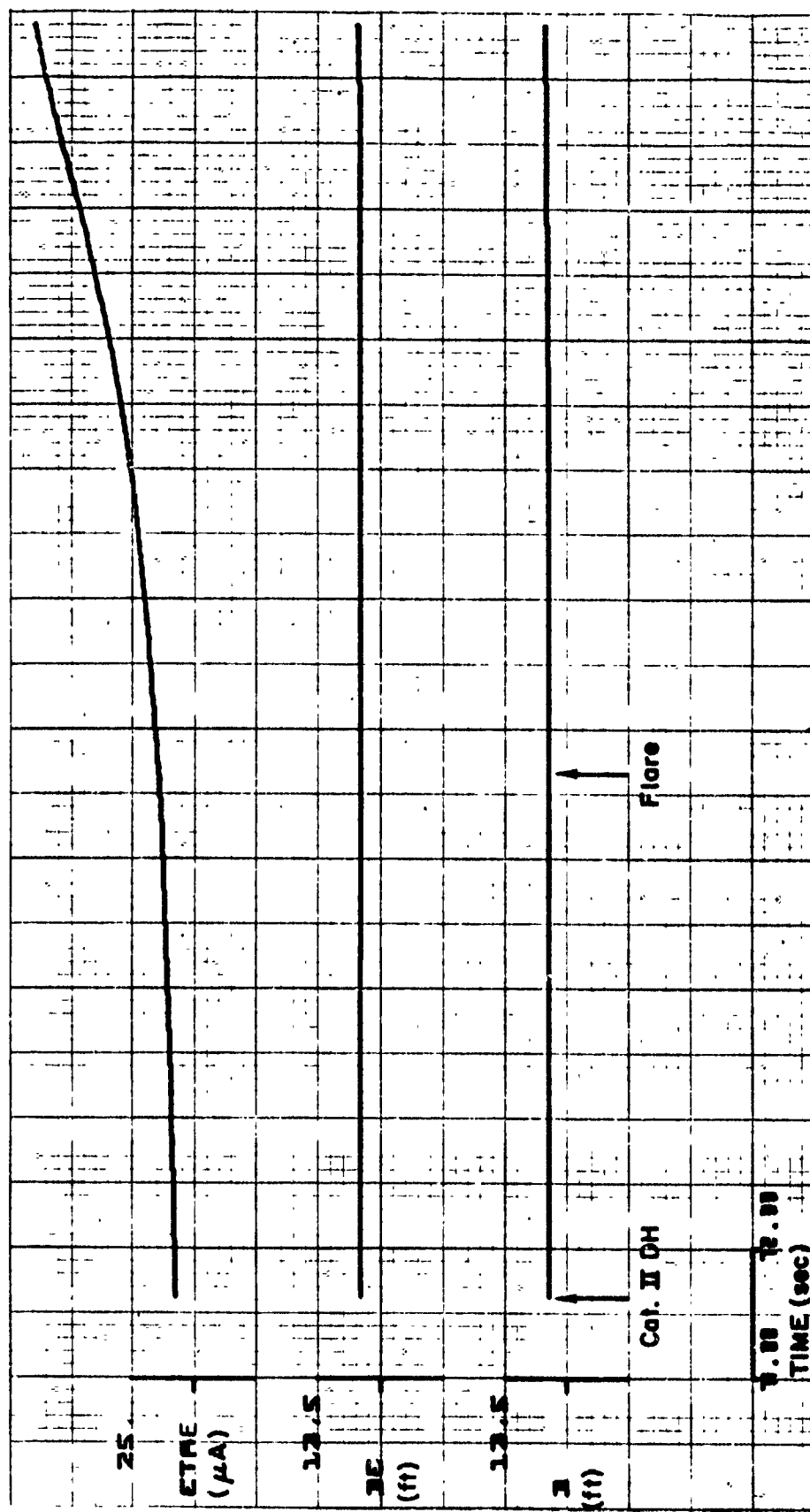


Figure D-14(c)

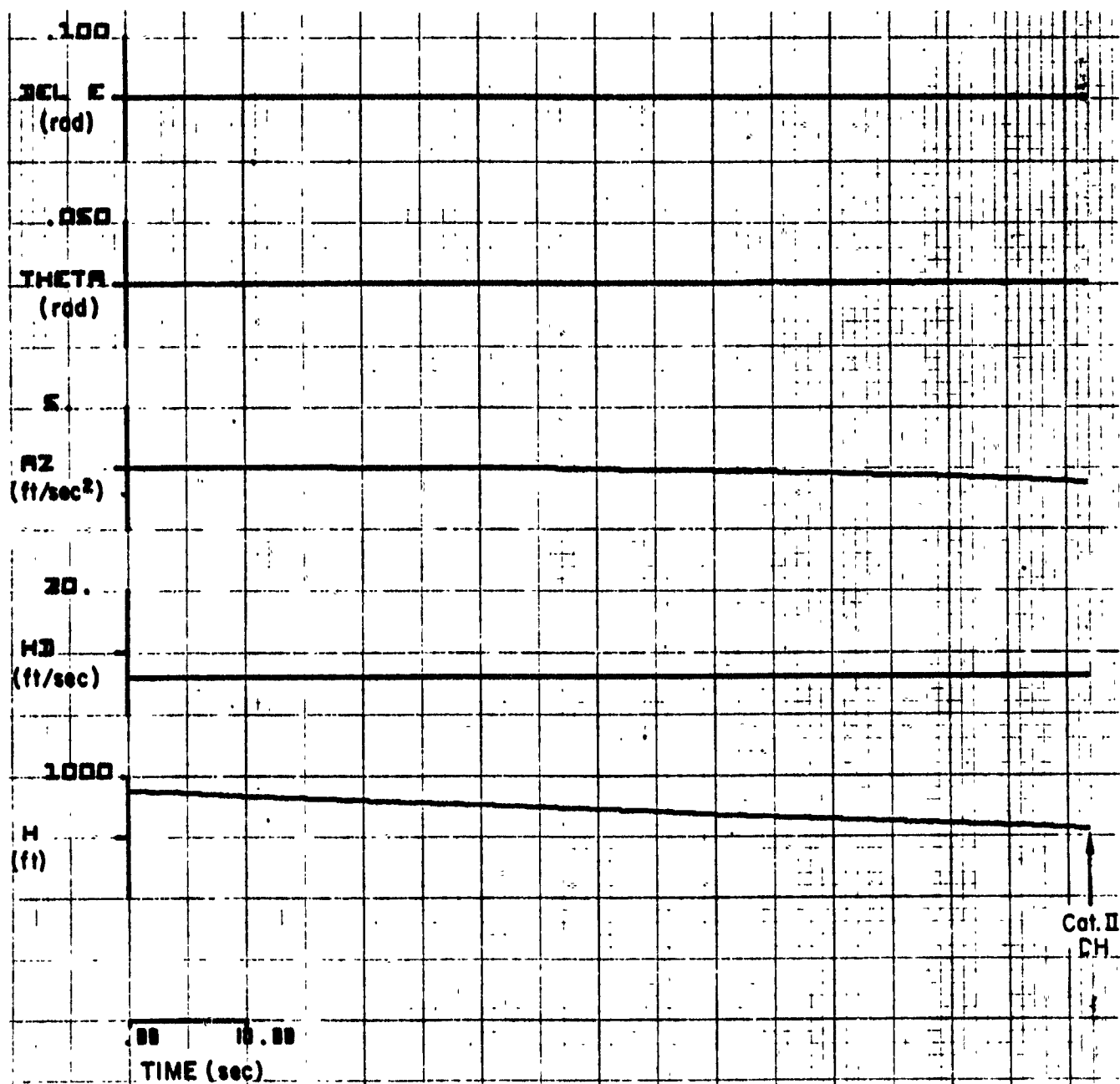


Figure D-15(a). Mean Responses: PA-30, Invented, Cat II, M

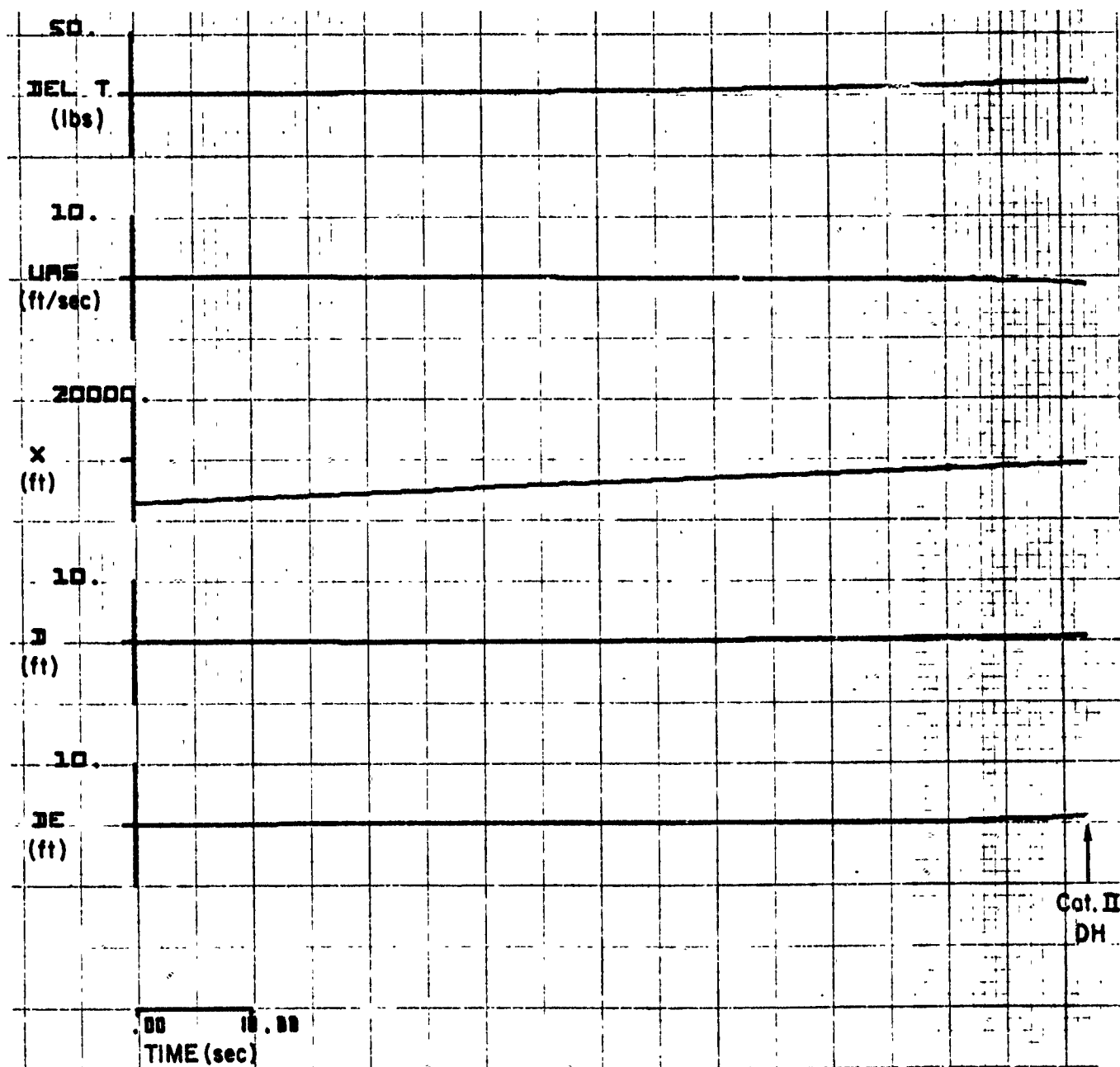


Figure D-15(b)

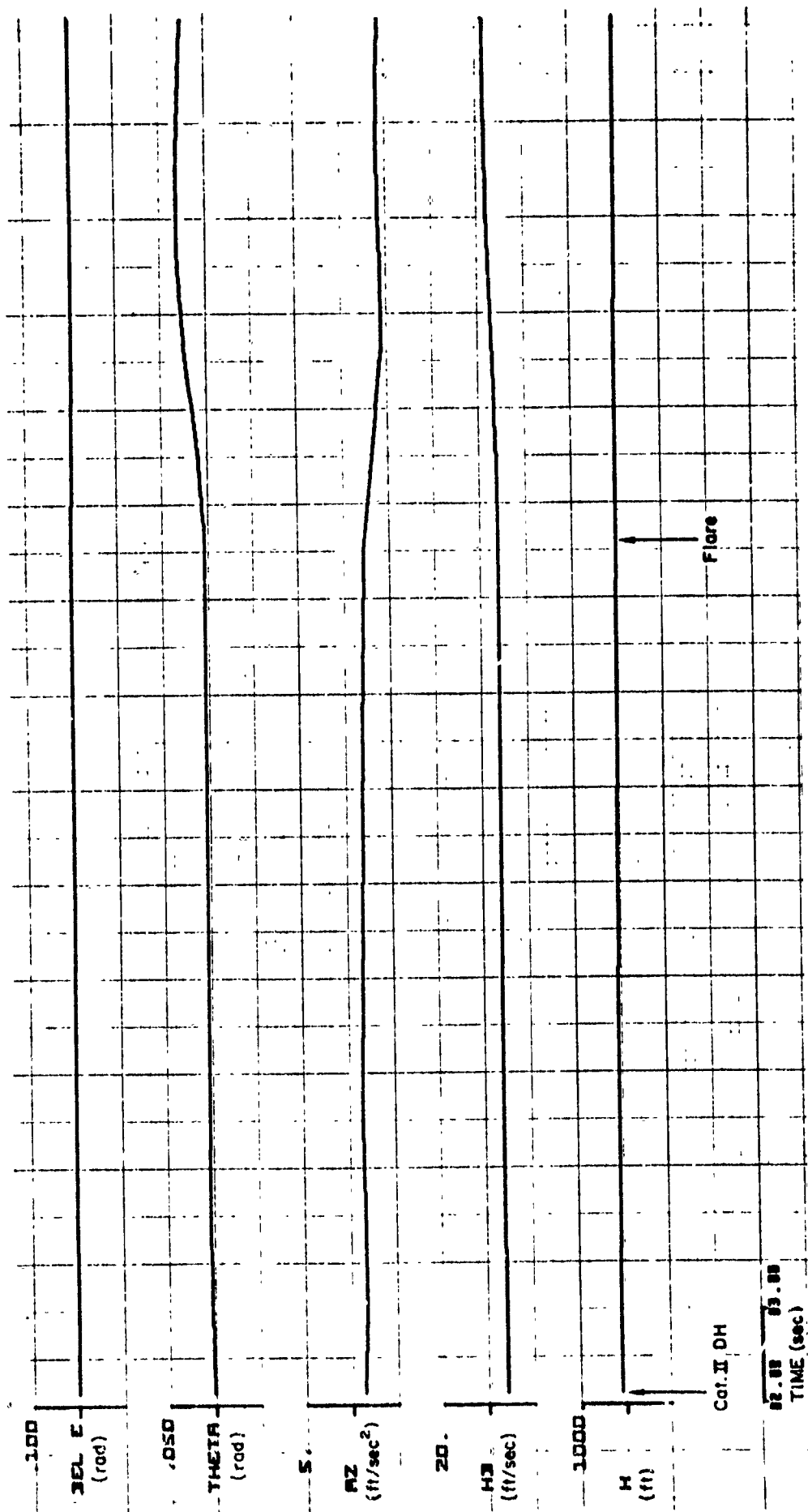


Figure D-16(a). Mean Responses: PA-30, Invented, Cat II, M

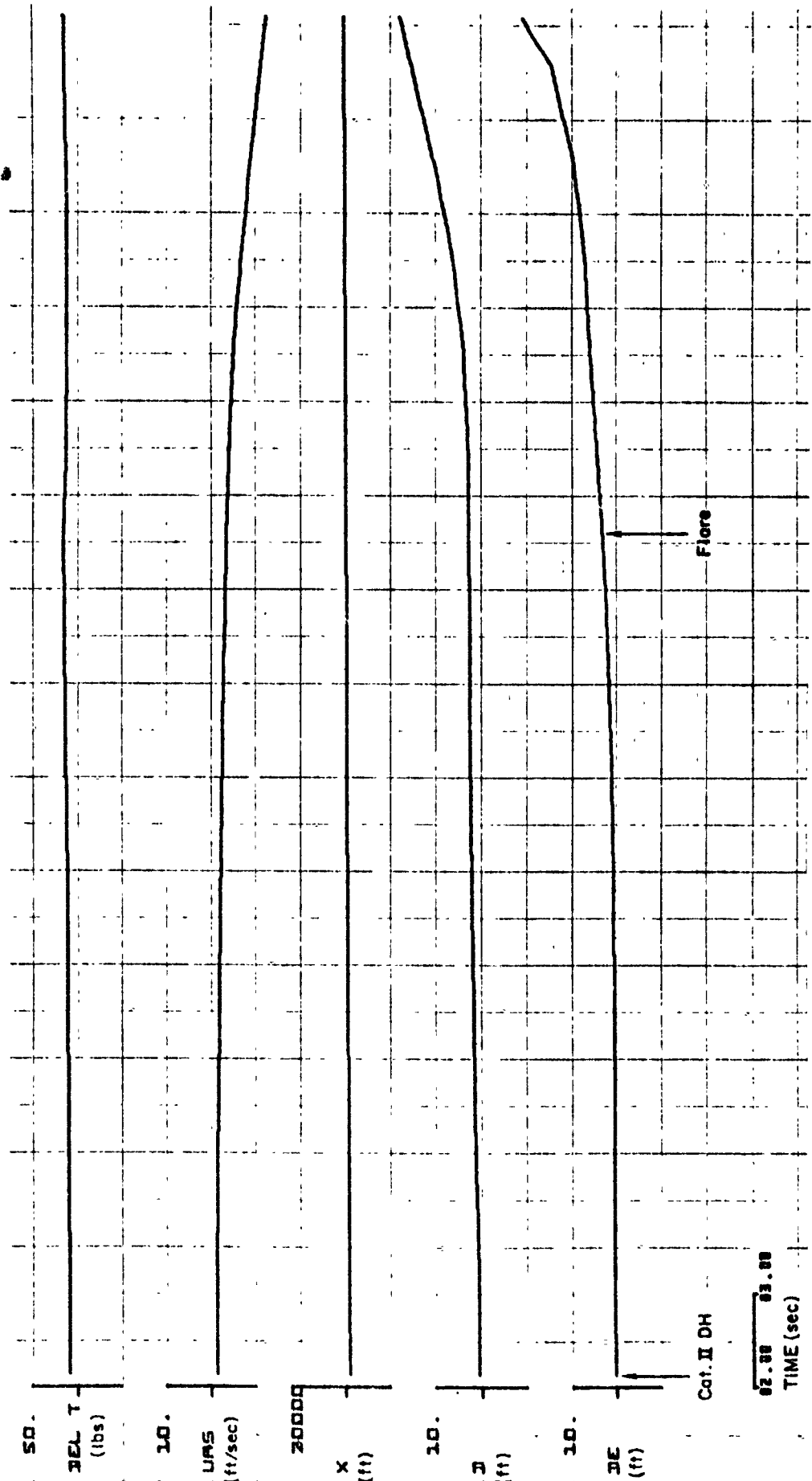
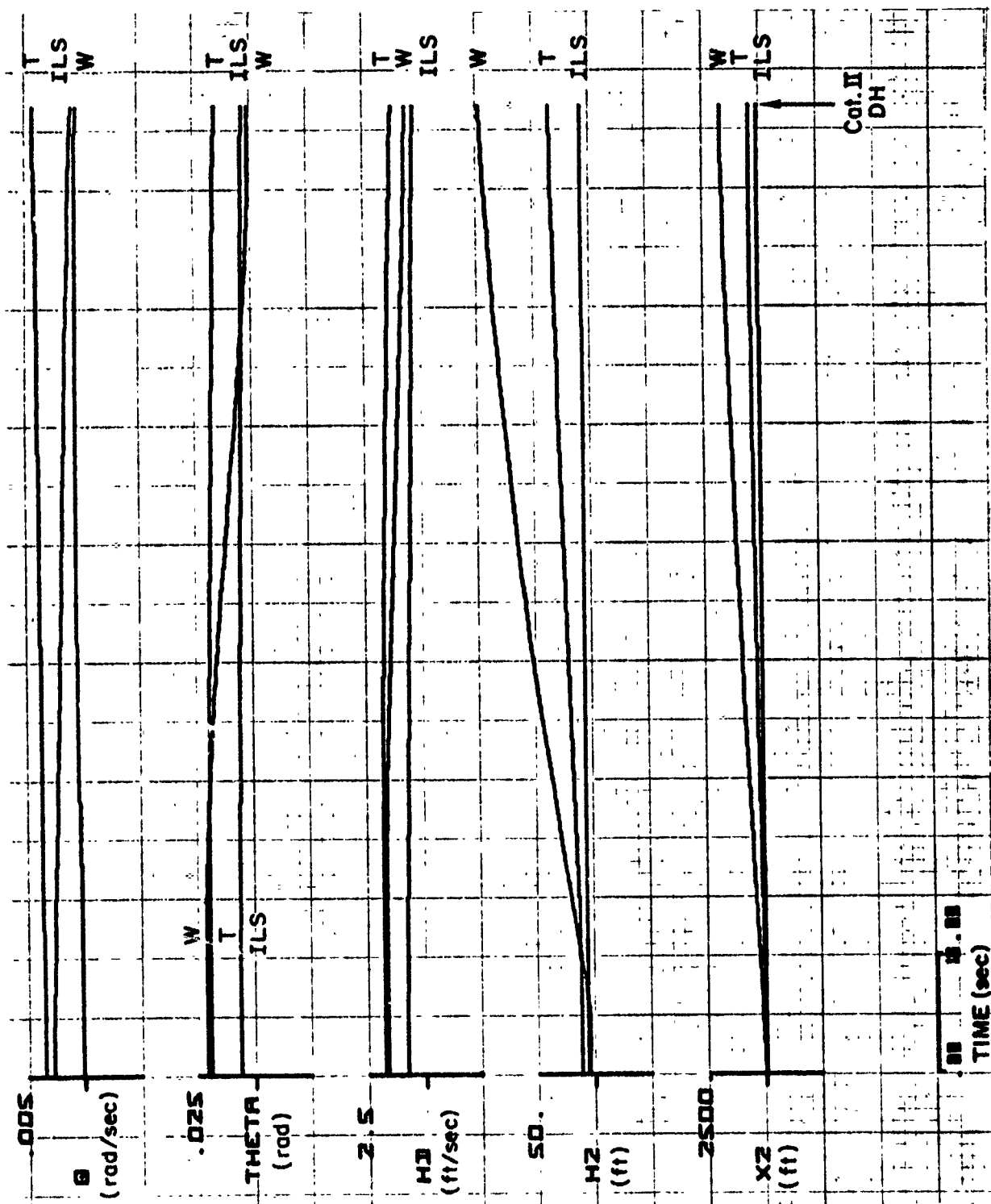


Figure D-16(b)



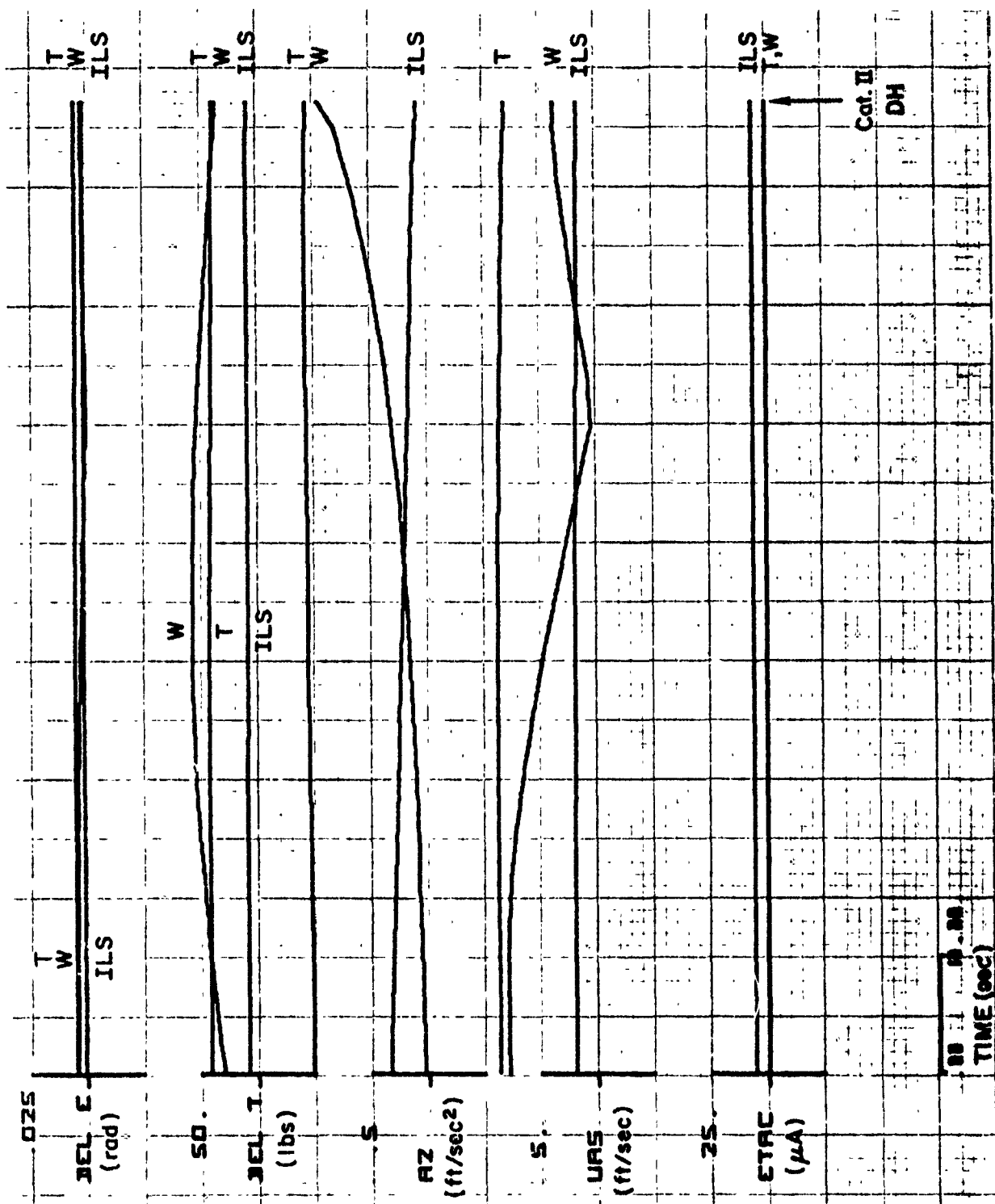


Figure D-17(b)

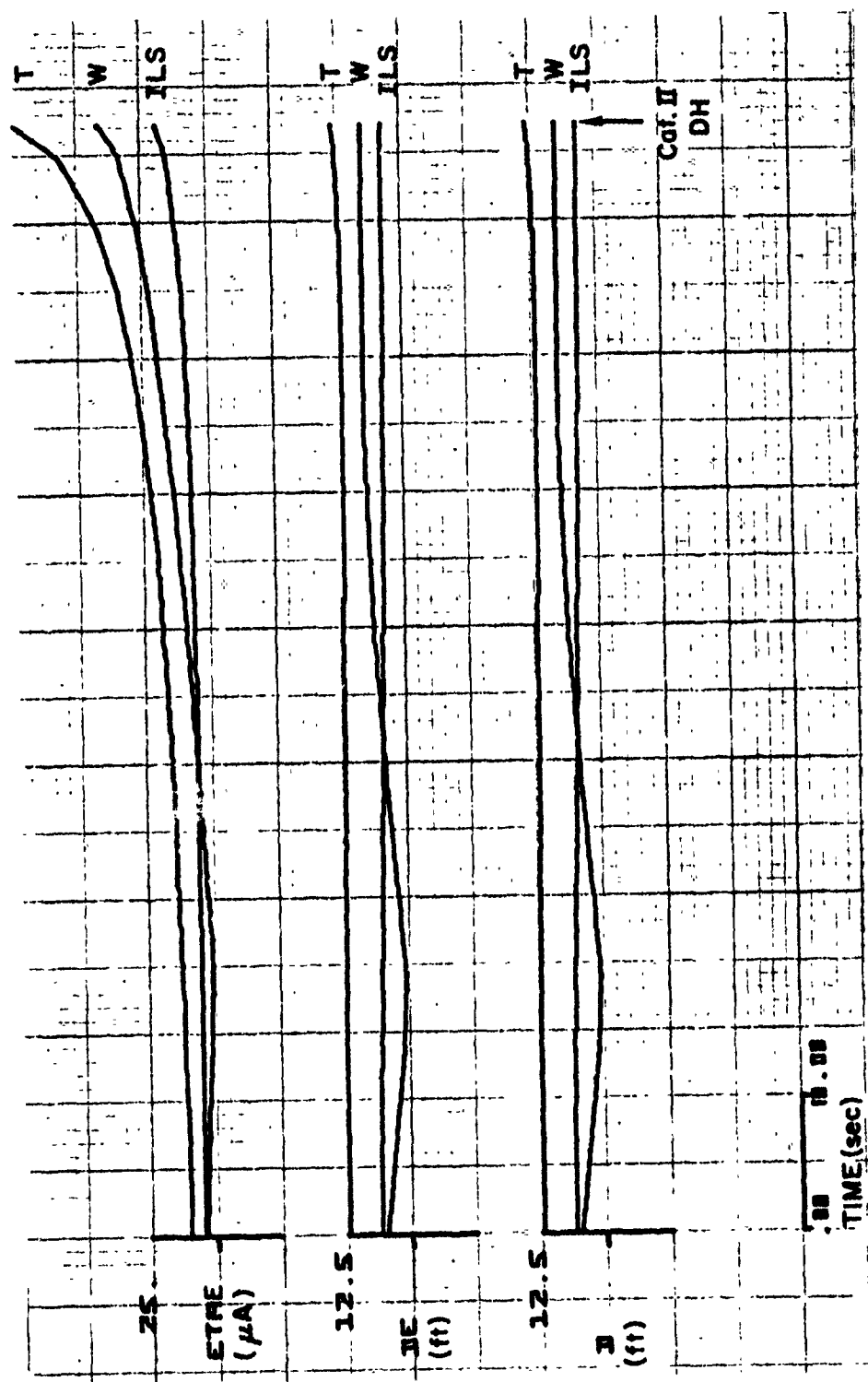


Figure D-17(c)

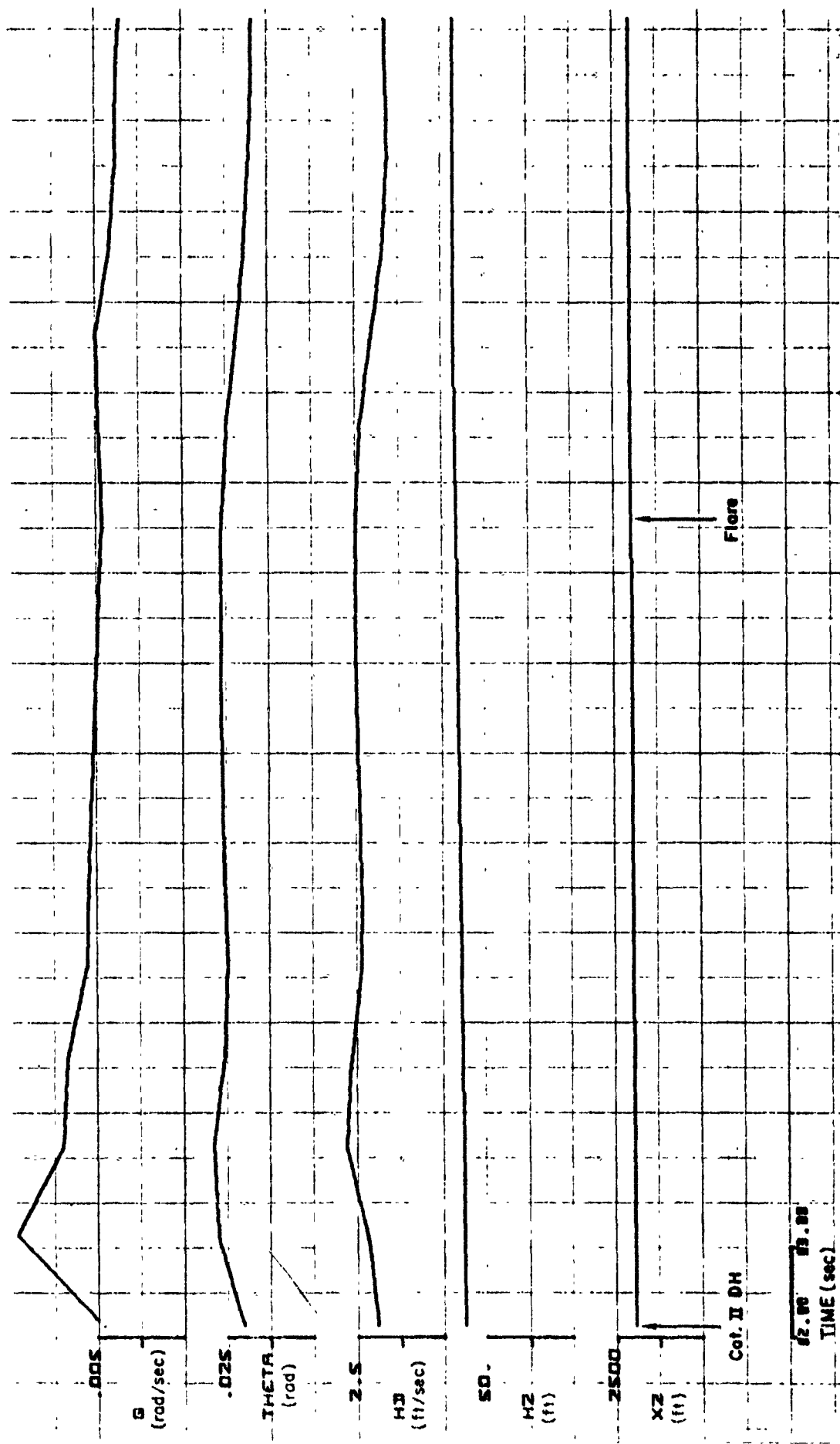


Figure D-18(a). Standard Deviation Responses: PA-30, Inverted, Cat II, M

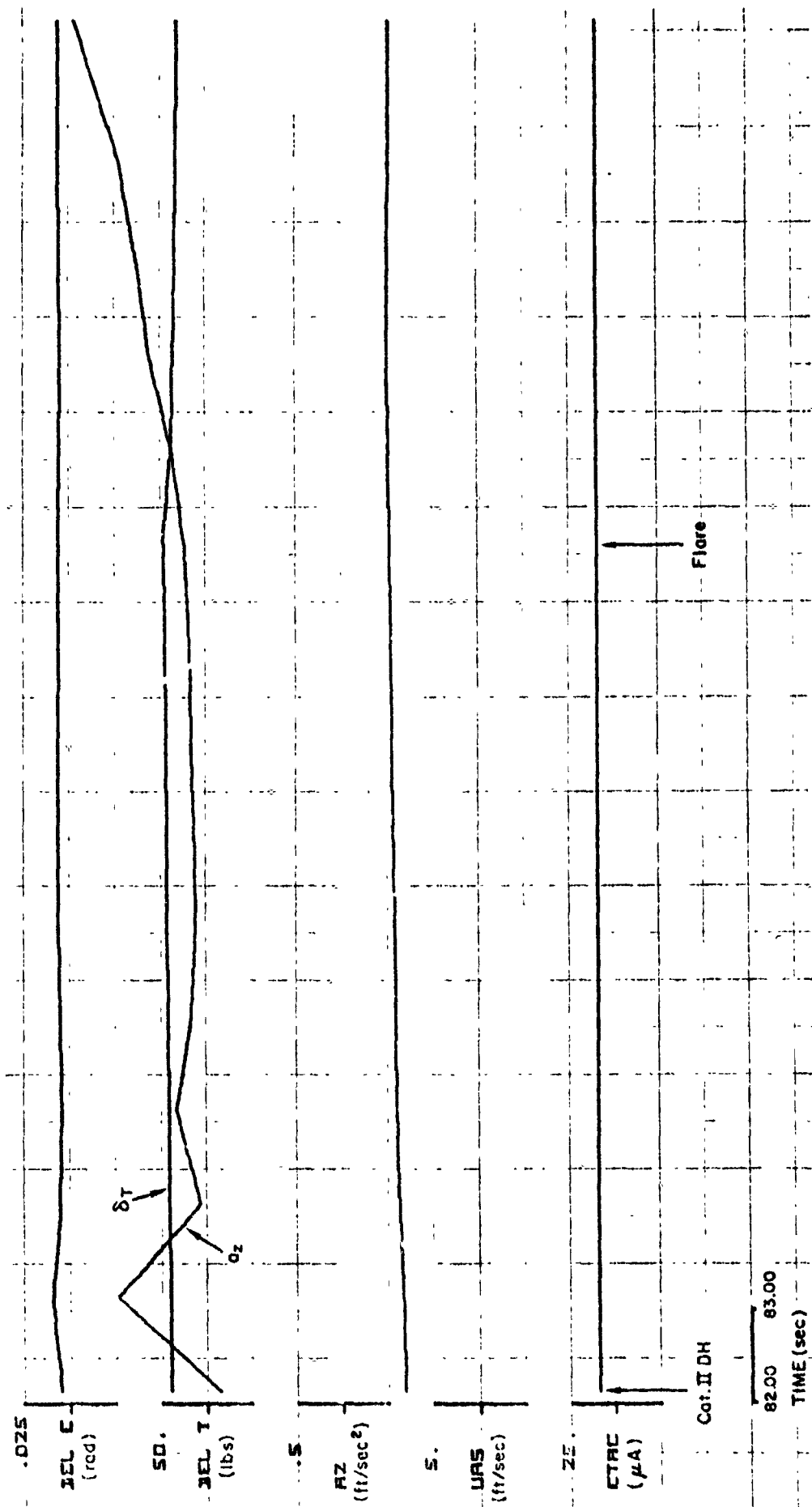


Figure D-18(b)



Figure D-18(c)

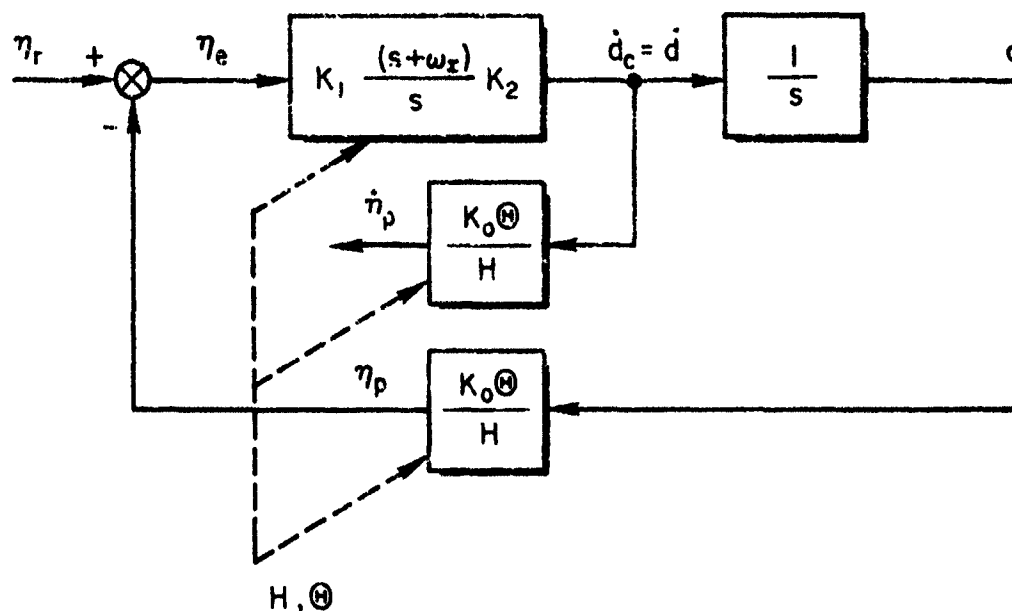
APPENDIX E

AN ALTERNATIVE FILTER SYSTEM FOR GENERATING TYPICAL AIRCRAFT RESPONSES TO GLIDE SLOPE STRUCTURE

An alternative to the filter system shown in Fig. 4 is presented in this Appendix. The alternative filter system is possibly more representative of typical aircraft/control system combinations insofar as ability to represent actual path deviation, actual path deviation rate and indicated path deviation responses is concerned. Final selection of one of these two filter systems must await comparison of transient responses to representative Glide Slope data and faults for Filter Systems No. 1 and No. 2 and complete aircraft/control system simulations in a sequel report.

A block diagram for the alternative filter system, Filter System No. 2, is Fig. E-1. The main difference between this filter system and that in Fig. 4 is that the proportional-plus-integral dynamics of the coupler are assumed to be predominant instead of the rate-of-climb response dynamics for the aircraft. The dynamic characteristics of Filter System No. 2 are dependent only upon Glide Slope coupler parameters, and are specifically independent of all aircraft and inner loop control system parameters. (Filter System No. 2 assumes perfect regulation of actual path deviation rate, \dot{d} , [or equivalently, in an approximate sense, pitch attitude or rate-of-climb]. The integration of \dot{d} to d represents a kinematic relationship.) The mechanization of the Filter System No. 2 portion of the airborne flight inspection equipment would be in the same manner discussed in Section II in connection with Filter System No. 1.

The 2σ tolerance levels calibrated to Filter System No. 2 are Fig. E-2, E-3 and E-4. These are for the actual path deviation, actual path deviation rate, and indicated path deviation respectively. These figures are the counterparts to Fig. 9, 10 and 11 respectively in Section II. The 2σ tolerance levels in Fig. E-2, E-3 and E-4 are qualitatively similar to their counterparts in Section II. However, the 2σ tolerance levels



- ω_I Typical glide slope coupler integral path gain, 0.20 rad/sec
- K_0 Conversion constant 12,278. ($\mu\text{A}/\text{rad}$)
- K_1 Course softening gain function; $K_1 = 1.0$, $H \geq 600$ ft; decreasing linearly to zero at $H = 0$; $K_1 = 0$, $H \leq 0$ ft
- K_2 Typical glide slope coupler gain, 0.2918 ($\text{ft}/\text{sec})/\mu\text{A}$

Figure E-1. Block Diagram for Alternative Filter System which Generates Typical Aircraft Indicated Deviation, Actual Path Deviation and Actual Path Deviation Rate Responses (Filter System No. 2)

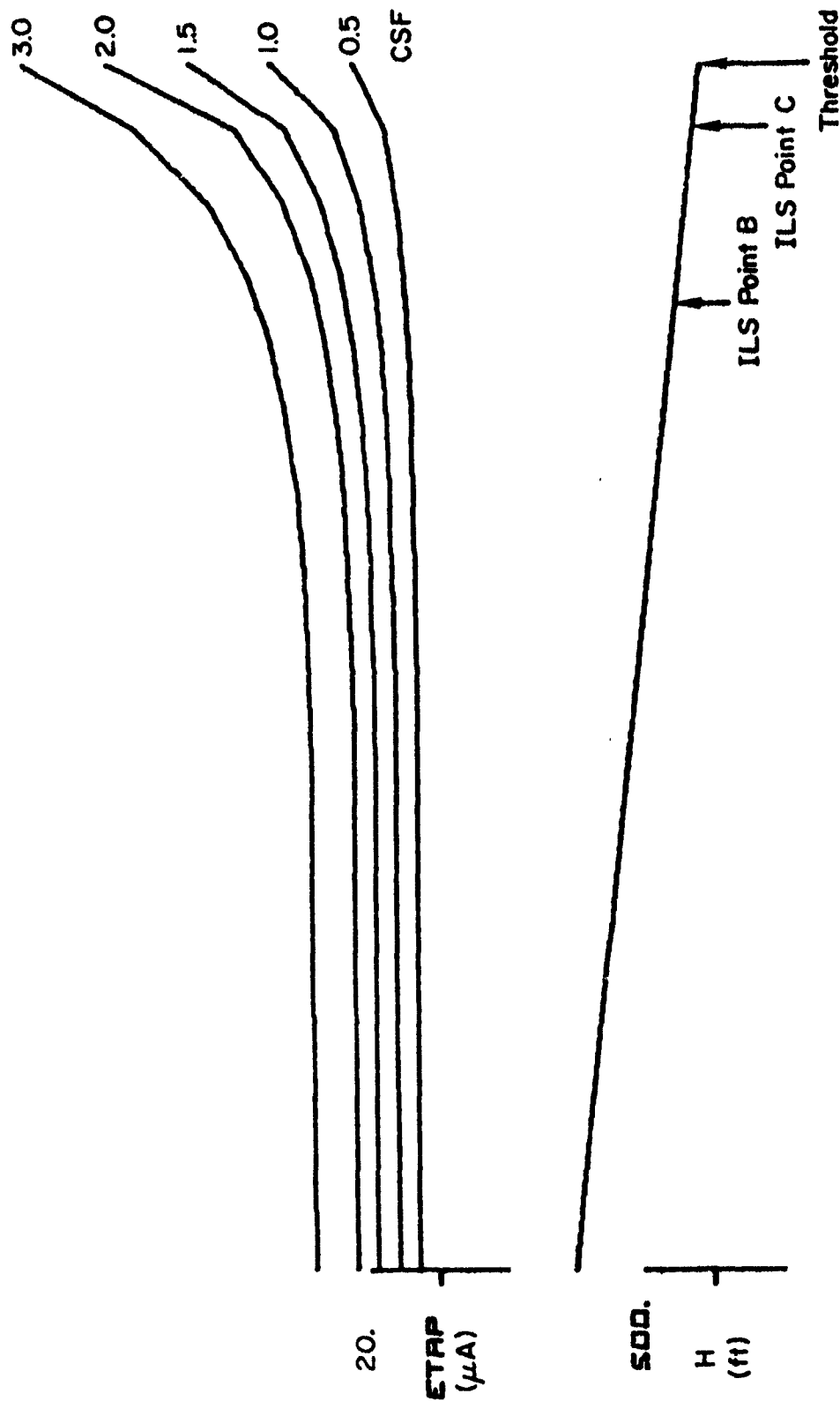


Figure E-2. 2σ Tolerance Level Curves for Typical Aircraft Actual Path Deviation Response (Filter System No. 2)

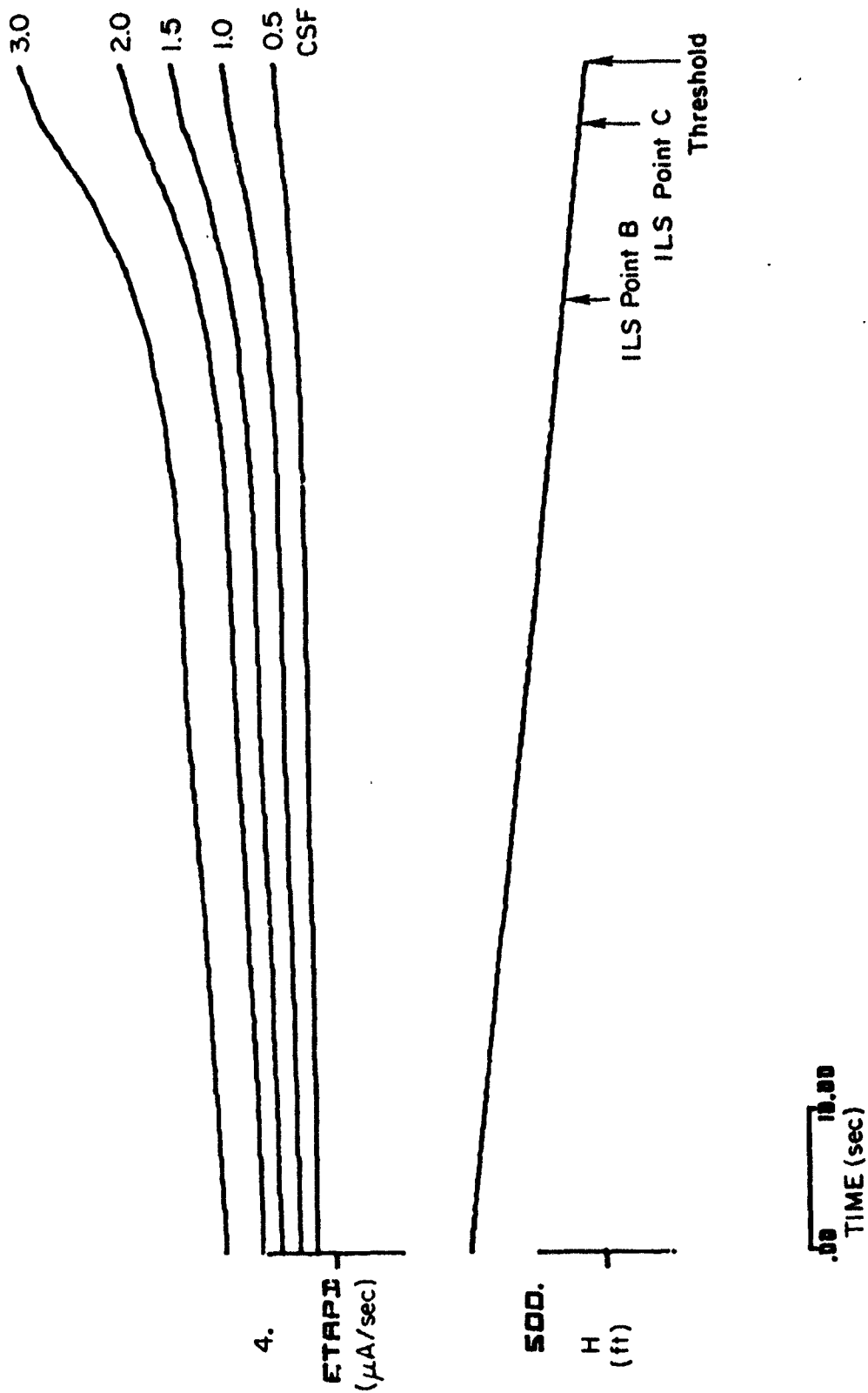


Figure E-3. 2σ Tolerance Level Curves for Typical Aircraft Actual Path Deviation Rate Response (Filter System No. 2)

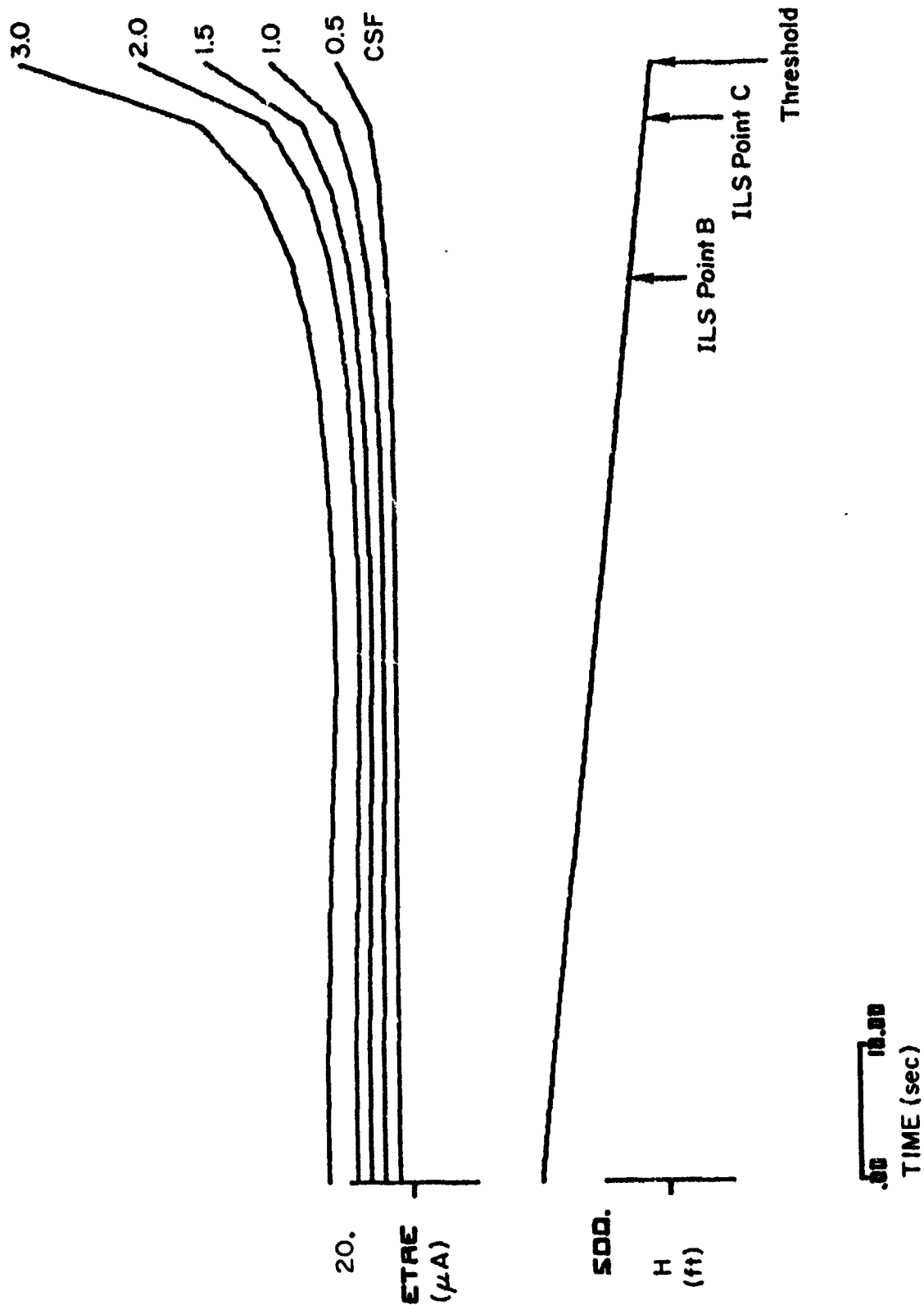


Figure E-4. 2 σ Tolerance Level Curves for Typical Aircraft Indicated
Glide Path Deviation Response (Filter System No. 2)

for actual path deviation and actual path deviation rate are slightly larger, and for indicated path deviation, slightly smaller, for Filter System No. 2.

Figure E-5 compares the current (absolute) standard for ILS Glide Slope change/reversal in slope with the 3σ tolerance levels for actual path deviation rate for Category I and Category II and III facilities. This figure is the counterpart of Fig. 14. The Filter System No. 2 tolerance level for Category I facilities is much larger than the current slope change/reversal standard throughout ILS Zone 2 and 3. For Category II facilities, however, the current slope change/reversal standard is slightly more conservative than the tolerance level upon actual path deviation rate throughout most of ILS Zone 2. At the end of Zone 2, and throughout Zone 3, the current standard becomes increasingly conservative as the runway threshold is approached.

Figure E-6 compares the current average glide path alignment standard with the tolerance level for actual path deviation for Category II ILS Glide Slope facilities. (Refer to Ref. 21.) This figure is the counterpart of Fig. 15. The current standard is conservative with respect to the tolerance level throughout ILS Zone 3. (Refer to Section II for a discussion of the limitations of this comparison and of cautions concerning the current standard.

Best Available Copy

3 σ Level of Tolerance for Category I

3 σ Level of Tolerance for Category II and III

Equivalent of Current FAA Standard (25 μ A/1000 ft) for Category I and II (Current Standard is Absolute)

5.4

6

ETAPD (μ A/sec)

500

H (ft)

ILS Point B

ILS Point C

Threshold

TIME (sec)

Figure 1-1. Comparison of Category I and Category II and III Tolerances for ETAPD vs. H

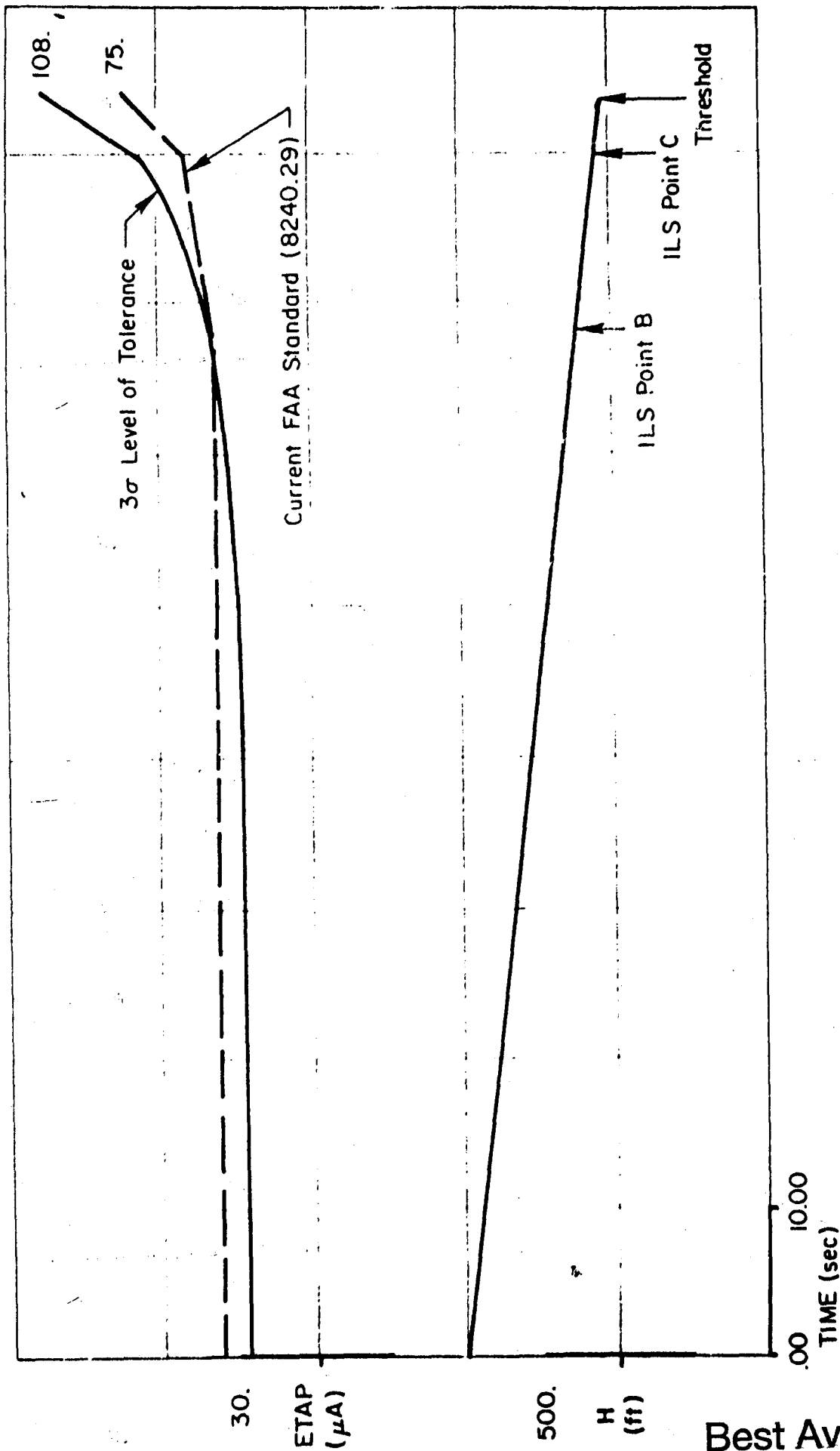


Figure E-1. Comparison of Current FAA Average Path Alignment Standard for Category II with the tolerance level of the typical Aircraft Path Deviation Response Filter System No. 2

Best Available Copy

REFERENCE:

1. Anonymous, Standard Performance Criteria for Autopilot/Coupler Equipment, RTCA Paper 31-63/DO-11E, 14 Mar. 1963.
2. Friedman, A. and J. Doniger, Analog Computer Study of Safe Low Approach Decision Regions and Effectiveness of Glide Path Extension Techniques, The Bendix Corp., Eclipse-Pioneer Div., Defense Documentation Center No. 603869, 31 Mar. 1964.
3. Moses, D., Analog Computer Study of Category III ILS Airborne and Ground Equipment Standards, The Bendix Corp., Eclipse-Pioneer Div., Defense Documentation Center No. AD616005, Sept. 1964.
4. Anonymous, International Standards and Recommended Practices Aeronautical Telecommunications, MLS-ICAO-TN001 (Excerpts), Annex 10, Vol. I, April 1968.
5. Anonymous, United States Standard Flight Inspection Manual, OA P 8200-1, through Change 17, 26 Aug. 1970.
6. Anonymous, Automatic Landing Systems (ALS), FAA AC-20-57A, 12 Jan. 1971.
7. Johnson, W. A., and R. H. Hoh, Determination of ILS Category II Decision Height Window Requirements, NASA CR-2024, May 1972.
8. Weir, D. H., Compilation and Analysis of Flight Control System Command Inputs, AFFDL-TR-65-119, Jan. 1966.
9. Welp, D. W., Disturbance Models for Automatic Flight Control System Simulation and Analysis, Collins Radio Company, TR70-31, 28 Aug. 1970.
10. Johnson, W. A., and R. J. DiMarco, Application of an Approach and Landing System Model to the Space Shuttle Orbiter Vehicle, Systems Technology, Inc., TR-1007-1, Feb. 1972.
11. Johnson, W. A. and D. T. McRuer, Development of a Category II Approach System Model, NASA CR-2022, May 1972.
12. Anonymous, Criteria for Approving Category I and Category II Landing Minima for FAR 121 Operators, FAA-AC-120-29, 25 Sept. 1970; Change 1, 15 Dec. 1971; Change 2, 26 Jul. 1972.
13. Anonymous, Criteria for Approval of Category IIIa Landing Weather Minima, FAA-AC-120-28A, 14 Dec. 1971.
14. Nelson, F. R., W. Koerner, and R. E. Trudel, Dynamics of the Airframe, Bu Aer Rept. AE-61-4II, Sept. 1952.

15. McRuer, D. T., I. L. Ashkenas, and D. Graham, Aircraft Dynamics and Automatic Control, Princeton Univ. Press, 1973.
16. DeRusso, P. M., R. J. Roy, and C. M. Close, State Variables for Engineers, John Wiley and Sons, Inc., New York, 1965.
17. Anonymous, Automatic Landing System for FAA Convair 880, N-112, FAA-RD-71-35, April 1971.
18. Koziol, J. S., Jr., Simulation Model for the Piper PA-30 Light Maneuverable Aircraft in the Final Approach, DOT-TSC-FAA-71-11, July 1971.
19. Anonymous, Category II Operations, General Aviation Airplanes, FAA-AC-91-16, 7 Aug. 1967.
20. Anonymous, Instrument Landing System Improvement Program, FAA-RD-72-71, June 1972, pp. 14-29.
21. Anonymous, ILS Glide Path Tolerance, FAA Change Order 3240.29, 3 Aug. 1973.
22. Anonymous, Minimum Performance Standards - Airborne ILS Glide Slope Receiving Equipment, RTCA Document No. DO-132, 15 Mar. 1966.
23. Bleeg, R. J., H. F. Tisdale and R. M. Vircks, Inertially Augmented Automatic Landing System: Autopilot Performance with Imperfect ILS Beams, FAA-RD-72-22, April 1972.
24. Blackman, R. B., and J. W. Tukey, The Measurement of Power Spectra, New York, Dover, 1958.
25. Weir, D. H., Analysis and Comparison of Carrier Air Wakes, Systems Technology, Inc., TR-158-1, Apr. 1966.
26. Aseltine, J. A., Transform Method in Linear System Analysis, New York, McGraw-Hill, 1958.
27. Anonymous, Wind Model for Space Shuttle Simulations, NASA Ames Research Center, circa 1970.
28. Anonymous, Flying Qualities of Piloted Airplanes, MIL-F-8785B(ASG), 7 Aug. 1969.